Marine isoprene - Formation, emissions and their impact on the atmospheric chemistry

Dissertation
zur Erlangung des Doktorgrades
der Mathematisch-Naturwissenschaftlichen Fakultät
der Christian-Albrechts-Universität zu Kiel

vorgelegt von

Dennis Booge

Kiel, 2017

Marine isoprene - Formation, emissions and their impact on the atmospheric chemistry

Dissertation
zur Erlangung des Doktorgrades
der Mathematisch-Naturwissenschaftlichen Fakultät
der Christian-Albrechts-Universität
zu Kiel

vorgelegt von

Dennis Booge

Kiel, 2017

Erste Gutachterin:	Prof. Dr. Christa A. Marandino
Zweiter Gutachter:	Prof. Dr. Hermann W. Bange
Tag der mündlichen Prüfung:	23.01.2018
Zum Druck genehmigt:	23.01.2018

gez. Prof. Dr. Natascha Oppelt, Dekanin

Eidesstattliche Erklärung

Hiermit erkläre ich, **Dennis Booge**, dass ich diese Doktorarbeit, abgesehen durch die Beratung meiner Betreuerin, selbstständig verfasst, sowie alle wörtlichen und inhaltlichen Zitate als solche gekennzeichnet habe.

Die Arbeit wurde unter Einhaltung der Regeln guter wissenschaftlicher Praxis der Deutschen Forschungsgemeinschaft verfasst.

Sie hat weder ganz, noch in Teilen, einer anderen Stelle im Rahmen eines Prüfungsverfahrens vorgelegen, ist nicht veröffentlicht und auch nicht zur Veröffentlichung eingereicht.

Kiel, Dezember 2017

_____

gez. Dennis Booge

ABSTRACT

Volatile organic compounds (VOCs) play an important role in influencing the oxidative capacity of the atmosphere. On a global scale, emissions of biogenic VOCs are dominating anthropogenic emissions by one order of magnitude. Isoprene, the most important biogenic VOC, has received increased attention in recent years as biogenic emissions of isoprene are the main contributor for secondary organic aerosols (SOA) formation. SOA in the atmosphere influence the radiative balance through scattering or absorption of solar radiation and, therefore, have a direct impact on the climate of our Earth's system. Although terrestrial isoprene emissions are quite well quantified, the strength of global marine isoprene emissions is highly debated, as only a few field measurements in the world oceans have been carried out to date. The knowledge about the spatial and seasonal distribution of isoprene, as well as its production and consumption processes in the surface ocean, is still lacking and is crucial to quantify marine isoprene emissions.

The main goal of this work was to increase the global dataset of marine isoprene measurements and provide a better understanding of the biogeochemical cycling in the surface ocean. This improved understanding was used to calculate the global surface isoprene distribution and the isoprene emission to the atmosphere in order to estimate the influence of marine isoprene on the Earth's atmosphere and climate.

In the first study, isoprene measurements from three different ocean basins were used to improve model simulations of global marine isoprene distributions. Remotely sensed monthly mean satellite data of chlorophyll a (chl-a), sea surface temperature, wind speed, and mixed layer depth were used in a steady-state model to estimate monthly mean global isoprene distributions. Compared to in-field isoprene data, the model underestimated the actual isoprene concentration by a factor of 19±12. The main improvement was achieved by replacing a single isoprene production rate by chl-a normalized isoprene production rates from different phytoplankton functional types. However, the improved model still could not sufficiently reproduce the distribution pattern and underestimated the measured concentrations by a factor of two suggesting at least one missing source or possibly other factors influencing surface ocean isoprene distributions. Global marine isoprene emissions were calculated (0.21 Tg C yr^{-1}), increasing earlier emission estimates by a factor of two. However, the calculated emissions had to be 10-20 times higher to account for measured atmospheric isoprene concentrations.

The goal of the second study was to better understand isoprene sources and sink processes of isoprene in the surface ocean. Isoprene and related field measurements were carried out in the oligotrophic Indian Ocean as well as in the East Pacific Ocean, in the coastal upwelling region off to Peru. The results of these two contrasting regions demonstrated that isoprene production is mainly influenced by light, ocean temperature, and salinity. Additionally, nutrient availability played a role in the strength of isoprene production by different phytoplankton types. For the first time, in-field isoprene production rates for different phytoplankton functional types under varying biogeochemical and physical conditions were calculated. By implementing these newly derived production rates into the improved model of the first study, the results indicated that an additional sink process was needed, which was attributed to heterotrophic bacterial respiration.

The results of different global marine isoprene emission estimates were used in the third study to estimate the influence of marine isoprene derived SOA (iSOA) on total atmospheric iSOA concentration. As a result of the first study three different monthly mean emission inventories were used and implemented into a global chemistry climate model (ECHAM-HAMMOZ). A novel framework within ECHAM-HAMMOZ connected the semi-explicit isoprene oxidation chemistry with an explicit treatment of aerosol tracers. The results showed that marine iSOA concentrations are very low (contribution: <1%) compared to total SOA concentrations on a global scale, but are important on regional and seasonal scales, as the atmosphere over remote ocean parts was significantly influenced by marine-derived iSOA. Although the annual mean direct radiative effect of marine-derived iSOA in different ocean regions was <0.2 W m^{-2}, the contribution to the total aerosol direct radiative effect on regional and seasonal scales was calculated to be up to 43% (boreal summer, North Atlantic region). However, the effect of marine-derived iSOA on the radiative balance seemed to be weakened due to the formation of larger aerosol particles compared to smaller particle formation over land. The different size distribution might indicate that marine-derived iSOA contributes to the growth of already existing particles instead of contributing to their initial formation.

Despite the low marine-derived iSOA concentrations on a global scale, this thesis illustrates that marine isoprene emissions significantly influence the atmospheric chemistry and the radiative balance in the open ocean regions. In these regions the terrestrial influence is only of minor importance or even absent which strengthens the influence of local marine sources of isoprene on the atmospheric chemistry over the ocean. Therefore, a better understanding of production and consumption of isoprene helps to determine missing sources and sinks influencing surface ocean isoprene distributions to finally quantify marine isoprene emissions and their atmospheric impact. The results show that isoprene emission estimates have to be incorporated into atmospheric chemistry climate models in order to predict SOA concentrations and their influence in a changing climate.

ZUSAMMENFASSUNG

Flüchtige organische Verbindungen (VOCs: volatile organic compounds) haben einen großen Einfluss auf die oxidative Kapazität der Atmosphäre. Weltweit gesehen sind die Emissionen biogener VOCs um eine Größenordnung stärker als menschengemachte Emissionen. Isopren, als wichtigster Vertreter der biogenen VOCs, wurde in den letzten Jahren zunehmende Aufmerksamkeit zuteil, da es als wichtiger Vorläuferstoff für die Bildung von sekundären organischen Aerosolen (SOA: seconary organic aerosols) verantwortlich ist. In der Atmosphäre beeinflusst SOA durch Streuung und Absorption von Sonnenstrahlung die Strahlungsbilanz der Erde und hat somit einen direkten Einfluss auf das Klima. Im Gegensatz zu terrestrischen Emissionen von Isopren ist die Stärke von ozeanischen Emissionen immer noch nicht ermittelt, da bis heute nur wenige Messungen von Isopren in den weltweiten Ozeanen durchgeführt wurden. Sowohl die räumliche und saisonale Verteilung als auch die Bildungs- und Abbauprozesse von Isopren im Oberflächenozean sind noch immer nicht ausreichend erforscht. Ein besseres Verständnis dieser Prozesse ist jedoch wichtig um die Stärke mariner Emissionen von Isopren zu quantifizieren.

Ziel dieser Arbeit war es Messungen von Isopren im Ozean durchzuführen und die Prozesse sowohl zur Bildung als auch zum Abbau von Isopren im Oberflächenozean zu untersuchen. Die hieraus gewonnenen Erkenntnisse wurden genutzt, um sowohl die globale Konzentrationsverteilung von Isopren im Oberflächenozean als auch die resultierenden Emissionen in die Atmosphäre zu berechnen, und um somit schlussendlich den globalen Einfluss von ozeanischem Isopren auf das Klima der Erde abschätzen zu können.

In der ersten Studie wurden Messungen von Isopren in drei verschiedenen Ozeanen genutzt, um die Modellsimulation der globalen Konzentrationsverteilung von Isopren im Oberflächenozean zu verbessern. Mithilfe monatlich gemittelter Satellitendaten von Chlorophyll *a* (chl-a), der Wassertemperatur, der Windstärke, sowie der Durchmischungstiefe wurden globale Konzentrationsverteilungen von Isopren im Oberflächenozean berechnet. Im Vergleich zu den Messungen unterschätzte das Modell die Oberflächenkonzentration von Isopren um den Faktor 19±12. Das Modell wurde durch den Einsatz von verschiedenen, je nach Phytoplanktonart abhängigen, chl-a normalisierten Isoprenproduktionsraten erheblich verbessert. Jedoch konnte das verbesserte Modell die Konzentrationsverteilung immer noch nicht vollständig wiedergeben. Außerdem

waren die Konzentrationsvorhersagen im Vergleich zu den Messungen immer noch um das zweifache zu gering. Dies weist auf wenigstens einen oder mehrere nicht berücksichtigte Prozesse von Isopren im Oberflächenozean hin. Die mit dem neuen Modell berechneten globalen Isoprenemissionen (0,21 Tg C yr^{-1}) waren doppelt so hoch wie frühere Berechnungen, allerdings um das 10-20 fache zu niedrig, um die gemessenen atmosphärischen Isoprenkonzentrationen zu erklären.

Das Ziel der zweiten Studie war es die Produktions- und Abbauprozesse von Isopren im Oberflächenozean zu untersuchen. Dafür wurden Messungen von Isopren und weiteren Parametern sowohl im nährstoffarmen indischen Ozean als auch im Ostpazifik, im nährstoffreichen Auftriebsgebiet vor Peru, durchgeführt. Die Ergebnisse aus den beiden unterschiedlichen Regionen zeigten, dass die Produktion von Isopren hauptsächlich durch Licht, Wassertemperatur und Salzgehalt beeinflusst wird. Zusätzlich spielte die Verfügbarkeit von Nährstoffen bei einigen Phytoplanktonarten eine Rolle. Zum ersten Mal überhaupt wurden Produktionsraten von Isopren unter verschiedenen biochemischen und physikalischen Bedingungen im Ozean berechnet. Diese neu berechneten Produktionsraten wurden in das Modell der ersten Studie implementiert. Die Ergebnisse des aktualisierten Modells zeigten, dass ein zusätzlicher Abbauprozess von Isopren, möglicherweise bakterielle Respiration, benötigt wird, um die gemessenen Isoprenkonzentrationen im Oberflächenozean zu erklären.

Die unterschiedlichen globalen Emissionsabschätzungen von ozeanischem Isopren aus der ersten Studie wurden in der dritten Studie genutzt, um den Einfluss des aus marinem Isopren gebildeten SOA (iSOA) auf die totale atmosphärische iSOA Konzentration abzuschätzen. Dazu wurden drei verschiedene marine Isoprenemissionsszenarien in ein globales, chemisches Klimamodell (ECHAM-HAMMOZ) implementiert. Ein neuer Bestandteil in ECHAM-HAMMOZ verband dabei die semi-explizite Oxidation von Isopren mit einer expliziten Betrachtung von Aerosoltracern. Die Ergebnisse zeigten, dass die marinen iSOA Konzentrationen auf globaler Ebene im Vergleich zu den totalen SOA Konzentrationen sehr gering waren (Anteil: <1%). Jedoch hatten die marinen iSOA Konzentrationen über dem offenen Ozean einen signifikanten Einfluss auf regionaler und saisonaler Skala. Der direkte Effekt auf die Strahlungsbilanz über verschiedenen Ozeanregionen war im jährlichen Mittel kleiner 0,2 W m^{-2}. Allerdings war der Anteil am totalen aerosolinduzierten direkten Effekt auf die Strahlungsbilanz je nach Jahreszeit und Region bis zu 43% (Sommer, Nordatlantik). Der Einfluss von marinem iSOA auf den direkten Strahlungseffekt wird jedoch dadurch geschwächt, dass es bei der Bildung von marinem iSOA zur Bildung von größeren Partikeln kommt als im Vergleich zur Bildung von iSOA über Land. Die unterschiedliche Größenverteilung legt den Verdacht nahe, dass marines iSOA zum Wachstum bereits existierender Partikel und nicht zur deren intitialen Bildung beiträgt.

Auch wenn die marinen iSOA Konzentrationen auf globaler Ebene gering erscheinen, zeigt diese Arbeit, dass marine Emissionen von Isopren die Chemie in der Atmosphäre und die Strahlungsbilanz über dem offenen Ozean signifikant beeinflussen. In diesen Regionen ist der Einfluss terrestrisch gebildeten Isoprens kaum noch vorhanden, was den Einfluss lokaler Ozeanquellen von Isopren auf die Chemie in der Atmosphäre über dem Ozean verstärkt. Dies zeigt, dass ein besseres Verständnis der Produktions- und

Abbauprozesse von Isopren hilft, um die noch fehlenden Quellen und Senken im Oberflächenozean zu bestimmen. Die gewonnen Erkenntnisse helfen weiter die globale Konzentrationsverteilung von Isopren im Oberflächenozean zu berechnen, um so letztendlich den Einfluss von marinen Isoprenemissionen auf die Chemie in der Atmosphäre zu bestimmen. Die Ergebnisse dieser Arbeit zeigen, dass die Emissionsabschätzungen von marinem Isopren in globale, atmosphärische Klimamodelle integriert werden müssen, um so die SOA Konzentration und deren Einfluss in einem sich verändernden Klima abschätzen zu können.

ACKNOWLEDGEMENTS

LIST OF FIGURES

LIST OF TABLES

MANUSCRIPT OVERVIEW

This thesis is based on the following manuscripts:

1. **Dennis Booge**, Christa A. Marandino, Cathleen Schlundt, Paul I. Palmer, Michael Schlundt, Elliot L. Atlas, Astrid Bracher, Eric S. Saltzman, Douglas W. R. Wallace: **Can simple models predict large scale surface ocean isoprene concentrations?**, published in: Atmos. Chem. Phys., 16, 11807–11821, 2016, doi:10.5194/acp-16-11807-2016.

   Author contribution: Dennis Booge designed the study together with Christa A. Marandino, performed the data analysis and wrote the manuscript. Christa A. Marandino measured oceanic isoprene on board together with Cathleen Schlundt and wrote parts of the manuscript. Astrid Bracher analyzed the pigment data and Elliot L. Atlas measured isoprene concentrations in the air. Paul I. Palmer helped to validate model calculations and Michael Schlundt calculated mixed layer depths of the cruises. All authors reviewed the manuscript.

2. **Dennis Booge**, Cathleen Schlundt, Astrid Bracher, Sonja Endres, Birthe Zäncker, Christa A. Marandino: **Marine isoprene production and consumption in the mixed layer of the surface ocean – A field study over 2 oceanic regions**, accepted for publication in Biogeosciences, doi:10.5194/bg-2017-257.

   Author contribution: Dennis Booge performed the isoprene measurements on board, analyzed the isoprene data, and wrote the manuscript. Cathleen Schlundt and Christa A. Marandino performed the isoprene measurements on board. Astrid Bracher analyzed the pigment and radiation data. Sonja Endres and Birthe Zäncker performed the HPLC measurements and analyzed the bacteria data. All authors reviewed the manuscript.

3. **Dennis Booge**, Scarlet Stadtler, Christa A. Marandino: **The influence of marine isoprene emissions on secondary organic aerosol concentration over the remote ocean**, manuscript in preparation.
   Author contribution: Dennis Booge designed the study together with Christa A. Marandino, performed the isoprene data analysis and wrote the manuscript with contribution from all authors. Scarlet Stadtler performed the secondary organic aerosol model calculations.

In addition, I contributed to the following manuscripts:

4. Lennartz, S. T., Marandino, C. A., von Hobe, M., Cortes, P., Quack, B., Simo, R., **Booge, D.**, Pozzer, A., Steinhoff, T., Arevalo-Martinez, D. L., Kloss, C., Bracher, A., Röttgers, R., Atlas, E., and Krüger, K.: Direct oceanic emissions unlikely to account for the missing source of atmospheric carbonyl sulfide, published in: Atmos. Chem. Phys., 17, 385-402, 2017, doi:10.5194/acp-17-385-2017, 2017.

5. Alex Zavarsky, **Dennis Booge**, Alina Fiehn, Kirstin Krüger, Elliot Atlas and Christa Marandino: The influence of air-sea fluxes on atmospheric aerosols during the summer monsoon over the tropical Indian Ocean, published in Geophys. Res. Lett., 45, doi:10.1002/2017GL076410, 2017.

6. Lennartz, S. T., Marandino, C. A., von Hobe, M., Fischer, T., Bittig, H., **Booge, D.**, Goncalves Araujo, R., Ksionzek, K., Koch, B. P., Bracher, A., Röttgers, R., Quack, B.: Production and Consumption processes of OCS and CS_2 in the Eastern Tropical South Pacific, manuscript in preparation for J. Geophys. Res .

CONTENTS

1 INTRODUCTION

Aerosols influence the radiative balance of our Earth's system directly through absorption and scattering of solar radiation, or indirectly, through formation of cloud condensation nuclei (IPCC, 2013). They have a negative radiative forcing potential and, therefore, counteract the warming potential of greenhouse gases (Figure 1.1a). Aerosols are either emitted directly (primary aerosols) from natural (e.g. volcanic eruption, sea spray) or anthropogenic sources (e.g. combustion process) or are formed in the atmosphere (secondary aerosols) by gas-particle processes through heterogeneous or multiphase chemical reactions (e.g. sulfates, nitrates, organic compounds). Organic aerosol (OA) represents the dominant component of global aerosol (KANAKIDOU et al., 2005) and is divided similarly into primary OA (POA) and secondary OA (SOA). SOA is formed by volatile organic compounds (VOC), which act as precursor gases in the atmosphere (PANDIS et al., 1992). Globally, 90% of SOA is due to biogenic emissions of VOCs (KANAKIDOU et al., 2005). However, in the northern hemisphere, anthropogenic sources are suggested to be equally important (DE GOUW and JIMENEZ, 2009; LIN et al., 2012) (Figure 1.1b).
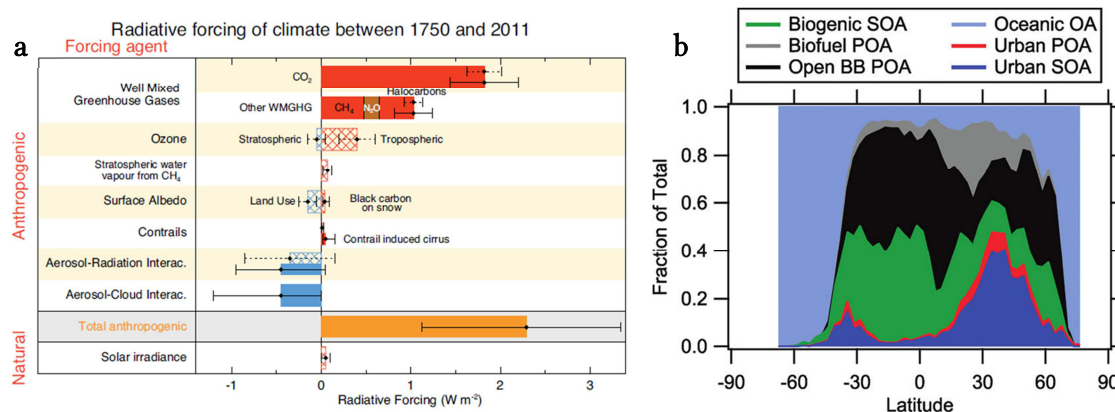
Figure 1.1: Different components of the climate system showing their radiative forcing (a) and mean zonal proportion of organic aerosol sources (b). (a) Globally averaged radiative forcing for the period 1750-2011 with uncertainties (5 to 95% confidence range) from IPCC (2013). (b) Estimated zonal mean distribution of different SOA and POA sources as fraction of total organic aerosol from DE GOUW and JIMENEZ (2009). BB: biomass burning. Note: no differentiation of primary and secondary derived marine OA.

One of the biogenic VOCs is isoprene (2-methyl-1,3-butadiene), which has received the most attention in recent years concerning its terrestrial importance for SOA for-

mation (CARLTON et al., 2009). Once emitted to the atmosphere, isoprene is highly reactive and influences more than SOA formation. Through reaction with OH, isoprene oxidation affects the lifetime of the greenhouse gas methane (COLLINS et al., 2002). Additionally, isoprene oxidation products can increase tropospheric ozone levels during high nitrogen oxides (NO_x) levels (HOFZUMAHAUS et al., 2009). On the other hand, during low NO_x levels, isoprene directly reacts with ozone, decreasing atmospheric ozone levels (ATKINSON and AREY, 2003).

Isoprene has the highest global emission estimate of all biogenic VOCs with flux estimates of 410 - 600 Tg C yr^{-1} (ARNETH et al., 2008). Terrestrial emissions from plants are dominant and only a minor amount (~1 Tg C yr^{-1}) is attributed to marine emissions (SHAW et al., 2010 and references therein). The contribution of marine-derived SOA to the total global SOA budget is highly discussed (MESKHIDZE and NENES, 2006). It appears relatively small on a global basis (GANTT et al., 2010) but could be up to 100% over the Southern Ocean (DE GOUW and JIMENEZ, 2009).

Determination and prediction of aerosol production and its radiative forcing potential in models is an important research topic in atmospheric chemistry and climate change research. However, there are large uncertainties in global models trying to estimate the current and future influence of aerosols on the radiative balance of the Earth's system. A part of these uncertainties can be reduced by fully understanding the formation of SOA through isoprene oxidation. Particularly, the understanding of the composition and formation of marine SOA is limited and needs further research to quantify the influence of oceanic isoprene emissions on atmospheric SOA formation. In the following sections the current knowledge of the formation of isoprene, its marine and terrestrial source, and its emissions to the atmosphere will be discussed. Furthermore, an overview of the mechanistic understanding of atmospheric isoprene oxidation to SOA formation will be given.

1.1 Terrestrial isoprene

1.1.1 Production

The emission of isoprene by plants was discovered 60 years ago (SANADZE, 1957) and was firstly quantified using mass spectrometry by SANADZE (1969) and RASMUSSEN (1970). Isoprene is synthesized in chloroplasts of plants from the precursor dimethylallyl pyrophosphate (DMAPP) using the enzyme isoprene synthase (SILVER and FALL, 1991). DMAPP is produced by the 2-methylerythritol 4-phosphate (MEP) pathway starting with the reaction of pyruvate and glyceraldehyde 3-phosphate (ROHMER et al., 1993). Figure 1.2 shows the MEP pathway, including the energetic costs. SHARKEY and SINGSAAS (1995) MILNE et al. (1995) MILNE et al. (1995) To date, it is still unclear if isopentenyl pyrophosphate (IPP) is produced first, which then can be isomerized to DMAPP, or if DMAPP is formed directly. Monoterpenes and carotenoids can also be formed via the
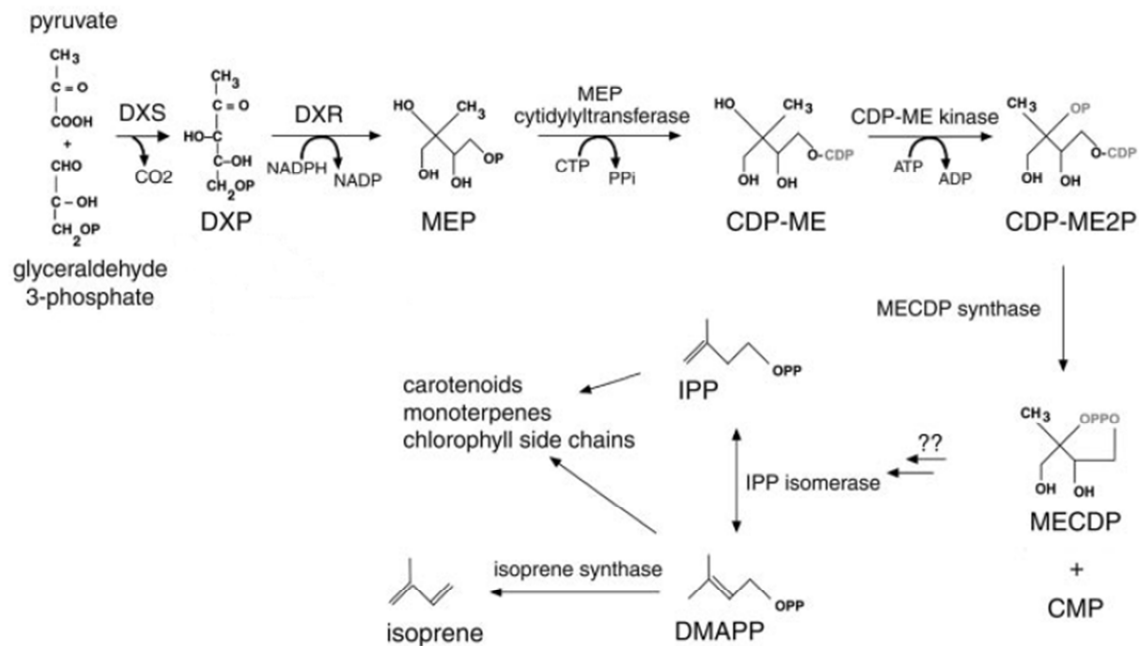
Figure 1.2: The MEP pathway. CDP-ME, 4-(cytidine 5'-diphospho)-2-C-methyl-D-erythritol; CDP-ME2P, 2-phospho-4-(cytidine 5'-diphospho)-2-C-methyl-D-erythritol; DMAPP, dimethylallyl pyrophosphate; DXR, deoxyxylulose-5-phosphate reductoisomerase; DXS, deoxyxylulose-5-phosphate synthase; IPP, isopentenyl pyrophosphate; MECDP, 2-C-methyl-D-erythritol 2,4-cyclodiphosphate. Modified from SHARKEY and YEH (2001).

MEP pathway. Plants that do not have the enzyme isoprene synthase are not able to produce and emit isoprene. The MEP pathway costs 6 carbon atoms, 20 adenosine triphosphates (ATP), and 14 nicotinamide adenine dinucleotide phosphates (NADPH) to produce isoprene. The benefits plants derive from isoprene emissions are highly debated, because some plants do emit isoprene whereas others do not (SHARKEY and YEH, 2001). The most discussed advantage plants may gain from producing isoprene is thermotolerance (Figure 1.3a), which was first observed by SHARKEY and SINGSAAS (1995). This protection against heat stress involves the protection from direct solar radiation resulting in heat or sunflecks (SHARKEY et al., 2008). Leaves at the top of a canopy, which are exposed to higher light levels than those at the bottom, emit up to four times more isoprene (HARLEY et al., 1996). The light dependence of isoprene emission in plants is well known and emissions increase with increasing light intensity (Figure 1.3b). Isoprene may also serve as antioxidant because it rapidly reacts with ozone or other reactive oxygen species (STOKES et al., 1998). Atmospheric CO_2 levels are also thought to influence isoprene emissions, but there are contradicting results. Some studies suggest that isoprene emissions are inhibited at high CO_2 levels (TINGEY et al., 1981), whereas other studies suggest that isoprene emissions are enhanced, which may also be plant dependent (SHARKEY et al., 1991).
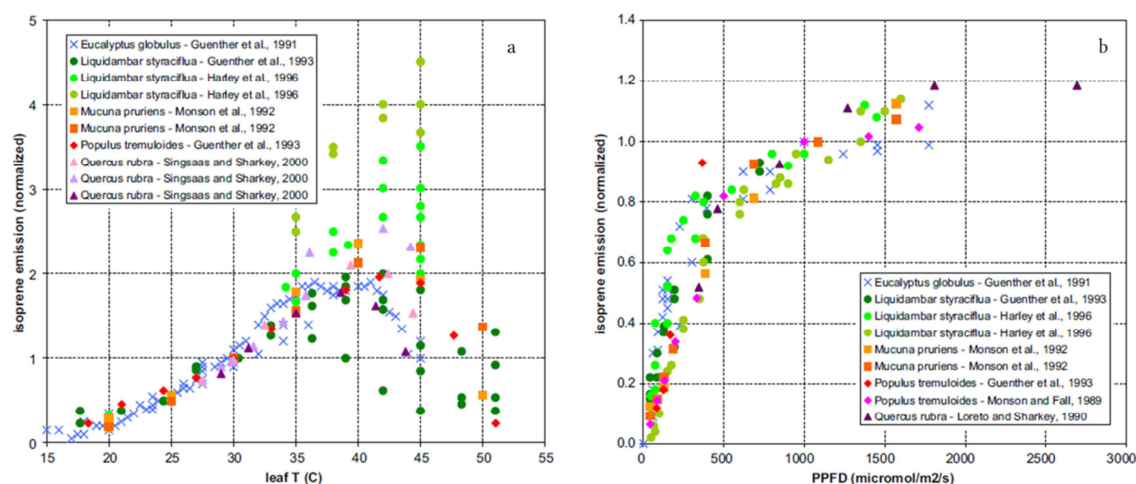
Figure 1.3: Response of isoprene emission to temperature (a) and light (b) from PACIFICO et al. (2009). PPFD: Photosynthetic photon flux density in μmol m^{-2} s^{-1}, T: temperature in °C.

1.1.2 Spatial distribution

Figure 1.4 shows monthly mean spatial distributions of terrestrial isoprene emissions using a terrestrial ecosystem emission model (MEGAN, GUENTHER et al., 2012). The global mean annual isoprene emission estimate over the period of 1980-2010 is 594 ± 34 Tg (SINDELAROVA et al., 2014), which is comparable to other global isoprene emission estimates ranging from 410 Tg yr^{-1} (MÜLLER et al., 2008) to 635 Tg yr^{-1} (POTTER et al., 2001). Although the emission estimates differ in various studies, the spatial distribution of terrestrial isoprene emissions is similar in each study. Strongest isoprene emissions can be seen in tropical and south-tropical regions, driven by high temperatures and incoming solar radiation. Northern and southern tropics account for 88% of total terrestrial isoprene emissions. The strength of isoprene emissions is shifted towards to the southern hemisphere during austral summer (Figure 1.4a) and to the northern hemisphere during boreal summer (Figure 1.4b).
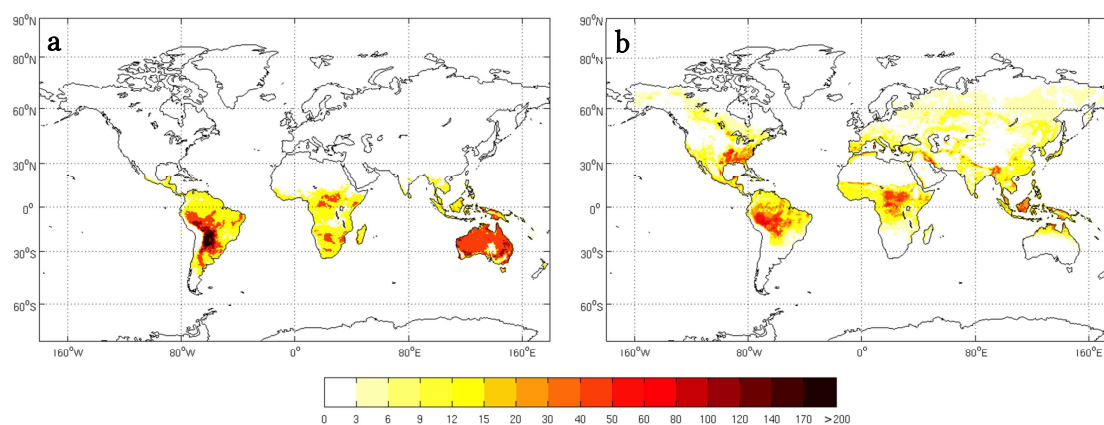
Figure 1.4: Modeled spatial distribution of monthly mean isoprene emissions in mg m^{-2} day^{-1} for (a) January and (b) July averaged over the period 1980-2010 from SINDELAROVA et al. (2014).

1.2　　Marine isoprene

Evidence for the marine production of isoprene was found for the first time in the early 1990s by Bonsang et al. (1992). They performed isoprene measurements in the atmosphere and in the ocean. Due to the supersaturation in the water they concluded that it has to be produced in the marine environment. Furthermore, they proposed that it is produced biologically because the isoprene concentration was mainly following the fluorescence signal of their measurements when performing vertical profiles. Since then, 15 more studies of field measurements were published in order to quantify isoprene concentrations in different parts of the ocean (general range: <1 - 200 pmol L^{-1}; references: Table 1.1). Furthermore, laboratory studies under varying conditions were performed in order to investigate the influence of physical and physiological parameters on the production and consumption of isoprene in the marine environment. A state-of-the-art overview of processes driving the isoprene production and consumption is given in the following sections.

Table 1.1: Literature review of published field studies of marine isoprene concentrations in pmol L^{-1}.

Reference	Region	Month	Concentration
Bonsang et al. (1992)	Pacific Ocean, Mediterranean Sea	April, May/October	3.6 - 98
Milne et al. (1995)	Florida Straits, Gulf Stream	September	9.8 - 51
Broadgate et al. (1997)	Southern Ocean, North Sea	November	0.7 - 90
Baker et al. (2000)	Eastern Atlantic Ocean	May	5 - 55
Matsunaga et al. (2002)	Western North Pacific	May	<12 - 94
Broadgate et al. (2004)	Mace Head, Ireland	September	10 - 21
Wingenter et al. (2004)	Southern Ocean	January	mean: 1.8
Moore and Wang (2006)	Eastern North Pacific	July	2 - 6.5
Kurihara et al. (2010)	Western North Pacific	April	4 - 68
Kurihara et al. (2012)	Sagami Bay	April - December	4.4 - 10
Tran et al. (2013)	Arctic Ocean	July	mean: 26 ± 31
Kameyama et al. (2014)	Southern (Indian) Ocean	January	0.2 - 395
Zindler et al. (2014)	Eastern Atlantic Ocean	November	mean: 25.7 ± 14.7
Ooki et al. (2015)	Southern Ocean, Indian Ocean, Northwest Pacific Ocean, Bering Sea, western Arctic Ocean	September - November, November - January, April - September, October, September	basin: 1.3 - 121 slope: 1.5 - 165 shelf: 2.7 - 136

Table 1.1: continued.

Reference	Region	Month	Concentration
LI et al. (2017)	East China Sea, South Yellow Sea	July	32 - 174
HACKENBERG et al. (2017)	Atlantic Ocean, Arctic Ocean	October/November, March/July	1 - 66

1.2.1 Sources

Biological production. Oceanic isoprene concentrations mainly follow the chlorophyll *a* (chl-a) depth profile (BONSANG et al., 1992; HACKENBERG et al., 2017; MILNE et al., 1995; TRAN et al., 2013). Using different monocultures of phytoplankton functional types (PFTs) in laboratory studies, MILNE et al. (1995) could prove that isoprene is produced biologically by phytoplankton. Figure 1.5 shows a typical depth profile of isoprene, which follows the shape of the chl-a profile and the profile of some abundant PFTs. However, further studies discovered that not every PFT has the same ability to produce isoprene (SHAW et al., 2010 and references therein). Measured chl-a normalized isoprene production rates from monocultures range from 0.36 ± 0.22 µmol $(\text{g chl-a})^{-1} \text{day}^{-1}$ (species of chlorophytes; BONSANG et al., 2010) up to 32.16 ± 5.76 µmol $(\text{g chl-a})^{-1} \text{day}^{-1}$ (species of prasinophytes; EXTON et al., 2013). The strength of isoprene emissions is mainly attributed to environmental conditions like light and temperature stress (EXTON et al., 2013; MESKHIDZE et al., 2015; SHAW et al., 2003) which is similar to terrestrial isoprene emissions. Generally, isoprene production rates increase with increasing light levels and increasing temperature, but also might level off or even decrease at higher light or temperature levels. The influence of light and temperature varies already within one group of phytoplankton (MESKHIDZE et al., 2015; SRIKANTA DANI et al., 2017). These results suggest a similar physiological function of isoprene for phytoplankton in the ocean as for terrestrial plants on land.

Chemical production. An additional source for isoprene could be the reaction of photochemically excited dissolved organic matter and fatty acids in the surface microlayer (SML) of the ocean. In reactor experiments CIURARU et al. (2015) measured isoprene in the gas phase immediately after illuminating sea water containing humic acid (acts as dissolved organic matter) and nonanoic acid (surfactant). If a surfactant was not added, no isoprene emission was observed. Surfactant concentration is known to be high in the SML (WURL et al., 2011), therefore a photochemical reaction of organic matter with surfactants could be a hint of non-biological production of isoprene in the marine environment.
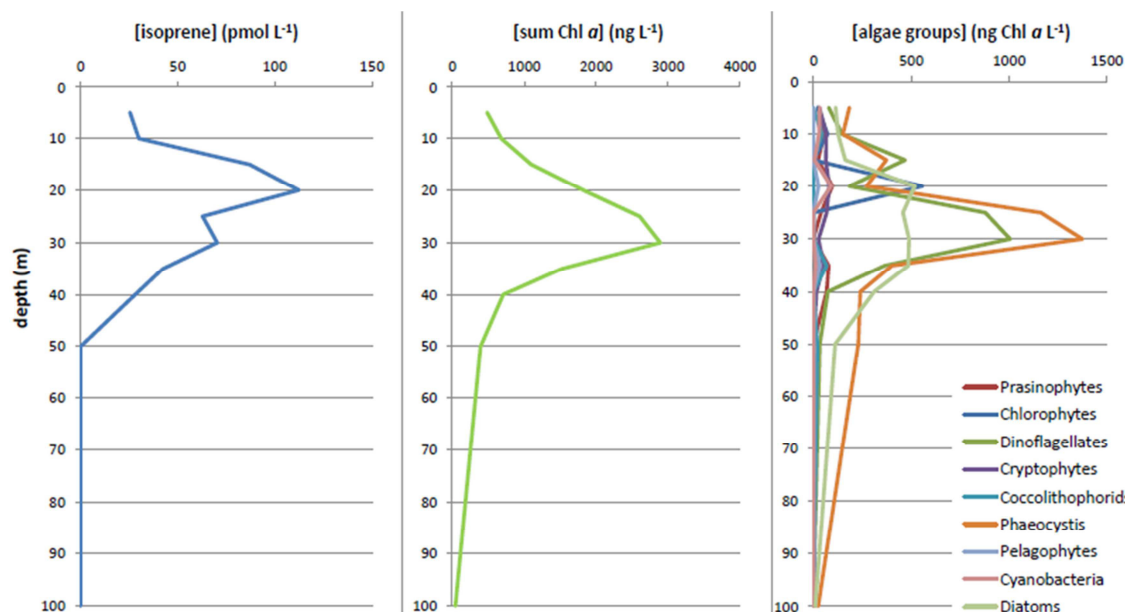
Figure 1.5: Depth profiles of isoprene (left), chl-a (middle), and different PFTs (right) in the Arctic Ocean during summer 2010 from TRAN et al. (2013).

1.2.2 Sinks

Biological consumption. Very little is known about bacterial degradation of isoprene in seawater. ACUÑA ALVAREZ et al. (2009) tested some bacteria species and could show that bacterial degradation might take place. Recently, JOHNSTON et al. (2017) identified isoprene degrading bacteria strains in estuarine and marine environments. However, these studies did not provide any isoprene loss rates and they are thought to be very small compared to the biological production (SHAW et al., 2003).

Chemical degradation. Even less is known about chemical degradation of isoprene in seawater and only assumptions were made to date. PALMER and SHAW (2005) used rates for the reaction with OH in the gas phase and for the reaction with singlet oxygen in chloroform (Figure 1.6). Scaling these rates with the oceanic concentration of each oxidant (OH=10^{-17} mol L^{-1}, singlet oxygen=10^{-14} mol L^{-1} from COOPER et al. (1988)) leads to mean isoprene loss rates <10% of the biological production rates of isoprene (PALMER and SHAW, 2005).

Air-sea gas exchange. The dominant loss of isoprene in the ocean is thought to be the gas exchange to the atmosphere. The lifetime of isoprene due to air-sea gas exchange is about seven days in the mixed layer of the ocean (PALMER and SHAW, 2005) and the loss rate is highest in the high latitudes during seasons of high wind speeds (Figure 1.6). Theoretically, air-sea gas exchange can also be a source for oceanic isoprene, but as isoprene is generally oversaturated in the surface ocean by up to three orders of magnitude (BONSANG et al., 1992; MILNE et al., 1995; WINGENTER et al., 2004), the air-sea gas exchange is a net loss for marine isoprene. The strength of isoprene emissions to the at-

mosphere depends on the concentration difference between the ocean and the atmosphere but also on parameters like wind speed and temperature. The concept of air-sea gas exchange and its driving processes are explained in section 1.3.
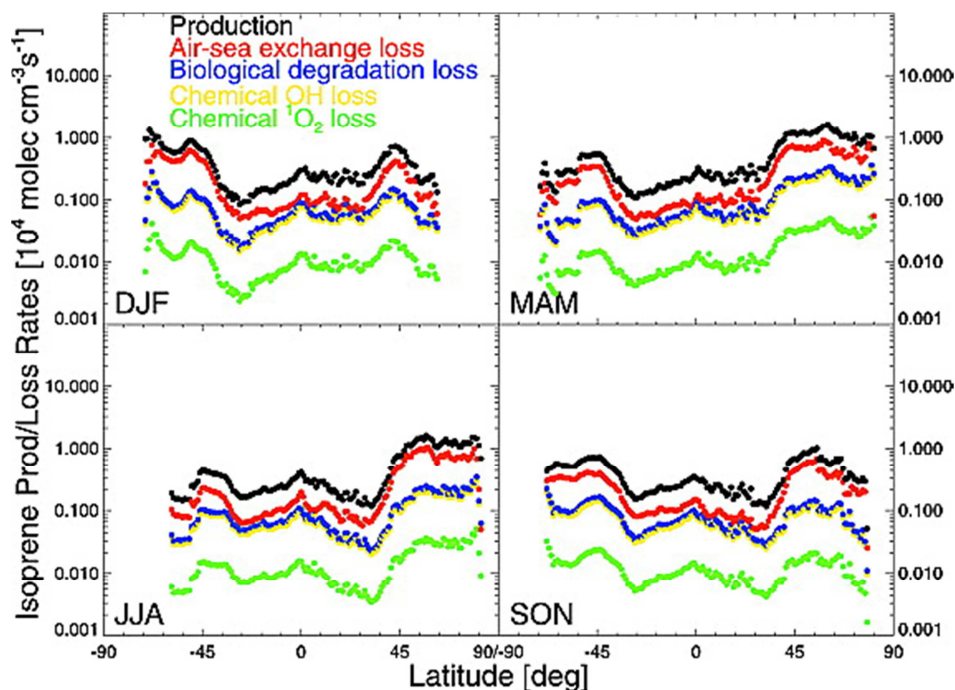
Figure 1.6: Modeled isoprene production and loss rates as a function of latitude and season using satellite data from PALMER and SHAW (2005).

1.2.3 Spatial distribution

Figure 1.7 shows the modeled monthly mean isoprene concentrations in the surface mixed layer of the ocean. PALMER and SHAW (2005) used chl-a concentrations as a proxy to parameterize surface ocean isoprene concentrations, as isoprene is produced biologically (see section 4.2.1). Therefore, surface ocean isoprene concentrations show a similar distribution pattern as the chl-a concentration distribution in the ocean with very low concentrations in the tropical ocean due to oligotrophic conditions. During boreal summer, open ocean isoprene concentrations increase in the northern hemisphere, with local hotspots of phytoplankton blooms. During austral summer, isoprene concentrations are higher in the southern hemisphere, also with local hotspots of phytoplankton blooms in the open ocean. However, surface ocean isoprene concentrations are lower, compared to the northern hemisphere summer time, because constant high wind speeds are pushing the air-sea gas exchange. Isoprene concentrations are enhanced in coastal regions, mainly due to regional and seasonal hotspots of biological activity.
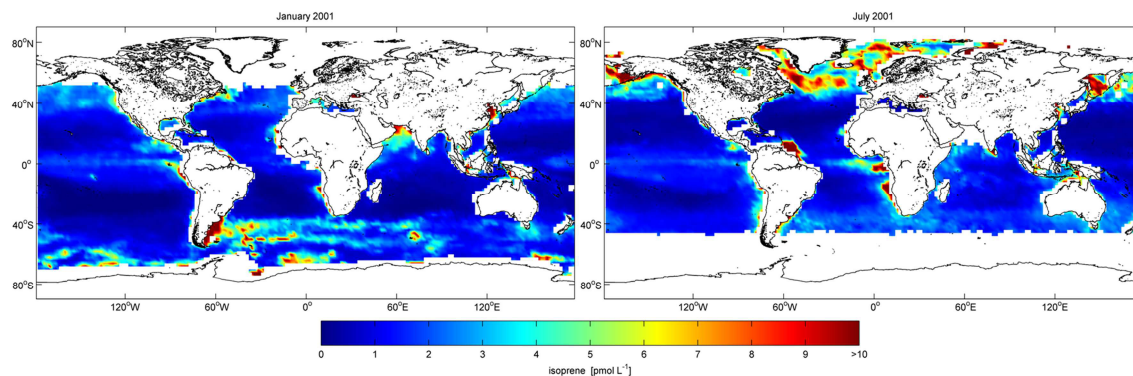
Figure 1.7: Modeled spatial distribution of monthly mean marine isoprene concentrations in the surface mixed layer in pmol L^{-1} for January 2001 (left) and July 2001 (right). Isoprene concentrations were calculated from isoprene emission estimates from PALMER and SHAW (2005).

1.3 Air-sea gas exchange

The flux across the air-sea-interface is the only source for atmospheric isoprene over the remote ocean, where the influence of terrestrially derived isoprene is negligible. The transfer (F) of a gas is controlled by the transfer velocity (k) and the concentration gradient (ΔC) between the water- (C_w) and the air-phase (C_a):

$$F = k\ \Delta C = k\ (C_w - C_a) \tag{1.1}$$

The physical and chemical properties influence the solubility of each gas in a liquid medium. Therefore the Ostwald coefficient (α) is used to correct for the solubility of each gas:

$$F = k\ (C_w - \alpha\ C_a) \tag{1.2}$$

The transfer of a gas at the interface depends on the solubility and is either controlled in the water or in the air-side and is described by the two-film model by LISS and SLATER (1974). In this conceptual model, shown in Figure 1.8a, the exchange depends on the molecular diffusion at the interface in between the turbulent layer of the air and the water. The resistance for soluble gases, like water vapor or sulfur dioxide ($\alpha \geq 100$), is air-side controlled (red line), whereas for insoluble gases like isoprene (blue line), the resistance is controlled by the aqueous-side diffusive sublayer (WANNINKHOF et al., 2009).

The transfer velocity (k) describes the kinetic force controlling the gas transfer. Many processes influence the transfer velocity and are mainly wind induced, including breaking waves and bubble entrainment (e.g. ASHER et al., 1996; ZHANG et al., 2006). Surface films (e.g. BROECKER, 1978) or rain (e.g. HO et al., 1997) also affect k. Today, different approaches are carried out in the field in order to determine k. The turbulent flux F above the interface can be directly measured using micrometeorological techniques, like the eddy covariance technique (e.g. MARANDINO et al., 2007; MCGILLIS et al., 2001). Values for k can be directly derived using equation (1.1) when both the F and ΔC are measured simultaneously. Another technique is the so called mass balance technique. The dual tracer method is one of several techniques, where the mass balance of a gas in the water is perturbed by adding a mixture of ^{3}He/SF$_6$-gas to the water (e.g. HO et al., 2006;

WANNINKHOF et al., 1993). As these gases are inert, measurements of C_w and C_a over time yield the flux F.

Measurements have shown that wind speed has a dominant effect and, therefore, is a good indicator to describe the gas transfer (e.g. BELL et al., 2013; HO et al., 2011; WANNINKHOF et al., 2009). Since LISS and MERLIVAT (1986) published the first wind speed based parameterization, different other parameterizations (e.g., quadratic, cubic) were published and are shown in Figure 1.8b. During this work three different wind speed (at 10 m height, U_{10}) based parameterizations were applied to calculate isoprene emissions:

$$k_{W92} = 0.31\ U_{10}^2 \left(\frac{S_C}{660}\right)^{-0.5},\ \text{WANNINKHOF (1992)} \tag{1.3}$$

$$k_{W99} = 0.0283\ U_{10}^3 \left(\frac{S_C}{660}\right)^{-0.5},\ \text{WANNINKHOF and MCGILLIS (1999)} \tag{1.4}$$

$$k_{N00} = \left(0.333\ U_{10} + 0.222\ U_{10}^2\right)\left(\frac{S_C}{660}\right)^{-0.5},\ \text{NIGHTINGALE et al. (2000)} \tag{1.5}$$

The temperature (T) dependent dimensionless Schmidt number (S_C) of isoprene, which is the ratio of the molecular diffusivity of isoprene in seawater and the kinematic viscosity of seawater, is taken from PALMER and SHAW (2005):

$$S_C = 3913.15 - 162.13T + 2.67T^2 - 0.012T^3 \tag{1.6}$$
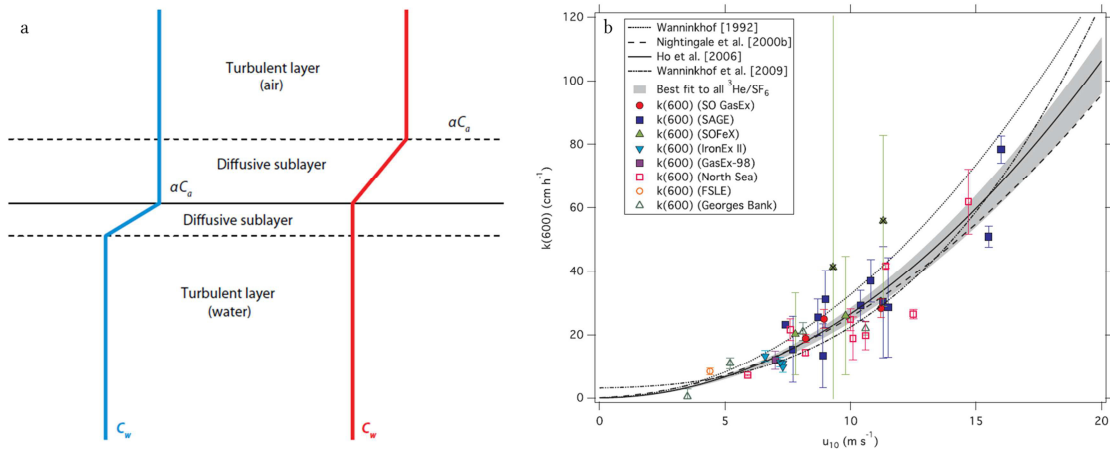
Figure 1.8: Conceptual two-film model (a) and different relationships of the transfer velocity (k) and wind speed (b). (a) Concentration profile of an insoluble gas (blue line) and a soluble gas (red line) from WANNINKHOF et al. (2009). (b) Parameterizations and results for k from ^{3}He/SF$_6$ dual tracer experiments dependent on the wind speed from HO et al. (2011).

The parameterizations are generally comparable in a wind regime <7 m s^{-1}, but the differences increase significantly at higher wind. Other factors like surface films or bubble entrainment are one hypothesis to explain the divergence in parameterizations at higher wind speeds. It is very important to reduce the uncertainties of theses parameterizations in the future, especially at high wind speeds. A better assessment of flux estimates of climate relevant gases will improve to estimate their influence on the chemistry in the atmosphere today and in a changing climate.

1.4   Isoprene in the atmosphere

1.4.1   Atmospheric distribution

Total global emissions of isoprene range from 410 to 600 Tg C yr^{-1} (ARNETH et al., 2008). Oceanic emissions of isoprene represent only a minor amount. Depending on model simulations ("bottom-up" or "top-down" approaches) global oceanic emission estimates range from 0.1 to 11.6 Tg C yr^{-1} (ARNOLD et al., 2009; GANTT et al., 2009; LUO and YU, 2010; PALMER and SHAW, 2005). Due to the short lifetime of 1 - 4 hours (SHAW et al., 2010 and references therein), mean daily atmospheric concentrations in the terrestrial boundary layer are generally <1 ppb but can be up to 11 ppb and 26 ppb during daytime over the central amazon forest and an oil palm plantation, respectively (JARDINE et al., 2016; MISZTAL et al., 2011). Isoprene concentrations in the atmosphere over the remote oceans are generally lower than 100 ppt (YOKOUCHI et al., 1999). Concentrations in the marine atmosphere are mainly influenced by light, as shown in Figure 1.9 (LIAKAKOU et al., 2007). This is due to higher emissions from phytoplankton during
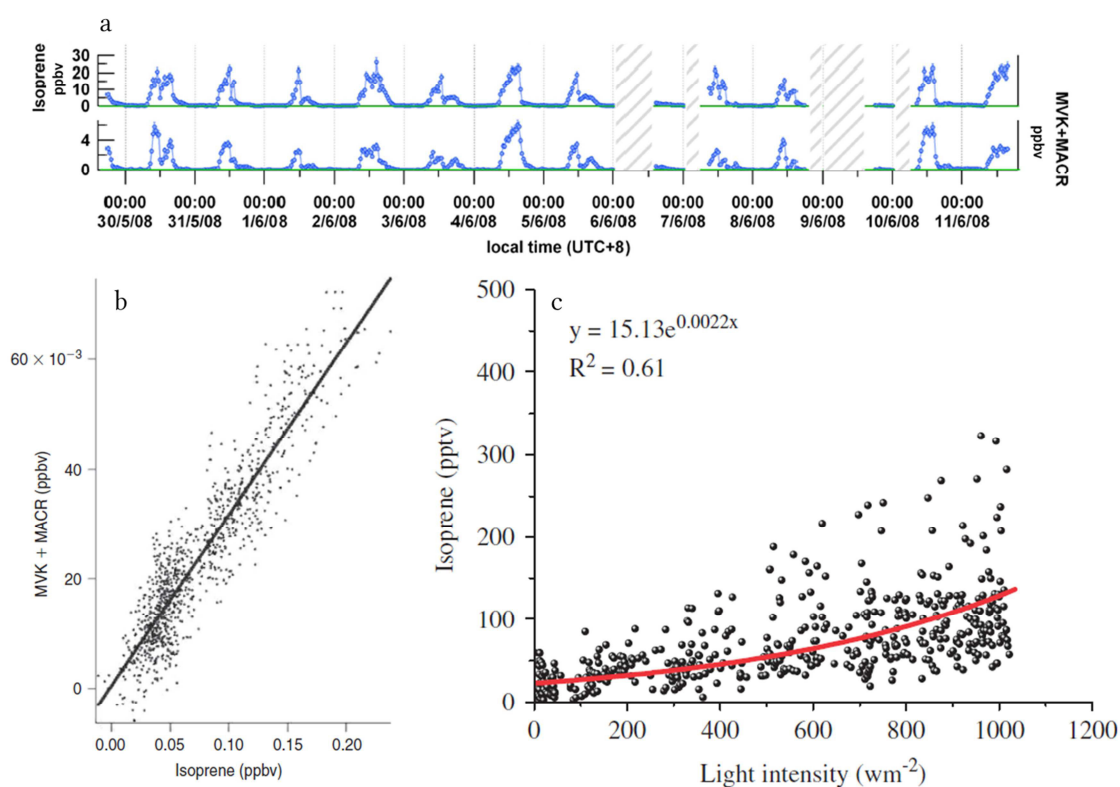
Figure 1.9: Time series of isoprene and methyl vinyl ketone+methacrolein mixing ratios (a), their correlation (b) and light dependent isoprene mixing ratio (c). (a) Time series of isoprene and MVK+MACR in ppbv over a palm oil plantation in Malaysian Borneo from MISZTAL et al. (2011). (b) Correlation of isoprene and its oxidation products MVK+MACR volume mixing ratios (r^2=0.80) in the atmosphere over the Southern Indian Austral Ocean from COLOMB et al. (2009). (c) Atmospheric isoprene mixing ratios in ppbv from unpolluted marine air dependent on light intensity (W m^{-2}) from a coastal site on the island of Crete in the East Mediterranean from LIAKAKOU et al. (2007).

daytime, which is similar to emissions from plants. LEWIS et al. (1997) measured a diel cycle of isoprene concentrations in marine influenced atmosphere at a coastal station in Mace Head, Ireland. The diel cycle was similar to the variation in concentration from terrestrial influenced air with the highest concentrations during 12 pm and 2 pm.

The spatial and seasonal distribution in the terrestrial atmosphere is similar to the terrestrial emission distributions of isoprene (Figure 1.4), as transport of atmospheric isoprene is of minor importance due to the short lifetime. Generally, the same is true for isoprene in the marine boundary layer. Atmospheric concentrations over the North Atlantic (during boreal winter) and the Southern Ocean (throughout the whole year) are comparatively higher than marine concentrations due to strong winds driving the isoprene gas exchange from the ocean to the atmosphere.

1.4.2 Atmospheric reactions

Once emitted to the atmosphere isoprene is highly reactive, due to the two double bonds, and influences the oxidative capacity of the atmosphere (CARLTON et al., 2009). The short lifetime of isoprene is mainly dependent on the atmospheric reactions with hydroxyl radicals (OH), nitrate (NO_3), and ozone (O_3). The rate constant (at 298 K) for the reaction of isoprene with OH is highest (1.0×10^{-11} cm^3 $molecule^{-1}$ s^{-1}), followed by the reaction with NO_3 (6.8×10^{-13} cm^3 $molecule^{-1}$ s^{-1}) and O_3 (1.3×10^{-17} cm^3 $molecule^{-1}$ s^{-1}) (ATKINSON et al., 2006). Isoprene directly modulates the O_3 concentration (WILLIAMS et al., 2010), but also, through oxidation with OH, indirectly influences the lifetime of methane (CH_4) in the atmosphere. Isoprene oxidation via OH is the most important reaction and will be discussed, with regard to SOA formation, in section 1.4.3.

Figure 1.10 shows a mechanistic overview of the isoprene reaction pathway initiated by O_3. Isoprene reacts with O_3 to form primary ozonides which react to carbonyl oxides (ZHANG and ZHANG, 2002). These so-called Criegee intermediates either stabilize or undergo unimolecular reactions to form dioxiranes followed by the formation of organic acids and methacrolein (MACR) or methyl vinyl ketone (MVK) (APLINCOURT and RUIZ-LÓPEZ, 2000). MACR and MVK are intermediates of the SOA formation pathway and are further discussed in section 1.4.3. However, Criegee intermediates can also form OH radicals due to collisional deactivation (OH yield: 0.25) (ATKINSON et al., 2006). The formed OH radicals, in turn, directly impact the formation or loss of O_3. In the remote clean atmosphere over the open ocean (low NO_x level) the O_3 loss rate is almost constant and independent of the NO_x concentration. However, the production rate of O_3 increases with increasing NO_x concentration leading to a threshold value of NO_x concentration of ~60 pptv, where production and loss rate of O_3 are balanced (LIU et al., 1992). Higher concentrations of NO_x lead to O_3 production, lower concentrations lead to O_3 destruction. Thus, during low NO_x conditions isoprene strengthens the O_3 depletion, during elevated NO_x conditions isoprene counteracts the O_3 production by reacting with O_3.
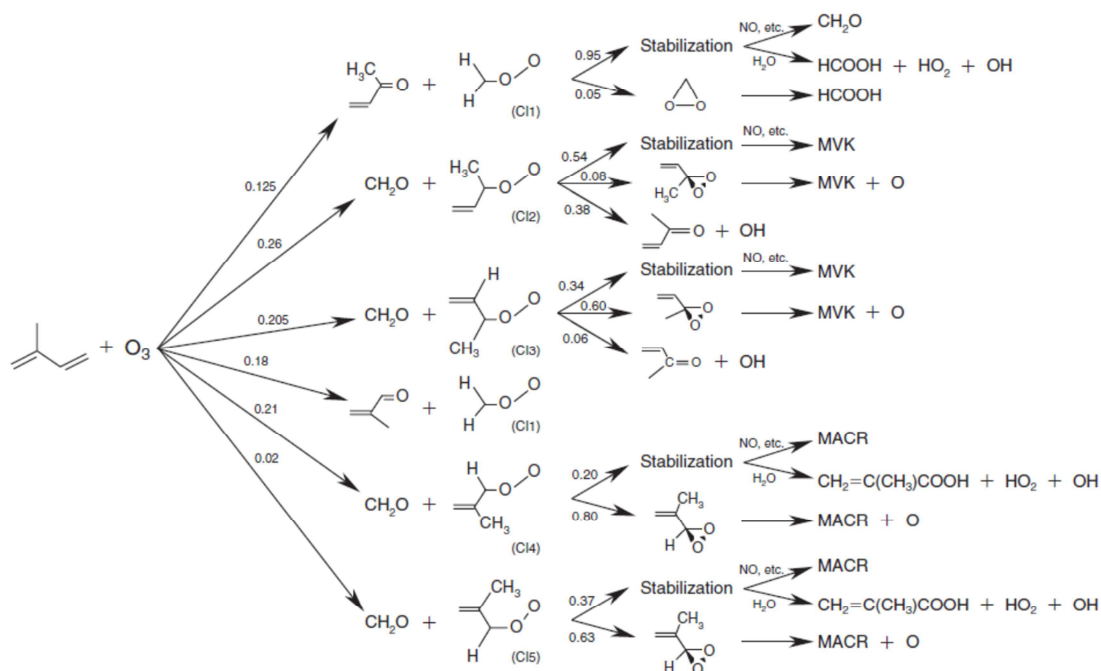
Figure 1.10: Mechanistic overview of the O_3 initiated reaction pathways of isoprenefrom FAN and ZHANG (2004). MVK: methyl vinyl ketone, MACR: methacrolein.

The reaction of isoprene with NO_3 is only important during the night, as OH concentrations decrease and NO_3 is not degraded photochemically to NO_2 and NO. Additionally, NO_3 concentrations over the remote oceans are low compared to concentrations over polluted terrestrial regions, due to low precursor (NO_x) concentrations. Isoprene oxidation via NO_3 is less understood, but may be similar to the initial OH oxidation step (FAN and ZHANG, 2004). The main products are organic nitrates, which act as a sink for NO_x and therefore indirectly influence the ozone level (HOROWITZ et al., 2007). MVK and MACR are also formed but in low yields (KWOK et al., 1996). Therefore, isoprene oxidation via NO_3 does not significantly contribute to SOA formation and will not be discussed in the next section.

1.4.3 SOA formation

General mechanism. Reaction with OH is the dominant loss for isoprene in the atmosphere (HENZE and SEINFELD, 2006) and the mechanism of OH initiated isoprene oxidation has received most study (Figure 1.11 shows as a simplified mechanism). Key products of the first generation oxidation with OH are MACR or MVK, which are still volatile. Measurements from a palm oil plantation (MISZTAL et al., 2011), as well as measurements of isoprene over the ocean (COLOMB et al., 2009), demonstrate the direct link between isoprene and its oxidation products MVK and MACR (Figure 1.9a, b). Those first generation products need to be further oxidized (second generation products) to semi volatile products with a low vapor pressure in order to contribute to SOA by partitioning into the particle phase or, in case of water-soluble intermediate products like glyoxal, through photooxidation in the aqueous-phase. During laboratory studies, meas-

urable, semi-volatile hygroscopic products, like methyl tetrols, are common indicators for the formation of SOA from isoprene oxidation (EDNEY et al., 2005). They contribute to particle growth or act as cloud condensation nuclei (CLAEYS et al., 2004b).

The reaction mechanism of isoprene oxidation with O_3 (Figure 1.10) is different than the OH pathway, but also leads to volatile intermediates like MACR and MVK (KAMENS et al., 1982). The isoprene oxidation with O_3 also initiates a peroxide-OH radical cycle (WANG et al., 2012), which in turn enhances the formation of SOA by organic compounds (CARLTON et al., 2006). Additionally, these highly-soluble peroxides increase the particle-phase acidity, which favors SOA formation from isoprene oxidation (SURRATT et al., 2007). However, the SOA yield from ozonolysis of isoprene is minor, compared to the oxidation via OH (KLEINDIENST et al., 2007).
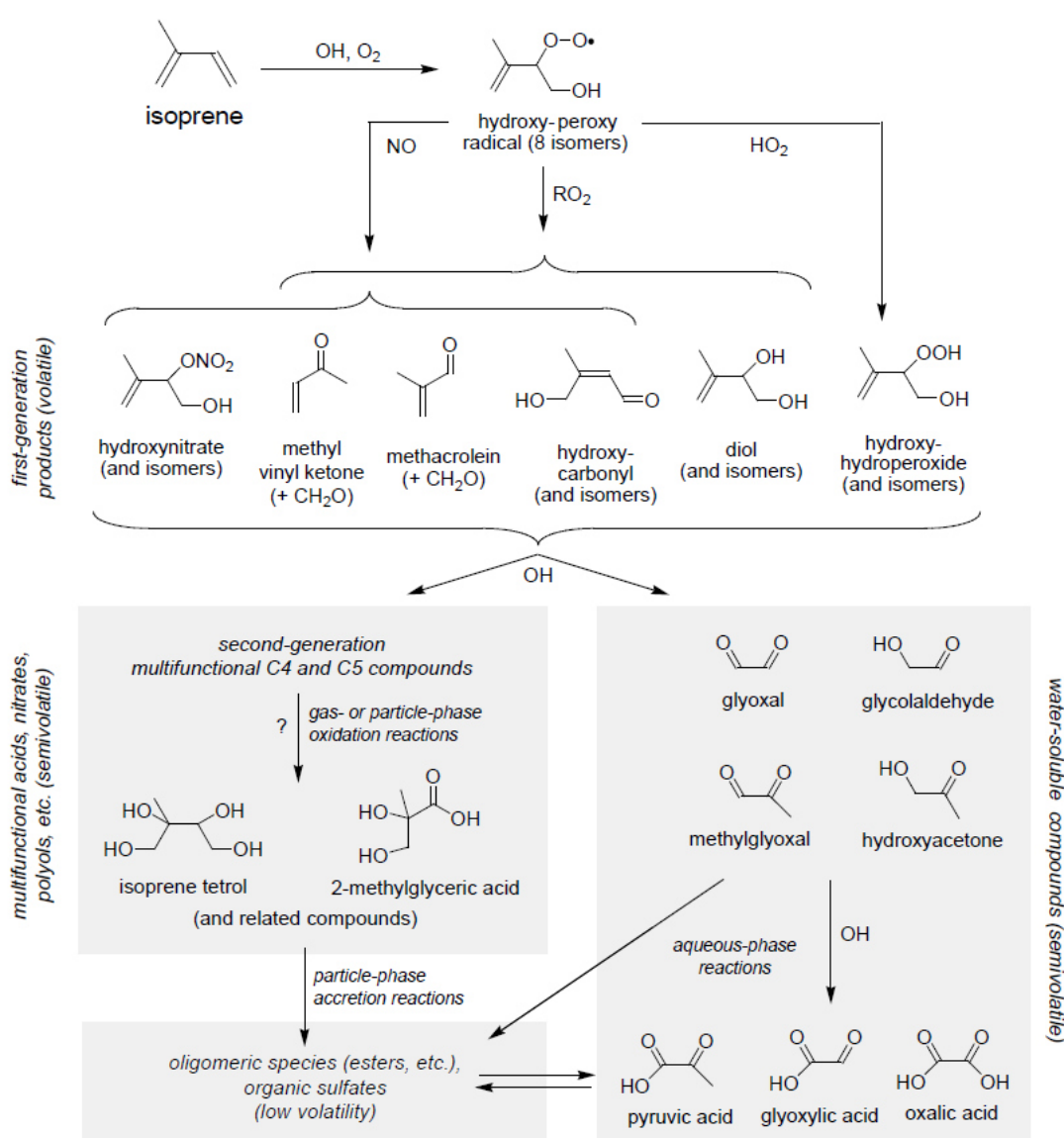
Figure 1.11: Simplified overview of OH initiated pathway of isoprene oxidation leading to SOA (e.g. isoprene tetrol, 2-methylglyceric acid) from CARLTON et al. (2009).

Environmental controls. Although field and laboratory studies demonstrate the contribution of isoprene to SOA formation, the strength is still unclear. Chamber experiments performed under different atmospheric conditions suggest that SOA yields are highly sensitive to environmental conditions. As the main oxidant, OH concentration controls the extent and the rate of the reaction (CARLTON et al., 2009). However, concentrations of NO_3 become more important during night, because OH concentrations decrease and NO_3 reacts rapidly with unsaturated alkenes as isoprene (ATKINSON and AREY, 2003). NO_3 concentrations are controlled by O_3 and NO_x levels. OH concentrations are also influenced by the NO_x level, which makes it complicated to determine the dependence of SOA formation solely on OH concentration (KROLL et al., 2006). Additionally, NO_x levels influence the yield of first-generation products of the isoprene oxidation with OH (Figure 1.11). SOA mass yields range from <1-3% (EDNEY et al., 2005) during "high NO_x" conditions (~630 ppbv) to 24% (NG et al., 2008) during "NO_x-free" conditions or even up to 29% under "low-NO_x-acid-catalyzed" conditions (SURRATT et al., 2010), dependent on conditions in chamber simulations. The SOA yield is also dependent on the organic aerosol loading, which controls the gas-particle partitioning of the semi-volatile substances (ODUM et al., 1996).

Global yields. Global models estimate yearly isoprene SOA (iSOA) production to be in the range from 6 Tg (HENZE and SEINFELD, 2006) to 19 Tg (HEALD et al., 2008). Global iSOA production estimates contribute up to 78 % (HEALD et al., 2008) to the total SOA, dependent on the model approach. However, the influence of marine-derived SOA is still highly debated. Some model studies demonstrate, that the marine isoprene emissions are too low to control the formation of SOA over the remote oceans (ANTTILA et al., 2010; ARNOLD et al., 2009; GANTT et al., 2009; MYRIOKEFALITAKIS et al., 2010; SPRACKLEN et al., 2008). However, field derived data from HU et al. (2013) suggest that high isoprene emissions during phytoplankton blooms are important for the formation of organic aerosols.

1.5   Climate feedbacks

The publication of the CLAW-hypothesis in 1987 (CHARLSON et al., 1987), describing the climate feedback mechanism of oceanic dimethyl sulfide (DMS) emission and production of aerosol particles, received the most attention in the field of atmospheric particle formation by oceanic trace gases in the last decades. QUINN and BATES (2011) demonstrated that this link is more complex than it was proposed in the late 1980s. To date, some hypotheses about potential feedbacks on the Earth's climate are postulated, however, the complete feedback is not yet understood. Even if the strength of the influence is not yet clear, emissions of isoprene influence atmospheric SOA formation (CLAEYS et al., 2004a). SOA scatters and absorbs light, which decreases the temperature of the Earth. On the other hand, isoprene reacts with OH, which modulates the lifetime of the greenhouse gas CH_4. Therefore, an increase of isoprene emissions would increase the atmospheric CH_4 concentrations leading to an increasing temperature. Generally, increasing temperature favors isoprene production and emission, but there might also be a decrease of iso-

prene production at a certain temperature maximum. These very simple conclusions demonstrate that the climate feedback of isoprene emissions is still very unclear.

Some studies already tried to quantify future global isoprene emissions and their influence on the atmospheric chemistry in different climate scenarios. SANDERSON et al. (2003) calculated that global isoprene emissions may increase by up to 34% in 2090 due to temperature increase. Using the RCP8.5 scenario (RIAHI et al., 2007) global isoprene emissions would increase until 2100 by 69% due to future climate (PACIFICO et al., 2012). Climate change alone (e.g. temperature effect, oxidative capacity) would not significantly change the mean SOA production, but would increase the SOA burden from biogenic sources by 35% (HEALD et al., 2008). However, the influence of marine isoprene emissions in these global models is still unknown. Additionally, these feedback models have large uncertainties, indicating the need to fully understand the marine strength of isoprene emissions and their impact on the complex processes of atmospheric SOA formation.

References

Acuña Alvarez, L., Exton, D. A., Timmis, K. N., Suggett, D. J., and McGenity, T. J.: Characterization of marine isoprene-degrading communities, *Environmental Microbiology*, 11, 3280-3291, 10.1111/j.1462-2920.2009.02069.x, 2009.

Anttila, T., Langmann, B., Varghese, S., and O'Dowd, C.: Contribution of isoprene oxidation products to marine aerosol over the north-east atlantic, *Advances in Meteorology*, 10.1155/2010/482603, 2010.

Aplincourt, P., and Ruiz-López, M. F.: Theoretical investigation of reaction mechanisms for carboxylic acid formation in the atmosphere, *Journal of the American Chemical Society*, 122, 8990-8997, 10.1021/ja000731z, 2000.

Arneth, A., Monson, R. K., Schurgers, G., Niinemets, Ü., and Palmer, P. I.: Why are estimates of global terrestrial isoprene emissions so similar (and why is this not so for monoterpenes)?, *Atmos. Chem. Phys.*, 8, 4605-4620, 10.5194/acp-8-4605-2008, 2008.

Arnold, S. R., Spracklen, D. V., Williams, J., Yassaa, N., Sciare, J., Bonsang, B., Gros, V., Peeken, I., Lewis, A. C., Alvain, S., and Moulin, C.: Evaluation of the global oceanic isoprene source and its impacts on marine organic carbon aerosol, *Atmos. Chem. Phys.*, 9, 1253-1262, 10.5194/acp-9-1253-2009, 2009.

Asher, W. E., Karle, L. M., Higgins, B. J., Farley, P. J., Monahan, E. C., and Leifer, I. S.: The influence of bubble plumes on air-seawater gas transfer velocities, *Journal of Geophysical Research: Oceans*, 101, 12027-12041, 10.1029/96JC00121, 1996.

Atkinson, R., and Arey, J.: Atmospheric degradation of volatile organic compounds, *Chemical reviews*, 103, 4605-4638, 2003.

Atkinson, R., Baulch, D. L., Cox, R. A., Crowley, J. N., Hampson, R. F., Hynes, R. G., Jenkin, M. E., Rossi, M. J., Troe, J., and Subcommittee, I.: Evaluated kinetic and photochemical data for atmospheric chemistry: Volume ii – gas phase reactions of organic species, *Atmos. Chem. Phys.*, 6, 3625-4055, 10.5194/acp-6-3625-2006, 2006.

Baker, A. R., Turner, S. M., Broadgate, W. J., Thompson, A., McFiggans, G. B., Vesperini, O., Nightingale, P. D., Liss, P. S., and Jickells, T. D.: Distribution and sea-air fluxes of biogenic trace gases in the eastern atlantic ocean, *Global Biogeochemical Cycles*, 14, 871-886, Doi 10.1029/1999gb001219, 2000.

Bell, T. G., De Bruyn, W., Miller, S. D., Ward, B., Christensen, K., and Saltzman, E. S.: Air–sea dimethylsulfide (dms) gas transfer in the north atlantic: Evidence for limited interfacial gas exchange at high wind speed, *Atmos. Chem. Phys.*, 13, 11073-11087, 10.5194/acp-13-11073-2013, 2013.

BONSANG, B., POLLE, C., and LAMBERT, G.: Evidence for marine production of isoprene, *Geophysical Research Letters*, 19, 1129-1132, Doi 10.1029/92gl00083, 1992.

BONSANG, B., GROS, V., PEEKEN, I., YASSAA, N., BLUHM, K., ZOELLNER, E., SARDA-ESTEVE, R., and WILLIAMS, J.: Isoprene emission from phytoplankton monocultures: The relationship with chlorophyll-a, cell volume and carbon content, *Environmental Chemistry*, 7, 554-563, 10.1071/En09156, 2010.

BROADGATE, W. J., LISS, P. S., and PENKETT, S. A.: Seasonal emissions of isoprene and other reactive hydrocarbon gases from the ocean, *Geophysical Research Letters*, 24, 2675-2678, 10.1029/97gl02736, 1997.

BROADGATE, W. J., MALIN, G., KUPPER, F. C., THOMPSON, A., and LISS, P. S.: Isoprene and other non-methane hydrocarbons from seaweeds: A source of reactive hydrocarbons to the atmosphere, *Marine Chemistry*, 88, 61-73, 10.1016/j.marchem.2004.03.002, 2004.

BROECKER, H. C.: The influence of wind on co_2-exchange in a wind-wave tunnel, including the effect of monolayers, *J. mar. Res.*, 36, 595-610, 1978.

CARLTON, A. G., TURPIN, B. J., LIM, H.-J., ALTIERI, K. E., and SEITZINGER, S.: Link between isoprene and secondary organic aerosol (soa): Pyruvic acid oxidation yields low volatility organic acids in clouds, *Geophysical Research Letters*, 33, n/a-n/a, 10.1029/2005GL025374, 2006.

CARLTON, A. G., WIEDINMYER, C., and KROLL, J. H.: A review of secondary organic aerosol (soa) formation from isoprene, *Atmospheric Chemistry and Physics*, 9, 4987-5005, 2009.

CHARLSON, R. J., LOVELOCK, J. E., ANDREAE, M. O., and WARREN, S. G.: Oceanic phytoplankton, atmospheric sulfur, cloud albedo and climate, *Nature*, 326, 655-661, 10.1038/326655a0, 1987.

CIURARU, R., FINE, L., PINXTEREN, M. v., D'ANNA, B., HERRMANN, H., and GEORGE, C.: Unravelling new processes at interfaces: Photochemical isoprene production at the sea surface, *Environmental Science & Technology*, 49, 13199-13205, 10.1021/acs.est.5b02388, 2015.

CLAEYS, M., GRAHAM, B., VAS, G., WANG, W., VERMEYLEN, R., PASHYNSKA, V., CAFMEYER, J., GUYON, P., ANDREAE, M. O., ARTAXO, P., and MAENHAUT, W.: Formation of secondary organic aerosols through photooxidation of isoprene, *Science*, 303, 1173-1176, 10.1126/science.1092805, 2004a.

CLAEYS, M., WANG, W., ION, A. C., KOURTCHEV, I., GELENCSER, A., and MAENHAUT, W.: Formation of secondary organic aerosols from isoprene and its gas-phase oxidation products through reaction with hydrogen peroxide, *Atmospheric Environment*, 38, 4093-4098, 10.1016/j.atmosenv.2004.06.001, 2004b.

COLLINS, W. J., DERWENT, R. G., JOHNSON, C. E., and STEVENSON, D. S.: The oxidation of organic compounds in the troposphere and their global warming potentials, *Climatic Change*, 52, 453-479, 10.1023/a:1014221225434, 2002.

COLOMB, A., GROS, V., ALVAIN, S., SARDA-ESTEVE, R., BONSANG, B., MOULIN, C., KLÜPFEL, T., and WILLIAMS, J.: Variation of atmospheric volatile organic compounds over the southern indian ocean (3049s), *Environmental Chemistry*, 6, 70-82, http://dx.doi.org/10.1071/EN08072, 2009.

COOPER, W. J., ZIKA, R. G., PETASNE, R. G., and FISCHER, A. M.: Sunlight-induced photochemistry of humic substances in natural waters: Major reactive species, in: Aquatic humic substances, Advances in chemistry, 219, American Chemical Society, 333-362, doi:10.1021/ba-1988-0219.ch022

10.1021/ba-1988-0219.ch022.

DE GOUW, J., and JIMENEZ, J. L.: Organic aerosols in the earth's atmosphere, *Environmental Science & Technology*, 43, 7614-7618, 10.1021/es9006004, 2009.

EDNEY, E. O., KLEINDIENST, T. E., JAOUI, M., LEWANDOWSKI, M., OFFENBERG, J. H., WANG, W., and CLAEYS, M.: Formation of 2-methyl tetrols and 2-methylglyceric acid in secondary organic aerosol from laboratory irradiated isoprene/nox/so2/air mixtures and their detection in ambient pm2.5 samples collected in the eastern united states, *Atmospheric Environment*, 39, 5281-5289, https://doi.org/10.1016/j.atmosenv.2005.05.031, 2005.

EXTON, D. A., SUGGETT, D. J., MCGENITY, T. J., and STEINKE, M.: Chlorophyll-normalized isoprene production in laboratory cultures of marine microalgae and implications for global models, *Limnology and Oceanography*, 58, 1301-1311, 2013.

FAN, J., and ZHANG, R.: Atmospheric oxidation mechanism of isoprene, *Environmental Chemistry*, 1, 140-149, https://doi.org/10.1071/EN04045, 2004.

GANTT, B., MESKHIDZE, N., and KAMYKOWSKI, D.: A new physically-based quantification of marine isoprene and primary organic aerosol emissions, *Atmospheric Chemistry and Physics*, 9, 4915-4927, 10.5194/acp-9-4915-2009, 2009.

GANTT, B., MESKHIDZE, N., ZHANG, Y., and XU, J.: The effect of marine isoprene emissions on secondary organic aerosol and ozone formation in the coastal united states, *Atmospheric Environment*, 44, 115-121, 10.1016/j.atmosenv.2009.08.027, 2010.

GUENTHER, A. B., JIANG, X., HEALD, C. L., SAKULYANONTVITTAYA, T., DUHL, T., EMMONS, L. K., and WANG, X.: The model of emissions of gases and aerosols from nature version 2.1 (megan2.1): An extended and updated framework for modeling biogenic emissions, *Geoscientific Model Development*, 5, 1471-1492, 10.5194/gmd-5-1471-2012, 2012.

HACKENBERG, S. C., ANDREWS, S. J., AIRS, R., ARNOLD, S. R., BOUMAN, H. A., BREWIN, R. J. W., CHANCE, R. J., CUMMINGS, D., DALL'OLMO, G., LEWIS, A. C., MINAEIAN, J. K., REIFEL, K. M., SMALL, A., TARRAN, G. A., TILSTONE, G. H., and CARPENTER, L. J.: Potential controls of isoprene in the surface ocean, *Global Biogeochemical Cycles*, n/a-n/a, 10.1002/2016GB005531, 2017.

HARLEY, P., GUENTHER, A., and ZIMMERMAN, P.: Effects of light, temperature and canopy position on net photosynthesis and isoprene emission from sweetgum (liquidambar styraciflua) leaves, *Tree Physiology*, 16, 25-32, 1996.

HEALD, C. L., HENZE, D. K., HOROWITZ, L. W., FEDDEMA, J., LAMARQUE, J. F., GUENTHER, A., HESS, P. G., VITT, F., SEINFELD, J. H., GOLDSTEIN, A. H., and FUNG, I.: Predicted change in global secondary organic aerosol concentrations in response to future climate, emissions, and land use change, *Journal of Geophysical Research-Atmospheres*, 113, 16, 10.1029/2007jd009092, 2008.

HENZE, D. K., and SEINFELD, J. H.: Global secondary organic aerosol from isoprene oxidation, *Geophysical Research Letters*, 33, 4, Artn L09812

10.1029/2006gl025976, 2006.

HO, D. T., BLIVEN, L. F., WANNINKHOF, R., and SCHLOSSER, P.: The effect of rain on air-water gas exchange, *Tellus B*, 49, 149-158, 1997.

HO, D. T., LAW, C. S., SMITH, M. J., SCHLOSSER, P., HARVEY, M., and HILL, P.: Measurements of air-sea gas exchange at high wind speeds in the southern ocean: Implications for global parameterizations, *Geophysical Research Letters*, 33, n/a-n/a, 10.1029/2006GL026817, 2006.

HO, D. T., WANNINKHOF, R., SCHLOSSER, P., ULLMAN, D. S., HEBERT, D., and SULLIVAN, K. F.: Toward a universal relationship between wind speed and gas exchange: Gas transfer velocities measured with 3he/sf6 during the southern ocean gas exchange experiment, *Journal of Geophysical Research: Oceans*, 116, n/a-n/a, 10.1029/2010JC006854, 2011.

HOFZUMAHAUS, A., ROHRER, F., LU, K., BOHN, B., BRAUERS, T., CHANG, C.-C., FUCHS, H., HOLLAND, F., KITA, K., KONDO, Y., LI, X., LOU, S., SHAO, M., ZENG, L., WAHNER, A., and ZHANG, Y.: Amplified trace gas removal in the troposphere, *Science*, 324, 1702-1704, 10.1126/science.1164566, 2009.

HOROWITZ, L. W., FIORE, A. M., MILLY, G. P., COHEN, R. C., PERRING, A., WOOLDRIDGE, P. J., HESS, P. G., EMMONS, L. K., and LAMARQUE, J.-F.: Observational constraints on the chemistry of isoprene nitrates over the eastern united states, *Journal of Geophysical Research: Atmospheres*, 112, n/a-n/a, 10.1029/2006JD007747, 2007.

HU, Q.-H., XIE, Z.-Q., WANG, X.-M., KANG, H., HE, Q.-F., and ZHANG, P.: Secondary organic aerosols over oceans via oxidation of isoprene and monoterpenes from arctic to antarctic, *Scientific Reports*, 3, 2280, 10.1038/srep02280

http://www.nature.com/articles/srep02280#supplementary-information, 2013.

IPCC: Clouds and aerosols, in: Climate change 2013: The physical science basis. Contribution of working group i to the fifth assessment report of the intergovernmental panel on climate change, Cambridge University Press, 571-657.

JARDINE, K. J., JARDINE, A. B., SOUZA, V. F., CARNEIRO, V., CERON, J. V., GIMENEZ, B. O., SOARES, C. P., DURGANTE, F. M., HIGUCHI, N., MANZI, A. O., GONÇALVES, J. F. C., GARCIA, S., MARTIN, S. T., ZORZANELLI, R. F., PIVA, L. R., and CHAMBERS, J. Q.: Methanol and isoprene emissions from the fast growing tropical pioneer species vismia guianensis (aubl.) pers. (hypericaceae) in the central amazon forest, *Atmos. Chem. Phys.*, 16, 6441-6452, 10.5194/acp-16-6441-2016, 2016.

JOHNSTON, A., CROMBIE, A. T., EL KHAWAND, M., SIMS, L., WHITED, G. M., MCGENITY, T. J., and COLIN MURRELL, J.: Identification and characterisation of isoprene-degrading bacteria in an estuarine environment, *Environmental Microbiology*, 19, 3526-3537, 10.1111/1462-2920.13842, 2017.

KAMENS, R. M., GERY, M. W., JEFFRIES, H. E., JACKSON, M., and COLE, E. I.: Ozone–isoprene reactions: Product formation and aerosol potential, *International Journal of Chemical Kinetics*, 14, 955-975, 10.1002/kin.550140902, 1982.

KAMEYAMA, S., YOSHIDA, S., TANIMOTO, H., INOMATA, S., SUZUKI, K., and YOSHIKAWA-INOUE, H.: High-resolution observations of dissolved isoprene in surface seawater in the southern ocean during austral summer 2010-2011, *Journal of Oceanography*, 70, 225-239, 10.1007/s10872-014-0226-8, 2014.

KANAKIDOU, M., SEINFELD, J. H., PANDIS, S. N., BARNES, I., DENTENER, F. J., FACCHINI, M. C., VAN DINGENEN, R., ERVENS, B., NENES, A., NIELSEN, C. J., SWIETLICKI, E., PUTAUD, J. P., BALKANSKI, Y., FUZZI, S., HORTH, J., MOORTGAT, G. K., WINTERHALTER, R., MYHRE, C. E. L., TSIGARIDIS, K., VIGNATI, E., STEPHANOU, E. G., and WILSON, J.: Organic aerosol and global climate modelling: A review, *Atmos. Chem. Phys.*, 5, 1053-1123, 10.5194/acp-5-1053-2005, 2005.

KLEINDIENST, T. E., LEWANDOWSKI, M., OFFENBERG, J. H., JAOUI, M., and EDNEY, E. O.: Ozone-isoprene reaction: Re-examination of the formation of secondary organic aerosol, *Geophysical Research Letters*, 34, n/a-n/a, 10.1029/2006GL027485, 2007.

KROLL, J. H., NG, N. L., MURPHY, S. M., FLAGAN, R. C., and SEINFELD, J. H.: Secondary organic aerosol formation from isoprene photooxidation, *Environmental Science & Technology*, 40, 1869-1877, 10.1021/es0524301, 2006.

KURIHARA, M., ISEDA, M., IORIYA, T., HORIMOTO, N., KANDA, J., ISHIMARU, T., YAMAGUCHI, Y., and HASHIMOTO, S.: Brominated methane compounds and isoprene in surface seawater of sagami bay: Concentrations, fluxes, and relationships with phytoplankton assemblages, *Marine Chemistry*, 134–135, 71-79, http://dx.doi.org/10.1016/j.marchem.2012.04.001, 2012.

KURIHARA, M. K., KIMURA, M., IWAMOTO, Y., NARITA, Y., OOKI, A., EUM, Y. J., TSUDA, A., SUZUKI, K., TANI, Y., YOKOUCHI, Y., UEMATSU, M., and HASHIMOTO, S.: Distributions of short-lived iodocarbons and biogenic trace gases in the open ocean and atmosphere in the western north pacific, *Marine Chemistry*, 118, 156-170, http://dx.doi.org/10.1016/j.marchem.2009.12.001, 2010.

KWOK, E. S. C., ASCHMANN, S. M., AREY, J., and ATKINSON, R.: Product formation from the reaction of the no3 radical with isoprene and rate constants for the reactions of methacrolein and methyl vinyl ketone with the no3 radical, *International Journal of Chemical Kinetics*, 28, 925-934, 1996.

LEWIS, C. A., D. BARTLE, K., E. HEARD, D., B. MCQUAID, J., J. PILLING, M., and W. SEAKINS, P.: Insitu, gas chromatographic measurements of non-methane hydrocarbons and dimethyl sulfide at a remote coastal location (mace head, eire) july-august 1996, *Journal of the Chemical Society, Faraday Transactions*, 93, 2921-2927, 10.1039/A701566F, 1997.

LI, J.-L., ZHANG, H.-H., and YANG, G.-P.: Distribution and sea-to-air flux of isoprene in the east china sea and the south yellow sea during summer, *Chemosphere*, 178, 291-300, http://doi.org/10.1016/j.chemosphere.2017.03.037, 2017.

LIAKAKOU, E., VREKOUSSIS, M., BONSANG, B., DONOUSIS, C., KANAKIDOU, M., and MIHALOPOULOS, N.: Isoprene above the eastern mediterranean: Seasonal variation and contribution to the oxidation capacity of the atmosphere, *Atmospheric Environment*, 41, 1002-1010, 10.1016/j.atmosenv.2006.09.034, 2007.

LIN, G., PENNER, J. E., SILLMAN, S., TARABORRELLI, D., and LELIEVELD, J.: Global modeling of soa formation from dicarbonyls, epoxides, organic nitrates and peroxides, *Atmos. Chem. Phys.*, 12, 4743-4774, 10.5194/acp-12-4743-2012, 2012.

LISS, P. S., and SLATER, P. G.: Flux of gases across the air-sea interface, *Nature*, 247, 181-184, 1974.

LISS, P. S., and MERLIVAT, L.: Air-sea gas exchange rates: Introduction and synthesis, in: The role of air-sea exchange in geochemical cycling, edited by: Buat-Ménard, P., Springer Netherlands, Dordrecht, 113-127, 10.1007/978-94-009-4738-2_5.

LIU, S. C., TRAINER, M., CARROLL, M. A., HÜBLER, G., MONTZKA, D. D., NORTON, R. B., RIDLEY, B. A., WALEGA, J. G., ATLAS, E. L., HEIKES, B. G., HUEBERT, B. J., and WARREN, W.: A study of the photochemistry and ozone budget during the mauna loa observatory photochemistry experiment, *Journal of Geophysical Research: Atmospheres*, 97, 10463-10471, 10.1029/91JD02298, 1992.

LUO, G., and YU, F.: A numerical evaluation of global oceanic emissions of α-pinene and isoprene, *Atmos. Chem. Phys.*, 10, 2007-2015, 10.5194/acp-10-2007-2010, 2010.

Marandino, C. A., De Bruyn, W. J., Miller, S. D., and Saltzman, E. S.: Eddy correlation measurements of the air/sea flux of dimethylsulfide over the north pacific ocean, *Journal of Geophysical Research: Atmospheres*, 112, n/a-n/a, 10.1029/2006JD007293, 2007.

Matsunaga, S., Mochida, M., Saito, T., and Kawamura, K.: In situ measurement of isoprene in the marine air and surface seawater from the western north pacific, *Atmospheric Environment*, 36, 6051-6057, 10.1016/s1352-2310(02)00657-x, 2002.

McGillis, W. R., Edson, J. B., Hare, J. E., and Fairall, C. W.: Direct covariance air-sea co2 fluxes, *Journal of Geophysical Research: Oceans*, 106, 16729-16745, 10.1029/2000JC000506, 2001.

Meskhidze, N., and Nenes, A.: Phytoplankton and cloudiness in the southern ocean, *Science*, 314, 1419-1423, 10.1126/science.1131779, 2006.

Meskhidze, N., Sabolis, A., Reed, R., and Kamykowski, D.: Quantifying environmental stress-induced emissions of algal isoprene and monoterpenes using laboratory measurements, *Biogeosciences*, 12, 637-651, 10.5194/bg-12-637-2015, 2015.

Milne, P. J., Riemer, D. D., Zika, R. G., and Brand, L. E.: Measurement of vertical-distribution of isoprene in surface seawater, its chemical fate, and its emission from several phytoplankton monocultures, *Marine Chemistry*, 48, 237-244, Doi 10.1016/0304-4203(94)00059-M, 1995.

Misztal, P. K., Nemitz, E., Langford, B., Di Marco, C. F., Phillips, G. J., Hewitt, C. N., MacKenzie, A. R., Owen, S. M., Fowler, D., Heal, M. R., and Cape, J. N.: Direct ecosystem fluxes of volatile organic compounds from oil palms in south-east asia, *Atmospheric Chemistry and Physics*, 11, 8995-9017, 10.5194/acp-11-8995-2011, 2011.

Moore, R. M., and Wang, L.: The influence of iron fertilization on the fluxes of methyl halides and isoprene from ocean to atmosphere in the series experiment, *Deep-Sea Research Part Ii-Topical Studies in Oceanography*, 53, 2398-2409, 10.1016/j.dsr2.2006.05.025, 2006.

Müller, J. F., Stavrakou, T., Wallens, S., De Smedt, I., Van Roozendael, M., Potosnak, M. J., Rinne, J., Munger, B., Goldstein, A., and Guenther, A. B.: Global isoprene emissions estimated using megan, ecmwf analyses and a detailed canopy environment model, *Atmos. Chem. Phys.*, 8, 1329-1341, 10.5194/acp-8-1329-2008, 2008.

Myriokefalitakis, S., Vignati, E., Tsigaridis, K., Papadimas, C., Sciare, J., Mihalopoulos, N., Facchini, M. C., Rinaldi, M., Dentener, F. J., Ceburnis, D., Hatzianastasiou, N., O'Dowd, C. D., van Weele, M., and Kanakidou, M.: Global modeling of the oceanic source of organic aerosols, *Advances in Meteorology*, 16, 10.1155/2010/939171, 2010.

Ng, N. L., Kwan, A. J., Surratt, J. D., Chan, A. W. H., Chhabra, P. S., Sorooshian, A., Pye, H. O. T., Crounse, J. D., Wennberg, P. O., Flagan, R. C., and Seinfeld, J. H.:

Secondary organic aerosol (soa) formation from reaction of isoprene with nitrate radicals (no$_3$), *Atmos. Chem. Phys.*, 8, 4117-4140, 10.5194/acp-8-4117-2008, 2008.

NIGHTINGALE, P. D., MALIN, G., LAW, C. S., WATSON, A. J., LISS, P. S., LIDDICOAT, M. I., BOUTIN, J., and UPSTILL-GODDARD, R. C.: In situ evaluation of air-sea gas exchange parameterizations using novel conservative and volatile tracers, *Global Biogeochemical Cycles*, 14, 373-387, 10.1029/1999GB900091, 2000.

ODUM, J. R., HOFFMANN, T., BOWMAN, F., COLLINS, D., FLAGAN, R. C., and SEINFELD, J. H.: Gas/particle partitioning and secondary organic aerosol yields, *Environmental Science & Technology*, 30, 2580-2585, 10.1021/es950943+, 1996.

OOKI, A., NOMURA, D., NISHINO, S., KIKUCHI, T., and YOKOUCHI, Y.: A global-scale map of isoprene and volatile organic iodine in surface seawater of the arctic, northwest pacific, indian, and southern oceans, *Journal of Geophysical Research: Oceans*, 120, 4108-4128, 10.1002/2014JC010519, 2015.

PACIFICO, F., FOLBERTH, G. A., JONES, C. D., HARRISON, S. P., and COLLINS, W. J.: Sensitivity of biogenic isoprene emissions to past, present, and future environmental conditions and implications for atmospheric chemistry, *Journal of Geophysical Research: Atmospheres*, 117, n/a-n/a, 10.1029/2012JD018276, 2012.

PALMER, P. I., and SHAW, S. L.: Quantifying global marine isoprene fluxes using modis chlorophyll observations, *Geophysical Research Letters*, 32, 10.1029/2005gl022592, 2005.

PANDIS, S. N., HARLEY, R. A., CASS, G. R., and SEINFELD, J. H.: Secondary organic aerosol formation and transport, *Atmospheric Environment. Part A. General Topics*, 26, 2269-2282, https://doi.org/10.1016/0960-1686(92)90358-R, 1992.

POTTER, C. S., ALEXANDER, S. E., COUGHLAN, J. C., and KLOOSTER, S. A.: Modeling biogenic emissions of isoprene: Exploration of model drivers, climate control algorithms, and use of global satellite observations, *Atmospheric Environment*, 35, 6151-6165, https://doi.org/10.1016/S1352-2310(01)00390-9, 2001.

QUINN, P. K., and BATES, T. S.: The case against climate regulation via oceanic phytoplankton sulphur emissions, *Nature*, 480, 51-56, 10.1038/nature10580, 2011.

RASMUSSEN, R. A.: Isoprene: Identified as a forest-type emission to the atmosphere, *Environmental Science & Technology*, 4, 667-671, 10.1021/es60043a008, 1970.

RIAHI, K., GRÜBLER, A., and NAKICENOVIC, N.: Scenarios of long-term socio-economic and environmental development under climate stabilization, *Technological Forecasting and Social Change*, 74, 887-935, https://doi.org/10.1016/j.techfore.2006.05.026, 2007.

ROHMER, M., KNANI, M., SIMONIN, P., SUTTER, B., and SAHM, H.: Isoprenoid biosynthesis in bacteria: A novel pathway for the early steps leading to isopentenyl diphosphate, *Biochemical Journal*, 295, 517-524, 1993.

SANADZE, G.: Nature of gaseous substances from the robinia pseudoacacia leaves, *Rep Akad Nauk GruzSSR*, 19, 3, 1957.

SANADZE, G.: Light-dependent excretion of molecular isoprene, *Progress in Photosynthesis Research*, 2, 701-706, 1969.

SANDERSON, M. G., JONES, C. D., COLLINS, W. J., JOHNSON, C. E., and DERWENT, R. G.: Effect of climate change on isoprene emissions and surface ozone levels, *Geophysical Research Letters*, 30, n/a-n/a, 10.1029/2003GL017642, 2003.

SHARKEY, T. D., LORETO, F., and DELWICHE, C. F.: High-carbon dioxide and sun shade effects on isoprene emission from oak and aspen tree leaves, *Plant Cell and Environment*, 14, 333-338, 10.1111/j.1365-3040.1991.tb01509.x, 1991.

SHARKEY, T. D., and SINGSAAS, E. L.: Why plants emit isoprene, *Nature*, 374, 769-769, 10.1038/374769a0, 1995.

SHARKEY, T. D., and YEH, S.: Isoprene emission from plants, *Annual Review of Plant Physiology and Plant Molecular Biology*, 52, 407-436, 10.1146/annurev.arplant.52.1.407, 2001.

SHARKEY, T. D., WIBERLEY, A. E., and DONOHUE, A. R.: Isoprene emission from plants: Why and how, *Annals of Botany*, 101, 5-18, 10.1093/aob/mcm240, 2008.

SHAW, S. L., CHISHOLM, S. W., and PRINN, R. G.: Isoprene production by prochlorococcus, a marine cyanobacterium, and other phytoplankton, *Marine Chemistry*, 80, 227-245, http://dx.doi.org/10.1016/S0304-4203(02)00101-9, 2003.

SHAW, S. L., GANTT, B., and MESKHIDZE, N.: Production and emissions of marine isoprene and monoterpenes: A review, *Advances in Meteorology*, 10.1155/2010/408696, 2010.

SILVER, G. M., and FALL, R.: Enzymatic synthesis of isoprene from dimethylallyl diphosphate in aspen leaf extracts, *Plant Physiology*, 97, 1588-1591, 1991.

SINDELAROVA, K., GRANIER, C., BOUARAR, I., GUENTHER, A., TILMES, S., STAVRAKOU, T., MULLER, J. F., KUHN, U., STEFANI, P., and KNORR, W.: Global data set of biogenic voc emissions calculated by the megan model over the last 30 years, *Atmospheric Chemistry and Physics*, 14, 9317-9341, 10.5194/acp-14-9317-2014, 2014.

SPRACKLEN, D. V., ARNOLD, S. R., SCIARE, J., CARSLAW, K. S., and PIO, C.: Globally significant oceanic source of organic carbon aerosol, *Geophysical Research Letters*, 35, 5, 10.1029/2008gl033359, 2008.

SRIKANTA DANI, K. G., SILVA BENAVIDES, A. M., MICHELOZZI, M., PELUSO, G., TORZILLO, G., and LORETO, F.: Relationship between isoprene emission and photosynthesis in diatoms, and its implications for global marine isoprene estimates, *Marine Chemistry*, 189, 17-24, http://dx.doi.org/10.1016/j.marchem.2016.12.005, 2017.

STOKES, N. J., TERRY, G. M., and HEWITT, C. N.: The impact of ozone, isoprene and propene on antioxidant levels in two leaf classes of velvet bean (mucuna pruriens l.), *Journal of Experimental Botany*, 49, 115-123, 10.1093/jexbot/49.318.115, 1998.

SURRATT, J. D., LEWANDOWSKI, M., OFFENBERG, J. H., JAOUI, M., KLEINDIENST, T. E., EDNEY, E. O., and SEINFELD, J. H.: Effect of acidity on secondary organic aerosol formation from isoprene, *Environmental Science & Technology*, 41, 5363-5369, 10.1021/es0704176, 2007.

SURRATT, J. D., CHAN, A. W. H., EDDINGSAAS, N. C., CHAN, M. N., LOZA, C. L., KWAN, A. J., HERSEY, S. P., FLAGAN, R. C., WENNBERG, P. O., and SEINFELD, J. H.: Reactive intermediates revealed in secondary organic aerosol formation from isoprene, *Proceedings of the National Academy of Sciences of the United States of America*, 107, 6640-6645, 10.1073/pnas.0911114107, 2010.

TINGEY, D. T., EVANS, R., and GUMPERTZ, M.: Effects of environmental-conditions on isoprene emission from live oak, *Planta*, 152, 565-570, 10.1007/bf00380829, 1981.

TRAN, S., BONSANG, B., GROS, V., PEEKEN, I., SARDA-ESTEVE, R., BERNHARDT, A., and BELVISO, S.: A survey of carbon monoxide and non-methane hydrocarbons in the arctic ocean during summer 2010, *Biogeosciences*, 10, 1909-1935, 10.5194/bg-10-1909-2013, 2013.

WANG, H. L., HUANG, D., ZHANG, X., ZHAO, Y., and CHEN, Z. M.: Understanding the aqueous phase ozonolysis of isoprene: Distinct product distribution and mechanism from the gas phase reaction, *Atmos. Chem. Phys.*, 12, 7187-7198, 10.5194/acp-12-7187-2012, 2012.

WANNINKHOF, R.: Relationship between wind speed and gas exchange over the ocean, *Journal of Geophysical Research: Oceans*, 97, 7373-7382, 10.1029/92JC00188, 1992.

WANNINKHOF, R., ASHER, W., WEPPERNIG, R., CHEN, H., SCHLOSSER, P., LANGDON, C., and SAMBROTTO, R.: Gas transfer experiment on georges bank using two volatile deliberate tracers, *Journal of Geophysical Research: Oceans*, 98, 20237-20248, 10.1029/93JC01844, 1993.

WANNINKHOF, R., and MCGILLIS, W. R.: A cubic relationship between air-sea co2 exchange and wind speed, *Geophysical Research Letters*, 26, 1889-1892, 10.1029/1999gl900363, 1999.

WANNINKHOF, R., ASHER, W. E., HO, D. T., SWEENEY, C., and MCGILLIS, W. R.: Advances in quantifying air-sea gas exchange and environmental forcing, *Annual Review of Marine Science*, 1, 213-244, 10.1146/annurev.marine.010908.163742, 2009.

WILLIAMS, J., CUSTER, T., RIEDE, H., SANDER, R., JOCKEL, P., HOOR, P., POZZER, A., WONG-ZEHNPFENNIG, S., BEYGI, Z. H., FISCHER, H., GROS, V., COLOMB, A., BONSANG, B., YASSAA, N., PEEKEN, I., ATLAS, E. L., WALUDA, C. M., VAN AARDENNE, J. A., and LELIEVELD, J.: Assessing the effect of marine isoprene and ship emissions on ozone, using modelling and measurements from the south atlantic ocean, *Environmental Chemistry*, 7, 171-182, 10.1071/en09154, 2010.

WINGENTER, O. W., HAASE, K. B., STRUTTON, P., FRIEDERICH, G., MEINARDI, S., BLAKE, D. R., and ROWLAND, F. S.: Changing concentrations of co, ch4, c5h8, ch3br, ch3i, and dimethyl sulfide during the southern ocean iron enrichment experiments, *Proceedings of the National Academy of Sciences of the United States of America*, 101, 8537-8541, 10.1073/pnas.0402744101, 2004.

WURL, O., WURL, E., MILLER, L., JOHNSON, K., and VAGLE, S.: Formation and global distribution of sea-surface microlayers, *Biogeosciences*, 8, 121-135, 10.5194/bg-8-121-2011, 2011.

YOKOUCHI, Y., LI, H. J., MACHIDA, T., AOKI, S., and AKIMOTO, H.: Isoprene in the marine boundary layer (southeast asian sea, eastern indian ocean, and southern ocean): Comparison with dimethyl sulfide and bromoform, *Journal of Geophysical Research-Atmospheres*, 104, 8067-8076, 10.1029/1998jd100013, 1999.

ZHANG, D., and ZHANG, R.: Mechanism of oh formation from ozonolysis of isoprene: A quantum-chemical study, *Journal of the American Chemical Society*, 124, 2692-2703, 10.1021/ja011518l, 2002.

ZHANG, W., PERRIE, W., and VAGLE, S.: Impacts of winter storms on air-sea gas exchange, *Geophysical research letters*, 33, 2006.

ZINDLER, C., MARANDINO, C. A., BANGE, H. W., SCHÜTTE, F., and SALTZMAN, E. S.: Nutrient availability determines dimethyl sulfide and isoprene distribution in the eastern atlantic ocean, *Geophysical Research Letters*, 41, 3181-3188, 10.1002/2014GL059547, 2014.

2 THESIS OUTLINE

Once emitted to the atmosphere, isoprene affects the oxidation capacity of the atmosphere and, as a precursor for secondary organic aerosol (SOA) formation, influences the radiative balance of the Earth's system. Current global climate chemistry models use isoprene emission inventories only from terrestrial sources in order to estimate the impact of global isoprene emissions on today's atmosphere and climate. Although terrestrial isoprene emissions are known to be higher than marine isoprene emissions, terrestrially derived isoprene is not likely to influence the open ocean regions due to its short lifetime of a few hours. The strength of oceanic emissions is highly debated, because less is known about global marine isoprene distributions as measurements of marine isoprene concentrations in the world oceans are sparse. Moreover, oceanic isoprene emissions are critically controlled by surface ocean biogeochemical and physical factors, which are poorly quantified. Understanding the biogeochemical cycling and quantifying source and sink processes of isoprene are crucial to estimate global oceanic isoprene concentrations and their emissions to the atmosphere in order to answer the overarching question of this thesis:

How important are marine isoprene emissions in influencing the Earth's climate?

This thesis is based on marine isoprene measurements from three different ocean basins (eastern Atlantic Ocean, Indian Ocean, eastern Pacific Ocean) and is subdivided into the following three chapters, each one addressing sub-questions, whose answers are combined and discussed together in the conclusions with regard to the main question.

1) Can simple models predict large scale surface ocean isoprene concentrations?

Only a few measurements of surface ocean isoprene have been carried out to date. Extrapolating these measurements globally may result in large uncertainties, as isoprene concentrations and emissions vary with location and season. In this chapter an existing model, based on a steady-state assumption for production and consumption of isoprene in the oceanic mixed layer, is used to predict global surface ocean isoprene concentrations. Monthly mean remotely sensed satellite data of chlorophyll *a*, sea surface temperature, wind speed, and mixed layer depth are used to-

gether with production and consumption rates to parameterize global isoprene concentrations on a monthly basis. This model is improved and verified with surface ocean isoprene field measurements from three different ocean basins. (CHAPTER 4: MODELING MARINE ISOPRENE CONCENTRATIONS)

2) What are the in-field production and consumption rates of isoprene in the surface ocean?

Isoprene is produced biologically by phytoplankton in the surface ocean. However, published isoprene production rates for different phytoplankton functional types (PFTs) are generally determined in laboratory studies with different monocultures. In this chapter, isoprene and pigment data, as well as related field measurements (e.g. nutrients, bacteria, salinity) are used to investigate the influence of varying biogeochemical and physical conditions on isoprene production. Furthermore, in-field production rates of different PFTs are calculated for two contrasting regions: the oligotrophic open ocean and the coastal upwelling region. Finally, different loss processes of isoprene in the surface ocean are discussed. (CHAPTER 5: PRODUCTION AND CONSUMPTION OF ISOPRENE)

3) How much do marine isoprene emissions impact the formation of total iSOA?

In this chapter, marine isoprene emission inventories are implemented into a global chemistry climate model ECHAM-HAMMOZ. In this framework, the model provides a novel, explicit coupling between the sectional aerosol model HAM-SALSA and the chemistry model MOZ. It connects semi-explicit isoprene oxidation with explicit treatment of aerosol tracers in order to calculate isoprene derived SOA formation. The global influence of marine isoprene on iSOA formation is investigated using different emission estimates based on the results of chapter 4. Monthly mean emission inventories are used to assess the seasonal influence, as well as the regional marine source strengths on total iSOA formation. Additionally, the impact of marine-derived iSOA in general, as well as the influence of their particle size distribution on the total aerosol direct radiative effect is discussed. (CHAPTER 6: INFLUENCE OF MARINE ISOPRENE EMISSIONS ON SOA FORMATION)

3 MethodS

3.1 Analytical quantification of isoprene

For all oceanic isoprene measurements performed during this work, discrete water samples were taken and quantified by purge & trap - gas chromatography - mass spectrometry (P&T-GC-MS). A general set-up of the analytical system is shown in Figure 3.1. The fundamentals of the different analytical techniques as well as their application to quantify isoprene in seawater are described in the following sections.
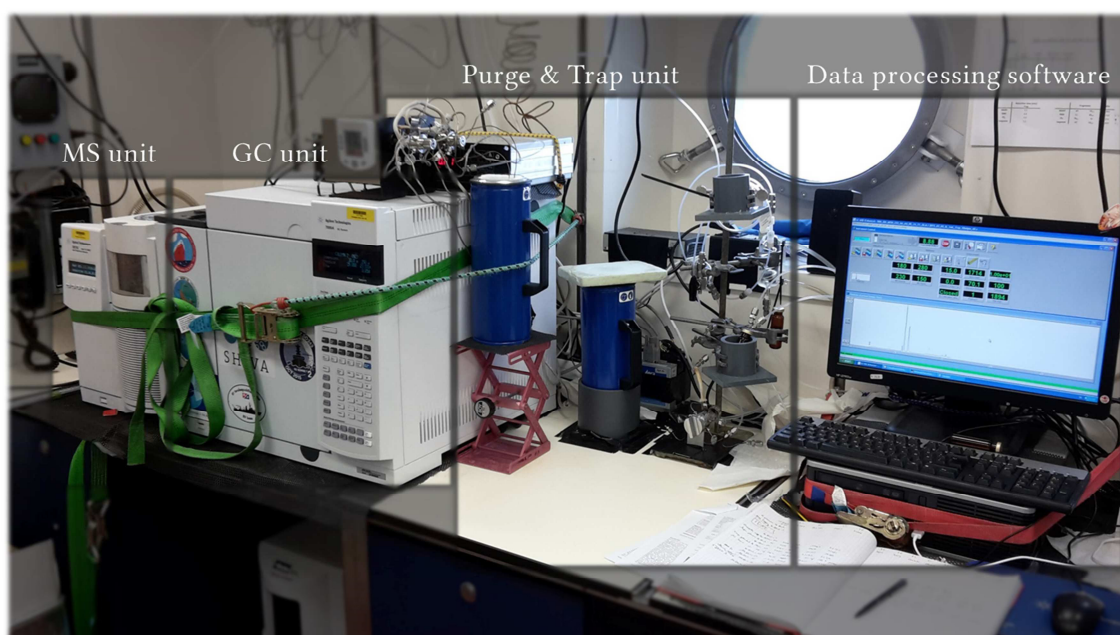
Figure 3.1: System set-up onboard R/V Sonne. MS: mass spectrometer, GC: gas chromatograph.

3.1.1 Purge & Trap technique

The P&T-technique is a common tool for separating gases from a water sample. Isoprene and other gases are swept out of a liquid sample over time using an inert gas (purge step). They are preconcentrated in an analytical trap (trap step), due to the very low concentrations of isoprene in seawater (10^{-12} -10^{-10} mol L^{-1}) and due to limits of de-

tection for many analytical systems. Details of the two steps of the P&T-technique are described below.

Purging. The seawater sample is purged with an inert gas using a needle sparger at a constant flow rate over time removing isoprene and other volatile dissolved gases from the liquid phase (Figure 3.2). Without purging, the vapor pressure of the respective gas would be the only driving force to achieve equilibrium between the water and the gas phase (headspace). The advantage of the purging method is that the partial pressure of the respective gas in the headspace above the sample can be assumed as zero. Hence, this accelerates the extraction of the gas from the water phase: The gas is stripped out. The time it takes to remove the gas from the sample depends on the physical properties of the gas itself. The solubility of a gas in water is described by the Henry's law constant, which is specific for every substance and is increasing with decreasing temperature. A comparison of properties of different gases, which were analyzed with the P&T-GC-MS set-up, is shown in Table 3.1. Also the temperature of the sample and the purge volume of the inert gas determine the time for extraction of a gas. The purge volume is the product of the purge flow rate and the purge time. A gas is extracted from the sample faster, the higher the flow rate and the higher the temperature of the sample. The purge efficiency is dependent on purge time, purge flow rate, sample volume, and sample temperature.

The purge efficiency, using helium as purge gas, was determined manually with regard to an efficient sample throughput and a sample volume which was large enough to detect isoprene at even low concentrations. A purge time of 15 min was sufficient to remove >99% of isoprene from the sample when a sample volume of 50 mL and a purge flow rate of 70 mL min^{-1} was used. The purge efficiency shown as percentage recovery (signal of first purge compared to the sum of the signals of all purge steps) depending on the purge time is shown in Figure 3.2.
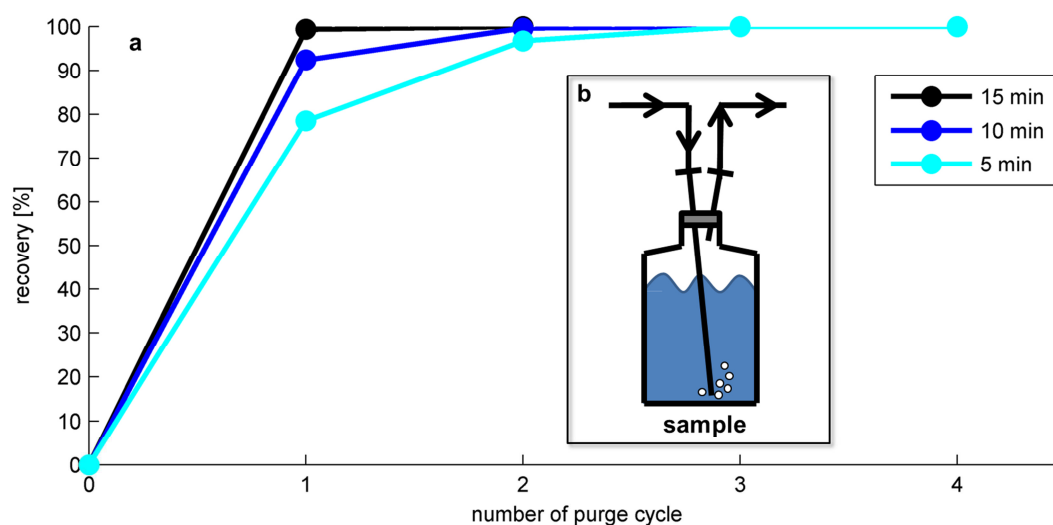
Figure 3.2: Isoprene recovery percentages of different purge times (a) and a schematic of a sample being purged (b).

Trapping. After purging, the extracted gas is trapped either in an adsorbent trap or a cryotrap. The adsorbent must be chosen depending on the properties of the gas to be trapped. A cryotrap works at temperatures which are low enough to retain the extracted gas while allowing the purge gas to flow unimpeded through the trap.

For the analysis of isoprene in this work, a cryotrap was chosen, because it is independent of the properties of different gases. The trap was a 1/16'' sulfinert stainless steel tubing in U-form, which was cooled with liquid nitrogen (liq. N₂) while trapping. Liq. N₂ has a boiling point of 77 K, retaining all compounds in the trap with a boiling point higher than 77 K. Helium, the purge gas, is not retained due to its lower boiling point (4 K). The concentrated trapped gas was quickly heated with hot water (~70°C) for injection to a GC for further analysis.

Water removal. Water vapor must be removed from the gas stream as it can freeze and could cause pressure problems by blocking the tubing. Furthermore, water vapor can reduce the lifetime of the column used in the GC. Therefore, the isoprene containing gas stream is dried, either using hygroscopic potassium carbonate (K_2CO_3) or a Nafion® membrane dryer.

During this work both drying systems were used. The desiccant K_2CO_3 dries the gas stream efficiently, but may not be suitable for all types of compounds (e.g. acidic compounds are absorbed). Also, the K_2CO_3 has to be changed after a certain amount of measurements, because the water containing solid K_2CO_3 is blocking the tubing. The Nafion® membrane dryer transfers the water vapor from the wet sample stream via a membrane (a copolymer of tetrafluoroethylene and perfluoro-3,6-dioxa-4-methyl-octene-sulfonic acid) to a counter-flowing dry gas stream. This set-up needs a constant dry gas supply when purging the sample and is also limited to compounds, as the membrane transfers gases, other than water vapor, dependent on their polarity. Both systems are suitable for isoprene. During this work, K_2CO_3 as drying agent was used first, but then replaced by a Nafion® dryer, due to easier handling.

Table 3.1: Properties and retention times of isoprene and other gases analyzed with the measurement set-up. Values of the boiling point, vapor pressure, and molar mass are from NIST (2017).

Compound	Boiling point [°C]	Vapor pressure (20°C) [10^4 Pa]	Molar mass [g mol^{-1}]	Henry constant (25°C) [mol m^{-3} Pa^{-1}]		GC method retention time [min]
Isoprene	34	6.07	68.12	3.4×10^{-4}	LENG et al. (2013)	5.2
Methanethiol	6	16.4	48.12	2.8×10^{-3}	STAUDINGER and ROBERTS (2001)	3.5
Dimethyl sulfide	38	5.27	62.13	5.3×10^{-3}	STAUDINGER and ROBERTS (2001)	4.8
Carbon disulfide	46	3.94	76.14	6.1×10^{-4}	WARNECK and WILLIAMS (2012)	4.9

3.1.2   Gas chromatography

In analytical chemistry, gas chromatography is a widely used method to separate individual compounds from a gas mixture. The gas mixture (mobile phase), carried through a column by an inert gas, interacts with a liquid stationary phase of the column. The column is located in a programmable column oven and constantly flushed with the inert carrier gas. The separation depends on the boiling point of each substance (Table 3.1) and the time of interaction of a substance with the stationary phase (difference in polarity). The lower the boiling point and the bigger the difference in polarity compared to the stationary phase (less interaction), the faster a component travels through the column. Besides the selection of an appropriate column, only the temperature program of the column oven can optimize the separation of the gas mixture. The time it takes for a component to travel through the column and being recorded as a gaussian curve (peak) is called retention time and is characteristic for each compound under identical chromatographic conditions.

During this work an Agilent 7890A GC was used. The column was a fused silica capillary column (Supel-Q^{TM} PLOT, length: 30 m, inner diameter: 0.32 mm, average thickness: 15 µm) containing divinylbenzene polymer as stationary phase. This column was suitable for C1-C4 hydrocarbons and for many sulfur gases. Helium (purity: 5.0) was used as the carrier gas and the column pressure was held constant at 15 psi (~1 bar). During the development of the method the temperature program as shown in Table 3.2 proved to be optimal for the separation of the isoprene peak (retention time: 5.2 min) from other compounds, such as sulfur gases, in a seawater sample (Figure 3.3, Table 3.1). The GC was connected to a detector for quantification of isoprene which is described in the following section.

Table 3.2: Temperature program of the used GC-method.

Rate [°C min^{-1}]	Temperature [°C]	Hold time [min]	Total run time [min]
	40	2.1	2.1
40	120	2	6.1
120	180	2.4	9
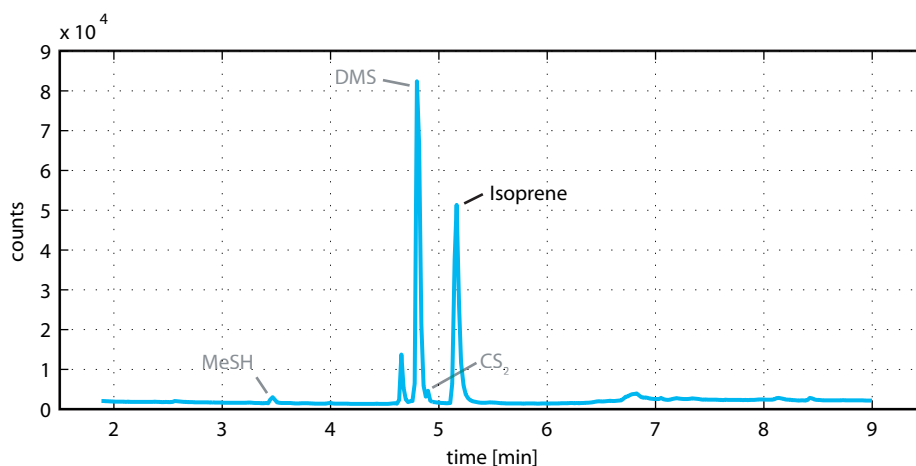
Figure 3.3: Chromatogram of a seawater sample, illustrating the separation of isoprene from other gases in the sample (retention times shown in Table 3.1). MeSH: methanethiol, DMS: dimethyl sulfide, CS$_2$: carbon disulfide.

3.1.3   Mass spectrometry

A mass spectrometer (MS) measures the molecular weight of a substance and is highly sensitive. Additionally, it can differentiate between substances with small mass differences. A GC-MS system can differentiate between compounds with the same retention times. The operation of a mass selective detector (MSD) can be split into three parts: ionization, mass separation, and mass detection. The fundamental analytical techniques on the basis of the ionization by the electron ionization method, the separation by a quadrupole mass filter, and the detection by an electron multiplier are explained in the following.

Electron ionization. The principle of this most common method is to transfer the neutral incoming molecules into positively charged ions. As shown in Figure 3.4a, an electron beam hits the incoming molecules from the GC. It interacts with the outer shell electrons of the molecules (M) forming positively charged ions (M$^{+\cdot}$):

$$M + e^- \rightarrow M^{+\cdot} + 2\,e^-$$

(3.1)

The potential difference between cathode and anode is typically set to 70 V (Figure 3.4) leading to a kinetic energy of 70 eV of the electrons. The needed energy for the abstraction of one electron is normally less than 15 eV. Hence, the excess energy destabilizes the radical cation by excitation of the vibrational and rotational energy levels, leading to fragmentation of the molecule. Every mass spectrum using a specific ionization energy is unique for a molecule. The ionization energy of 70 eV is commonly used due to a good ion yield and for a comparable mass spectra database (Nist, 2017). The mass spectrum of isoprene, using an ionization energy of 70 eV, is shown in Figure 3.4b (relative intensity vs. mass-to-charge ratio (m/z)). Fragmentation of one hydrogen atom has the highest probability (m/z=67), followed by the fragmentation of a methyl group

(m/z=53). The radical cations leave the ionization source and are focused through ion lenses and accelerated using a potential gradient towards the quadrupole.
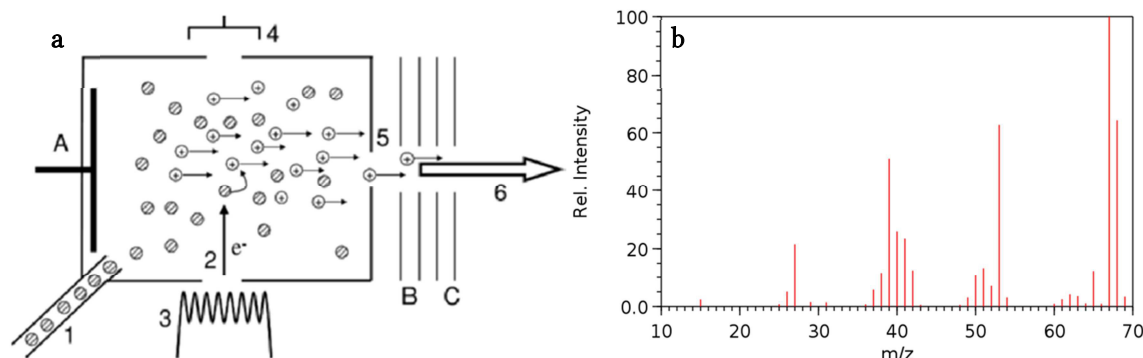
Figure 3.4: Schematic of the electron ionization chamber (a) and mass spectrum of isoprene (b). a: incoming molecules (1), electron beam of 70 eV (2), cathode (3), anode (4), outlet (5), ion beam to mass filter (6), repeller (A), acceleration potentials (B,C) from BUDZIKIEWICZ and SCHÄFER (2013). b: mass spectrum of isoprene at 70 eV (relative intensity vs. ratio of mass m to number of charges z (m/z)) taken from NIST (2017).

Quadrupole mass filter. The separation of ions of different masses is dependent on the interaction with the electric fields in the quadrupole mass filter. The quadrupole consists of four metal rods where each opposing rods are connected via an alternating current (AC) voltage V in a radio frequency (f=ω/2π) with a direct current (DC) offset voltage U establishing alternating fields with a negative and positive potential (Figure 3.5). The cations are traveling through the system and are directed to the center of the quadrupole during a positive phase and towards the rods during a negative phase. A stable flight path of the ions, and its amplitude, is dependent on the DC voltage, the frequency of the AC voltage, and the mass of the ion. Ions with a mass that have no stable flight path at a certain AC and DC voltage are diverted into one of the rods and are discharged. By varying the two voltages appropriately, only an ion with a certain m/z can travel through the system on a stable flight path and is detected by the ion collector. During a measurement the voltages can be changed in order to measure ions of different m/z within one sample. The time the system is measuring one m/z is called the dwell time. Higher dwell times result in higher sensitivity of the measurement. However, it is not possible to use the highest dwell time available, as there are finite retention times for each m/z. Typically a dwell time is chosen that yields 15-20 scans across a peak of a specific mass.

Ions

Ions

Quadrupole mass filter

Dynodes

Electron
multiplier

U + V ×cos ωt

Ion collector
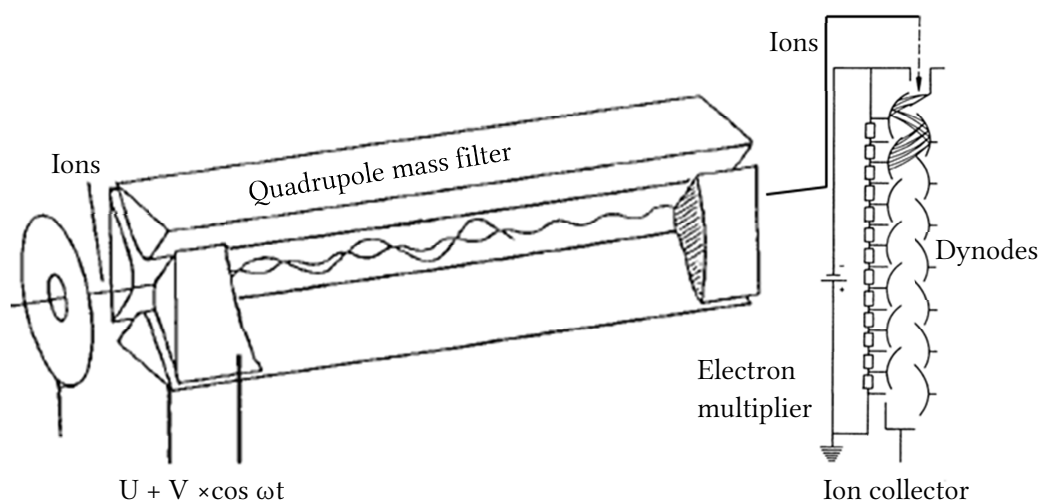
Figure 3.5: Schematic of a quadrupole mass filter modified from HÜBSCHMANN (2009) and schematic of an electron multiplier modified from SCHRÖDER (1991).

Electron multiplier. The electron multiplier is the detector of the MS. The operating principle is to amplify the signal of one ion arriving at the electron multiplier by emitting an electron cascade of secondary electrons (Figure 3.5). The ions collide with a high energy dynode which emits primary electrons. The emitted primary electrons strike a surface to emit secondary electrons. In typical electron multipliers, the electron cascades through 12 to 24 dynodes, is transferred to a signal amplifier board and is displayed as counts per time. The formation of secondary electrons depends on the surface of the dynode and the energy of the primary electron.

During this work an Agilent 5975C (inert XL MSD with triple axis detector) was used. The compounds were 1) ionized by the electron ionization method using an ionization energy of 70 eV, 2) separated by a quadrupole mass filter using a dwell time of 100 ms, and 3) detected by an electron multiplier. For analysis of the resulting chromatogram the software MSD ChemStation (Agilent Technologies) was used.

3.2   General sampling and analytical procedure

Seawater samples for isoprene measurements were taken bubble-free with a transparent glass vial (Chromatographie Handel Müller, Fridolfing, Germany). A gastight syringe (VICI Precision Sampling, Series A-2, Baton Rouge, Louisiana) was used to push 10 mL of helium (5.0, AirLiquide, Düsseldorf, Germany) into the sampling vial replacing 10 mL of seawater to supply a headspace for purging. Isoprene was completely removed from the sample (>99%, see section 3.1.1) by purging with helium at a flow rate of 70 mL min^{-1} for 15 min at room temperature (RT). The helium purge flow contained 500 µL gaseous deuterated isoprene (isoprene-d5; 98%, Polymer Source, Montreal, Canada), which was inserted within the helium flow into the sample vial from a Sulfinert® stainless steel

sample loop (1/16'' O.D., Restek, Bad Homburg, Germany) (Figure 5.2: purge unit, load position). The sample flow was dried using either K_2CO_3 (Carl Roth GmbH, Karlsruhe, Germany) or a Nafion® membrane dryer (Perma Pure, Ansyco GmbH, Karlsruhe, Germany). While using a Nafion® membrane dryer, CO_2- and hydrocarbon-free dry, pressurized air (flow: 180 mL min^{-1}) was used as counter flow. Isoprene was trapped in a Sulfinert® stainless steel trap (1/16'' O.D.) cooled with liq. N_2 (Figure 5.2: trap unit, load position). The GC-method was started after a purge time of 15 min using the software MSD ChemStation (Agilent Technologies) following the temperature program described in Table 3.2. After 0.1 min the trapped isoprene was injected into the GC by switching the 6-port valve (VICI Valco Instruments, Houston, Texas) to "load position" and changing from liq. N_2 to hot water (Figure 5.2: trap unit, load position). After 2.1 min the trap was decoupled from the GC by switching the 6-port valve back to "load position". The trap was flushed and cleaned with helium for at least one minute before a new sample was purged. The new sample was already purged while the method for the actual sample was still running which lead to a higher throughput and less storage time for each sample.

The MS was operated in selected ion mode (SIM) by quantifying isoprene and isoprene-d5 using m/z-ratios of 68 and 73, respectively. As qualifier ions, ions with a m/z-ratio of 67 and 72 were measured for isoprene and isoprene-d5, respectively. After method completion the amount of isoprene was determined from the peak area of the quantifier ion at the corresponding retention time using daily calibrations (section 3.4.1).

3.3   Storage tests

Depending on the amount of samples taken at once, samples had to be stored a certain amount of time prior to analysis, as only one sample could be analyzed immediately after sampling, due to the purge time and the analytical method. Furthermore, in some cases, the sample had to be transported to the laboratory, when the GC-MS was not at the same location as the sampling site. However, isoprene samples may not be stable, because isoprene is produced biologically in the surface ocean. The biological production or any other production/consumption process could influence the concentration of isoprene in the sample vial between sampling and analysis. The influence of sample storage while waiting for analysis, was tested in three storage experiments. Samples were treated and prepared for analysis as described in section 3.2. Storage experiments were performed under four different conditions: at RT next to the window (light), at RT in the cupboard (dark), in the fridge (+5°C), and in the freezer (-20°C). Samples were measured 1-2 hours, 3-4 hours, 6-7 hours, 24 hours, 48 hours, and 5-7 days after sampling, for light and dark conditions, respectively. Samples from the fridge were measured earliest 3-4 hours after sampling to account for the time it takes to cool down the sample. Frozen samples (-20°C) were only measured 1 day, 2 days, and 5-7 days after sampling to account for the time it takes to freeze and melt the seawater. Figure 3.6 shows the change in % to the initial concentration immediately after sampling. Storing the sample under dark conditions in the fridge appeared to be the best choice for storing isoprene samples

up to 4 hours before analysis (mean: 0.3±3.9%). The mean change during dark conditions was also very small after 3-4 hours (5.4%), although coming along with a very high standard deviation (27.7%) resulting from three experiments. Samples under light conditions where highly influenced after 1 hour of sampling. Freezing the samples appeared not to be a solution for long time storage, as the concentrations decreased by ~70% after being in the freezer for longer than 1 day.
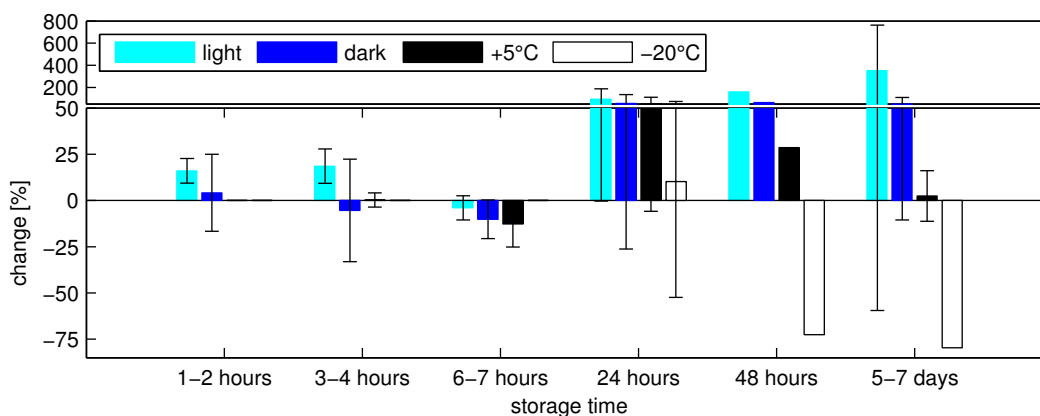
Figure 3.6: Isoprene storage experiment. Mean change in percent of concentration (± standard deviation) under different conditions (light: RT, dark: RT, 5°C: fridge, -20°C: freezer).

As a result of the storage experiment, analysis during this work was performed within two hours of collection while storing the samples in the fridge, when the GC-MS was onboard of the research vessel or at the same site the sample was taken at. When samples had to be transported to the analytical system, they were measured as fast as possible but within four hours of collection.

3.4   Data analysis

3.4.1   Calibrations

Three to five point calibration curves with known quantities of isoprene were performed in order to calculate the isoprene concentration from the resulting peakarea of a seawater sample. The preparation of a standard solution in ethylene glycol (≥99.5%, Merck, Darmstadt, Germany) was performed gravimetrically:

Two 25 mL brown glass vials (Chromatographie Handel Müller, Fridolfing, Germany) were weighed before and after the addition of ~24 mL ethylene glycol. A specific amount (generally ~10 µL) of isoprene (99%, stab. with ca. 0.02% 4-tert-butylcatechol, Alfa Aesar, Karlsruhe, Germany) was added and weighed to the first vial. The amount of isoprene n_{iso} in mol was calculated using the added mass m_{iso} and the molar mass M_{iso} (68.12 g mol^{-1}) of isoprene:

$$n_{iso} = \frac{m_{iso}}{M_{iso}} \tag{3.2}$$

The density of ethylene glycol (1.11 g cm^{-3}) and isoprene (0.68 g cm^{-3}) were used to convert the added masses into the corresponding volumes (V_{Eth} and V_{iso}). The concentration of isoprene in the first standard $Std1c_{iso}$ was calculated as follows using n_{iso}, $V_{Eth,}$ and V_{iso}:

$$Std1c_{iso} = \frac{n_{iso}}{V_{Eth} + V_{iso}} \tag{3.3}$$

About 5 μL of standard 1 (V_{Std1}) were added to the second vial and weighed. The concentration of isoprene in the second standard $Std2c_{iso}$ was calculated as follows:

$$Std2c_{iso} = \frac{V_{Std1} \times Std1c_{iso}}{V_{Eth} + V_{Std1}} \tag{3.4}$$

Three point calibrations were obtained by diluting three different amounts of Standard 2 in 10 mL of Milli-Q water and performing the analysis in the same way as the samples. Three Blanks were measured prior to the calibration to account for significant amounts of isoprene in the Milli-Q water. The mean peak area of the m/z=68 signal (PA_{68}) of the Milli-Q blanks was abstracted from each calibration measurement. An example of a five point calibration is shown in Figure 3.7. The amount of isoprene n_{iso} in a sample was calculated from the peak area of the sample, the slope s, and the intercept b of the linear regression:

$$n_{iso} = \frac{PA_{68} - b}{s} \tag{3.5}$$
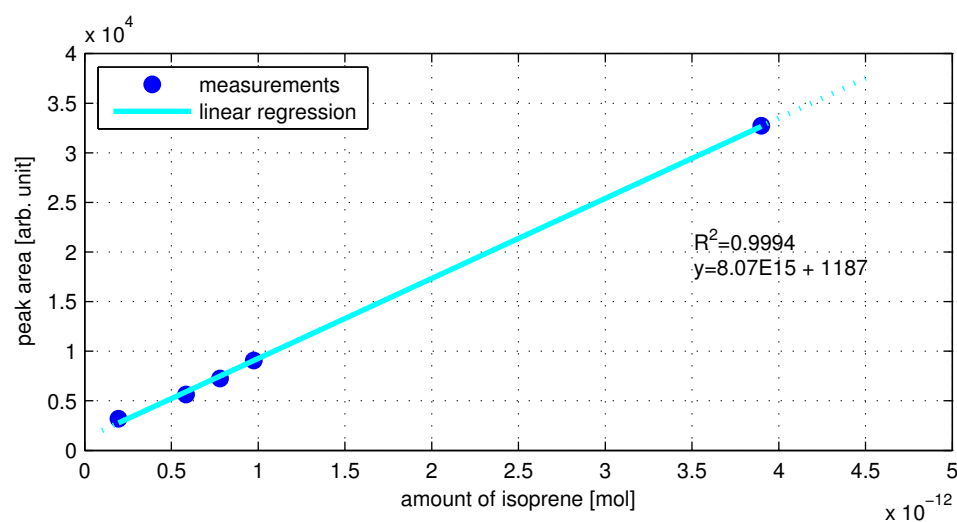
Figure 3.7: Example of a five point calibration using a liquid standard solution.

3.4.2   Sensitivity drift

Sensitivity is defined as the change of signal to the change of analyte concentration described by the signal-to-noise ratio (S/N). An increased signal and decreased noise, or a combination of both is increasing the sensitivity. Sensitivity in the MS is influenced by the ion creation in the ion source, the ion transmission through the lenses, and the ion detection by the electron multiplier. The ion source has to be cleaned or/and the MS conditions have to be readjusted (tuning) to improve sensitivity. However, these operations cannot be done frequently, as the system has to be shut down (ion source cleaning) and the system has to be recalibrated.

Once the MS conditions are set it is common to experience sensitivity loss in the GC-MS. With every sample being measured, the ion source gets dirty and the ions are less focused by the lenses. This change in sensitivity over time is negligible when measuring samples a few hours before and after performing a calibration. However, serious drift can occur when the system is in operation for long periods of time (e.g. during research cruises). Liquid calibrations can only account partially for a sensitivity change as they are done once in 24 h assuming that the change in sensitivity is linear between two calibrations, which is not always correct (Figure 3.8). 500 µL gaseous isoprene-d5 was added to every measurement as an internal standard to account for the sensitivity drift of the system between two calibrations. Figure 3.8 shows the sensitivity drift of the system during ASTRA-OMZ in 2015. The system was tuned three times during the cruise to improve the sensitivity.
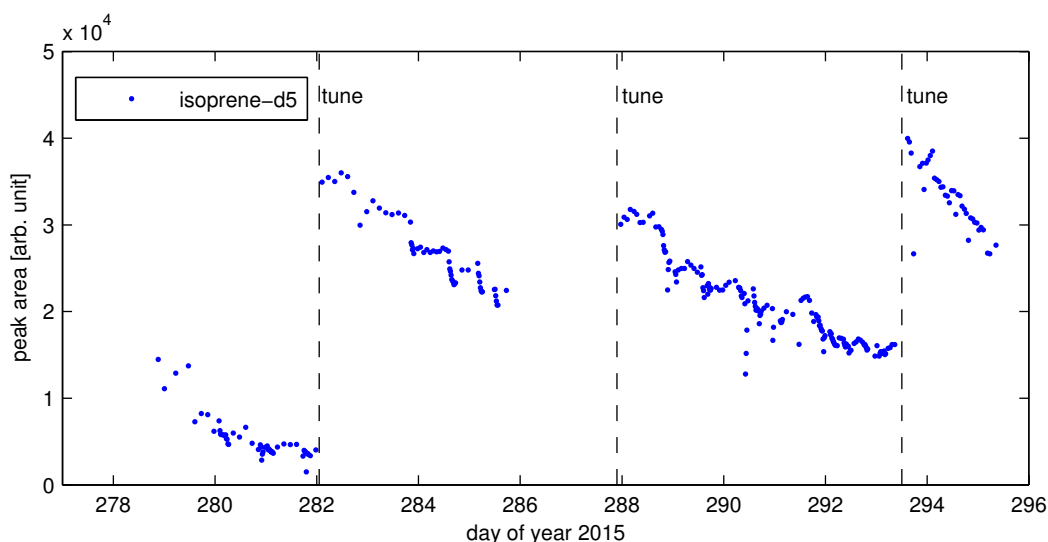
Figure 3.8: Sensitivity drift of the system during ASTRA-OMZ cruise 2015. Data points show raw peak area of isoprene-d5 (m/z=73) acting as internal standard. The system was tuned (dashed line: "tune") three times during the cruise to improve the sensitivity of the system.

The procedure to account for the sensitivity drift in between two calibrations is described in the following: Isotopically labeled isoprene is 98% pure and, therefore, contains low levels of natural isoprene. The proportion m/z=68 (unlabeled isoprene) in iso-

prene-d5 (m/z=73) was determined to be 0.102. Hence, the signal of isoprene-d5 (m/z=73) was multiplied by 0.102 and subtracted from the measured m/z=68 signal of the sample.

The magnitude of peak area counts of the internal standard had to be transferred to the magnitude of peak area counts of the liquid calibrations. Therefore, the ratio R_n of the peak area of the actual liquid calibration measurement PA_{68} (m/z=68) and the corresponding peak area of the internal standard PA_{73} (m/z=73) was calculated for n calibrations:

$$R_n = \frac{PA_{73}}{PA_{68}}$$

(3.6)

The ratios R_n and R_{n+1} were plotted over time t_n and t_{n+1} and a linear regression was applied resulting in a time dependent ratio R over time t with the slope s and intercept b:

$$R = s \times t + b$$

(3.7)

The ratio R was received from equation (3.7) dependent on the time t for every measurement in between these two calibrations. PA_{68} of each measurement was calculated by dividing the corresponding PA_{73} of each measurement by R using equation (3.6).

This procedure was done for all three volumes of the standard calibration resulting in three different calculated PA_{68} for every single measurement. These peak areas were used for a three point calibration. Calibration curves were performed for every single measurement as described in section 3.4.1 in order to calculate the isoprene concentration. An example of this calibration including the sensitivity drift is shown in Figure 3.9. The signal of the internal standard (m/z=73) was used according to equations (3.6) and (3.7) to calculate a "pseudo" calibration signal of m/z=68 for each measurement in between two actual calibrations at times t_n and t_{n+1}.
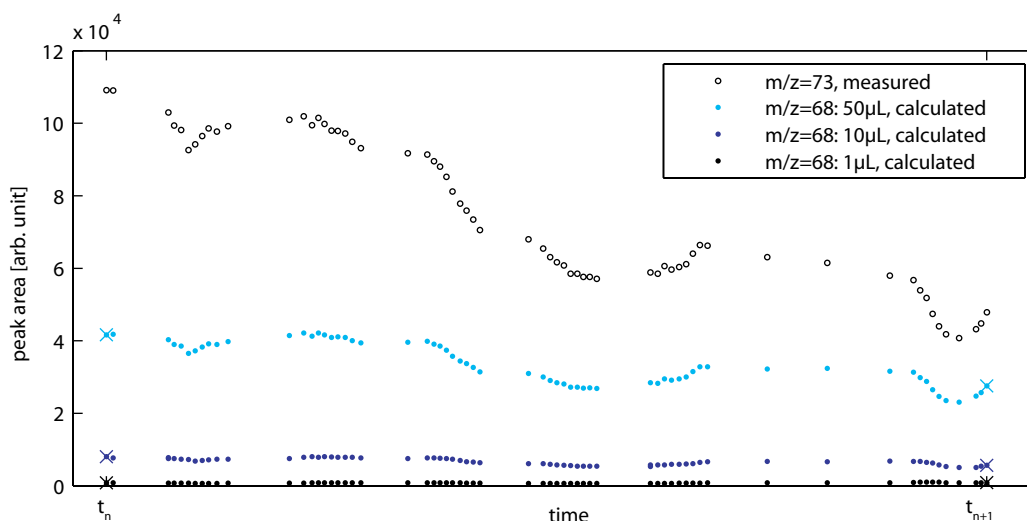
Figure 3.9: Example for calculated m/z=68 calibration peak areas for 1 µL, 10 µL, and 50 µL standard addition. Crosses show peak areas of m/z=68 signal of measured calibrations at times t_n and t_{n+1}. The "pseudo" peak areas were used for three point calibration at each point of measurement.

3.4.3   Error analysis

The total error estimate for the measurements performed for this work was calculated using error propagation. The following variables contributed to the overall error:
- Volume of the sea water sample
- Peak integration
- Concentration of the standard solution
- Linear calibration

Sample volume. Sample volumes were always filled headspace free. The volumes of the sample vials were tested and, due to manufacturing, were not identical. The systematic error of the sample volume was calculated from eight sample vials of one batch. The mean volume of a sample vial is 60.86 mL with a standard deviation of 0.24 mL.

The amount of seawater replaced by helium when creating headspace is dependent on the temperature difference of the helium in the gas bottle (T_{bottle}, outside temperature) and in the sea water sample (T_{water}). The volume of helium changes in proportion to the temperature change (in K) according to Gay-Lussac's law and following the ideal gas law. The volume of helium in the sample vial (V_{water}) is then described as follows:

$$V_{water} = V_{bottle} \times \frac{T_{water}}{T_{bottle}}$$

(3.8)

The seawater temperature for 75% of the data in this work ranged from 17 - 27°C, depending on the region and the depth a sample was taken. The temperature of the sample is converging to the surrounding air temperature while sampling from the CTD. For the following error calculation it is assumed that the difference of the sample and air temperature is ±5°C, when pushing 10 mL of helium into the sample vial. Combining

$$T_{water} = T_{bottle} \pm 5 \text{ K}$$

(3.9)

and equation (3.8) gives:

$$V_{water} = V_{bottle} \times \frac{T_{bottle} \pm 5 \text{ K}}{T_{bottle}} = V_{bottle} \times \left(1 \pm \frac{5 \text{ K}}{T_{bottle}}\right)$$

(3.10)

The error for the volume of helium in the sample (V_{water}) replacing 10 mL of sea water is calculated following

$$\Delta V_{water} = \sqrt{\left(\frac{\partial V_{water}}{\partial V_{bottle}} \Delta V_{bottle}\right)^2} = \left|\left(1 \pm \frac{5 \text{ K}}{T_{bottle}}\right) \cdot \Delta V_{bottle}\right|$$

(3.11)

The error of the syringe which is used to take 10 mL of helium from the gas bottle (ΔV_{bottle}) is assumed to be maximum 0.1 mL (10% of the main graduation interval of the syringe). It can be seen from equation (3.11), that ΔV_{water} is dependent on the outside temperature T_{bottle}, but as this influence is negligible ($1 \pm (5/T_{bottle}) \approx 1$), ΔV_{water} is 0.1 mL ($= \Delta V_{bottle}$).

Summing up the two error estimations (the volume of the sample vial and the volume of helium replacing the sea water) yields in an absolute error of 0.34 mL (0.67%) for the volume of the analyzed seawater (ΔV).

Peak integration. The relative error by manual peak integration increases with decreasing peak area. The limit of detection (LOD) of this system set-up is 3×10^{-13} mol ($\hat{=}$ 6 pmol L^{-1}), which is 10 times the standard deviation of the baseline noise. An error of ± half a standard deviation of the baseline noise due to manual integration would lead to an error of 5% ($\hat{=}$ 0.3 pmol L^{-1}) for the manual peak area integration at the LOD. In general, the peak height was higher than 100 times one standard deviation of the baseline noise, leading to a relative error of <0.5% for manual peak integration. This is considered negligible for further error propagation and will no longer be included.

Standard solution. As described in section 3.4.1, the preparation of the standard solution was performed gravimetrically. Every weighing step was done three times. The error of the isoprene concentration in the standard solution is 1% on average calculated from the standard deviation and the absolute amount of added isoprene.

The amounts of standard solution which were added to the Milli-Q were taken with a microliter syringe (Hamilton, Reno, Nevada), which has a volume error of 1% of the nominal volume (specifications of Hamilton syringe). Hence, combining the volume error and the weighing error, the amount of isoprene added from the standard solution has a total error of $\sqrt{1\% + 1\%} = 1.41\%$.

Linear calibration. The amount of isoprene in the sample is calculated by the linear regression of the calibration according to equation (3.5). The standard errors for the slope Δs and the intercept Δb were derived from the linear regression of each calibration. Equation (3.12) gives the error for the amount of isoprene in the sample (Δn_{iso}):

$$\Delta n_{iso} = \sqrt{\left(\frac{\partial n_{iso}}{\partial s} \Delta s\right)^2 + \left(\frac{\partial n_{iso}}{\partial b} \Delta b\right)^2} = \sqrt{\left(\frac{PA_{68} - b}{s^2} \cdot \Delta s\right)^2 + \left(-\frac{1}{s} \cdot \Delta b\right)^2} \tag{3.12}$$

The amount of isoprene (in mol) in the sample divided by the analyzed volume (in L) of sea water gives the isoprene concentration (c_{iso}, mol L^{-1}):

$$c_{iso} = \frac{n_{iso}}{V} \tag{3.13}$$

The total error calculated for each isoprene concentration (Δc_{iso}) during this work was calculated with the given error for the amount of isoprene in the sample (Δn_{iso}) and the error of the water volume (ΔV):

$$\Delta c_{iso} = \sqrt{\left(\frac{\partial c_{iso}}{\partial n_{iso}} \Delta n_{iso}\right)^2 + \left(\frac{\partial c_{iso}}{\partial V} \Delta V\right)^2} = \sqrt{\left(\frac{1}{V} \cdot \Delta n_{iso}\right)^2 + \left(-\frac{n_{iso}}{V^2} \cdot \Delta V\right)^2} = \sqrt{\left(\frac{\Delta n_{iso}}{50.9 mL}\right)^2 + \left(-\frac{0.34 mL\ n_{iso}}{(50.9 mL)^2}\right)^2} \tag{3.14}$$

Over all the mean Δc_{iso} for each measurement was about ±3.0 pmol L^{-1}. The mean measured concentration of isoprene was ~30 pmol L^{-1}, which leads to a precision of ±10% of the isoprene analysis during this work.

3.5 The chemistry climate model ECHAM-HAMMOZ

ECHAM-HAMMOZ is an atmospheric chemistry climate model that describes gas-phase reactions and aerosol chemistry in the troposphere and stratosphere. The current model version ECHAM6.3-HAM2.3-MOZ1.0 is described in SCHULTZ et al. (2017). The sixth generation of ECHAM (ECHAM6) is an atmospheric general circulation model, focusing on large-scale circulations and diabatic processes, which are driven by radiative forcing (STEVENS et al., 2013). The original version, a branch of the European Center for Medium Range Weather Forecasts model, was developed by the Max Planck Institute for Meteorology in Hamburg (ECHAM). The second version of the Hamburg Aerosol Model (HAM2) describes the composition and size distribution of aerosols including aerosol-cloud interactions (ZHANG et al., 2012). The atmospheric chemistry is described by the gas-phase tropospheric and stratospheric module MOZ from the Model for Ozone and Related chemical Tracers MOZART (EMMONS et al., 2010).

In order to simulate atmospheric concentrations, different emission inventories of trace gases and aerosols are used. Anthropogenic emissions are taken from the ACCMIP (Atmospheric Chemistry and Climate Model Intercomparison Project) interpolated inventory (LAMARQUE et al., 2010) and biogenic emissions are taken and simulated from version 2.1 of the Model of Emissions of Gases and Aerosols from Nature (MEGAN) (GUENTHER et al., 2012). Parameterized emissions of NO due to lightning are described in GREWE et al. (2001).

3.5.1 Modification for isoprene derived SOA formation

In the current version 2.3 of HAM all relevant aerosol processes are parameterized, including nucleation, condensation, coagulation, cloud activation, dry and wet deposition, and sedimentation (SCHULTZ et al., 2017). HAM is combined with the Sectional Aerosol module for Large Scale Applications SALSA to calculate the aerosol micro physics (KOKKOLA et al., 2008). The combination of HAM and SALSA is coupled to MOZ in order to calculate secondary organic aerosol (SOA) precursors.

An isoprene oxidation mechanism, including isoprene oxidation via OH, O_3 and NO_3, was implemented by TARABORRELLI et al. (2009) and further developed to include variation of low volatility organic compounds (LVOCs), resulting in a detailed gas-phase chemistry scheme JAM003 (Jülich Atmospheric Mechanism). JAM003, including its 147 isoprene oxidation reactions, is used in MOZ in order to calculate compounds contributing to isoprene derived SOA (iSOA). This chemical mechanism contains 779 chemical reactions, including eight tropospheric and 16 stratospheric heterogeneous reactions, as well as 146 photolysis reactions from in total 254 gas species (STADTLER et al., 2017a). Four LVOCs from isoprene oxidation products were identified in this model set-up to be low volatile enough (saturation vapor pressure <0.01 Pa) to contribute to iSOA and are shown in Table 3.3.

Table 3.3: Four low volatility organic compound oxidation products contributing to isoprene derived secondary organic compounds. Calculated saturation vapor pressure p and Henry's law coefficient H are listed at a temperature of 298 K. ΔH_{vap} is the evaporation enthalpy. Data from STADTLER et al. (2017a).

Compound	p_0^* [Pa]	ΔH_{vap}[kJ mol^{-1}]	H [atm^{-1}]	empirical formula
LNISOOH	2.2×10^{-4}	11.7	2.1×10^5	$C_5H_9NO_7$
LISOPOOHOOH	3.8×10^{-7}	155.3	2.0×10^{16}	$C_5H_{12}O_6$
LC578OOH	2.0×10^{-4}	123.2	3.0×10^{11}	$C_5H_{10}O_5$
C59OOH	1.0×10^{-4}	125.0	3.0×10^{11}	$C_5H_{10}O_5$

Starting from isoprene the exact chemical reaction steps leading to one of the four LVOCs are shown in STADTLER et al. (2017a) and SCHULTZ et al. (2017). An overview, including the main steps of multiple isoprene oxidations, is shown in Figure 3.10. Isoprene reacts with a NO$_3$ radical to form a nitrate peroxy radical in a NO$_x$ dominated environment. This radical is further oxidizes in different steps to form LNISOOH (name following the MCM nomenclature (JENKIN et al., 1997)) in a very low yield of 0.1%. The other three LVOCs contributing to iSOA are generated through oxidation with OH as first step. The formed isoprene peroxy radical isomers undergo self/cross reactions as well as reactions with other radicals yielding LC578OOH, C59OOH and LISOPOOHOOH in 1%, 2% and 9%, respectively. C59OOH can also be formed via a second oxidation pathway starting from an isoprene peroxy radical, when NO radicals are present. Isoprene oxidation with O$_3$ is also included in JAM003, but none of the products is volatile enough to act as iSOA.
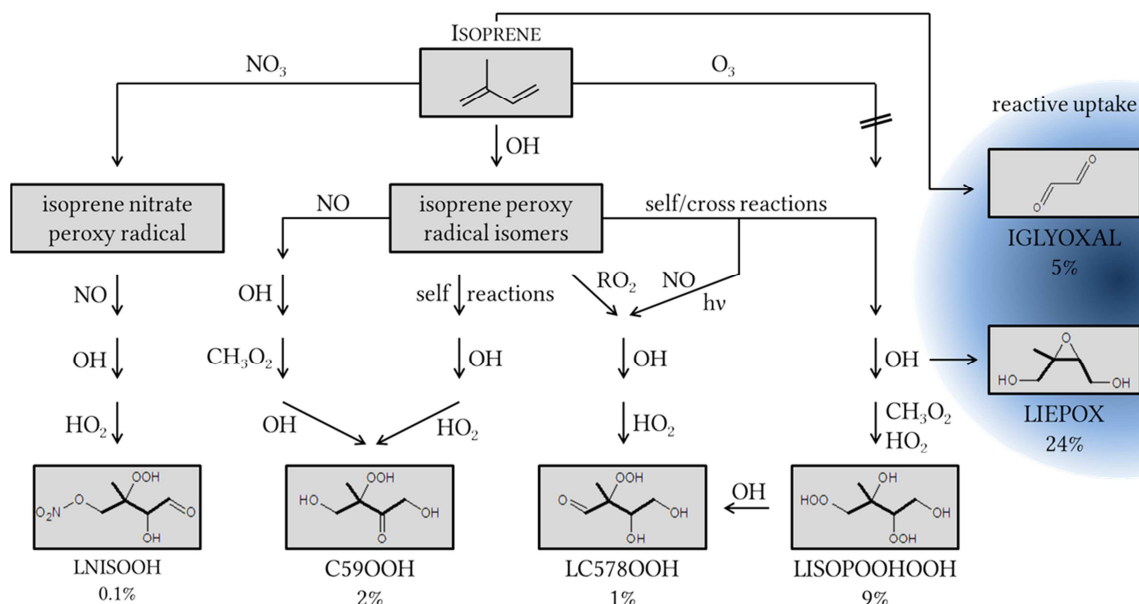
Figure 3.10: Simplified overview of oxidation pathways of isoprene in HAMMOZ leading to iSOA. Each arrow indicates a reaction step. Various formation pathways of IGLYOXAL are not shown due to readability of the figure. Numbers indicate the yield from isoprene in percent. Bold bonds in oxidation products highlight the isoprene skeleton. Modified from STADTLER et al. (2017a).

In addition to the production of the four LVOCs the chemical mechanism in MOZ includes the production of LIEPOX, which is formed during the LISOPOOHOOH reaction chain (see Figure 3.10) and isoprene derived glyoxal (IGLYOXAL), which is formed during numerous steps of all isoprene oxidation pathways, including the ozone oxidation pathway. LIEPOX (24% yield) and IGLYOXAL (5% yield) undergo reactive uptake by particles which is described in STADTLER et al. (2017b) and are accounting for the multiphase chemical iSOA formation in the model.

In total, six compounds (C59OOH, LC578OOH, LISOPOOHOOH, LNISOOH, IGLYOXAL, LIEPOX) account for the iSOA formation in this model set-up.

References

BUDZIKIEWICZ, H., and SCHÄFER, M.: Massenspektrometrie : Eine einführung, Wiley-VCH, Weinheim, 2013.

EMMONS, L. K., WALTERS, S., HESS, P. G., LAMARQUE, J. F., PFISTER, G. G., FILLMORE, D., GRANIER, C., GUENTHER, A., KINNISON, D., LAEPPLE, T., ORLANDO, J., TIE, X., TYNDALL, G., WIEDINMYER, C., BAUGHCUM, S. L., and KLOSTER, S.: Description and evaluation of the model for ozone and related chemical tracers, version 4 (mozart-4), *Geosci. Model Dev.*, 3, 43-67, 10.5194/gmd-3-43-2010, 2010.

GREWE, V., BRUNNER, D., DAMERIS, M., GRENFELL, J. L., HEIN, R., SHINDELL, D., and STAEHELIN, J.: Origin and variability of upper tropospheric nitrogen oxides and ozone at northern mid-latitudes, *Atmospheric Environment*, 35, 3421-3433, http://dx.doi.org/10.1016/S1352-2310(01)00134-0, 2001.

GUENTHER, A. B., JIANG, X., HEALD, C. L., SAKULYANONTVITTAYA, T., DUHL, T., EMMONS, L. K., and WANG, X.: The model of emissions of gases and aerosols from nature version 2.1 (megan2.1): An extended and updated framework for modeling biogenic emissions, *Geoscientific Model Development*, 5, 1471-1492, 10.5194/gmd-5-1471-2012, 2012.

JENKIN, M. E., SAUNDERS, S. M., and PILLING, M. J.: The tropospheric degradation of volatile organic compounds: A protocol for mechanism development, *Atmospheric Environment*, 31, 81-104, http://dx.doi.org/10.1016/S1352-2310(96)00105-7, 1997.

KOKKOLA, H., KORHONEN, H., LEHTINEN, K. E. J., MAKKONEN, R., ASMI, A., JÄRVENOJA, S., ANTTILA, T., PARTANEN, A. I., KULMALA, M., JÄRVINEN, H., LAAKSONEN, A., and KERMINEN, V. M.: Salsa – a sectional aerosol module for large scale applications, *Atmos. Chem. Phys.*, 8, 2469-2483, 10.5194/acp-8-2469-2008, 2008.

LAMARQUE, J. F., BOND, T. C., EYRING, V., GRANIER, C., HEIL, A., KLIMONT, Z., LEE, D., LIOUSSE, C., MIEVILLE, A., OWEN, B., SCHULTZ, M. G., SHINDELL, D., SMITH, S. J., STEHFEST, E., VAN AARDENNE, J., COOPER, O. R., KAINUMA, M., MAHOWALD, N., MCCONNELL, J. R., NAIK, V., RIAHI, K., and VAN VUUREN, D. P.: Historical (1850–2000) gridded anthropogenic and biomass burning emissions of reactive gases and aerosols: Methodology and application, *Atmos. Chem. Phys.*, 10, 7017-7039, 10.5194/acp-10-7017-2010, 2010.

LENG, C., KISH, J. D., KELLEY, J., MACH, M., HILTNER, J., ZHANG, Y., and LIU, Y.: Temperature-dependent henry's law constants of atmospheric organics of biogenic origin, *The Journal of Physical Chemistry A*, 117, 10359-10367, 10.1021/jp403603z, 2013.

NIST MASS SPEC DATA CENTER, S., S.E., director: Mass spectra, in: Nist chemistry webbook, nist standard reference database number 69, edited by: Linstrom, P. J., and Mallard, W. G., National Institute of Standards and Technology, Gaithersburg MD, 20899, 10.18434/T4D303.

SCHULTZ, M. G., STADTLER, S., SCHRÖDER, S., TARABORRELLI, D., FRANCO, B., KREFTING, J., HENROT, A., FERRACHAT, S., LOHMANN, U., NEUBAUER, D., SIEGENTHALER-LE DRIAN, C., WAHL, S., KOKKOLA, H., KÜHN, T., RAST, S., SCHMIDT, H., STIER, P., KINNISON, D., TYNDALL, G. S., ORLANDO, J. J., and WESPES, C.: The chemistry climate model echam6.3-ham2.3-moz1.0, *Geosci. Model Dev. Discuss.*, 2017, 1-43, 10.5194/gmd-2017-191, 2017.

STADTLER, S., KÜHN, T., SCHRÖDER, S., TARABORRELLI, D., SCHULTZ, M. G., and KOKKOLA, H.: Isoprene derived secondary organic aerosol in a global aerosol chemistry climate model, *Geosci. Model Dev. Discuss.*, 2017, 1-35, 10.5194/gmd-2017-244, 2017a.

STADTLER, S., SIMPSON, D., SCHRÖDER, S., TARABORRELLI, D., BOTT, A., and SCHULTZ, M.: Ozone impacts of gas-aerosol uptake in global chemistry transport models, *Atmos. Chem. Phys. Discuss.*, 2017, 1-35, 10.5194/acp-2017-566, 2017b.

STAUDINGER, J., and ROBERTS, P. V.: A critical compilation of henry's law constant temperature dependence relations for organic compounds in dilute aqueous solutions, *Chemosphere*, 44, 561-576, https://doi.org/10.1016/S0045-6535(00)00505-1, 2001.

STEVENS, B., GIORGETTA, M., ESCH, M., MAURITSEN, T., CRUEGER, T., RAST, S., SALZMANN, M., SCHMIDT, H., BADER, J., BLOCK, K., BROKOPF, R., FAST, I., KINNE, S., KORNBLUEH, L., LOHMANN, U., PINCUS, R., REICHLER, T., and ROECKNER, E.: Atmospheric component of the mpi-m earth system model: Echam6, *Journal of Advances in Modeling Earth Systems*, 5, 146-172, 10.1002/jame.20015, 2013.

TARABORRELLI, D., LAWRENCE, M. G., BUTLER, T. M., SANDER, R., and LELIEVELD, J.: Mainz isoprene mechanism 2 (mim2): An isoprene oxidation mechanism for regional and global atmospheric modelling, *Atmos. Chem. Phys.*, 9, 2751-2777, 10.5194/acp-9-2751-2009, 2009.

WARNECK, P., and WILLIAMS, J.: The atmospheric chemist's companion: Numerical data for use in the atmospheric sciences, Springer Science & Business Media, 2012.

ZHANG, K., O'DONNELL, D., KAZIL, J., STIER, P., KINNE, S., LOHMANN, U., FERRACHAT, S., CROFT, B., QUAAS, J., WAN, H., RAST, S., and FEICHTER, J.: The global aerosol-climate model echam-ham, version 2: Sensitivity to improvements in process representations, *Atmos. Chem. Phys.*, 12, 8911-8949, 10.5194/acp-12-8911-2012, 2012.

4 MODELING MARINE ISOPRENE CONCENTRATIONS

Abstract. We use isoprene and related field measurements from three different ocean data sets together with remotely sensed satellite data to model global marine isoprene emissions. We show that using monthly mean satellite-derived chl-a concentrations to parameterize isoprene with a constant chl-a normalized isoprene production rate underpredicts the measured oceanic isoprene concentration by a mean factor of 19±12. Improving the model by using phytoplankton functional type dependent production values and by decreasing the bacterial degradation rate of isoprene in the water column results in only a slight underestimation (factor 1.7±1.2). We calculate global isoprene emissions of 0.21 Tg C for 2014 using this improved model, which is twice the value calculated using the original model. Nonetheless, the sea-to-air fluxes have to be at least 1 order of magnitude higher to account for measured atmospheric isoprene mixing ratios. These findings suggest that there is at least one missing oceanic source of isoprene and, possibly, other unknown factors in the ocean or atmosphere influencing the atmospheric values. The discrepancy between calculated fluxes and atmospheric observations must be reconciled in order to fully understand the importance of marine-derived isoprene as a precursor to remote marine boundary layer particle formation.

4.1   Introduction

Remote marine boundary layer aerosol and cloud formation is important for both the global climate system/radiative budget and for atmospheric chemistry (TWOMEY, 1974) and has been investigated, with contentious results, for decades. The question remains: what are the precursors to aerosol and cloud formation over the ocean? Earlier studies pinpointed dimethyl sulfide (DMS) as the main precursor, as described in the CLAW hypothesis (CHARLSON et al., 1987). More recently, this hypothesis has been debated controversially (QUINN and BATES, 2011) because primary organic aerosols (POA; O'DOWD et al., 2008)) and small sea salt particles (ANDREAE and ROSENFELD, 2008; DE LEEUW et al., 2011) have been identified as cloud condensation nuclei (CCN) precursors with higher CCN production potential than DMS. In addition to POA, other gases besides DMS have been hypothesized as important for remote marine secondary organic aerosol formation (SOA), including isoprene (2-methyl-1,3-butadiene), which has received the most attention in recent years (CARLTON et al., 2009).

Isoprene is a byproduct of plant metabolism and one of the most abundant of the atmospheric volatile non-methane hydrocarbons (NMHC). On a global basis, as much as 90% of atmospheric isoprene comes from terrestrial plant emissions (400-600 TgC yr-1; ARNETH et al., 2008; GUENTHER et al., 2006). Isoprene is very short lived in the atmosphere, with a lifetime ranging from minutes to a few hours. The principal loss mechanism is reaction with hydroxyl radicals (OH), but reactions with ozone and nitrate radicals are also important sinks (ATKINSON and AREY, 2003; LELIEVELD et al., 2008).

The importance of the ocean as a source of atmospheric isoprene is unclear, as only few studies have directly measured isoprene concentrations in the euphotic zone. Throughout most of the world oceans, near-surface seawater isoprene concentrations range between <1 and 200 pmol L^{-1}, depending on season and region (BAKER et al., 2000; BONSANG et al., 1992; BROADGATE et al., 1997; BROADGATE et al., 2004; MATSUNAGA et al., 2002; MILNE et al., 1995; OOKI et al., 2015; ZINDLER et al., 2014). Higher isoprene levels have been measured in Southern Ocean and Arctic waters (395 and 541 pmol L-1, respectively; KAMEYAMA et al., 2014; TRAN et al., 2013). Atmospheric isoprene levels can be as high as 300 parts per trillion (ppt), varying with location and time of day (SHAW et al., 2010). Generally, the mixing ratios are lower than 100 ppt in remote areas not influenced by terrestrial sources (YOKOUCHI et al., 1999), but they can also increase up to 375 ppt during a phytoplankton bloom (YASSAA et al., 2008). MATSUNAGA et al. (2002) found that the sea-to-air flux estimated from measurements could not explain the atmospheric concentrations observed in the western North Pacific. This agrees with the model calculations of (HU et al., 2013), who found that top-down and bottom-up models estimating isoprene emissions disagree by 2 orders of magnitude.

Assessing the importance of isoprene for marine atmospheric chemistry and SOA formation requires extrapolations of measurements to develop global emissions climatologies and inventories. Model studies suggest that oceanic sources of isoprene are too weak to control marine SOA formation (ANTTILA et al., 2010; ARNOLD et al., 2009; GANTT et al., 2009; MYRIOKEFALITAKIS et al., 2010; SPRACKLEN et al., 2008) and field studies indicate that the organic carbon (OC) contribution from oceanic isoprene is less than

2% and out of phase with the peak of OC in the Southern Indian Ocean (ARNOLD et al., 2009). In contrast, HU et al. (2013) found that, despite sometimes low isoprene fluxes calculated by models, oceanic isoprene emissions can increase abruptly in association with phytoplankton blooms, resulting in regionally and seasonally important isoprene-derived SOA formation. Further experiments showed that isoprene oxidation products can increase the level of CCN when the number of CCN is low (EKSTROM et al., 2009). LANA et al. (2012) used both model-calculated fluxes of isoprene and remote sensing products to investigate isoprene-derived SOA formation in the marine atmosphere. Their results illustrated that the oxidation products of marine trace gases seemed to influence the condensation growth and the hygroscopic activation of small primary particles. Fluxes of isoprene (and other marine-derived trace gases) showed greater positive correlations with CCN number and greater negative correlations with aerosol effective radius than POA and sea salt over most of the world's oceans.

Since isoprene concentration measurements from the open ocean are sparse, it is essential to combine laboratory and field measurements, remote sensing, and modeling if we want to understand marine isoprene emissions. This study utilizes measurements of surface ocean isoprene and associated biological and physical parameters on three oceanographic cruises to refine and validate the model of PALMER and SHAW (2005) for estimating marine isoprene concentrations and emissions. The resulting model, with satellite-derived input, is used to compute monthly climatologies and annual average estimates of isoprene in the world ocean.

4.2   Methods

4.2.1   Model description

In this study we use a simple steady-state model for surface ocean isoprene consisting of a mass balance between biological production, chemical and biological losses, and emission to the atmosphere (PALMER and SHAW, 2005):

$$P - C_W \left(\sum k_{CHEM,i} C_{Xi} + k_{BIOL} + \frac{k_{AS}}{MLD} \right) - L_{MIX} = 0, \tag{4.1}$$

where biological production (P) is balanced by all loss processes, C_W is the seawater concentration of isoprene, k_{CHEM} is the chemical rate constant for all possible loss pathways (i) with all reactants (X) (X=OH and O_2), k_{BIOL} is the biological loss rate constant, which takes into account the biodegradation of isoprene, k_{AS} is the air−sea gas transfer coefficient that considers the loss processes due to air−sea gas exchange scaled with the depth of the ocean mixed layer (MLD), and L_{MIX} is the loss due to physical mixing (Table 4.1). The model equation was rearranged to solve for C_W as follows:

$$C_W = \frac{P - L_{MIX}}{\sum k_{CHEM,i} C_{Xi} + k_{BIOL} + \frac{k_{AS}}{MLD}} \tag{4.2}$$

The air−sea flux of isoprene (F) was calculated using the equation

$$F = k_{AS}(C_W - C_A/K_H) = \sim k_{AS}(C_W) \tag{4.3}$$

where C_A is the air-side concentration of isoprene and K_H is the dimensionless form of the Henry's law constant (equilibrium ratio of C_A and C_W). C_A is assumed to be negligible compared to C_W as noted above (Eq. (4.3)). As a result, the air–sea isoprene gradient is assumed equal to the surface ocean isoprene level, and emissions are assumed to be first order in C_W. This assumption is justified over the open ocean because of the short atmospheric lifetime of isoprene. In coastal regions downwind of strong isoprene sources, this assumption may not be valid. The air–sea exchange transfer coefficient (k_{AS}) is computed using the WANNINKHOF (1992) wind-speed-based (U_{10}) parameterization and the Schmidt number S_C of isoprene (PALMER and SHAW, 2005):

$$k_{AS} = 0.31\, U_{10}^2 \left(\frac{S_C}{660}\right)^{-0.5}. \tag{4.4}$$

Further details about the rate constants and input parameters are described in Table 4.1. Monthly mean wind speed (U_{10}) and sea surface temperature (SST) were obtained from the Quick Scatterometer (QuickSCAT) satellite and the Moderate Resolution Imaging Spectroradiometer (MODIS) instrument on board the Aqua satellite, respectively, and from in situ shipboard measurements. MLDs were obtained from climatological monthly means (DE BOYER MONTÉGUT et al., 2004) and compared to those calculated by in situ conductivity, temperature, and depth (CTD) profile measurements during each cruise. MLD was defined as the depth at which temperature is at least 0.2°C higher or lower than the temperature at 10 m depth (DE BOYER MONTÉGUT et al., 2004). Chlorophyll a (chl-a) concentrations were obtained either from the MODIS instrument on board the Terra satellite or from in situ shipboard measurements (here chl-a is defined as the sum of monovinyl chl-a, divinyl chl-a, and chlorophyllide a). Model calculations were carried out using MATLAB (Mathworks).

The steady-state model assumption is justified by the relatively short lifetime of isoprene in seawater as air–sea exchange is the dominant loss term over all latitudes and seasons (lifetime: 7–14 days) followed by k_{BIOL} and k_{CHEM} (PALMER and SHAW, 2005). In this study, model runs were carried out using three different sets of model parameters (Table 4.1).

1. ISO_{PS05}: the original configuration used by PALMER and SHAW (2005). In this configuration, the production of isoprene is parameterized as the product of the bulk chl-a concentration and a chl-a normalized isoprene production rate (P_{chloro}) inferred from laboratory phytoplankton monocultures of several cyanobacteria, eukaryotes, eukaryotes, and coccolithophores (SHAW et al., 2003). This approach inherently assumes that all phytoplankton have the same isoprene production characteristics. PALMER and SHAW (2005) also assumed that biological degradation of isoprene occurs in the water column, based on indirect evidence of a biological sink for isoprene (MOORE and WANG, 2006), but no isoprene loss rate constants have been published to date. They assumed a global average lifetime of ~17 days

(k_{BIOL} = 0.06 day^{-1}) based on the biological degradation rates of different data sets of methyl bromide (TOKARCZYK et al., 2003; YVON-LEWIS et al., 2002).

2. ISO$_{PFT}$: different P_{chloro} values are applied for different phytoplankton functional types (PFTs). Laboratory studies have shown that isoprene production rates vary significantly across different PFTs (ARNOLD et al., 2009; BONSANG et al., 2010; COLOMB et al., 2008; EXTON et al., 2013; SHAW et al., 2003). We use the PFT-dependent isoprene production rate constants and field observations of PFT distributions to estimate isoprene production rates. The chl-a normalized isoprene production rates of the different algae species are averaged within each PFT to obtain an estimated P_{chloro} value of isoprene for each PFT. PFT distributions along our cruise tracks were derived from the soluble organic pigment concentrations obtained from filtered water samples through Whatman GF/F filters using high-pressure liquid chromatography (HPLC) according to the method of BARLOW et al. (1997). This method was adjusted to our temperature-controlled instruments as detailed in TAYLOR et al. (2011b). We determined the list of pigments shown in Table 2 of TAYLOR et al. (2011b) and applied the method of AIKEN et al. (2009) for quality control of the pigment data. Pigment data from expedition ANT-XXV/1 have been already published in TAYLOR et al. (2011b). From the HPLC pigment concentration we calculated PFT groups using the diagnostic pigment (DP) analysis developed by VIDUSSI et al. (2001) and adapted in UITZ et al. (2006) to relate the weighted sum of seven, for each PFT representative DP. Using this approach, the chl-a concentrations for diatoms, dinoflagellates, haptophytes, chrysophytes, cryptophytes, cyanobacteria (excluding prochlorophytes), and chlorophytes were derived. The chl-a concentration of prochlorophytes was derived directly from the divinyl-chl-a concentration (the marker pigment for this group).

3. ISO$_{PFT-kBIO}$: the PFT approach is utilized to parameterize isoprene production as in ISO$_{PFT}$ and assumes that biological losses of isoprene in the water column are significantly slower than assumed by PALMER and SHAW (2005). Seawater incubation experiments carried out in temperature-controlled water baths over periods ranging from 48 to 72 h under natural light conditions, using deuterated isoprene (isoprene-d5), showed significantly longer lifetimes (manuscript in preparation). In the ISO$_{PFT-kBIO}$ configuration, we test a biological degradation lifetime of minimum 100 days (k_{BIOL} = 0.01 day^{-1}).

Table 4.1: List of parameters used in each model.

Parameter	Abbreviation	Unit	Model approach		
			ISO$_{PS05}$	ISO$_{PFT}$	ISO$_{PFT-kBIO}$
Isoprene production rate	P	pmol L^{-1} day^{-1}	P$_{chloro}$ x [chl-a]	P$_{chloro}$ x [PFT]	P$_{chloro}$ x[PFT]
Chemical loss rate	k$_{OH}$*C$_{OH}$	day^{-1}	0.0518	0.0518	0.0518
	k$_{O2}$*C$_{O2}$	day^{-1}	0.0009	0.0009	0.0009
Biological loss rate	k$_{BIOL}$	day^{-1}	0.06	0.06	0.01
Gas transfer coefficient	k$_{AS}$	m s^{-1}	WANNINKHOF (1992)		
Mixed layer depth	MLD	m	DE BOYER MONTÉGUT et al. (2004)		
Mixing loss rate	L$_{MIX}$	pmol L^{-1} day^{-1}	0.0459	0.0459	0.0459
Chl-a normalized isoprene production rate	P$_{chloro}$	μmol (g chl-a)$^{-1}$ day^{-1}	1.8	PFT dependent (Table 4.2)	

4.2.2 Cruise tracks

Isoprene was measured in the surface seawater during three separate cruises: the ANT-XXV/1 in the eastern Atlantic Ocean, the SPACES/OASIS cruises in the Indian Ocean, and the ASTRA-OMZ cruise in the eastern Pacific Ocean. ANT-XXV/1 took place in November 2008 on board the R/V Polarstern from Bremerhaven, Germany, to Cape Town, South Africa (Figure 4.1; for details about isoprene and ancillary data see also (Figure 4.1; for details about isoprene and ancillary data see also ZINDLER et al., 2014). The SPACES/OASIS cruises took place in June−July 2014 on board the R/V Sonne from Durban, South Africa, via Port Louis, Mauritius, to Malé, Maldives, and the AS-TRA-OMZ cruise took place in October 2015 on board the R/V Sonne from Guayaquil, Ecuador, to Antofagasta, Chile (Figure 4.1). Air mass backward trajectories (12 h; starting altitude: 50 m) from the Hybrid Single-Particle Lagrangian Integrated Trajectory (HYSPLIT; http://www.arl.noaa.gov/HYSPLIT.php) model were calculated for the sampling sites. The trajectories, in combination with atmospheric measurements, suggest that the air masses encountered on these cruises were from over the ocean for more than 12 h prior to sampling and are therefore unlikely to contain significant isoprene derived from terrestrial sources (Figure 4.1).
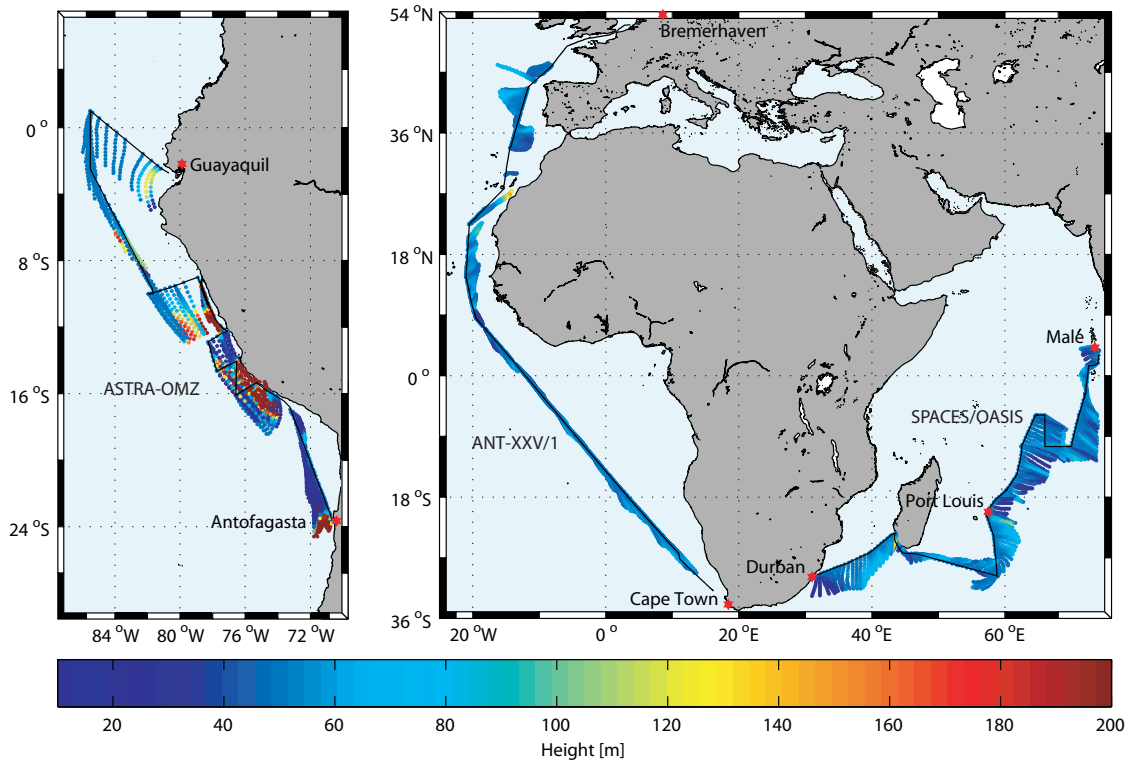
Figure 4.1: Cruise tracks (black) of ANT-XXV/1 (November 2008, East Atlantic Ocean), SPACES/OASIS (June/July 2014, Indian Ocean) and ASTRA-OMZ (October 2015, East Pacific Ocean). Air mass back trajectories calculated for 12 hours with a starting height of 50 m using HYSPLIT are superimposed on the cruise track. Color coding indicates altitude about sea level.

Isoprene measurements

4.2.3.1   Eastern Atlantic Ocean

The isoprene measurements from the ANT-XXV/1 (November 2008, eastern Atlantic Ocean) cruise are described in detail in ZINDLER et al. (2014). Seawater from approximately 2 m depth was continuously pumped on board and flowed through a porous Teflon membrane equilibrator. Isoprene was equilibrated by using a counterflow of dry air and was measured using an atmospheric pressure chemical ionization mass spectrometer (mini-CIMS), which consists of a ^{63}Ni atmospheric pressure ionization source coupled to a single quadrupole mass analyzer (Stanford Research Systems, SRS RGA200). Isoprene from a standard tank was added to the equilibrated air stream every 12 h to calibrate the system. The precision for isoprene measurements was ±13%. The isoprene data used here are 5 min averages.

4.2.3.2   Indian and eastern Pacific Oceans

The isoprene measurements on the SPACES/OASIS (June-July 2014, Indian Ocean) and ASTRA-OMZ (October 2015, eastern Pacific Ocean) cruises have not been published previously. Water samples (50 mL) were taken every 3 h from a continuously running seawater pump system located in the ship's moon pool at approximately 6m depth. All samples were analyzed on board within 15 min of collection using a purge and trap sys-

tem attached to a gas chromatograph/mass spectrometer operating in single ion mode (GC/MS; Agilent 7890A/Agilent 5975C; inert XL MSD with triple axis detector). Isoprene was purged from the water sample with helium for 15 min and dried using a Nafion membrane dryer (Perma Pure; ASTRA-OMZ) or potassium carbonate (SPACES/OASIS). Before being injected into the GC, isoprene was preconcentrated in a trap cooled with liquid nitrogen. Gravimetrically prepared liquid standards in ethylene glycol were measured in the same way as the samples and used to perform daily calibrations for quantification. Gaseous deuterated isoprene (isoprene-d5) was measured together with each sample as an internal standard to account for possible sensitivity drift between calibrations. The precision for isoprene measurements was ±8%.

Air samples were collected in electropolished stainless steel flasks and pressurized to approximately 2.5 atm with a metal bellows pump. Analysis was conducted after samples were returned to the laboratory. Isoprene was measured along with a range of halocarbons, hydrocarbons, and other gases using a combined GC/MS/FID/ECD system with a modified Markes Unity II/CIA sample preconcentrator. The modifications incorporated a water removal system consisting of a cold trap (-20°C) and a Perma Pure dryer (MD-050-24). Isoprene and >C4 hydrocarbons were quantified using selected ion MS and were calibrated against a whole air sample that is referenced to a NIST hydrocarbon mixture using GC/FID. Precision for isoprene is estimated at approximately ±0.4 ppt +5%.

4.3 Results and discussion

4.3.1 Comparison of modeled and in situ measured isoprene data

The shipboard isoprene measurements from the ANT-XXV/1 cruise ranged from 2 to 157 pmol L^{-1}, with the highest levels in the subtropics of the Southern Hemisphere and lower levels in the tropics (Figure 4.2). Model simulations were carried out along the cruise track using monthly mean satellite data from November 2008 for chl-a, surface winds, SST, and MLD as input parameters. The simulations underestimated the measured isoprene concentrations significantly, by as much as a factor of 20 over most of the cruise track (mean error of 19.1 pmol L^{-1}). Simulations were also carried out using in situ shipboard measurements (chl-a, wind speed, SST, MLD) as the input parameters. In both cases, the model simulations show a peak in the calculated isoprene levels at 13−17°N which is not present in the observations, whereas the peak, using in situ data as input parameter, is much smaller. This peak corresponds to elevated chl-a concentrations, suggesting that while there may have been high biological activity in this region, isoprene-producing species were not abundant (Figure 4.3, Figure 4.4). These results demonstrate that a single isoprene production factor and bulk chl-a concentration do not adequately describe the variability in isoprene production. When isoprene-producing PFTs are dominant, however, the modeled isoprene values follow the observed isoprene values (increasing isoprene concentration north of 33°N; Figure 4.2, Figure 4.5). The elevated iso-

prene concentrations in the subtropics of the Southern Hemisphere are not represented by the model.
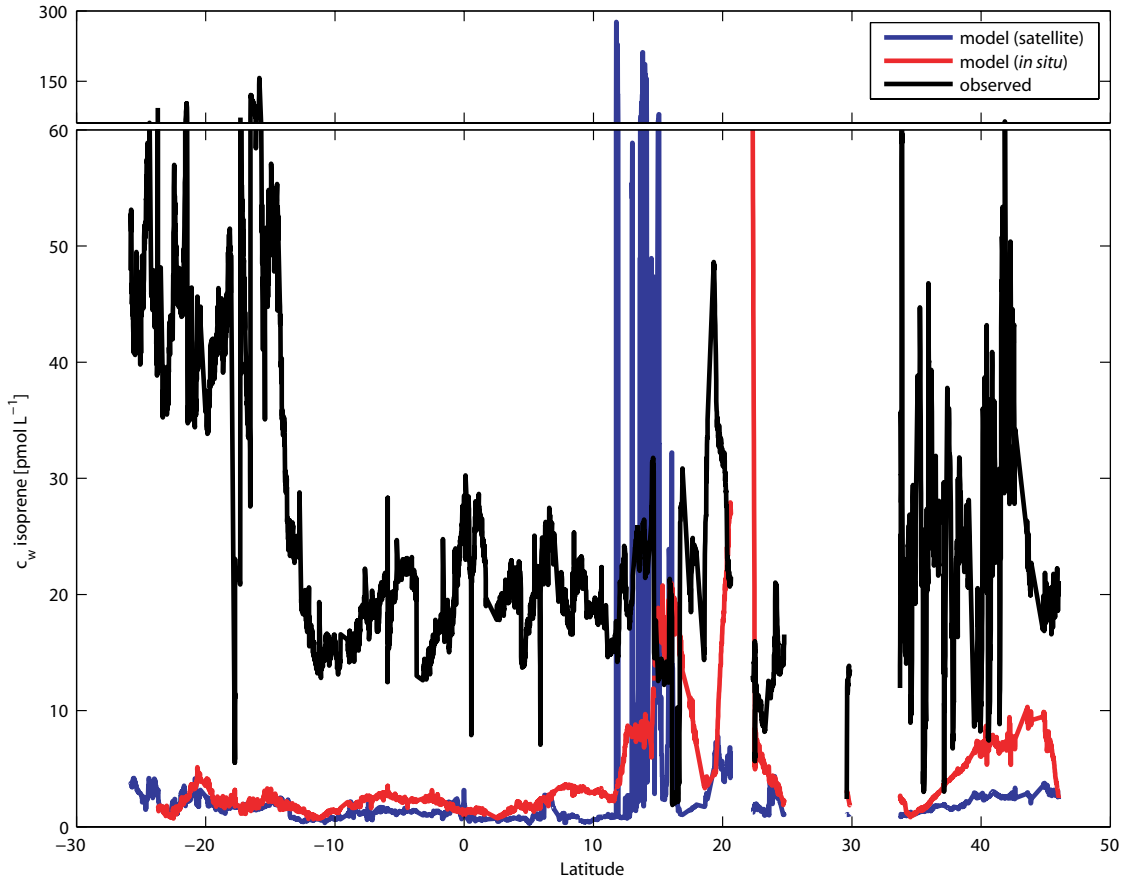
Figure 4.2: Comparison of observed (black) and modeled seawater isoprene concentrations for the ANT-XXV/1 cruise. Model calculations were carried out using the ISOPS05 model configuration, with monthly mean satellite data (blue) for chl-a, wind speed, SST, and MLD (climatology) and in situ shipboard measurements (red).

Monthly mean satellite data cannot resolve rapid changes like short phytoplankton blooms or wind events. We compared the satellite data to the ship's in situ measurements of SST, wind speed, calculated MLD, and in situ measured chl-a concentration as input parameters for the model (Figure 4.3) in order to determine if the resolution of the satellite data does resolve important features. The modeled isoprene concentrations closely follow the variability in chl-a, demonstrating that chl-a has the strongest influence of the four input parameters to the model. The differences between modeled isoprene concentrations using in situ data vs. satellite data are due primarily to the differences in chl-a (in situ data are in general 2 times higher than satellite data) with the largest differences in the regions from 10–25 to 40–45°N. As the discrepancies between in situ and satellite data are significant, in situ measured data of chl-a are used from now on for further calculations with the ISO_{PS05} model. Using monthly mean satellite data for wind speed, SST, and climatological values for MLD does not bias the model results significantly relative to the in situ data. Eight-day mean chl-a and weekly wind speed satel-

lite data (not shown) are also available and could lower the discrepancies to the in situ data. For this study, 8-day values were not useful for this region and time due to cloud coverage (loss of 46% of data points). A compromise between the two would be to average the 8-day values over a larger area grid to increase the amount of satellite-derived data, but this would lower the resolution and therefore the accurate comparison with the cruise track.
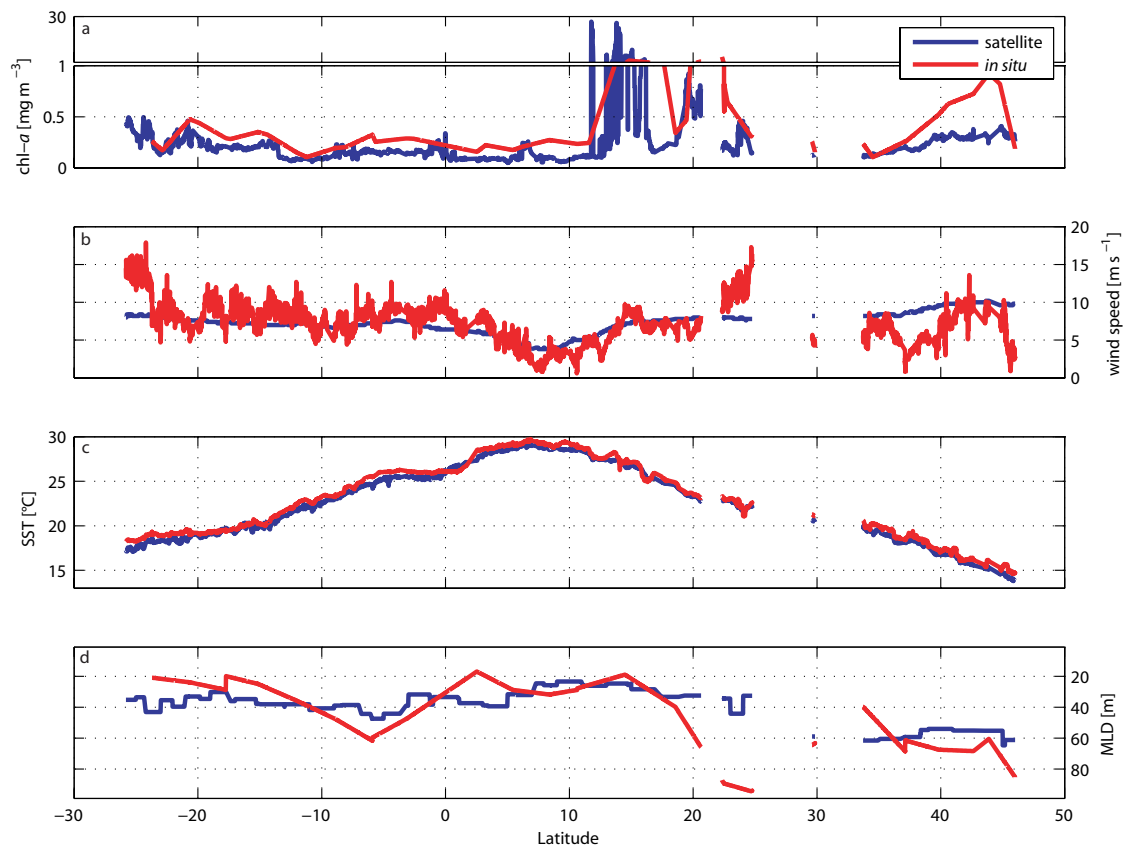
Figure 4.3: Satellite and in situ data for the ANT-XXV/1 cruise. Monthly mean satellite derived data (blue) and in situ measurements (red) of (a) chl-a, (b) wind speed, (c) SST. (d) Monthly mean climatology values (blue) and in situ measurements (red) of MLD.
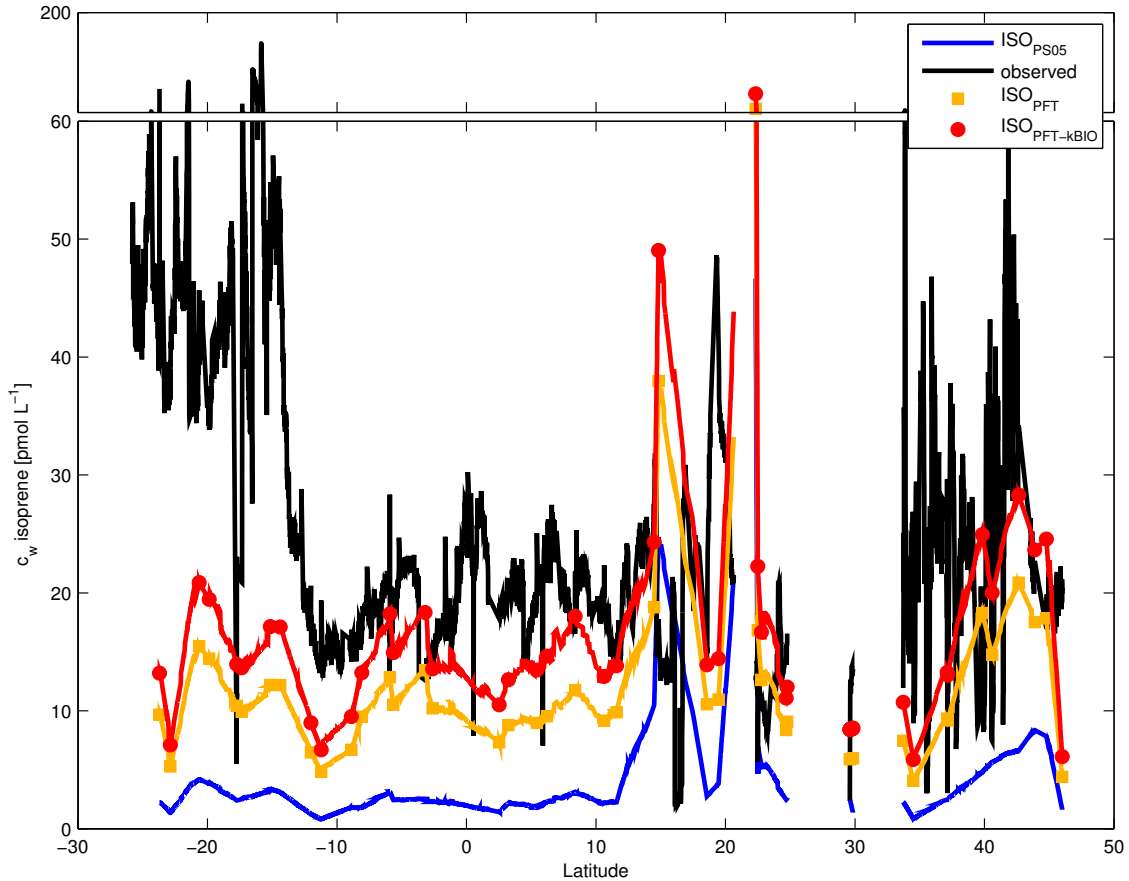
Figure 4.4: Comparison of in situ measured isoprene (black) with model derived isoprene concentrations for the ANT-XXV/1 cruise using ISO_{PS05} (blue), ISO_{PFT} (orange) and $ISO_{PFT\text{-}kBIO}$ (red); squares and circles: direct measurements; solid lines: interpolated data.

4.3.2   Modeling isoprene production using PFTs and revised k_{BIOL}

PALMER and SHAW (2005) used a universal P_{chloro} value of 1.8±0.7 µmoles (g chl-a)$^-$^{1} day^{-1} based on laboratory phytoplankton monoculture experiments with several cyanobacteria, eukaryotes, and coccolithophores (Table 4.1; SHAW et al., 2003). Subsequent laboratory experiments with monocultures of different phytoplankton species have shown generally higher isoprene production rates with large variations between PFTs (ARNOLD et al., 2009; BONSANG et al., 2010; COLOMB et al., 2008; EXTON et al., 2013). In addition, TRAN et al. (2013) observed that isoprene concentrations in the field are highly PFT dependent.

We averaged the P_{chloro} values of different PFTs (Table 4.2) and multiplied these values by the amount of the corresponding PFT. Using PFTs instead of total biomass of phytoplankton (chl-a) in the model run results in higher isoprene model concentrations (orange, Figure 4.4), which match the overall isoprene concentration levels measured north of 10°N quite well. However, there are also regions where the model still cannot reproduce the measured isoprene concentrations. Between 10°N and 25°S, the calculated

isoprene concentrations are quite stable with only small variations between 6 and 23 pmol L^{-1}. Measured concentrations are slightly higher between 10°N and 12°S (15-30 pmol L^{-1}) and sharply increase to 40-60 pmol L^{-1} south of 12°S with a maximum concentration of 150 pmol L^{-1} (16°S). As there were no significant differences in wind speed, SST, or MLD in these two regions during the cruise, there must be at least one additional source which is not captured in the model. In contrast, at 15°N and at 22°N the model overestimates the isoprene concentration (Figure 4.4). Chl-a concentrations are 10−20 times higher in these two areas than elsewhere on the cruise (Figure 4.3) and dominated by diatoms. However, the calculated isoprene is not 10−20 times higher, since diatoms have a relatively low P_{chloro} value (2.54 µmol (g chl-a)$^{-1}$ day^{-1}) and, therefore, using their respective PFT value modulates the influence of the increased chl-a on isoprene concentrations (Figure 4.5).
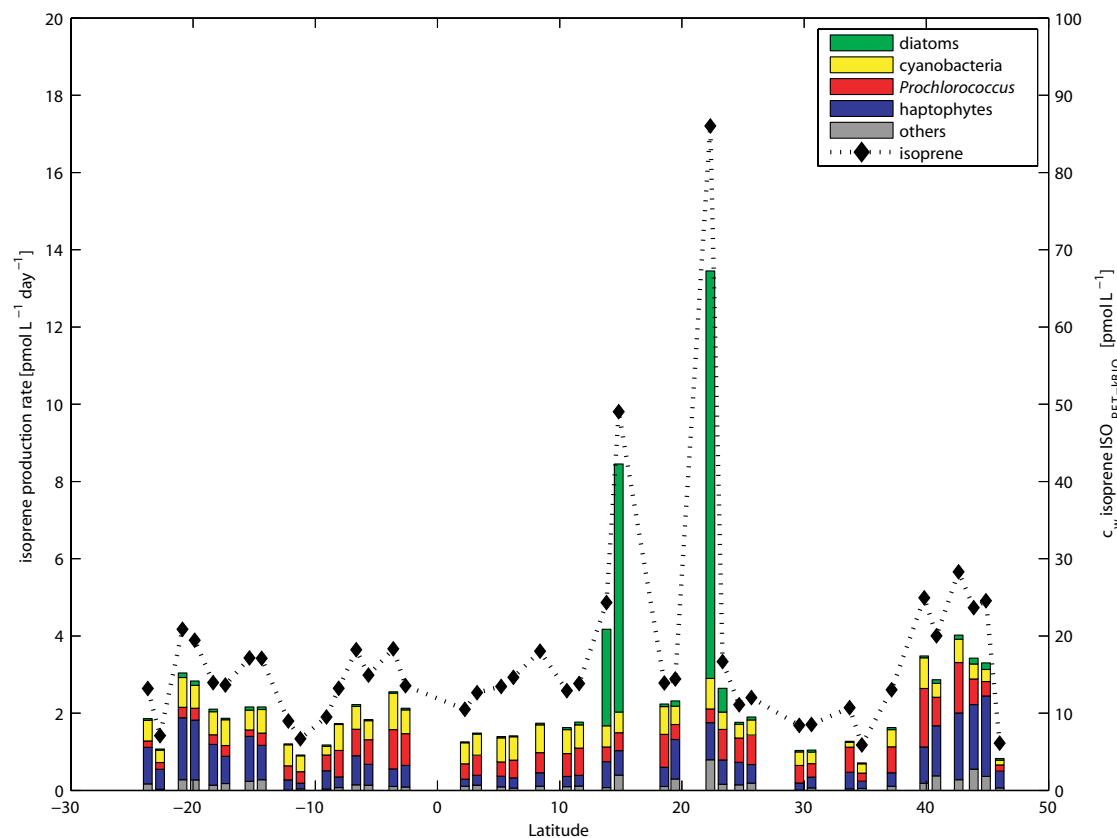
Figure 4.5: Proportion of main PFTs contributing to the total isoprene production rate for each station during ANT-XXV/1.

Excluding the two bloom areas, the main PFTs contributing to the modeled isoprene concentrations were prokaryotic phytoplankton (cyanobacteria and *Prochlorococcus*) and haptophytes (Figure 4.5, see also TAYLOR et al., 2011b). It should be noted that the PFTs considered in our study are only part of the full phytoplankton community. In addition, these values can be easily over- or underestimated due to a high variability in the Pc$_{hloro}$ values within one group of PFTs (e.g., haptophytes: 1-15.36 µmol isoprene (g chl-

a)$^{-1}$ day^{-1}; Table 4.2). Using the ISO$_{PFT-kBIO}$ model approach, the isoprene concentrations increase by a factor of 1.35, resulting in better agreement with the observations (Figure 4.4). Overall for the conditions of this cruise, the ISO$_{PFT-kBIO}$ model simulation yields 12-fold higher isoprene levels than ISO$_{PS05}$ (mean error of 11.8 pmol L^{-1}).

It is obvious that even after implementing these changes the model does not reproduce all the measured isoprene values or their distribution pattern. One particular problem is that marine isoprene emissions are very low in comparison to terrestrial isoprene emissions. Coastal emissions have to be calculated and interpreted carefully due to this terrestrial influence. We assume no terrestrial influence in the open ocean, since the atmospheric lifetime of isoprene is short. Despite the terrestrial influence on atmospheric isoprene values over the ocean, calculating surface ocean isoprene concentrations, other assumptions in the model should be scrutinized in order to understand the discrepancies between measured and calculated values:

1. The model assumes well-mixed isoprene concentrations through the MLD, which is, in fact, not the case. Measurements of depth profiles show a vertical gradient with a maximum of isoprene at the depth of the chl-a maximum slightly below the MLD (BONSANG et al., 1992; MILNE et al., 1995; MOORE and WANG, 2006), which was also measured during our three campaigns (data not shown). GANTT et al. (2009) tried to solve this problem using a light-dependent isoprene production rate, but this resulted in high fluxes in the tropics that are questionable when compared to field measurements.

2. Using PFT-dependent production rates strongly improved the model by adding more specific and realistic product information. Nonetheless, we may still be missing some important species within the PFTs, and the average taken over the isoprene measurements among the cultured species within one PFT carries some uncertainty. We used up to eight different PFTs, illustrating that only the four main groups (haptophytes, cyanobacteria, *Prochlorococcus*, and diatoms) produce the most isoprene (Figure 4.5). These groups are also the only four detected by the satellite product PHYSAT (ALVAIN et al., 2005), which has been used previously for predictions of isoprene (ARNOLD et al., 2009; GANTT et al., 2009). However, neglecting the other PFTs might lead to different results (others, Figure 4.5). This highlights the need to measure the isoprene emission of more species within each PFT group under different physiological conditions. Emissions in laboratory culture experiments can vary depending on the growth stage of the phytoplankton species (MILNE et al., 1995). SHAW et al. (2003) showed that the health conditions of the phytoplankton species directly influence the emission rates of isoprene when using phage-infected cultures. However, also environmental stress factors, such as temperature and light, influence the ability of different species to produce isoprene (EXTON et al., 2013; MESKHIDZE et al., 2015; SHAW et al., 2003). More exact data would also, potentially, lower the uncertainty of global marine isoprene emissions, which was found to be in the range of 20% when using the upper or lower bounds of PFT-dependent production rates (GANTT et al., 2009).

3. The temporal resolution of the simple model may also not be adequate. GANTT et al. (2009) could show that their model, using remote sensing input in combination with the light dependence of isoprene production, overestimated daytime isoprene concentrations and underestimated nighttime concentrations compared to the high temporal resolution field measurements of MATSUNAGA et al. (2002). The possible diurnal cycle of isoprene could not be resolved with remote sensing data obtained only at a specific local time during the day (e.g., 10:00 for MODIS Terra and 13:00 for MODIS Aqua).

4. The role of bacteria in producing isoprene is also unclear and may be a missing variable in the steady-state equation. ACUÑA ALVAREZ et al. (2009) observed bacterial isoprene production in estuary sediments and discovered isoprene production using different cultures of bacteria. However, SHAW et al. (2003) could not find any evidence of bacterial isoprene production in separate experiments.

Table 4.2: Chlorophyll-normalized isoprene production rates (P_{chloro}) determined from analysis of phytoplankton cultures experiments described in the literature (EXTON et al. (2013) and references therein). P_{chloro}-values are given in µmol (g chl-a)$^{-1}$ day^{-1}.

Species	Literature P_{chloro} value	Averaged P_{chloro} values for specific PFTs	References
Bacillariophyceae			
Chaetoceros neogracilis (CCMP1318)	28.48		COLOMB et al. (2008)
Cheatoceros neogracilis (CCMP 1318)	1.26 ±1.19		BONSANG et al. (2010)
Thalassiosira pseudonana (CCAP 1085/12)	5.76 ±0.24		EXTON et al. (2013)
Pelagomonas calceolate (CCMP 1214)	1.6 ±1.6		SHAW et al. (2003)
Phaeodactylum tricornutum (Falkowski)	2.85		COLOMB et al. (2008)
Phaeodactylum tricornutum (UTEX646)	1.12 ±0.32	2.54	BONSANG et al. (2010)
Skeletonema costatum	1.32 ±1.21		BONSANG et al. (2010)
Skeletonema costatum (CCMP 1332)	1.8		SHAW et al. (2003)
Thalassiosira weissflogii (CCMP 1051)	4.56 ±0.24		EXTON et al. (2013)
Diatoms (elsewhere)	2.48 ±1.75		ARNOLD et al. (2009)
Cylindrotheca sp.	2.64		EXTON et al. (2013)
cold adapted Bacillariophyceae			
Fragilariopsis kerguelensis	0.56 ±0.35		BONSANG et al. (2010)
Chaetoceros debilis	0.65 ±0.2		BONSANG et al. (2010)
Chaetoceros muelleri (CCAP 1010/3)	9.36 ±1.2	Excluded from the average isoprene production rate	EXTON et al. (2013)
Fragilariopsis cylindrus	0.96 ±0.24		EXTON et al. (2013)
Nitzschia sp. (CCMP 1088)	0.96 ±0.24		EXTON et al. (2013)
Synedropsis sp. (CCMP 2745)	0.72 ±0.24		EXTON et al. (2013)
Diatoms (Southern Ocean)	1.21 ±0.57		ARNOLD et al. (2009)

Species	Literature P_{chloro} value	Averaged P_{chloro} values for specific PFTs	References
Dinophyceae			
Prorocentrum minimum	10.08 ±1.44		EXTON et al. (2013)
Symbiodinium sp. (CCMP 2464)	4.56 ±3.12		EXTON et al. (2013)
Symbiodinium sp. (CCMP 2469)	17.04 ±8.4	13.78	EXTON et al. (2013)
Symbiodinium sp.	9.6 ±2.8		EXTON et al. (2013)
Symbiodinium sp. (CCMP 2463)	27.6 ±1.68		EXTON et al. (2013)
Cyanophyceae			
Prochlorococcus sp. (axenic MED4) (high light)	1.5 ±0.9	1.5	SHAW et al. (2003)
Prochlorococcus	9.66 ±5.78	9.66	ARNOLD et al. (2009)
Synechococcus sp. (RCC 40)	4.97 ±2.87		BONSANG et al. (2010)
Synechococcus sp. (WH 8103)	1.4	6.04	SHAW et al. (2003)
Synechococcus sp. (CCMP 1334)	11.76 ±0		EXTON et al. (2013)
Chlorophyceae			
Dunaliella tertiolecta	0.36 ±0.22		BONSANG et al. (2010)
Dunaliella tertiolecta (DUN, Falkowski)	2.85	1.47	COLOMB et al. (2008)
Dunaliella tertiolecta (CCMP 1320)	1.2		EXTON et al. (2013)
Cryptophyceae			
Rhodomonas lacustris (CCAP 995/3)	9.36 ±0.72	9.36	EXTON et al. (2013)
Prasinophyceae			
Micromonas pusilla (CCMP 489)	1.4 ±0.8		SHAW et al. (2003)
Prasinococcus capsulatus (CCMP 1614)	32.16 ±5.76	12.47	EXTON et al. (2013)
Tetraselmis sp. (CCMP 965)	3.84 ±0.24		EXTON et al. (2013)
Prymnesiophyceae			
Calcidiscus leptoporus (AC365)	5.4		COLOMB et al. (2008)
Emiliania huxleyi (CCMP 371)	11.54		COLOMB et al. (2008)
Emiliania huxleyi (CCMP 371)	1		BONSANG et al. (2010)
Emiliania huxleyi (CCMP 373)	1 ±0.5	6.92	SHAW et al. (2003)
Emiliania huxleyi (CCMP 373)	2.88 ±0.48		EXTON et al. (2013)
Emiliania huxleyi (CCMP 1516)	11.28 ±0.96		EXTON et al. (2013)
Gephyrocapsa oceanica	15.36 ±4.1		EXTON et al. (2013)

4.3.3 Verification of the ISO$_{PFT-kBIOL}$ model using data from the Indian and eastern Pacific Oceans

Isoprene concentrations calculated with the original (ISO$_{PS05}$) and revised (ISO$_{PFT-kBIOL}$) model are compared to measured isoprene in the surface ocean at two additional campaigns in two widely differing ocean basins (Indian Ocean, SPACES/OASIS, 2014; eastern Pacific Ocean, ASTRA-OMZ, 2015). The original model ISO$_{PS05}$ predicts on average 19±12 times lower isoprene concentrations compared with measured values for the additional two ship campaigns (circles, Figure 4.6), which confirms the results obtained for ANT-XXV/1. With the newly determined (lower) value for k$_{BIOL}$ and PFT-dependent P$_{chloro}$ values, the ISO$_{PFT-kBIO}$ model predicts concentrations that are 10 times higher than the original model ISO$_{PS05}$ output (crosses, Figure 4.6). This leads to a mean underestimation of 1.7±1.2 between modeled and measured isoprene concentrations. The main cause of the better agreement between measured and modeled isoprene concentrations is the isoprene production rate related to the production input parameter (color coding, Figure 4.6). The mean isoprene production rate using chl-a as an input parameter multiplied
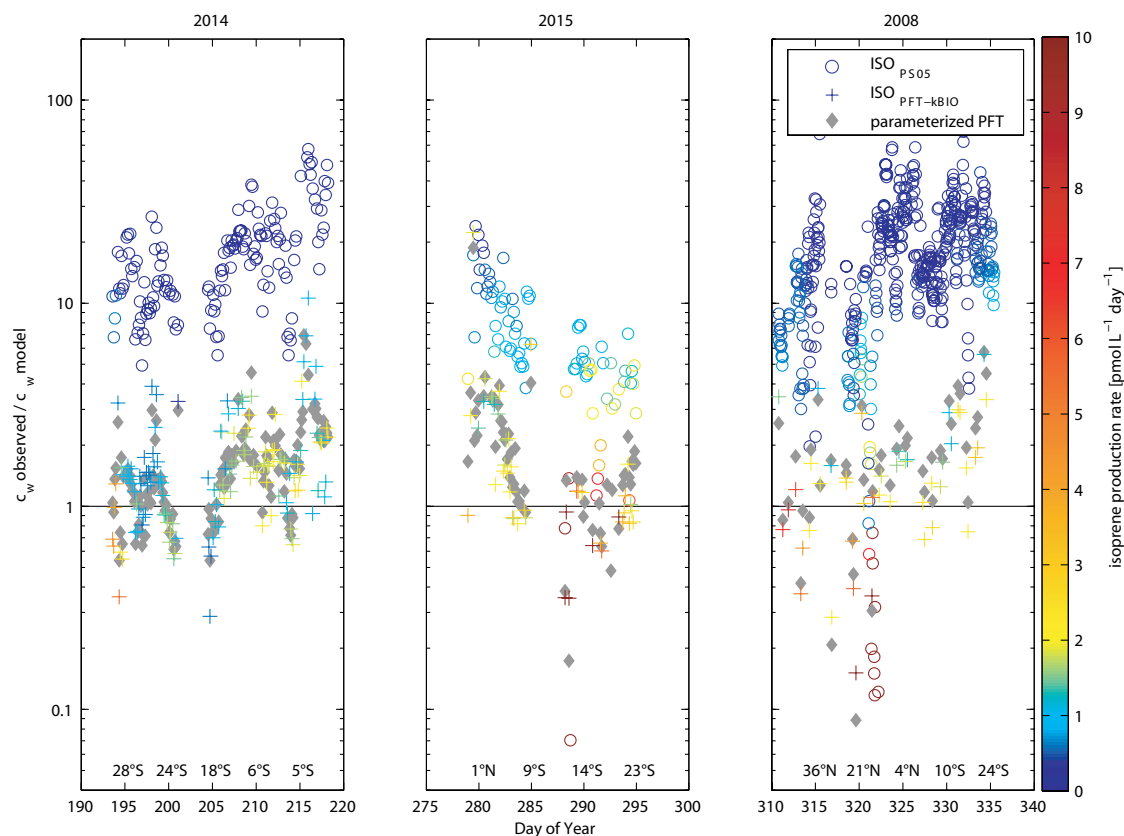
Figure 4.6: Observed isoprene concentration divided by modeled isoprene concentration on a logarithmic scale for three different cruises; left: SPACES/OASIS 2014, middle: ASTRA-OMZ 2015, right: ANT-XXV/1 2008; circles and crosses represent data derived by the original ISO$_{PS05}$ and revised ISO$_{PFT-kBIO}$ model, respectively; every data point is color coded with the corresponding isoprene production rate input parameter; grey diamonds represent data using parameterized PFT data by HIRATA et al. (2011); the black line represents a ratio of 1.

by a factor of 1.8 µmol (g chl-a)$^{-1}$ day^{-1} is less than 0.5 pmol L^{-1} day^{-1}, which is insufficient to explain the measured concentrations in all three campaigns. Using P$_{chloro}$ values multiplied with the concentration of the related PFT yields in an isoprene production rate of 1–2 pmol L^{-1} day^{-1} in non-bloom areas and even higher rates during phytoplankton blooms, resulting in isoprene concentrations that are comparable to the measured ones. The opposite can also occur, as seen on DOY 322 (Figure 4.6), when PFT specific production rates are smaller than those using chl-a only, due to the dominance of a low isoprene-producing PFT. Even though the improved model is tested in three widely different ocean basins, there are still different regions where the model should be tested with direct isoprene measurements to verify the model output.

4.4 Global oceanic isoprene emissions and implications for marine aerosol formation
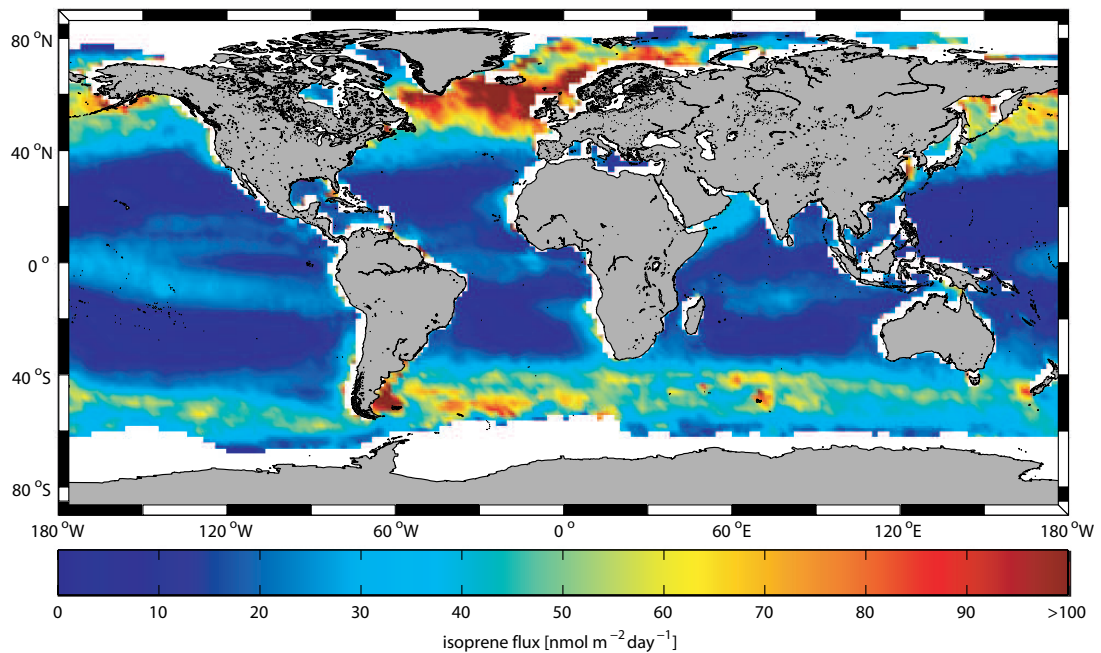
Figure 4.7: Global marine isoprene fluxes in nmol m^{-2} day^{-1} for 2014.

Monthly mean global ocean isoprene concentrations were calculated using the revised model ISO$_{PFT-kBIO}$ (2° x 2° grid). As there were no PFT satellite data readily available, we used an empirical relationship between chl-a and PFTs as parameterized by HIRATA et al. (2011). The quality of this parameterization was verified against the PFT data sets from all three campaigns (coefficient of determination: R^2=0.89, Figure S4.1 in the supplement) and is shown in Figure 4.6 (grey diamonds). Monthly mean global ocean isoprene emissions (Figures S4.2-S4.13 in the supplement) were averaged in order to compute global sea-to-air fluxes of isoprene for 2014 (Figure 4.7). An annual emission of 0.21 Tg C was calculated, which is 2 times higher than the value estimated by PALMER and SHAW (2005) (0.11 Tg C yr^{-1}). The highest emissions, more than 100 nmol m^{-2} day^{-1},

can be seen in the North Atlantic Ocean and the Southern Ocean, associated with high biological productivity and strong winds driving the air–sea gas exchange. The influence of regional hot spots of biological productivity, such as the upwelling off Mauretania or the Brazil–Malvinas Confluence Zone, can also be seen. The tropics (23.5°S–23.5°N) account for only 28% of global isoprene emissions, but they represent ~47% of the world oceans.

Yearly emissions of 0.21 Tg C are at the lower end of the range of previously published studies (Arnold et al., 2009, 0.27 Tg C yr-1; Gantt et al., 2009, 0.92 Tg C yr-1). Both studies use remotely sensed PFT data instead of chl-a to evaluate the isoprene production. Unlike this study, they implemented the Alvain et al. (2005) approach using PHYSAT data, which uses spectral information to produce global distributions of the dominant PFT but is limited to four phytoplankton groups (haptophytes, *Prochlorococcus*, *Synechococcus*, and diatoms). It should be noted that PHYSAT does not provide actual concentrations but rather only the relative dominance of the four groups. Arnold et al. (2009) used similar assumptions as Palmer and Shaw (2005) to calculate isoprene loss, namely that loss in the water column by advective mixing and aqueous oxidation is on a longer timescale than loss by air-sea gas exchange and, therefore, negligible. Thus, their calculated emissions of 0.27 TgC yr^{-1} are an upper estimate. The approach of had two main differences compared to our study. (1) Instead of using the MLD climatology of de Boyer Montégut et al. (2004), they used a maximum depth where isoprene production can occur as calculated by the downwelling irradiance (using the diffuse attenuation coefficient values at 490 nm) and the light propagation throughout the water column that is estimated by using the Lambert–Beer law. (2) They tested two of the detectable PFTs in laboratory experiments using monocultures of diatoms and coccolithophores growing under different light conditions to evaluate light-intensity-dependent isoprene production rates. Light-intensity-dependent production rates of *Prochlorococcus* and *Synechococcus* were derived after Gantt et al. (2009) using the original production rates at a specified wavelength measured by Shaw et al. (2003). Their isoprene emission calculations are more than 4 times higher than calculated with our approach, probably as a result of the light-dependent isoprene production rates. Whereas our global map shows very low emissions in the tropics due to a low phytoplankton productivity, the emissions modeled by Gantt et al. (2009) are comparable to those of high productivity areas like the Southern Ocean or the North Atlantic Ocean, likely as a consequence of the high solar radiation in the tropics. The data from our three cruises contradict this model-derived result and show very low concentrations in the tropical regions, which implies a very low flux of isoprene to the atmosphere. Furthermore, Meskhidze et al. (2015) showed that, at a specific light intensity, the isoprene production rate of tested monocultures sharply decreases.

Using atmospheric isoprene concentrations measured in two of the three campaigns, we were able to use a top-down approach to calculate isoprene emissions in order to compare with the bottom-up flux estimates. We used a box model with an assumed marine boundary layer height (MBLH) of 800 m, which reflected the local conditions during the two campaigns. The only source of isoprene for the air was assumed to be the sea-to-air flux (emission) and the atmospheric lifetime (τ) was assumed to be determined by

reaction with OH (chemical loss, 1 h). The sea-to-air flux was calculated by multiplying k_{AS} with the measured isoprene concentration (C_W) in the ocean (Eq.(4.3)). We assumed C_A to be zero in order to have the highest possible sea-to-air-flux, following a conservative approach. The concentration outside the box was assumed to be the same as inside to neglect advection into and out of the box. The resulting calculated steady-state isoprene air concentration for every box (1-day mean value of all individual measurements at daytime) is shown in Figure 4.8 (for a 1 h lifetime it takes approximately 10 h to achieve steady state) and is calculated as follows:

$$C_A = (k_{AS} \times C_W) \frac{\tau}{MBLH}. \tag{4.5}$$
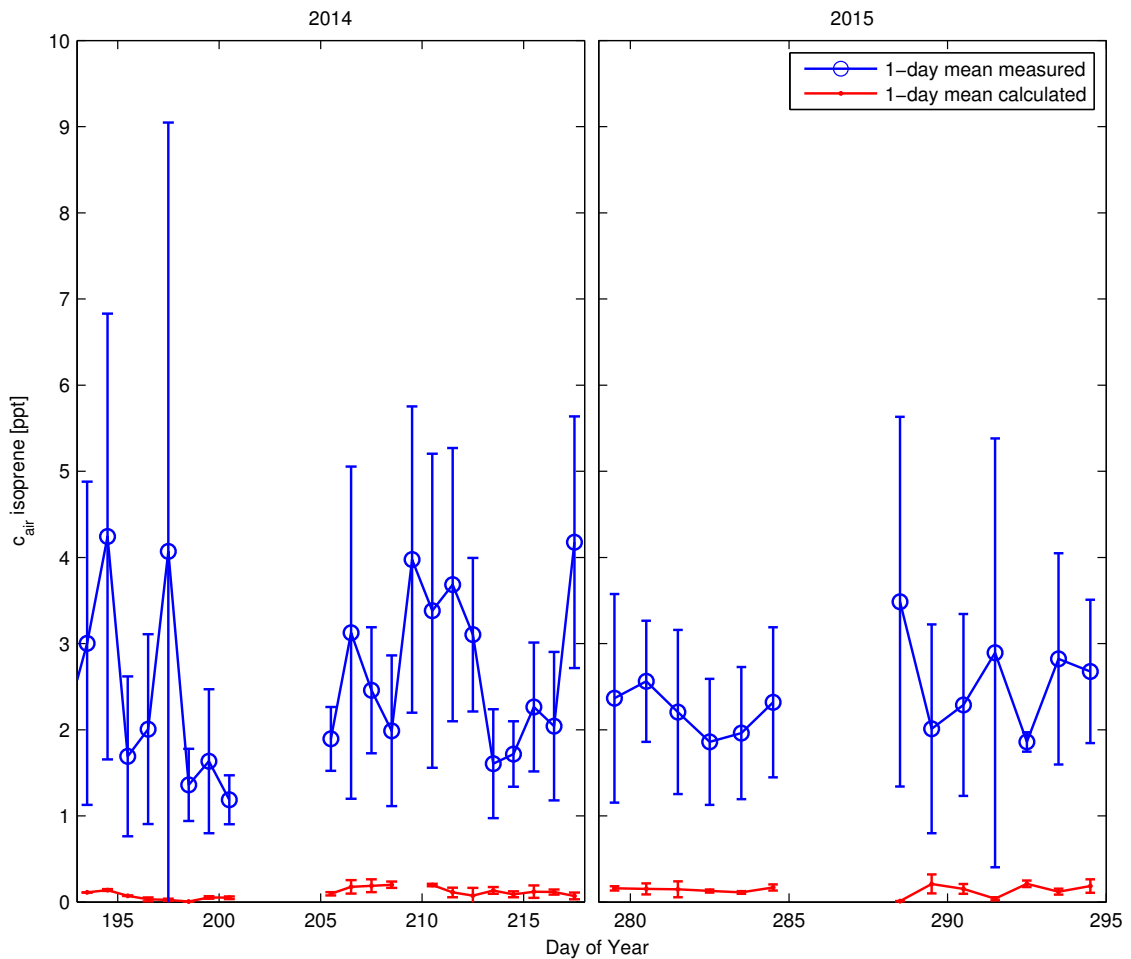
Figure 4.8: 1-day mean measured (blue) and calculated (red) daytime isoprene mixing ratios (ppt) during SPACES/OASIS (2014) and ASTRA-OMZ (2015). Calculated isoprene air values were derived by using the sea-to-air flux, a marine boundary layer height of 800 m and the one hour atmospheric lifetime based on a simple box model approach for each individual measurement.

For comparison, the mean measured concentration of isoprene in the atmosphere during the two cruises is 2.5±1.5 ppt and therefore 45 times higher than the calculated isoprene air values. The measured concentrations match previously measured remote open ocean atmospheric values (Shaw et al., 2003). We only used atmospheric measurements which were obtained during daytime (to reflect reaction with OH) and were not influenced by terrestrial sources. This was determined by omitting data points with concomitant high levels of anthropogenic hydrocarbons (concentrations of butane higher 20 ppt).

Reported mean atmospheric lifetime estimates of isoprene range from minutes up to 4 h, depending mainly on the atmospheric concentration of OH (PFISTER et al., 2008). We calculate that for an estimated lifetime of 1 and 4 h, a sea-to-air flux of at least 2000 and 500 nmol m^{-2} day^{-1}, respectively, is needed to reach the atmospheric concentration measured during SPACES/OASIS and ASTRA-OMZ, which is approximately 10−20 times higher than computed (even when assuming C_A as zero). Recent studies showed that the measured fluxes of isoprene range from 4.6−148 nmol m^{-2} day^{-1} in June−July 2010 in the Arctic (TRAN et al., 2013) to 181.0−313.1 nmol m^{-2} day^{-1} in the productive Southern Ocean during austral summer 2010/2011 (KAMEYAMA et al., 2014). Despite these high literature values, it appears that the calculated fluxes cannot explain the measured atmospheric concentrations even when a conservative lifetime of 4 h is assumed.

4.5 Conclusions

The revised PALMER and SHAW (2005) isoprene emission model was evaluated against direct surface ocean isoprene measurements from three different ocean basins, yielding comparable ocean concentrations that were slightly underestimated (factor of 1.7±1.2). The resulting annual global oceanic isoprene emissions are 2 times higher than the calculated flux with the original model. However, using a simple top-down approach based on measured atmospheric isoprene levels, we calculate that emissions from the ocean are required to be more than 1 order of magnitude greater than those computed using the bottom-up estimate based on measured oceanic isoprene levels. This result is consistent with a numerical evaluation of global ocean isoprene emissions by LUO and YU (2010). One possible explanation could be production in the surface microlayer (SML) that is not simulated by the model. CIURARU et al. (2015) showed that isoprene is produced photochemically by surfactants in an organic monolayer at the air−sea interface. As the SML is enriched with surfactants (WURL et al., 2011), the isoprene flux from the SML could range from 1000 to 33000 nmol m^{-2} day^{-1}, which is much larger (about 2 orders of magnitude) than the highest fluxes calculated from our observations. To date, there is no evidence of such a large gradient in the surface ocean between the surface and 10 m. Thus, further field measurements probing the SML could be a step forward in reconciling the role of the ocean for the atmospheric isoprene budget. Using the bottom-up approach, isoprene emissions are much smaller and given this scenario, isoprene consequently appears to be a relatively insignificant source of OC in the remote marine atmosphere. ARNOLD et al. (2009) calculated a yield of 0.04 Tg yr^{-1} OC derived from marine isoprene by using yearly emissions of 1.9 Tg yr^{-1} and a SOA yield of 2% (HENZE and SEINFELD, 2006). This is equivalent to 0.5% of estimated 8 Tg yr^{-1} global source of oceanic OC (SPRACKLEN et al., 2008). Using our bottom-up emission of 0.21 TgC yr^{-1} will even lower this small influence. Until this discrepancy between bottom-up and top-down approaches is resolved, the question of whether isoprene is a main precursor to remote marine boundary layer particle formation still remains open.

4.6   Data availability

All isoprene data are available from the corresponding author. Pigment data from ANT-XXV/1 are available from PANGAEA (Taylor et al., 2011a). Pigment data from SPACES/OASIS and ASTRA-OMZ will be available from PANGAEA but for now can be obtained through the corresponding author.

4.7   Acknowledgements

4.8   Supplementary material

Figure S4.1 shows the comparison between the measured isoprene production rate and the isoprene production rate derived from the phytoplankton functional type (PFT)-parameterization by Hirata et al. (2011). The comparison shows very good linear correlation in less productive regions (dashed regression line) whereas it is not linear over the whole range of isoprene production rates. The parameterization is dependent on the chl-a concentration and Figure S4.1 shows, fairly clearly, that the parameterization overestimates the PFT concentration and, therefore, the isoprene production rate (dotted regression line) in productive regions. The phytoplankton pigment data used in the parameterization of Hirata et al. (2011) is well distributed in the Atlantic Ocean, sparsely distributed in the Indian Ocean region of SPACES/OASIS, and there has been no data used

for the parameterization in the region off to Peru where ASTRA-OMZ took place. This may also cause some discrepancies between the measured and calculated values. But as these overestimated PFT values only account for 5% of our data set the overall coefficient of determination between the derived data using HIRATA et al. (2011) and the measured isoprene production rate is 0.89.
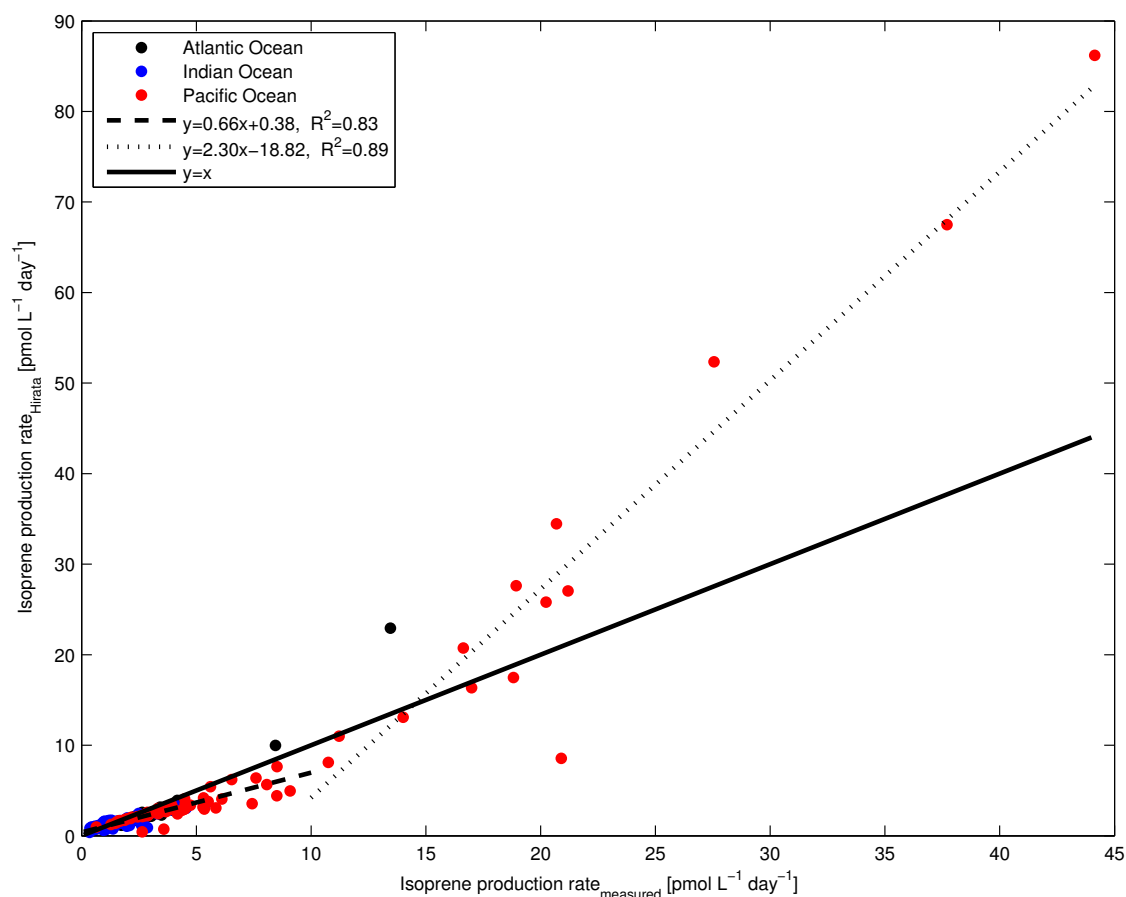
Figure S4.1: Measured isoprene production rates versus parameterized isoprene production rates from three different cruises (black: ANT-XXV/1; blue: SPACES/OASIS; red: ASTRA-OMZ). The dashed line and dotted line represent the regression line of isoprene production rates between 0 and 10 pmol L^{-1} day^{-1} and higher than 10 pmol L^{-1} day^{-1}, respectively. The solid line represents the 1:1 line.
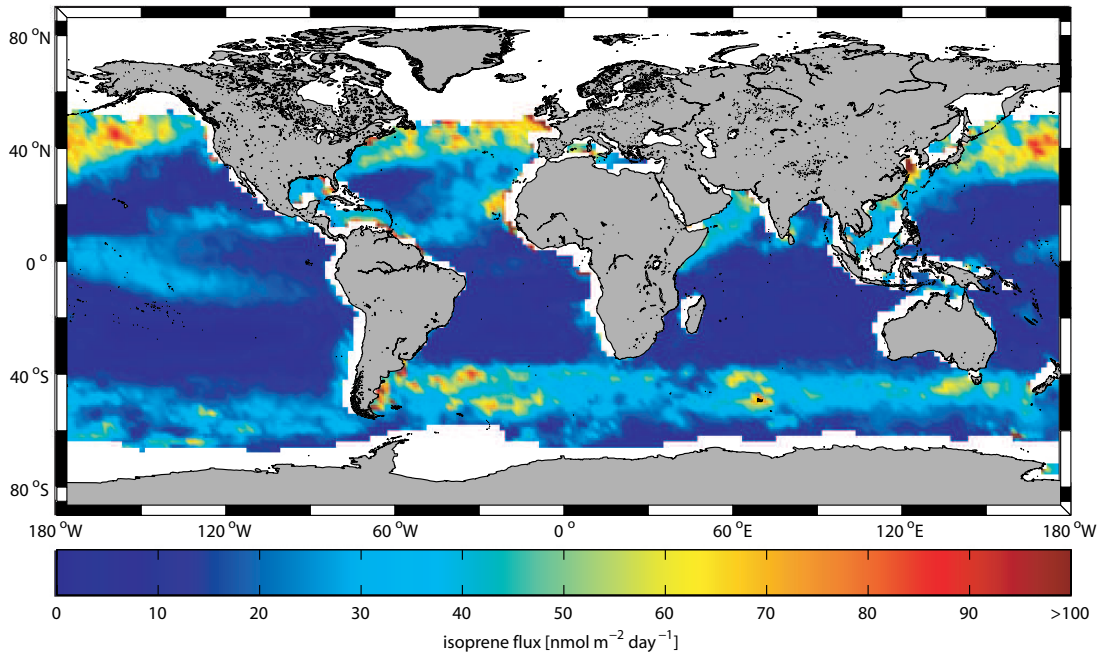
Figure S4.2: Global monthly mean marine isoprene fluxes in nmol m^{-2} day^{-1} for January 2014.
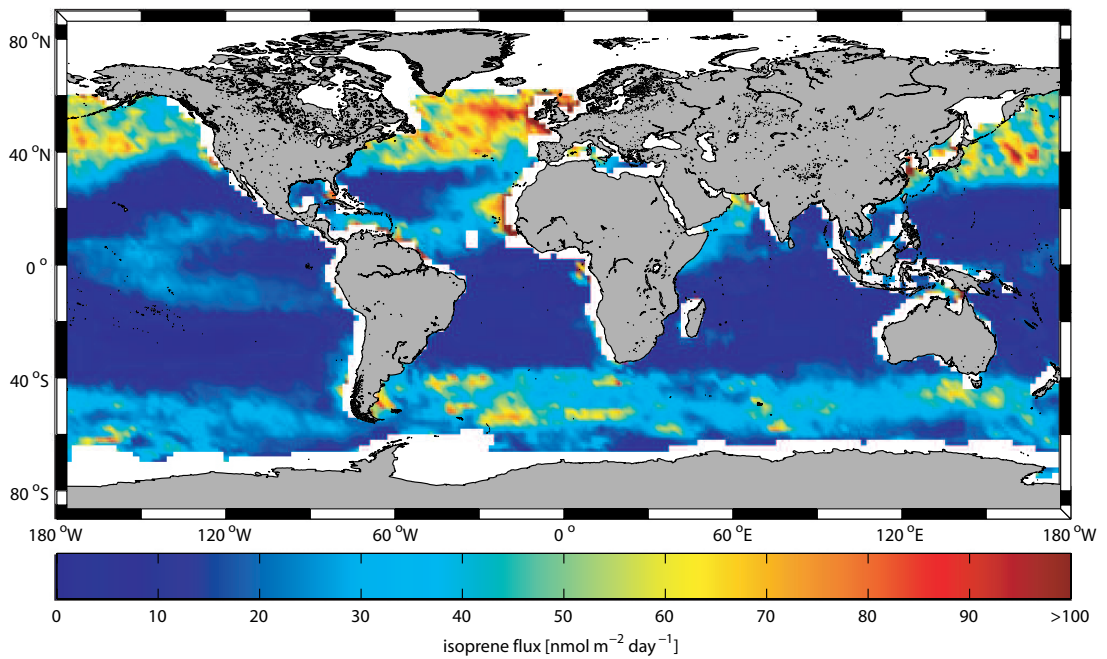
Figure S4.3: Global monthly mean marine isoprene fluxes in nmol m^{-2} day^{-1} for February 2014.
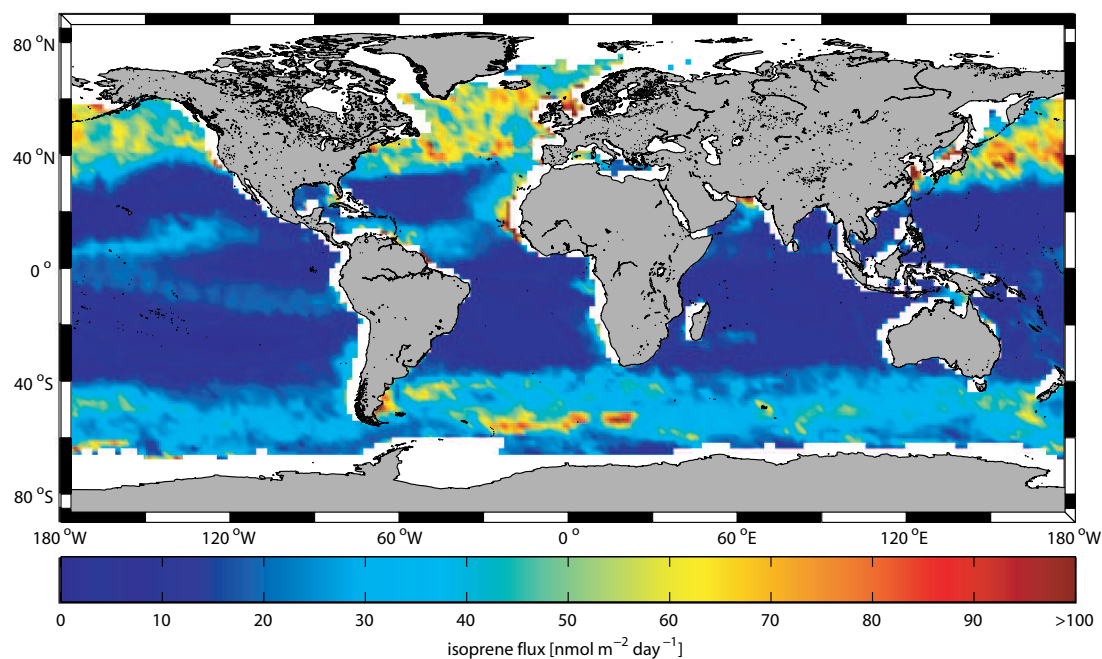
Figure S4.4: Global monthly mean marine isoprene fluxes in nmol m^{-2} day^{-1} for March 2014.
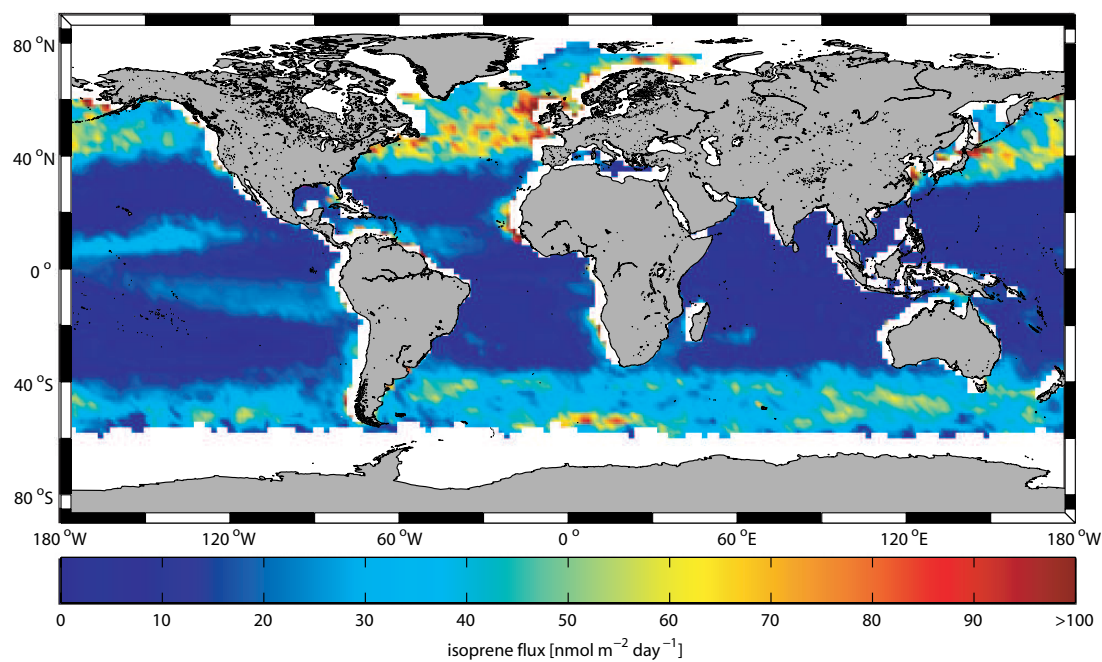
Figure S4.5: Global monthly mean marine isoprene fluxes in nmol m^{-2} day^{-1} for April 2014.
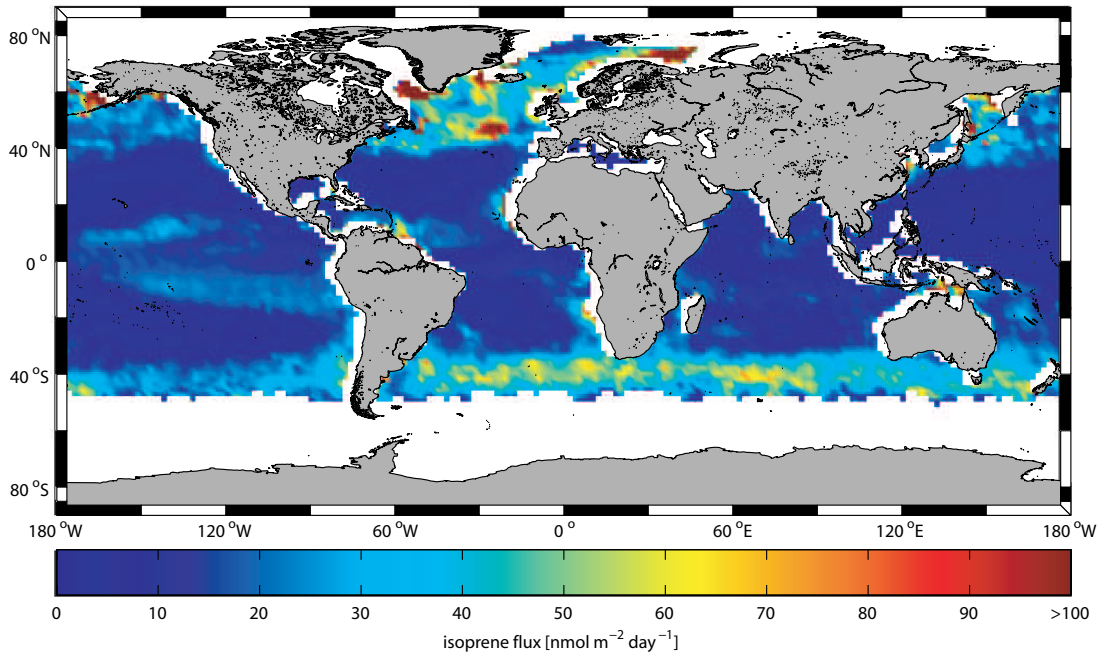
Figure S4.6: Global monthly mean marine isoprene fluxes in nmol m^{-2} day^{-1} for May 2014.
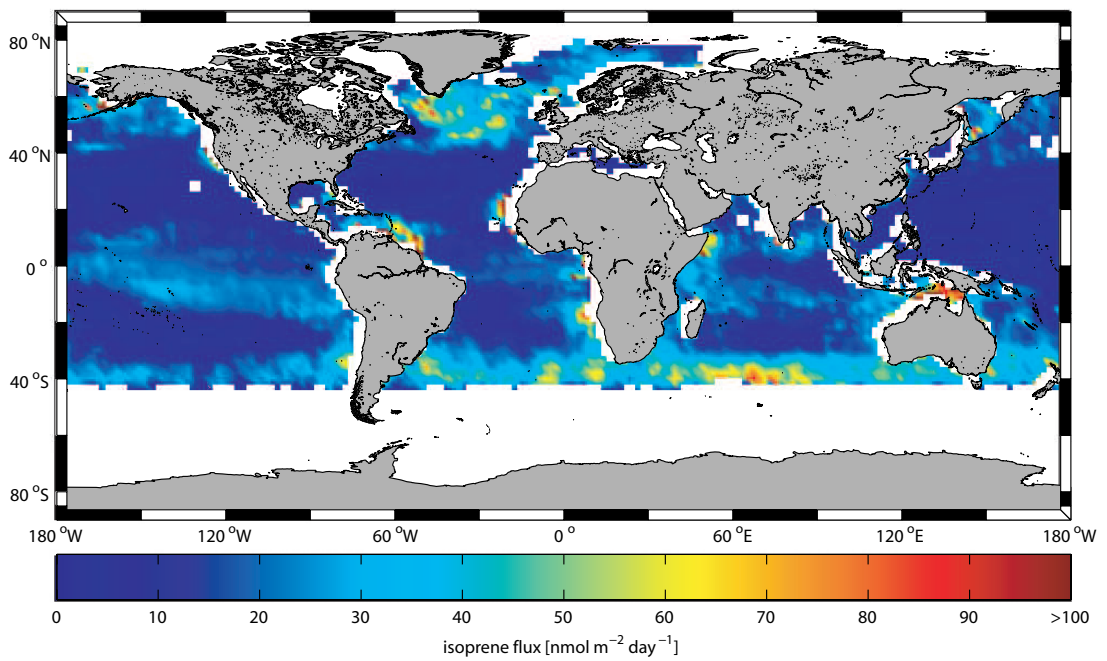
Figure S4.7: Global monthly mean marine isoprene fluxes in nmol m^{-2} day^{-1} for June 2014.
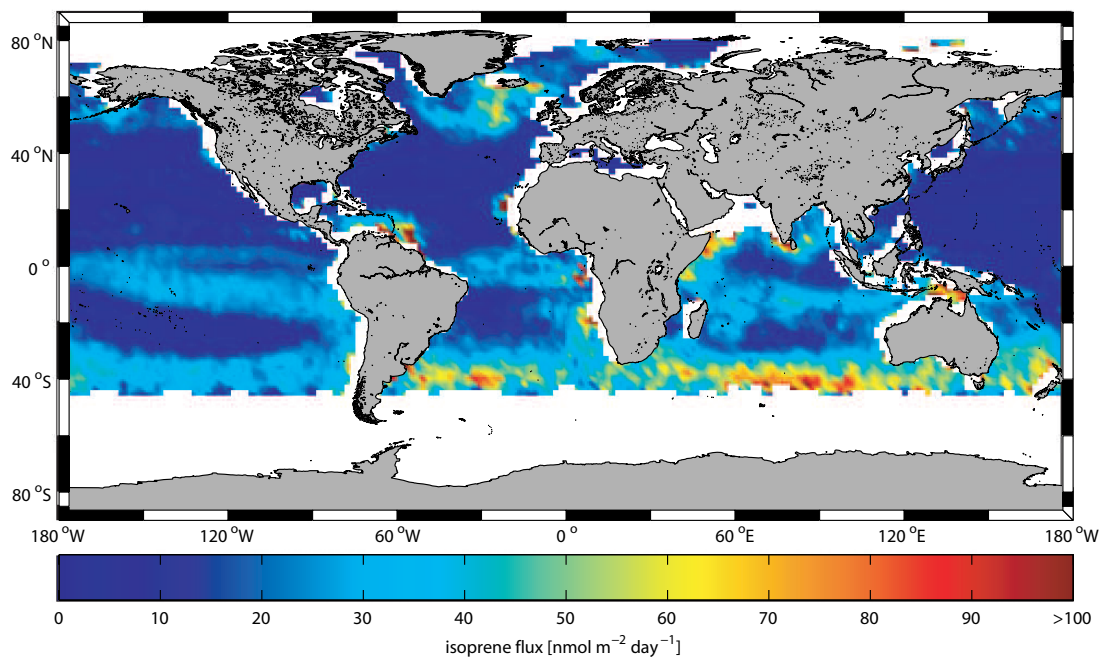
Figure S4.8: Global monthly mean marine isoprene fluxes in nmol m^{-2} day^{-1} for July 2014.
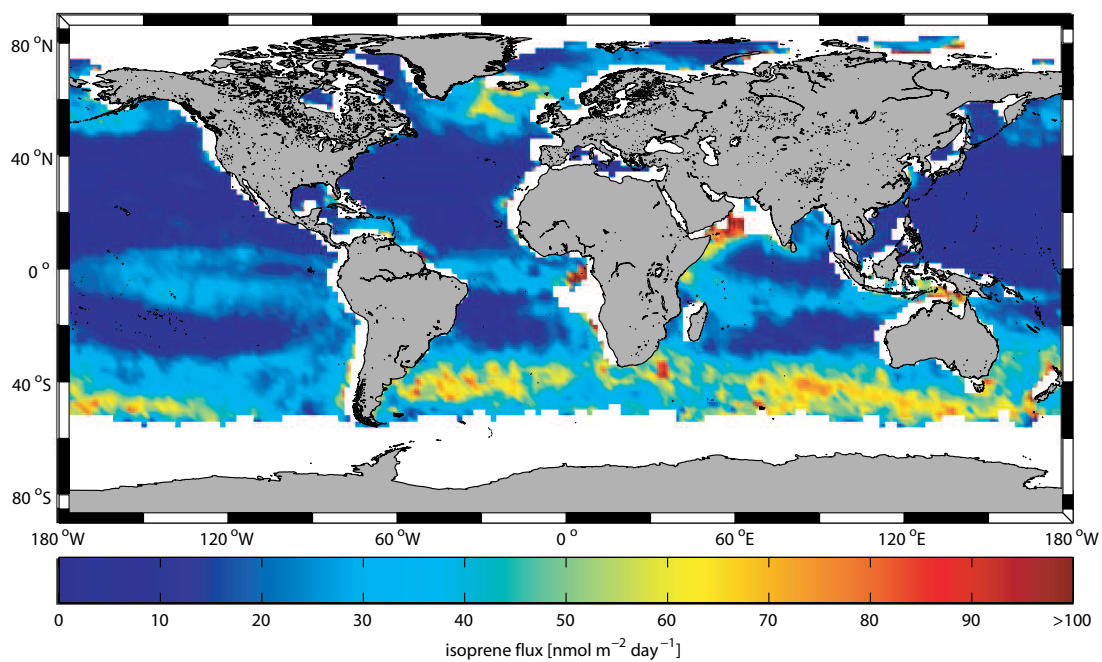
Figure S4.9: Global monthly mean marine isoprene fluxes in nmol m^{-2} day^{-1} for August 2014.
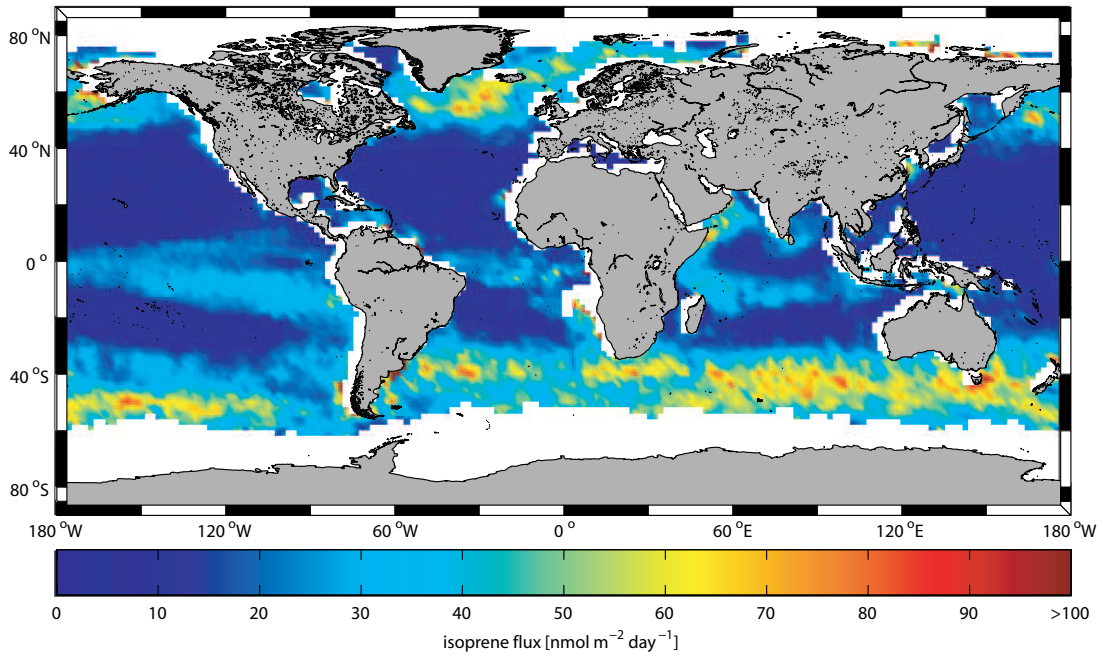
Figure S4.10: Global monthly mean marine isoprene fluxes in nmol m^{-2} day^{-1} for September 2014.
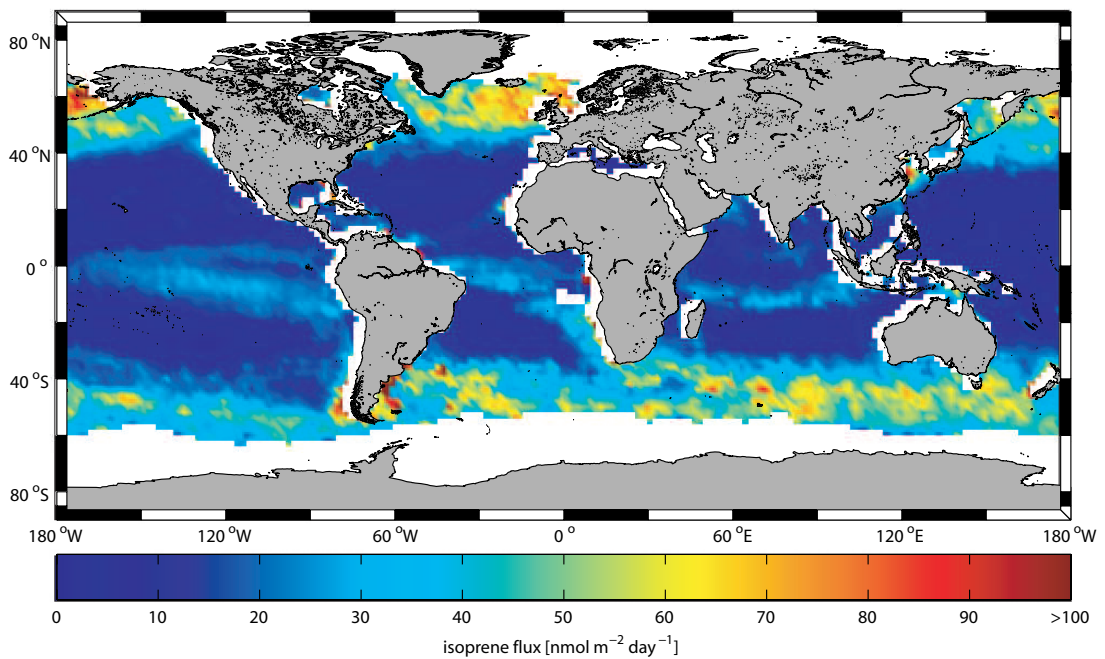
Figure S4.11: Global monthly mean marine isoprene fluxes in nmol m^{-2} day^{-1} for October 2014.
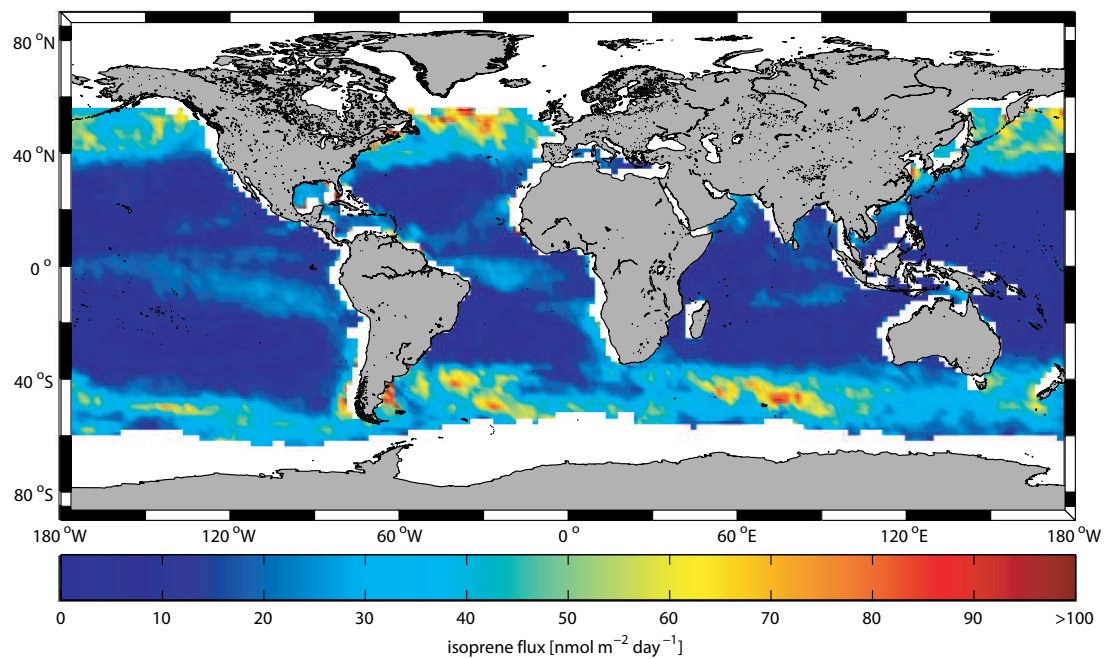
Figure S4.12: Global monthly mean marine isoprene fluxes in nmol m^{-2} day^{-1} for November 2014.
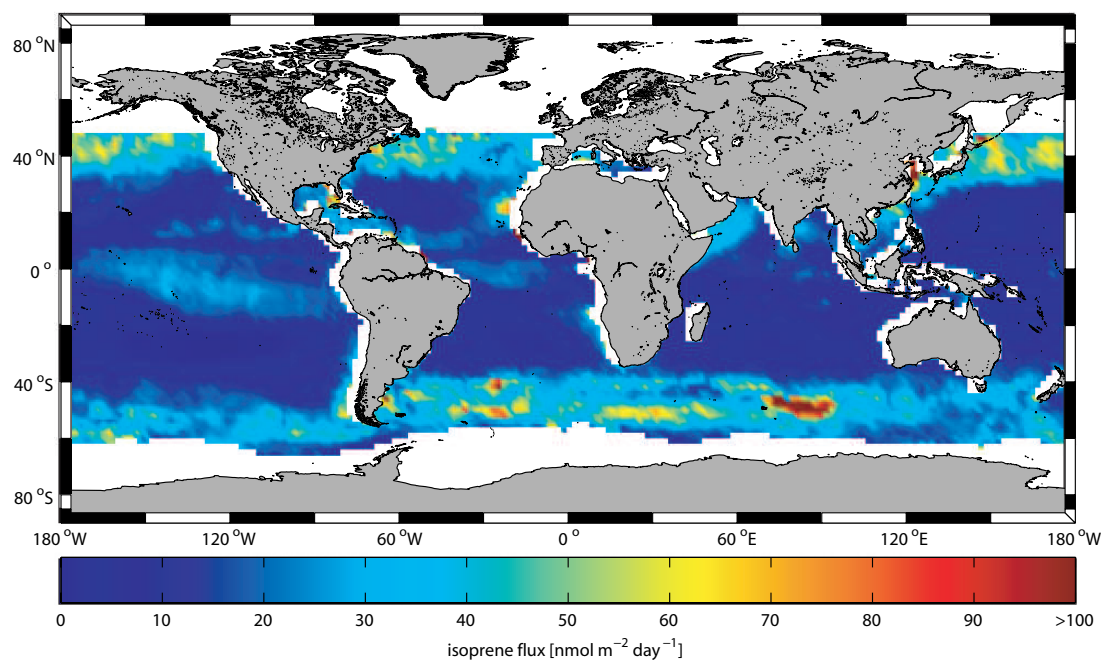
Figure S4.13: Global monthly mean marine isoprene fluxes in nmol m^{-2} day^{-1} for December 2014.

References

ACUÑA ALVAREZ, L., EXTON, D. A., TIMMIS, K. N., SUGGETT, D. J., and MCGENITY, T. J.: Characterization of marine isoprene-degrading communities, *Environmental Microbiology*, 11, 3280-3291, 10.1111/j.1462-2920.2009.02069.x, 2009.

AIKEN, J., PRADHAN, Y., BARLOW, R., LAVENDER, S., POULTON, A., HOLLIGAN, P., and HARDMAN-MOUNTFORD, N.: Phytoplankton pigments and functional types in the atlantic ocean: A decadal assessment, 1995-2005, *Deep-Sea Research Part Ii-Topical Studies in Oceanography*, 56, 899-917, 10.1016/j.dsr2.2008.09.017, 2009.

ALVAIN, S., MOULIN, C., DANDONNEAU, Y., and BREON, F. M.: Remote sensing of phytoplankton groups in case 1 waters from global seawifs imagery, *Deep-Sea Research Part I-Oceanographic Research Papers*, 52, 1989-2004, 10.1016/j.dsr.2005.06.015, 2005.

ANDREAE, M. O., and ROSENFELD, D.: Aerosol–cloud–precipitation interactions. Part 1. The nature and sources of cloud-active aerosols, *Earth-Science Reviews*, 89, 13-41, 10.1016/j.earscirev.2008.03.001, 2008.

ANTTILA, T., LANGMANN, B., VARGHESE, S., and O'DOWD, C.: Contribution of isoprene oxidation products to marine aerosol over the north-east atlantic, *Advances in Meteorology*, 10.1155/2010/482603, 2010.

ARNETH, A., MONSON, R. K., SCHURGERS, G., NIINEMETS, Ü., and PALMER, P. I.: Why are estimates of global terrestrial isoprene emissions so similar (and why is this not so for monoterpenes)?, *Atmos. Chem. Phys.*, 8, 4605-4620, 10.5194/acp-8-4605-2008, 2008.

ARNOLD, S. R., SPRACKLEN, D. V., WILLIAMS, J., YASSAA, N., SCIARE, J., BONSANG, B., GROS, V., PEEKEN, I., LEWIS, A. C., ALVAIN, S., and MOULIN, C.: Evaluation of the global oceanic isoprene source and its impacts on marine organic carbon aerosol, *Atmos. Chem. Phys.*, 9, 1253-1262, 10.5194/acp-9-1253-2009, 2009.

ATKINSON, R., and AREY, J.: Atmospheric degradation of volatile organic compounds, *Chemical reviews*, 103, 4605-4638, 2003.

BAKER, A. R., TURNER, S. M., BROADGATE, W. J., THOMPSON, A., MCFIGGANS, G. B., VESPERINI, O., NIGHTINGALE, P. D., LISS, P. S., and JICKELLS, T. D.: Distribution and sea-air fluxes of biogenic trace gases in the eastern atlantic ocean, *Global Biogeochemical Cycles*, 14, 871-886, Doi 10.1029/1999gb001219, 2000.

BARLOW, R. G., CUMMINGS, D. G., and GIBB, S. W.: Improved resolution of mono- and divinyl chlorophylls a and b and zeaxanthin and lutein in phytoplankton extracts using reverse phase c-8 hplc, *Marine Ecology Progress Series*, 161, 303-307, 10.3354/meps161303, 1997.

BONSANG, B., POLLE, C., and LAMBERT, G.: Evidence for marine production of isoprene, *Geophysical Research Letters*, 19, 1129-1132, Doi 10.1029/92gl00083, 1992.

BONSANG, B., GROS, V., PEEKEN, I., YASSAA, N., BLUHM, K., ZOELLNER, E., SARDA-ESTEVE, R., and WILLIAMS, J.: Isoprene emission from phytoplankton monocultures: The relationship with chlorophyll-a, cell volume and carbon content, *Environmental Chemistry*, 7, 554-563, 10.1071/En09156, 2010.

BROADGATE, W. J., LISS, P. S., and PENKETT, S. A.: Seasonal emissions of isoprene and other reactive hydrocarbon gases from the ocean, *Geophysical Research Letters*, 24, 2675-2678, 10.1029/97gl02736, 1997.

BROADGATE, W. J., MALIN, G., KUPPER, F. C., THOMPSON, A., and LISS, P. S.: Isoprene and other non-methane hydrocarbons from seaweeds: A source of reactive hydrocarbons to the atmosphere, *Marine Chemistry*, 88, 61-73, 10.1016/j.marchem.2004.03.002, 2004.

CARLTON, A. G., WIEDINMYER, C., and KROLL, J. H.: A review of secondary organic aerosol (soa) formation from isoprene, *Atmospheric Chemistry and Physics*, 9, 4987-5005, 2009.

CHARLSON, R. J., LOVELOCK, J. E., ANDREAE, M. O., and WARREN, S. G.: Oceanic phytoplankton, atmospheric sulfur, cloud albedo and climate, *Nature*, 326, 655-661, 10.1038/326655a0, 1987.

CIURARU, R., FINE, L., PINXTEREN, M. v., D'ANNA, B., HERRMANN, H., and GEORGE, C.: Unravelling new processes at interfaces: Photochemical isoprene production at the sea surface, *Environmental Science & Technology*, 49, 13199-13205, 10.1021/acs.est.5b02388, 2015.

COLOMB, A., YASSAA, N., WILLIAMS, J., PEEKEN, I., and LOCHTE, K.: Screening volatile organic compounds (vocs) emissions from five marine phytoplankton species by head space gas chromatography/mass spectrometry (hs-gc/ms), *Journal of Environmental Monitoring*, 10, 325-330, 10.1039/b715312k, 2008.

DE BOYER MONTÉGUT, C., MADEC, G., FISCHER, A. S., LAZAR, A., and IUDICONE, D.: Mixed layer depth over the global ocean: An examination of profile data and a profile-based climatology, *Journal of Geophysical Research: Oceans*, 109, n/a-n/a, 10.1029/2004JC002378, 2004.

DE LEEUW, G., ANDREAS, E. L., ANGUELOVA, M. D., FAIRALL, C. W., LEWIS, E. R., O'DOWD, C., SCHULZ, M., and SCHWARTZ, S. E.: Production flux of sea spray aerosol, *Reviews of Geophysics*, 49, n/a-n/a, 10.1029/2010RG000349, 2011.

EKSTROM, S., NOZIERE, B., and HANSSON, H. C.: The cloud condensation nuclei (ccn) properties of 2-methyltetrols and c3-c6 polyols from osmolality and surface tension measurements, *Atmospheric Chemistry and Physics*, 9, 973-980, 2009.

EXTON, D. A., SUGGETT, D. J., MCGENITY, T. J., and STEINKE, M.: Chlorophyll-normalized isoprene production in laboratory cultures of marine microalgae and implications for global models, *Limnology and Oceanography*, 58, 1301-1311, 2013.

GANTT, B., MESKHIDZE, N., and KAMYKOWSKI, D.: A new physically-based quantification of marine isoprene and primary organic aerosol emissions, *Atmospheric Chemistry and Physics*, 9, 4915-4927, 10.5194/acp-9-4915-2009, 2009.

GUENTHER, A., KARL, T., HARLEY, P., WIEDINMYER, C., PALMER, P. I., and GERON, C.: Estimates of global terrestrial isoprene emissions using megan (model of emissions of gases and aerosols from nature), *Atmos. Chem. Phys.*, 6, 3181-3210, 10.5194/acp-6-3181-2006, 2006.

HENZE, D. K., and SEINFELD, J. H.: Global secondary organic aerosol from isoprene oxidation, *Geophysical Research Letters*, 33, 4, Artn L09812

10.1029/2006gl025976, 2006.

HIRATA, T., HARDMAN-MOUNTFORD, N. J., BREWIN, R. J. W., AIKEN, J., BARLOW, R., SUZUKI, K., ISADA, T., HOWELL, E., HASHIOKA, T., NOGUCHI-AITA, M., and YAMANAKA, Y.: Synoptic relationships between surface chlorophyll-a and diagnostic pigments specific to phytoplankton functional types, *Biogeosciences*, 8, 311-327, 10.5194/bg-8-311-2011, 2011.

HU, Q.-H., XIE, Z.-Q., WANG, X.-M., KANG, H., HE, Q.-F., and ZHANG, P.: Secondary organic aerosols over oceans via oxidation of isoprene and monoterpenes from arctic to antarctic, *Scientific Reports*, 3, 2280, 10.1038/srep02280, 2013.

KAMEYAMA, S., YOSHIDA, S., TANIMOTO, H., INOMATA, S., SUZUKI, K., and YOSHIKAWA-INOUE, H.: High-resolution observations of dissolved isoprene in surface seawater in the southern ocean during austral summer 2010-2011, *Journal of Oceanography*, 70, 225-239, 10.1007/s10872-014-0226-8, 2014.

LANA, A., SIMÓ, R., VALLINA, S. M., and DACHS, J.: Potential for a biogenic influence on cloud microphysics over the ocean: A correlation study with satellite-derived data, *Atmos. Chem. Phys.*, 12, 7977-7993, 10.5194/acp-12-7977-2012, 2012.

LELIEVELD, J., BUTLER, T. M., CROWLEY, J. N., DILLON, T. J., FISCHER, H., GANZEVELD, L., HARDER, H., LAWRENCE, M. G., MARTINEZ, M., TARABORRELLI, D., and WILLIAMS, J.: Atmospheric oxidation capacity sustained by a tropical forest, *Nature*, 452, 737-740, 10.1038/nature06870, 2008.

LUO, G., and YU, F.: A numerical evaluation of global oceanic emissions of α-pinene and isoprene, *Atmos. Chem. Phys.*, 10, 2007-2015, 10.5194/acp-10-2007-2010, 2010.

MATSUNAGA, S., MOCHIDA, M., SAITO, T., and KAWAMURA, K.: In situ measurement of isoprene in the marine air and surface seawater from the western north pacific, *Atmospheric Environment*, 36, 6051-6057, 10.1016/s1352-2310(02)00657-x, 2002.

MESKHIDZE, N., SABOLIS, A., REED, R., and KAMYKOWSKI, D.: Quantifying environmental stress-induced emissions of algal isoprene and monoterpenes using laboratory measurements, *Biogeosciences*, 12, 637-651, 10.5194/bg-12-637-2015, 2015.

MILNE, P. J., RIEMER, D. D., ZIKA, R. G., and BRAND, L. E.: Measurement of vertical-distribution of isoprene in surface seawater, its chemical fate, and its emission from several phytoplankton monocultures, *Marine Chemistry*, 48, 237-244, Doi 10.1016/0304-4203(94)00059-M, 1995.

MOORE, R. M., and WANG, L.: The influence of iron fertilization on the fluxes of methyl halides and isoprene from ocean to atmosphere in the series experiment, *Deep-Sea Research Part Ii-Topical Studies in Oceanography*, 53, 2398-2409, 10.1016/j.dsr2.2006.05.025, 2006.

MYRIOKEFALITAKIS, S., VIGNATI, E., TSIGARIDIS, K., PAPADIMAS, C., SCIARE, J., MIHALOPOULOS, N., FACCHINI, M. C., RINALDI, M., DENTENER, F. J., CEBURNIS, D., HATZIANASTASIOU, N., O'DOWD, C. D., VAN WEELE, M., and KANAKIDOU, M.: Global modeling of the oceanic source of organic aerosols, *Advances in Meteorology*, 16, 10.1155/2010/939171, 2010.

O'DOWD, C. D., LANGMANN, B., VARGHESE, S., SCANNELL, C., CEBURNIS, D., and FACCHINI, M. C.: A combined organic-inorganic sea-spray source function, *Geophysical Research Letters*, 35, n/a-n/a, 10.1029/2007GL030331, 2008.

OOKI, A., NOMURA, D., NISHINO, S., KIKUCHI, T., and YOKOUCHI, Y.: A global-scale map of isoprene and volatile organic iodine in surface seawater of the arctic, northwest pacific, indian, and southern oceans, *Journal of Geophysical Research: Oceans*, 120, 4108-4128, 10.1002/2014JC010519, 2015.

PALMER, P. I., and SHAW, S. L.: Quantifying global marine isoprene fluxes using modis chlorophyll observations, *Geophysical Research Letters*, 32, 10.1029/2005gl022592, 2005.

PFISTER, G. G., EMMONS, L. K., HESS, P. G., LAMARQUE, J. F., ORLANDO, J. J., WALTERS, S., GUENTHER, A., PALMER, P. I., and LAWRENCE, P. J.: Contribution of isoprene to chemical budgets: A model tracer study with the ncar ctm mozart-4, *Journal of Geophysical Research: Atmospheres*, 113, n/a-n/a, 10.1029/2007JD008948, 2008.

QUINN, P. K., and BATES, T. S.: The case against climate regulation via oceanic phytoplankton sulphur emissions, *Nature*, 480, 51-56, 10.1038/nature10580, 2011.

SHAW, S. L., CHISHOLM, S. W., and PRINN, R. G.: Isoprene production by prochlorococcus, a marine cyanobacterium, and other phytoplankton, *Marine Chemistry*, 80, 227-245, http://dx.doi.org/10.1016/S0304-4203(02)00101-9, 2003.

SHAW, S. L., GANTT, B., and MESKHIDZE, N.: Production and emissions of marine isoprene and monoterpenes: A review, *Advances in Meteorology*, 10.1155/2010/408696, 2010.

SPRACKLEN, D. V., ARNOLD, S. R., SCIARE, J., CARSLAW, K. S., and PIO, C.: Globally significant oceanic source of organic carbon aerosol, *Geophysical Research Letters*, 35, 5, 10.1029/2008gl033359, 2008.

TAYLOR, B. B., TORRECILLA, E., BERNHARDT, A., TAYLOR, M. H., PEEKEN, I., RÖTTGERS, R., PIERA, J., and BRACHER, A.: Pigments of phytoplankton during polarstern cruise ant-xxv/1, In supplement to: Taylor, BB et al. (2011): Bio-optical provinces in the eastern Atlantic Ocean and their biogeographical relevance. Biogeosciences, 8, 3609-3629, doi:10.5194/bg-8-3609-2011, 10.1594/PANGAEA.819070, 2011a.

TAYLOR, B. B., TORRECILLA, E., BERNHARDT, A., TAYLOR, M. H., PEEKEN, I., RÖTTGERS, R., PIERA, J., and BRACHER, A.: Bio-optical provinces in the eastern atlantic ocean and their biogeographical relevance, *Biogeosciences*, 8, 3609-3629, 10.5194/bg-8-3609-2011, 2011b.

TOKARCZYK, R., GOODWIN, K. D., and SALTZMAN, E. S.: Methyl chloride and methyl bromide degradation in the southern ocean, *Geophysical Research Letters*, 30, n/a-n/a, 10.1029/2003GL017459, 2003.

TRAN, S., BONSANG, B., GROS, V., PEEKEN, I., SARDA-ESTEVE, R., BERNHARDT, A., and BELVISO, S.: A survey of carbon monoxide and non-methane hydrocarbons in the arctic ocean during summer 2010, *Biogeosciences*, 10, 1909-1935, 10.5194/bg-10-1909-2013, 2013.

TWOMEY, S.: Pollution and planetary albedo, *Atmospheric Environment*, 8, 1251-1256, 10.1016/0004-6981(74)90004-3, 1974.

UITZ, J., CLAUSTRE, H., MOREL, A., and HOOKER, S. B.: Vertical distribution of phytoplankton communities in open ocean: An assessment based on surface chlorophyll, *Journal of Geophysical Research: Oceans*, 111, n/a-n/a, 10.1029/2005JC003207, 2006.

VIDUSSI, F., CLAUSTRE, H., MANCA, B. B., LUCHETTA, A., and MARTY, J.-C.: Phytoplankton pigment distribution in relation to upper thermocline circulation in the eastern mediterranean sea during winter, *Journal of Geophysical Research: Oceans*, 106, 19939-19956, 10.1029/1999JC000308, 2001.

WANNINKHOF, R.: Relationship between wind speed and gas exchange over the ocean, *Journal of Geophysical Research: Oceans*, 97, 7373-7382, 10.1029/92JC00188, 1992.

WURL, O., WURL, E., MILLER, L., JOHNSON, K., and VAGLE, S.: Formation and global distribution of sea-surface microlayers, *Biogeosciences*, 8, 121-135, 10.5194/bg-8-121-2011, 2011.

YASSAA, N., PEEKEN, I., ZÖLLNER, E., BLUHM, K., ARNOLD, S., SPRACKLEN, D., and WILLIAMS, J.: Evidence for marine production of monoterpenes, *Environmental Chemistry*, 5, 391-401, 10.1071/En08047, 2008.

YOKOUCHI, Y., LI, H. J., MACHIDA, T., AOKI, S., and AKIMOTO, H.: Isoprene in the marine boundary layer (southeast asian sea, eastern indian ocean, and southern ocean): Comparison with dimethyl sulfide and bromoform, *Journal of Geophysical Research-Atmospheres*, 104, 8067-8076, 10.1029/1998jd100013, 1999.

YVON-LEWIS, S. A., BUTLER, J. H., SALTZMAN, E. S., MATRAI, P. A., KING, D. B., TOKARCZYK, R., MOORE, R. M., and ZHANG, J.-Z.: Methyl bromide cycling in a warm-core eddy of the north atlantic ocean, *Global Biogeochemical Cycles*, 16, 88-81-88-86, 10.1029/2002GB001898, 2002.

ZINDLER, C., MARANDINO, C. A., BANGE, H. W., SCHÜTTE, F., and SALTZMAN, E. S.: Nutrient availability determines dimethyl sulfide and isoprene distribution in the eastern atlantic ocean, *Geophysical Research Letters*, 41, 3181-3188, 10.1002/2014GL059547, 2014.

5 PRODUCTION AND CONSUMP-TION OF ISOPRENE

Abstract. Parameterizations of surface ocean isoprene concentrations are numerous, despite the lack of source/sink process understanding. Here we present isoprene and related field measurements in the mixed layer from the Indian Ocean and the East Pacific Ocean to investigate the production and consumption rates in two contrasting regions, namely oligotrophic open ocean and coastal upwelling region. Our data show that the ability of different phytoplankton functional types (PFTs) to produce isoprene seems to be mainly influenced by light, ocean temperature, and salinity. Our field measurements also demonstrate that nutrient availability seems to have a direct influence on the isoprene production. With the help of pigment data, we calculate in-field isoprene production rates for different PFTs under varying biogeochemical and physical conditions. Using these new calculated production rates we demonstrate that an additional, significant and variable loss, besides a known chemical loss and a loss due to air sea gas exchange, is needed to explain the measured isoprene concentration. We hypothesize that this loss, with a lifetime for isoprene between 10 and 100 days depending on the ocean region, is potentially due to degradation or consumption by bacteria.

5.1   Introduction

Isoprene (2-methyl-1,3-butadiene, C_5H_8), a biogenic volatile organic compound (VOC), accounts for half of the total global biogenic VOCs in the atmosphere (GUENTHER et al., 2012). 400-600 Tg C yr^{-1} are emitted globally from terrestrial vegetation (ARNETH et al., 2008; GUENTHER et al., 2006). Emitted isoprene influences the oxidative capacity of the atmosphere and acts as a source for secondary organic aerosols (SOA)(CARLTON et al., 2009). It reacts with hydroxyl radicals (OH), as well as ozone and nitrate radicals (ATKINSON and AREY, 2003; LELIEVELD et al., 2008), forming low-volatility species, such as methacrolein or methyl vinyl ketone, which are then further photooxidized to SOA via more semi-volatile intermediate products (CARLTON et al., 2009). Model studies suggest that isoprene accounts for 27% (HOYLE et al., 2007), 48% (HENZE and SEINFELD, 2006) or up to 79% (HEALD et al., 2008) of the total SOA production globally.

Whereas the terrestrial isoprene emissions are well known to act as a source for SOA, the oceanic source strength is highly discussed (CARLTON et al., 2009). Marine derived isoprene emissions only account for a few percent of the total emissions and are suggested, based on model studies, to be generally lower than 1 Tg C yr^{-1} (ARNOLD et al., 2009; BOOGE et al., 2016; GANTT et al., 2009; PALMER and SHAW, 2005). Some model studies suggest that these low emissions are not enough to control the formation of SOA over the ocean (ANTTILA et al., 2010; ARNOLD et al., 2009; GANTT et al., 2009; MYRIOKEFALITAKIS et al., 2010; SPRACKLEN et al., 2008). However, due to its short atmospheric lifetime of minutes to a few hours, terrestrial isoprene is not reaching the atmosphere over remote regions of the oceans. In these regions, oceanic emissions of isoprene could play an important role in SOA formation on regional and seasonal scales, especially in association with increased emissions during phytoplankton blooms (HU et al., 2013). In addition, the isoprene SOA yield could be up to 29% under acid-catalyzed particle phase reactions during low-NO_x conditions, which occur over the open oceans (SURRATT et al., 2010). This SOA yield is significantly higher than a SOA burden of 2% during neutral aerosol experiments calculated by HENZE and SEINFELD (2006).

Marine isoprene is produced by phytoplankton in the euphotic zone of the oceans, but only a few studies have directly measured the concentration of isoprene to date and the exact mechanism of isoprene production is not known. The concentrations generally range between < 1 and 200 pmol L^{-1} (BAKER et al., 2000; BONSANG et al., 1992; BROADGATE et al., 1997; BROADGATE et al., 2004; HACKENBERG et al., 2017; KURIHARA et al., 2010; MATSUNAGA et al., 2002; MILNE et al., 1995; OOKI et al., 2015; ZINDLER et al., 2014). Depending on region and season, concentrations of isoprene in surface waters can reach up to 395 and 541 pmol L^{-1} during phytoplankton blooms in the highly productive Southern Ocean and Arctic waters, respectively (KAMEYAMA et al., 2014; TRAN et al., 2013).

Studies have shown that the depth profile of isoprene mainly follows the chlorophyll-a (chl-a) profile suggesting phytoplankton as an important source (BONSANG et al., 1992; HACKENBERG et al., 2017; MILNE et al., 1995; TRAN et al., 2013) and furthermore, BROADGATE et al. (1997) and KURIHARA et al. (2010) show a direct correlation between isoprene and chl-a concentrations in surface waters and between 5 and 100 m depth,

respectively. However, this link is not consistent enough on global scales to predict marine isoprene concentrations using chl-a (Table 5.1). Laboratory studies with different monocultures illustrate that the isoprene production rate varies widely depending on the phytoplankton functional type (PFT) (BOOGE et al., 2016 and references therein). In addition, environmental parameters, such as temperature and light, have been shown to influence isoprene production (EXTON et al., 2013; MESKHIDZE et al., 2015; SHAW et al., 2003). In general, the production rates increase with increasing light levels and higher temperature, similar to the terrestrial vegetation (GUENTHER et al., 1991). However, this trend cannot easily be generalized to all species, because each species-specific growth requirement is linked differently to the environmental conditions. For example, SRIKANTA DANI et al. (2017) showed that two diatom species, *Chaetoceros calcitrans* and *Phaeodyctylum tricornutum,* have their maximum isoprene production rate at light levels of 600 and 200 μmol m^{-2} s^{-1}, respectively, which decreases at even higher light levels. Furthermore, MESKHIDZE et al. (2015) measured the isoprene production rates of different diatoms at different temperature and light levels on two consecutive days. Their results showed a less variable, but higher emission on day two, suggesting that phytoplankton must acclimate physiologically to the environment. This should also hold true for dynamic regions of the ocean and has to be taken into account when using field data to model isoprene production.

The main loss of isoprene in seawater is air-sea gas exchange, with a minor physical loss due to advective mixing and chemical loss by reaction with OH and singlet oxygen (PALMER and SHAW, 2005). The existence of biological losses still remains an open question, as almost no studies were conducted concerning this issue. SHAW et al. (2003) assumed the biological loss by bacterial degradation to be very small. However, ACUÑA ALVAREZ et al. (2009) showed that isoprene consumption in culture experiments from marine and coastal environments did not exhibit first order dependency on isoprene concentration. They observed faster isoprene consumption with lower initial isoprene concentration.

This study significantly increases the small dataset of marine isoprene measurements in the world oceans with new observations of the distribution of isoprene in the surface mixed layer of the oligotrophic subtropical Indian Ocean and in the nutrient rich upwelling area of the East Pacific Ocean along the Peruvian coast. These two contrasting and, in terms of isoprene measurements, highly undersampled ocean basins are interesting regions to compare the diversity of isoprene producing species. With the help of concurrently measured physical (temperature, salinity, radiation), chemical (nutrients, oxygen), and biological (pigments, bacteria) parameters, we aim to improve the understanding of isoprene production and consumption processes in the surface ocean under different environmental conditions.

Table 5.1: Factors of different regression equations from different studies ([isoprene]=u*[chl-a]+v*SST+intercept) compared to factors from this study. Bold/*italic*/regular R^2 value: correlation significant/not significant/significance not known (significant: $p<0.05$). [chl-a] in µg L^{-1}, SST in °C, [isoprene] in pmol L^{-1}.

reference	cruise/region	SST bins	u	v	intercept	R²
HACKENBERG et al. (2017)	AMT 22 (Atlantic O.)	<20°C	37.9	---	17.5	**0.37** (n=39)
	AMT 23 (Atlantic O.)		15.1	---	18.4	**0.55** (n=11)
	ACCACIA 2 (Arctic)		34.1	---	11.1	**0.61** (n=34)
	AMT 22 (Atlantic O.)	≥20°C	300	---	-3.35	**0.60** (n=93)
	AMT 23 (Atlantic O.)		103	---	5.58	**0.82** (n=22)
OOKI et al. (2015)	Southern Ocean, Indian Ocean, Northwest Pacific Ocean, Bering Sea, western Arctic Ocean	3.3-17°C	14.3	2.27	2.83	**0.64**
		17-27°C	20.9	-1.92	63.1	**0.77**
		>27°C	319	8.55	-244	**0.75**
KURIHARA et al. (2012)	Sagami Bay	no bin	10.7	---	5.9	**0.49** (n=8)
KURIHARA et al. (2010)	Western North Pacific	no bin	18.8	---	6.1	**0.79** (n=60)
BROADGATE et al. (1997)	North Sea	no bin	6.4	---	1.2	0.62
This study	whole study	no bin	2.45	---	22.1	**0.07**(n=138)
	SPACES (Indian Ocean)		20.2	---	8.01	**0.30** (n=37)
	OASIS (Indian Ocean)		42.6	---	12.6	**0.10** (n=59)
	ASTRA-OMZ (Southeast Pacific O.)		1.26	---	26.5	*0.07* (n=42)
		<20°C	3.92	---	11.5	**0.59** (n=46)
		≥20°C	25.6	---	16.6	**0.14** (n=92)
		3.3-17°C	1.30	10.0	-144	**0.84** (n=10)
		17-27°C	10.4	0.76	-3.70	**0.41** (n=97)
		>27°C	40.4	-0.58	39.7	*0.17* (n=31)

5.2 Methods

5.2.1 Sampling sites

Measurements of oceanic isoprene were performed during three separate cruises, the SPACES (Science Partnerships for the Assessment of Complex Earth System Processes) and OASIS (Organic very short-lived substances and their air-sea exchange from the Indian Ocean to the stratosphere) cruises in the Indian Ocean and the ASTRA-OMZ (Air sea interaction of trace elements in oxygen minimum zones) cruise in the eastern Pacific Ocean. The SPACES/OASIS cruises took place in July/August 2014 on board the R/V Sonne I from Durban, South Africa via Port Louis, Mauritius to Malé, Maldives and the ASTRA-OMZ cruise took place in October 2015 on board the R/V Sonne II from Guayaquil, Ecuador to Antofagasta, Chile (Figure 5.1).
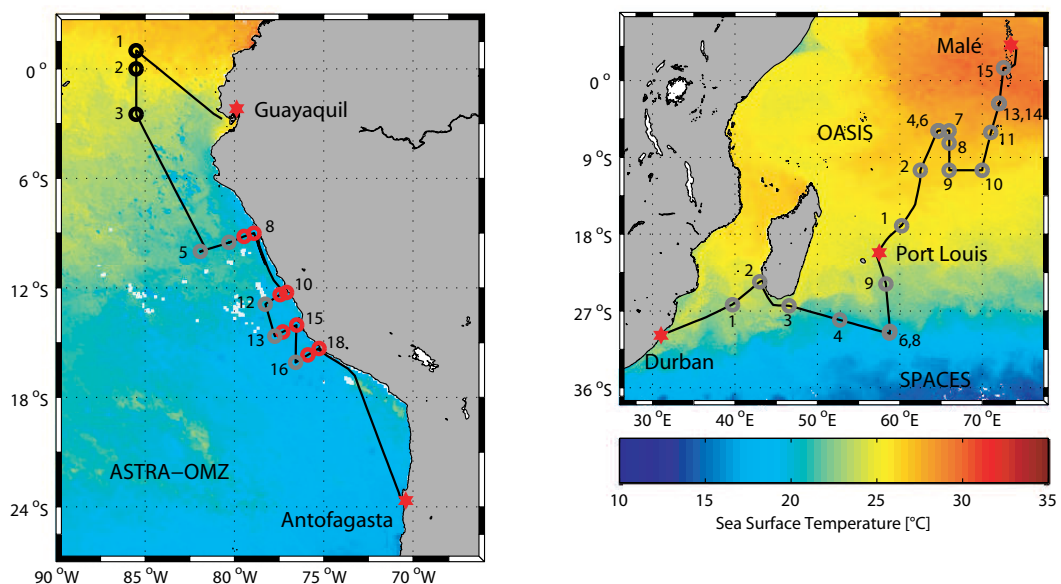
Figure 5.1: Cruise tracks (black) of ASTRA-OMZ (October 2015, East Pacific Ocean) and SPACES/OASIS (July/August 2014, Indian Ocean) plotted on top of monthly mean sea surface temperature detected by the Moderate Resolution Imaging Spectroradiometer (MODIS) instrument on board the Aqua satellite. Circles indicate CTD stations (grey: SPACES/OASIS and open ocean stations during ASTRA-OMZ, black: equatorial stations during ASTRA-OMZ, red: coastal stations during ASTRA-OMZ). Numbers indicate stations, where a CTD depth profile was performed. Stations 6 & 8 (SPACES) as well as stations 4 & 6 and 13 & 14 (OASIS) have almost the same geographical coordinates. If a station number is omitted (SPACES: stations 5 & 7; OASIS: stations 3, 5 & 12; ASTRA-OMZ: stations 4 & 9) no CTD cast was performed.

5.2.2   Isoprene measurements

During all cruises, up to 7 samples (50 mL) from 5 to 150 m depth for each depth profile were taken bubble-free from a 24 L-Niskin bottle rosette equipped with a CTD (conductivity-temperature-depth; described in STRAMMA et al. (2016)). 10 mL of helium were pushed into each transparent glass vial (Chromatographie Handel Müller, Fridolfing, Germany) replacing the same amount of sea water and providing a headspace for the upcoming analysis. The water samples were, if necessary, stored in the fridge and analyzed on board, within 1 h of collection, using a purge and trap system attached to a gas chromatograph/mass spectrometer (GC/MS; Agilent 7890A/Agilent 5975C; inert XL MSD with triple axis detector) (Figure 5.2). Isoprene was purged for 15 minutes from the water sample with helium (70 mL min^{-1}) containing 500 µL of gaseous deuterated isoprene (isoprene-d5) as an internal standard to account for possible sensitivity drift (Figure 5.2: purge unit, load position). The gas stream was dried using potassium carbonate (SPACES/OASIS) or a Nafion$^{®}$ membrane dryer (Perma Pure; ASTRA-OMZ). CO_2- and hydrocarbon-free dry, pressurized air with a flow of 180 mL min^{-1} was used as counter flow in the Nafion$^{®}$ membrane dryer (Figure 5.2: water removal). Before being injected into the GC (Figure 5.2: trap unit, inject position), isoprene was preconcentrated in a Sulfinert$^{®}$ stainless steel trap (1/16'' O.D.) cooled with liquid nitrogen (Figure 5.2: trap unit, load position). The mass spectrometer was operated in single ion mode quantifying isoprene and d5-isoprene using m/z - ratios of 67, 68 and 72, 73, respectively. In order to perform daily calibrations for quantification, gravimetrically prepared liquid isoprene standards in ethylene glycol were diluted in Milli-Q water and measured in the same way as the samples. The precision for isoprene measurements was ± 8%.
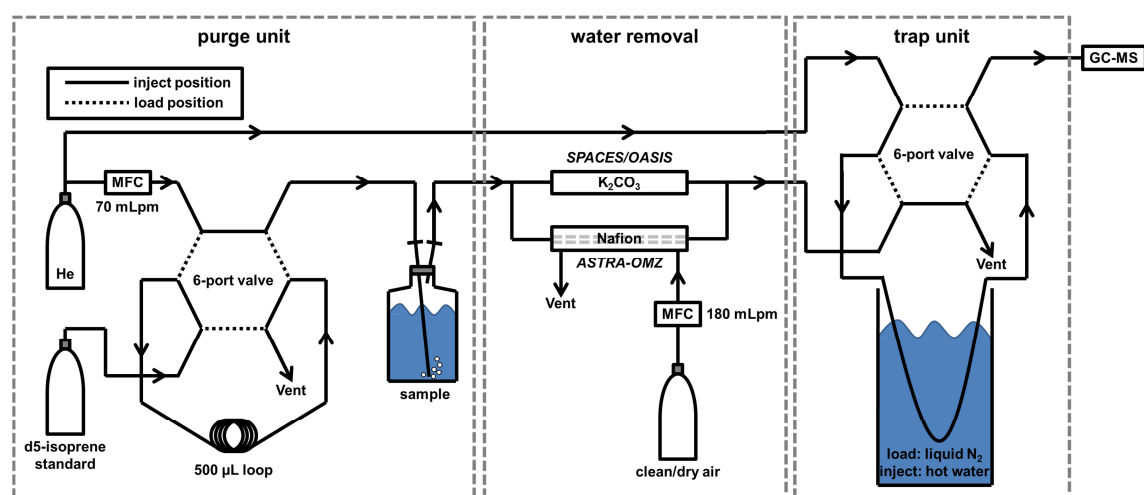
Figure 5.2: Schematic overview of the analytical purge-and-trap-system, divided into three parts: purge unit (left), water removal (middle) and trap unit (right). He: helium, MFC: Mass flow controller, K_2CO_3: potassium carbonate, GC-MS: gas chromatograph/mass spectrometer.

5.2.3   Nutrient measurements

Micronutrient samples were taken on every cruise from the CTD bottles (covering all sampled depths). The samples from SPACES were stored in the fridge at -20°C and measured during OASIS. Samples from OASIS and ASTRA-OMZ were directly measured on-board with a QuAAtro auto-analyzer (Seal Analytical). Nitrate was measured as nitrite following reduction on a cadmium coil. The precision of nitrate measurements was calculated to be ±0.13 µmol L^{-1}.

5.2.4   Bacteria measurements

For bacterial cell counts, 4 mL samples were preserved with 200 µL glutaraldehyde (1% v/v final concentration) and stored at -20°C for up to three months until measurement. A stock solution of SybrGreen I (Invitrogen) was prepared by mixing 5 µL of the dye with 245 µL dimethyl sulfoxide (Sigma Aldrich). 10 µL of the dye stock solution and 10 µL fluoresbrite YG microspheres beads (diameter 0.94 µm, Polysciences) were added to 400 µL of the thawed sample and incubated for 30 min in the dark. The samples were then analyzed at low flow rate using a flow cytometer (FACS Calibur, Becton Dickinson) (GASOL and DEL GIORGIO, 2000). TruCount beads (Becton Dickinson) were used for calibration and in combination with Fluoresbrite YG microsphere beads (0.5-1 µm, Polysciences) for absolute volume calculation. Calculations were done using the software program "Cell Quest Pro".

5.2.5   Phytoplankton functional types from marker pigment measurements

Different PFTs were derived from marker phytoplankton pigment concentrations and chlorophyll concentrations. To determine PFT chl-a, 0.5 to 6 L of sea water were filtered through Whatman GF/F filters at the same stations as isoprene was sampled. The soluble organic pigment concentrations were determined using high-pressure liquid chromatography (HPLC) according to the method of BARLOW et al. (1997) adjusted to our temperature-controlled instruments as detailed in TAYLOR et al. (2011). We determined the list of pigments shown in Table 2 of TAYLOR et al. (2011) and applied the method by AIKEN et al. (2009) for quality control of the pigment data. PFT chl-a was calculated using the diagnostic pigment analysis developed by VIDUSSI et al. (2001) and adapted in UITZ et al. (2006). This method uses specific phytoplankton pigments which are (mostly) common only in one specific PFT. These pigments are called marker or diagnostic pigments (DP) and the method relates for each measurement point the weighted sum of the concentration of seven, for each PFT representative DP to the concentration of monovinyl chlorophyll a concentration and by that PFT group specific coefficients are derived which enable to derive the PFT chl-a concentration. The latter is an ubiquitous pigment in all PFT except *Prochlorococcus* sp. which contains divinyl chlorophyll a instead. In general, chl-a

is a valid proxy for the overall phytoplankton biomass. In the DP analysis as DP concentrations of fucoxanthin, peridinin, 19'hexanoyloxy-fucoxanthin, 19'butanoyloxy-fucoxanthin, alloxanthin, and chlorophyll *b* indicative for diatoms, dinoflagellates, haptophytes, chrysophytes, cryptophytes, cyanobacteria (excluding *Prochlorococcus* sp.), and chlorophytes, respectively, are used. With the DP analysis then finally the chl-a concentration of these PFTs were derived. The chl-a concentration of *Prochlorococcus* sp. was directly derived from the concentration of divinyl chlorophyll *a.*

5.2.6 Photosynthetic available radiation within the water column measurements

Since no underwater light data were available for all cruises, we used global radiation data from the ship's meteorological station together with the light attenuation coefficients (determined from the chl-a concentration profiles) to calculate the photosynthetic available radiation) within the water column during a day. In detail we processed these data the following way:

We fitted the hourly resolved global radiation data with a sine function to account for the light variation during the day and converted into PAR just above surface, $PAR(0^+)$ in $\mu mol\ m^{-2}\ s^{-1}$ during the course of a day, by multiplying these daily global radiation values with a factor of 2 (JACOVIDES et al., 2004) (Figure S5.1a).

The subsurface PAR ($PAR(0^-)$) was calculated using the refractive index of water (n=1.34) and 0.98 for transmission assuming incident light angles <49°:

$$PAR(0^-)=E_d PAR(0^+) \times 1.34^2/0.98 \tag{5.1}$$

In order to derive the diffuse attenuation coefficient for PAR ($K_d PAR$) we calculated the euphotic depth (Z_{eu}) from the chl-a profile for all stations using the approximation by MOREL and BERTHON (1989) further refined by MOREL and MARITORENA (2001). In detail the following was done: From the chl-a profiles at each station the total chl-a integrated for Z_{eu} (C_{tot}) was determined. A given profile was progressively integrated with respect to increasing depth (z). The successive integrated chl-a values were introduced in Equation 2 or 3 accordingly, thus providing successive Z_{eu} values that were progressively decreasing. Once the last Z_{eu} value, as obtained, became lower than the actual depth z used when integrating the profile, these C_{tot} and Z_{eu} values from the last integration were taken. Profiles which did not reach Z_{eu} were excluded.

$$Z_{eu}=912.5 \times C_{tot}^{-0.839} \text{ ;if } 10m<Z_{eu}<102m \tag{5.2}$$

$$Z_{eu}=426.3 \times C_{tot}^{-0.547} \text{ ;if } Z_{eu}>102m \tag{5.3}$$

$K_d PAR$ of each station was then calculated from Z_{eu} as follows:

$$K_d PAR=\frac{4.6}{Z_{eu}} \tag{5.4}$$

The plane photosynthetic available irradiance at each depth (z) in the water column, $PAR(z)$, is then calculated applying Beer-Lambert's law (Figure S5.1b):

$$PAR(z) = PAR_{surface} \times e^{-K_d\, z} \qquad\qquad (5.5)$$

An example of two *PAR* fitted depth profiles for the time of the two specific stations is shown in the supplement (Figure S5.2), which have been compared to directly measured downwelling photosynthetic available radiation (*$E_d PAR$*) profiles. The comparison shows that the fitted PAR profiles obtained from ship's global radiation data and chlorophyll profiles were reliable.

$E_d PAR$ profiles were only measured during ASTRA daytime stations with a hyperspectral radiometer (RAMSES, TriOS GmbH, Germany) covering a wavelength range of 320 nm to 950 nm with an optical resolution of 3.3 nm and a spectral accuracy of 0.3 nm (for more details on the measurements see TAYLOR et al. (2011)). The downwelling irradiance *$E_d(z,\lambda)$* RAMSES data were interpolated to 1 nm resolution and then the *$E_d(z)$* given in W m^{-2} at each nm wavelength step between 400 to 700 nm was converted to µmol quanta m^{-2} s^{-1} by following the principle that one photon contains the energy $E_p = (h^*c)/\lambda$ (with the Planck's constant h=6.6266*10^{-34} Js and the speed of light c=299792458 m s^{-1}). Finally, the *$E_d(z, \lambda)$* were integrated from 400 to 700 nm to receive the downwelling photosynthetic available plane irradiance (*$E_d PAR(z)$*).

5.2.7 Calculation of isoprene production

We calculated the isoprene production rate (*P*) in two different ways: a direct and an indirect calculation, which will be explained in the following paragraphs. For all calculations made we came up with one production rate per station within the mixed layer. This was either due to the shallow mixed layer depth (MLD) resulting in only one measurement within the mixed layer (coastal stations ASTRA-OMZ) or due to well mixed isoprene concentrations showing almost no gradient within the mixed layer (data explained in section 5.3.2).

5.2.7.1 Direct calculation of isoprene production rates

Isoprene production rates of different PFTs were determined in laboratory phytoplankton culture experiments (see a collection of literature values: Table 2 in BOOGE et al. (2016)) and were used here to calculate isoprene production from measured PFTs in the field. These literature studies showed that isoprene production rates are light dependent, with increasing production rates at higher light levels (BONSANG et al., 2010; GANTT et al., 2009; MESKHIDZE et al., 2015; SHAW et al., 2003). To include the light dependency in our calculations, we followed the approach of GANTT et al. (2009) for each PFT by applying a log squared fit between all single literature laboratory chl-a normalized isoprene production rates *P_{chloro}* (µmol isoprene (g chl-a)$^{-1}$ h^{-1}) (references in Table 5.2) and their measured light intensity *I* (µmol m^{-2} s^{-1}) during individual experiments to determine an emission factor (*EF*) for each PFT (Figure S5.3):

$$P_{chloro} = EF \times \ln(I)^2 \qquad\qquad (5.6)$$

The resulting *EF* from this log squared fit is unique for each PFT and is listed in Table 5.2: The higher the *EF* of a PFT, the higher its P_{chloro} value at a specific light intensity. It should be noted that we are not sure what species were actually present during the cruises. We realize, therefore, that this method of calculating *EF*s is limited. In order to calculate the isoprene production at each sampled depth (*z*) at each station, we used the scalar photosynthetic available radiation in the water column, *PAR(z)*, (see section 5.2.6) as input for *I*, which was used with the respective, calculated *EF* of each PFT using Equation (5.6). The product was integrated over the course of the day, resulting in a P_{chloro} value (μmol isoprene (g chl-a)$^{-1}$ day^{-1}) for each PFT and day depending on the depth in the water column (Figure S5.4). The light and depth dependent individual $P_{chloro,i}$ values of each PFT at the sampled depth *z* were multiplied with the corresponding, measured PFT chl-a concentration (*[PFT]$_i$*). The sum of all products gives the directly calculated isoprene production rate at each sampled depth *z*:

$$P_{direct}(z) = \sum \left(P_{chloro_i} \times [PFT]_i \right)$$

(5.7)

Integrating over all measurements within the mixed layer and scaling with the MLD results in a "mean" direct isoprene production rate (P_{direct}) for each station.

Table 5.2: Emission factor (*EF*) of each PFT determined by applying a log squared relationship between light intensity and isoprene production rates resulting from published phytoplankton cultures experiments.

PFT	emission factor	references of literature values used for fitting*
Diatoms	0.0064	SHAW et al. (2003), BONSANG et al. (2010), EXTON et al. (2013), MESKHIDZE et al. (2015)
Chlorophytes	0.0168	SHAW et al. (2003), BONSANG et al. (2010), EXTON et al. (2013)
Dinoflagellates	0.0176	EXTON et al. (2013)
Haptophytes	0.0099	SHAW et al. (2003), BONSANG et al. (2010), EXTON et al. (2013)
Cyanobacteria	0.0097	SHAW et al. (2003), BONSANG et al. (2010), EXTON et al. (2013)
Cryptophytes	0.0120	EXTON et al. (2013)
Prochlorococcus	0.0053	SHAW et al. (2003)

*exact species within a PFT tested for calculation production rates can be found in the references cited for each PFT

5.2.7.2 Indirect calculation of isoprene production rates

The indirect calculation of the isoprene production rate is dependent on our measured isoprene concentrations ($C_{Wmeasured}$). We used the simple model concept of PALMER and SHAW (2005), assuming that the measured isoprene concentration is in steady state, meaning that the production (*P*) is balanced by all loss processes:

$$P - C_{Wmeasured} \left(\Sigma k_{CHEM,i} C_{Xi} + k_{BIOL} + \frac{k_{AS}}{MLD} \right) - L_{MIX} = 0, \tag{5.8}$$

where k_{CHEM} is the chemical loss rate constant for all possible loss pathways (i) with the concentrations of the reactants (C_X = OH and O_2), k_{BIOL} is the biological loss rate constant due to biological degradation, and L_{MIX} is the loss due to physical mixing. These constants are further described in PALMER and SHAW (2005). k_{AS} is the loss rate constant due to air-sea gas exchange scaled with the MLD. The MLD at each station was calculated from CTD profile measurements applying the temperature threshold criterion (±0.2°C) of DE BOYER MONTÉGUT et al. (2004). k_{AS} was computed using the Schmidt number (S_C) of isoprene (PALMER and SHAW, 2005) and the quadratic wind-speed-based (U_{10}) parameterization of WANNINKHOF (1992):

$$k_{AS} = 0.31 \, U_{10}^2 \left(\frac{S_C}{660} \right)^{-0.5}. \tag{5.9}$$

As we assume steady state isoprene concentration, we used the mean wind speed and the mean sea surface temperature of the last 24 h of shipboard observations before taking the isoprene sample to calculate U_{10} and S_C, respectively.

We modified equation (5.8) to calculate the needed production rate (P_{need}) by multiplying $C_{Wmeasured}$ with the sum of k_{CHEM} (0.0527 day^{-1}) and k_{AS} scaled with the MLD:

$$P_{need} = C_{Wmeasured} \left(k_{CHEM} + \frac{k_{AS}}{MLD} \right). \tag{5.10}$$

We neglected the loss rates of isoprene due to biological degradation and physical mixing because they are low compared to k_{CHEM} and k_{AS} (BOOGE et al., 2016; PALMER and SHAW, 2005), meaning that the resulting P_{need} value can be seen as a minimum needed production rate.

5.3 Results and discussion

5.3.1 Cruise settings

The first part of the Indian Ocean cruise, SPACES, started in Durban, travelled eastwards while passing the Agulhas current and the southern tip of Madagascar (Toliara reef) with relatively warm water masses (mean: 23.4°C) and southerly winds. Southeast of Madagascar wind direction changed to easterly winds and we encountered the Antarctic circumpolar current with significantly lower mean sea surface temperatures of 19.7°C before heading north to Mauritius. Mean wind speed during the cruise was 8.2±3.7 m s^{-1} and mean salinity was 35.5±0.2. Global radiation over the course of the day was on average ~360±70 W m^{-2}. As shown in Figure 5.3, within the mixed layer, chl-a concentrations were very low (average value < 0.3 µg L^{-1}) during the whole cruise, coinciding with generally low nutrient levels in the mixed layer (mean values for nitrate and phosphate were 0.14 and 0.15 µmol L^{-1}, respectively).

The second part of Indian ocean cruise, OASIS, covered open ocean regimes, upwelling regions, such as the equatorial overturning cell as described in SCHOTT et al. (2009) and the shallow Mascarene Plateau (8°-12°S, 59°-62°E). Constant south easterly winds (mean: 10.3±4.2 m s^{-1}) were observed that were characteristic for the season of the southwest monsoon. During the cruise, sea surface temperature was constantly increasing with latitude from 24.4°C (Port Louis) to 29.7°C (southern tip of the Maldives) with mean daily light levels of ~457±64 W m^{-2}. Salinity ranged from 34.4 to 35.4. As for the SPACES cruise, the chl-a concentration in the western tropical Indian Ocean was low (0.2-0.5 μg L^{-1} on average, Figure 5.3). Nitrate levels (mean: 0.42 μmol L^{-1}) in the mixed layer were higher than during SPACES, but not phosphate (mean: 0.17 μmol L^{-1}).
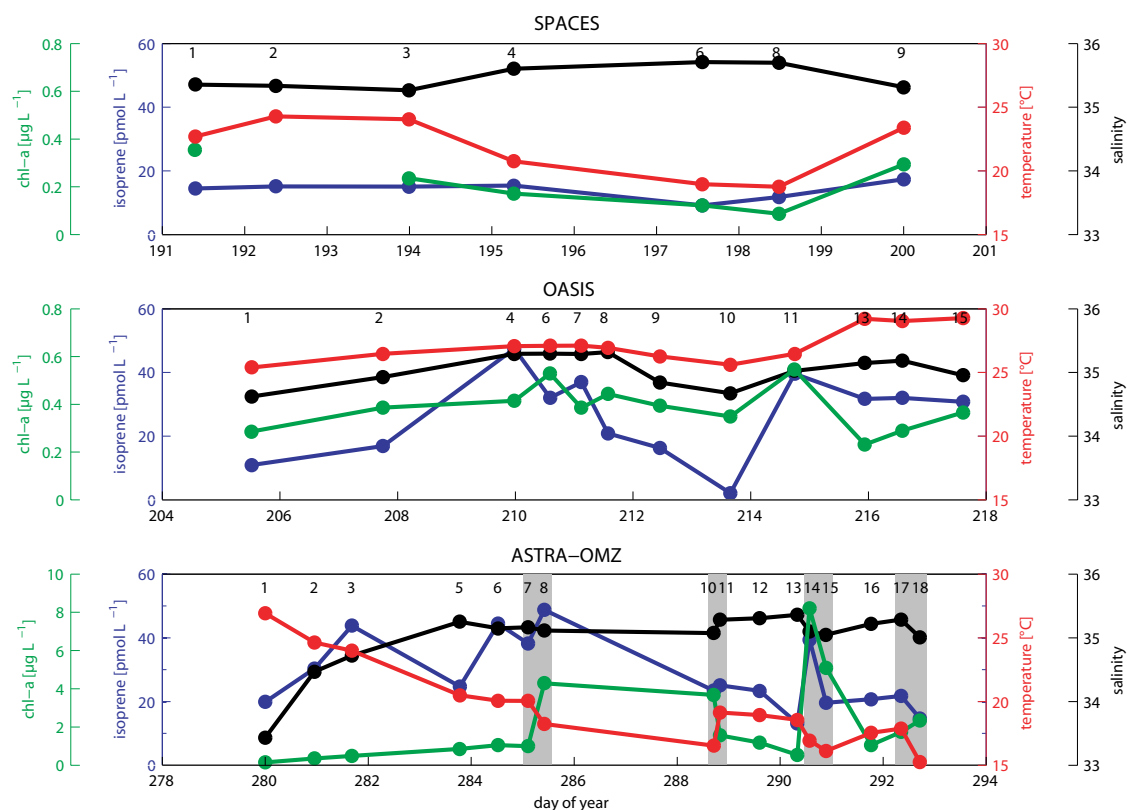
Figure 5.3: Mean salinity (black), isoprene concentration (blue), temperature (red), and chl-a concentration (green) in the MLD at each station during SPACES (upper panel), OASIS (middle panel), and ASTRA-OMZ (bottom panel). Grey rectangles highlight the 8 coastal stations during ASTRA-OMZ. Numbers in each panel refer to corresponding number of station.

The ASTRA-OMZ cruise took place in the coastal, wind driven Peruvian upwelling system (16°S - 6°S). This area is a part of one of the four major eastern boundary upwelling systems (CHAVEZ and MESSIÉ, 2009) and is highly influenced by the El Niño-Southern Oscillation. We observed constant southeasterly winds (8.2±2.5 m s^{-1}) travelling parallel to the Peruvian coast. During neutral surface conditions or La Niña conditions, cold, nutrient rich water is being upwelled at the shelf of Peru resulting in high biological productivity. However, in early 2015 a strong El Niño developed, which brought warmer, low salinity waters from the western Pacific to the coast of Peru, result-

ing in suppressed upwelling with lower biological activity due to the presence of nutrient-poor water masses. The cruise started with a section passing the equator from north to south at 85.5°W east of the Galapagos Islands with mean sea surface temperatures of 25.0°C and low salinity waters (mean for profiles: 34.2), as well as low chl-a concentrations (mean for profiles: 0.5 µg L^{-1}). Levels of incoming shortwave radiation were ~508±67 W m^{-2}. Afterwards, we performed 4 onshore-offshore transects at about 9, 12, 14, and 16°S off the coast of Peru (Figure 5.1) where the incoming shortwave radiation was significantly decreased by clouds (~300 W m^{-2}). Upwelled waters identified by higher salinity (mean: 35.2) and lower sea surface temperatures (mean: 18.9°C) were found during the second part of the cruise. Chl-a values were highest directly at the coast (max: 13.1 µg L^{-1}), coinciding with lower sea surface temperatures (Figure 5.3) showing that some upwelling was still present.

5.3.2   Isoprene distribution in the mixed layer

The isoprene concentrations during the SPACES cruise were generally very low, ranging from 6.1 pmol L^{-1} to 27.1 pmol L^{-1} in the mixed layer (mean for the average of a profile: 12.3 pmol L^{-1}) in the southern Indian Ocean, mainly due to very low biological productivity. During the OASIS cruise, the isoprene concentrations south of 10°S were comparable to the concentrations of the SPACES cruise. North of 10°S, the isoprene values in the mixed layer were significantly higher (mean: 35.9 pmol L^{-1}) (Figure 5.3). These results are in good agreement with the sea surface isoprene concentrations of Ooki et al. (2015) in the same area east of 60°E, who measured concentrations lower than 20 pmol L^{-1} south of 12°S and concentrations of ~40 pmol L^{-1} north of 12°S during a campaign between November 2009 and January 2010. During ASTRA-OMZ the concentrations ranged from 12.7 pmol L^{-1} to 53.2 pmol L^{-1} with a mean isoprene concentration of 29.5 pmol L^{-1} in the mixed layer. Although the chl-a concentrations at the coastal stations (3.8 µg L^{-1}) were significantly higher than open ocean values (0.7 µg L^{-1}), the isoprene values did not show the same trend (Figure 5.3).

A mean normalized depth profile of each cruise for isoprene (blue), water temperature (black), oxygen (red), and chl-a (green) is shown in Figure 5.4. In order to compare the depth profiles of each cruise with respect to the different concentration regimes, we normalized the measured values by dividing the concentration of each depth of each station by the mean concentration in the mixed layer from the same station profile. A normalized value >1 means that the value at a certain depth is higher than the mean value in the mixed layer, a value <1 means less than in the mixed layer. As the sampled depths at each station were not the same at every cruise, we binned the data into seven equally spaced depth intervals (15 m) and averaged each data of an interval over each of the three cruises. The calculated mean mixed layer depths of the SPACES and OASIS cruises, using the temperature threshold criterion (±0.2°C) of DE BOYER MONTÉGUT et al. (2004), were about 60 m, the mean mixed layer depth of the ASTRA-OMZ cruise was 30 m excluding the four coastal stations, which had only a MLD of 20 m resulting in only one bin interval in the MLD. Figure 5.4 shows, that during all three cruises almost no gradient of isoprene in the mixed layer was detectable. In contrast to the isoprene con-

centration, the highest chl-a concentration was measured slightly above or below the MLD during SPACES/OASIS, whereas during ASTRA-OMZ chl-a showed the same trend as isoprene. These results suggest a very fast mixing of isoprene after it is produced by phytoplankton and released to the water column above the MLD.
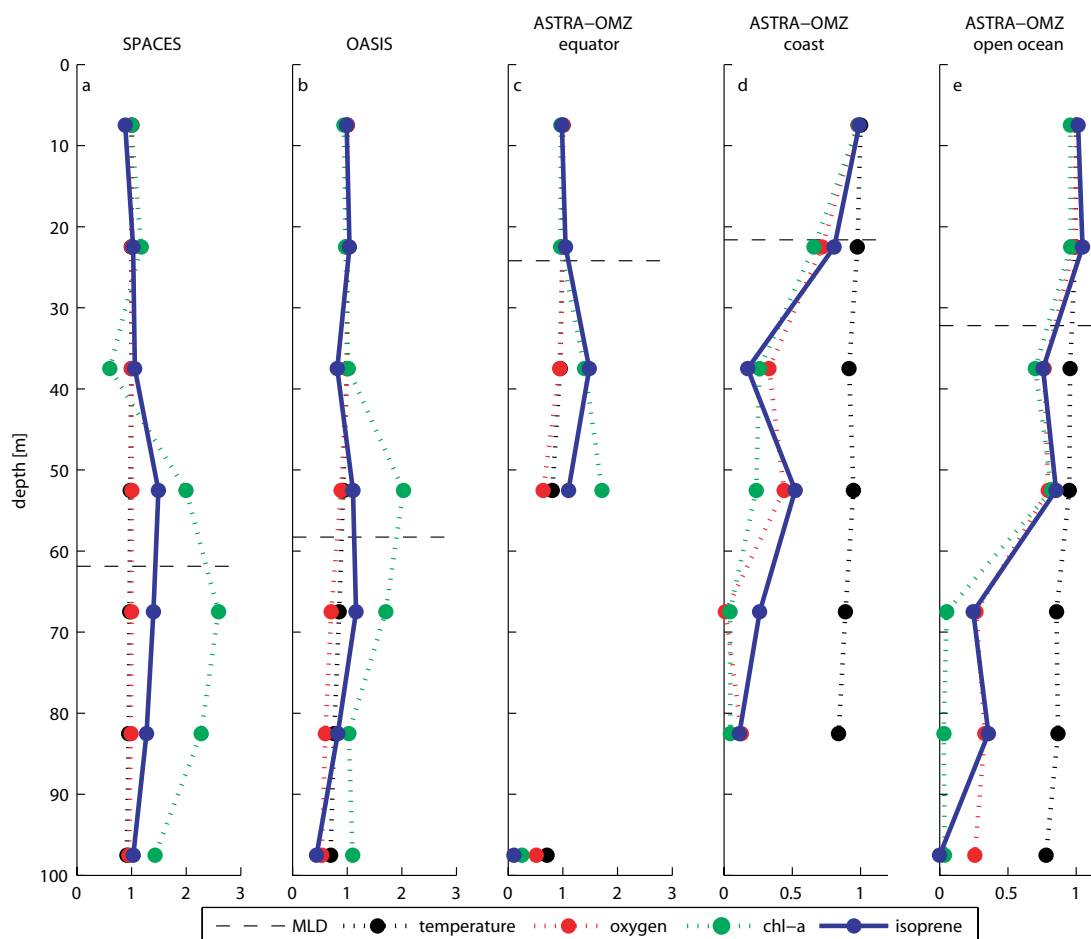
Figure 5.4: Mean normalized depth profiles of temperature (black), oxygen (red), chl-a (green) and isoprene (blue) during (a) SPACES, (b) OASIS, and (c,d,e) ASTRA-OMZ. The black dashed line represents the mean MLD for each cruise.

As isoprene is produced biologically by phytoplankton, many studies attempted to find a correlation between chl-a and isoprene, but found very different results. BONSANG et al. (1992), MILNE et al. (1995) and ZINDLER et al. (2014) did not find a significant correlation, whereas other studies could show a significant correlation and, therefore, attempted a linear regression to show a relationship between isoprene and chl-a, as well as SST (BROADGATE et al., 1997; HACKENBERG et al., 2017; KURIHARA et al., 2012; KURIHARA et al., 2010; OOKI et al., 2015). Comparing the different factors of each regression equation (Table 5.1), it can be seen that, even if the correlations for most of the datasets are significant, there is no globally unique regression factor to adequately describe the relationship between chl-a (and SST) and isoprene. As shown in Table 5.1, during ASTRA-OMZ there was no significant correlation between chl-a and isoprene, whereas during

SPACES and OASIS the correlation was significant but with low R^2-values (SPACES: R^2=0.30, OASIS: R^2=0.10) and different regression coefficients. HACKENBERG et al. (2017) split their data from three different cruises into two SST bins with SST values higher and lower than 20°C, resulting in significant correlations with R^2-values from 0.37 to 0.82 depending on the cruise (Table 5.1). OOKI et al. (2015) described a multiple linear relationship between isoprene, chl-a and SST when using three different SST regimes (Table 5.1). Our correlations, using the approaches of OOKI et al. (2015) and HACKENBERG et al. (2017), were significant, except for SST values higher than 27°C, but the regression coefficients were also significantly different to those found by OOKI et al. (2015) and HACKENBERG et al. (2017). These varying equations demonstrate that bulk chl-a concentrations, or linear combinations of chl-a concentration and SST, do not adequately predict the variability of isoprene in the global surface ocean, but do point to these variables as among the main controls on isoprene concentration in the euphotic zone.

5.3.3 Modeling chl-a normalized isoprene production rates

The directly calculated production rate (P_{direct}) using Equation 7 and the indirectly calculated production rate (P_{need}) using Equation 10 were compared and were found to be significantly different (Figure 5.5a, difference in percent: (P_{direct} - P_{need})/P_{need}*100). The difference of more than -70% between P_{direct} and P_{need} during SPACES/OASIS means that P_{direct} is too low to account for the measured isoprene concentrations, which is also true for the equatorial region of ASTRA-OMZ. In the open ocean region of ASTRA-OMZ, the average difference between P_{direct} and P_{need} is the lowest but still highly variable from station to station. However, in the coastal region of ASTRA-OMZ the directly calculated isoprene production rate is highly overestimating the needed production by 75% on average. There are three possible explanations for this difference: 1) the presence of a missing sink, which is not accounted for in the calculation of P_{need}. Adding an additional loss term to equation 10 would increase the needed production to reach the measured isoprene concentration. This sink would only be valid for this specific coastal region, but would increase the discrepancy between P_{direct} and P_{need} for all other performed cruises. Furthermore, this possible loss rate constant would have to be on average 0.22 day^{-1} and, therefore, higher than the main loss due to air sea gas exchange in the coastal region (see section 5.3.5 and Figure 5.8). Thus, it is highly unlikely that this additional loss term is the only reason for the discrepancy between P_{direct} and P_{need}; 2) uncertainty of using a light dependent log squared fit. Measurements from different laboratory studies used different species within one group of PFTs. All species within one PFT group were combined to produce a light dependent isoprene production rate (Figure S5.3), although the isoprene production variability of different species within one PFT group is quite high. This will certainly influence P_{direct}, but cannot explain the 70% difference between P_{direct} and P_{need} measured at SPACES/OASIS and ASTRA-OMZ (equator) (Figure 5.5); 3) incorrect literature derived chl-a normalized isoprene production rate (P_{chloro}) for one or more groups of PFTs. For example, the high P_{direct} values,

compared to the P_{need} values, during ASTRA-OMZ coincided with high chl-a concentrations in the coastal area. These coastal stations were, in contrast to all other measured stations, highly dominated by diatoms (up to 7.67 µg L^{-1}, Figure S5.5). This might point to a possibly incorrect P_{chloro} value (too high) for diatoms (and other PFTs).
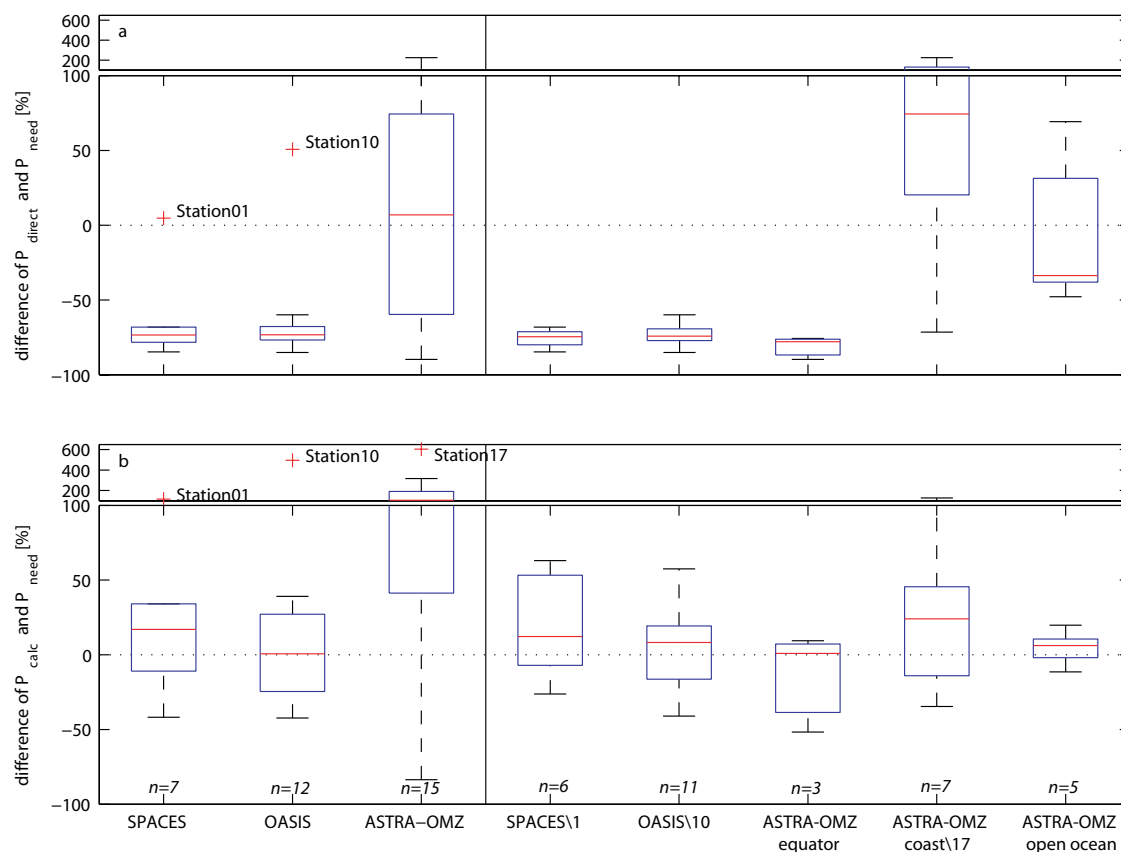
Figure 5.5: Percent differences between (a) P_{direct} and P_{need} ((P_{direct}-P_{need})/P_{need}) and (b) P_{calc} and P_{need} ((P_{calc}-P_{need})/P_{need}) for the different cruises / cruise regions. Left of the vertical black line data is divided into the three different cruises, right of the vertical black line data is shown for the three cruises where outliers from left part are excluded. Additionally, ASTRA-OMZ was split into three regions (equator, coast, open ocean). Number of stations (n) used for each set of data is shown in italics. The red line represents the median, the boxes show the first to third quartile and the whiskers illustrate the highest and lowest values that are not outliers. The red plus signs represent outliers. The number indicated after \ denotes a station that has been excluded from the analysis.

Therefore, we calculated new individual chl-a normalized production rates of each PFT ($P_{chloronew}$) within the MLD. We used the concentrations of haptophytes, cyanobacteria and *Prochlorococcus* for SPACES/OASIS and the concentrations of haptophytes, chlorophytes and diatoms for ASTRA-OMZ, as these PFT were the three most abundant PFTs of each cruise, accounting on average for ≥80% of total PFTs. We performed a multiple linear regression by fitting a linear equation between the P_{need} values for each station and the corresponding PFT chl-a concentrations (analogous to equation (5.7)) to derive one new calculated $P_{chloronew}$ value for each PFT and cruise, which is listed in Table 5.3. The lower and upper limit of the $P_{chloronew}$ value was set to 0.5 and 50 µmol (g chl-a)$^{-1}$ day^{-1}, respectively, when performing the multiple linear regression, to

avoid mathematically possible but biologically unreasonable negative chl-a normalized isoprene production rates. The upper limit was chosen in relation to the maximum published chl-a normalized isoprene production rate of *Prasinococcus capsulatus* by EXTON et al. (2013) (32.16±5.76 µmol (g chl-a)$^{-1}$ day^{-1}). This rate was measured during common light levels of 300 µmol m^{-2} s^{-1}. Applying a same log squared relationship between light levels and the isoprene production rate as for the other PFTs would increase this value up to 50 µmol (g chl-*a*)$^{-1}$ day^{-1} at light levels of ~1000 µmol m^{-2} s^{-1}. Our tests using the whole PFT community for the multiple linear regression did not change our results and, in some cases, led to highly unlikely production rates for the less abundant PFTs.

With the help of the multiple linear regression derived $P_{chloronew}$ values, we calculated the new direct isoprene production rate (P_{calc}) in the same way as P_{direct} in equation 7. We compared our calculated P_{calc} values with the P_{need} values, which are shown in Figure 5.5b (difference in percent between P_{calc} and P_{need}). We found one outlier station for each cruise (SPACES: Station 1, OASIS: Station 10, ASTRA-OMZ: Station 17), when using the new $P_{chloronew}$ values for each PFT for each whole cruise (Figure 5.5b, left part). We excluded these stations from every following calculation and redid the multiple linear regression. Furthermore, we split the ASTRA-OMZ into three different regions (equator, coast and open ocean), due to their contrasting biomass to isoprene concentration ratio, and calculated new $P_{chloronew}$ values for each of the three most abundant PFTs for SPACES, OASIS, and each part of ASTRA-OMZ.

Haptophytes were one of the three most abundant PFTs during all three cruises (Figure S5.5) and their $P_{chloronew}$ values range from 0.5 to 47.9 µmol (g chl-*a*)$^{-1}$ day^{-1} with a mean value of 17.9 ± 18.3 µmol (g chl-*a*)$^{-1}$ day^{-1} for all cruises. The haptophyte production rates exhibited two interesting features. First, this range is highly variable depending on the oceanic region (tropical ocean (SPACES), subtropical ocean (OASIS)) and different ocean regimes (coastal, open ocean). Second, the average value is different from the mean value of all laboratory study derived isoprene production rates of haptophytes (6.92±5.78 µmol (g chl-*a*)$^{-1}$ day^{-1}, Table 5.3). During SPACES/OASIS the $P_{chloronew}$ values of *Prochlorococcus* (both 0.5 µmol (g chl-*a*)$^{-1}$ day^{-1}) are slightly lower but in good agreement with the mean literature value (1.5 µmol (g chl-*a*)$^{-1}$ day^{-1}, Table 5.3), whereas the cyanobacteria values are higher (44.7 and 13.9 µmol (g chl-*a*)$^{-1}$ day^{-1}) than the literature value (6.04 µmol (g chl-*a*)$^{-1}$ day^{-1}, Table 5.3). Chlorophytes, as well as diatoms, are known to be low isoprene producers with mean P_{chloro} values of 1.47 µmol (g chl-*a*)$^{-1}$ day^{-1} and 2.51 µmol (g chl-*a*)$^{-1}$ day^{-1}, respectively (Table 5.3). For diatoms, this is verified with our calculated rates during ASTRA-OMZ (all values ≤ 0.6 µmol (g chl-*a*)$^{-1}$ day^{-1}), whereas the rate for chlorophytes in the coastal regions (6.1 µmol (g chl-*a*)$^{-1}$ day^{-1}) is significantly higher than in the open ocean and equatorial region during ASTRA-OMZ (0.5 µmol (g chl-*a*)$^{-1}$ day^{-1}). Over all three cruises no significant correlations were found between the new multiple linear regression derived $P_{chloronew}$ values of each PFT and any other parameter measured on the cruise. This may be caused by the high variability of the chl-a normalized production rates of different PFTs (Table 5.3). Another explanation could be the high variability of isoprene production of different species within one PFT group. For instance, in the PFT group of haptophytes, the isoprene production rates of two different strains of *Emiliania huxleyi* meas-

ured by Exton et al. (2013) were 11.28 ± 0.96 and 2.88 ± 0.48 µmol (g chl-a)$^{-1}$ day^{-1} for strain CCMP 1516 and CCMP 373, respectively. Laboratory culture experiments show that stress factors, like temperature and light, also influence the emission rate within one species (Exton et al., 2013; Meskhidze et al., 2015; Shaw et al., 2003). Srikanta Dani et al. (2017) showed that in a light regime of 100-600 µmol m^{-2} s^{-1} the isoprene emission rate was constantly increasing with higher light levels for the diatom *Chaetoceros calcitrans*, whereas the diatom *Phaeodyctylum tricornutum* was highest at 200 µmol m^{-2} s^{-1} and decreased at higher light levels. Furthermore, health conditions (Shaw et al., 2003), as well as the growth stage of the phytoplankton species (Milne et al., 1995), can also influence the isoprene emission rate.

With the new P_{calc} values, we slightly overestimate the needed production P_{need} by up to 20% on average (Figure 5.5b, right part). For SPACES and OASIS, except for stations 1 and 10, using one $P_{chloronew}$ value for each PFT for the whole cruise is reasonable because the biogeochemistry in these regions did not differ much within one cruise. This was not true for ASTRA-OMZ, due to the biogeochemically contrasting open ocean region and the coastal upwelling region. Using just one $P_{chloronew}$ value for each PFT for the whole cruise resulted in a highly overestimated and variable P_{calc} value (Figure 5.5b, "ASTRA-OMZ"). Therefore splitting this cruise into three different parts (equator, coast, open ocean), due to their different chl-a concentration and nutrient availability, resulted in less variable P_{calc} values. However, in the coastal region, the variability is still the highest, but with the new derived P_{calc} the agreement with P_{need} is significantly better than with P_{direct} (compare Figure 5.5a and b).

Table 5.3: Calculated chl-a normalized isoprene production rates ($P_{chloronew}$, µmol (g chl-a)$^{-1}$ day^{-1}) of the three most abundant PFTs during SPACES/OASIS (haptophytes, cyanobacteria, *Prochlorococcus*) and ASTRA-OMZ (haptophytes, chlorophytes, diatoms). Number indicated after \ denotes a station that has been excluded from the analysis. For explanation of the omission, please refer to section 5.3.3.

cruise		haptophytes	cyanobacteria	*Prochlorococcus*	chlorophytes	diatoms
SPACES\1		0.5	44.7	0.5	--	--
OASIS\10		21.2	13.9	0.5	--	--
ASTRA-OMZ	equator	47.9	--	--	0.5	0.5
	coast\17	9.6	--	--	6.1	0.6
	open ocean	10.3	--	--	0.5	0.5
Collection of literature values in Booge et al. (2016)		6.92	6.04	1.5*	1.47	2.51*

*production rates from Arnold et al. (2009) were excluded from literature values listed in Booge et al. (2016)

5.3.4   Drivers of isoprene production

As mentioned above, no significant correlations between each calculated $P_{chloronew}$ value and any other parameter during the three cruises were found. *Prochlorococcus* was one of the three most abundant PFTs during SPACES and OASIS, but concentrations decrease to almost zero in the colder open ocean and upwelling regions of ASTRA-OMZ (Figure 5.1), which confirms the general knowledge that *Prochlorococcus* is absent at temperatures <15°C (JOHNSON et al., 2006). Our newly derived production rates confirm the actual laboratory derived rates, demonstrating *Prochlorococcus* as a minor contributor to isoprene concentration. However, *Prochlorococcus* is especially abundant at high ocean temperatures, where isoprene production rates from the other PFTs show evidence of decreasing. Cyanobacteria concentrations (excluding *Prochlorococcus*) were also related to temperature, but, in contrast to *Prochlorococcus*, other cyanobacteria taxa can be abundant in colder waters during ASTRA-OMZ. The different derived isoprene production rates for SPACES and OASIS might be related to the different mean ocean temperature and light levels during these cruises. During SPACES, with lower ocean temperatures and lower light levels, compared to OASIS, the production rate is higher. This relationship would confirm the findings of two independent laboratory studies of BONSANG et al. (2010) and SHAW et al. (2003). BONSANG et al. (2010) tested two species of cyanobacteria at 20°C and found higher isoprene production rates than a different species tested by SHAW et al. (2003) at 23°C and even stronger light intensities. However, EXTON et al. (2013) measured the same rate as SHAW et al. (2003) at 26°C for one species, but a 5-times higher production rate for another species at the same temperature. Because we do not know which species were present, we hypothesize that the production rate is not dependent on one environmental parameter and varies from species to species within the group of cyanobacteria.

Comparing the calculated isoprene production rates of the haptophytes with global radiation, ocean temperature, salinity and nitrate results in some interesting qualitative trends (Figure 5.6). Mean global radiation during SPACES (~360 W m^{-2}) was lower than during OASIS (~457 W m^{-2}). Highest mean values were measured during ASTRA-OMZ (at equator, ~508 W m^{-2}). The same trend can be seen in the $P_{chloronew}$ values of the haptophytes. Within the open ocean and coastal regimes of ASTRA-OMZ, the isoprene production rate was lower than around the equator (mean global radiation decreased to ~310 W m^{-2}). A similar trend can be seen with the mean ocean temperature and the $P_{chloronew}$ values of the haptophytes. These results are similar to several laboratory experiments with monocultures: Higher light intensities and water temperatures enhance phytoplankton ability to produce isoprene (EXTON et al., 2013; MESKHIDZE et al., 2015; SHAW et al., 2003). However, MESKHIDZE et al. (2015) showed in laboratory experiments that isoprene production rates from two diatoms species were highest when incubated in water temperatures of 22 to 26°C. Higher temperatures caused a decrease in isoprene production rate. During OASIS, mean water temperatures were 27.3°C with up to 29.2°C near the Maldives. Increasing ocean temperatures influence the growth rate of phytoplankton generally, but also differently within one group of PFTs. For haptophytes, HUERTAS et al. (2011) show that two strains of *Emiliania huxleyi* were not tolerant to a

temperature increase from 22°C to 30°C, whereas *Isochrysis galbana* could adapt to the increased temperature. In general, the optimal growth rate temperature decreases with higher latitude (CHEN, 2015), but the link between growth rate of phytoplankton and isoprene production rate is still not known. Assuming this temperature dependence can be transferred from diatoms also to haptophytes, the high seawater temperatures during OASIS could explain why the calculated isoprene production rate is lower than in the ASTRA-OMZ-equatorial regime. Additionally, as mentioned before, the temperature as well as the light dependence of isoprene production might vary between different species of haptophytes when comparing different ocean regimes. Another reason for the very high isoprene production rate of haptophytes in the equatorial regime during ASTRA-OMZ, apart from temperature and light intensity, could be stress-induced production caused by low saline waters, which was already shown for dimethylsulphoniopropionate, a precursor for the climate relevant trace gas dimethyl sulfide (DMS), produced by phytoplankton (SHENOY et al., 2000). The salinity is considerably lower at the equator during ASTRA-OMZ than for all other cruise regions, with values down to 33.4. We observed that the $P_{chloronew}$ values decrease again in regions with more saline waters, where phytoplankton likely experience less stress due to salinity, temperature or light levels (Figure 5.6).
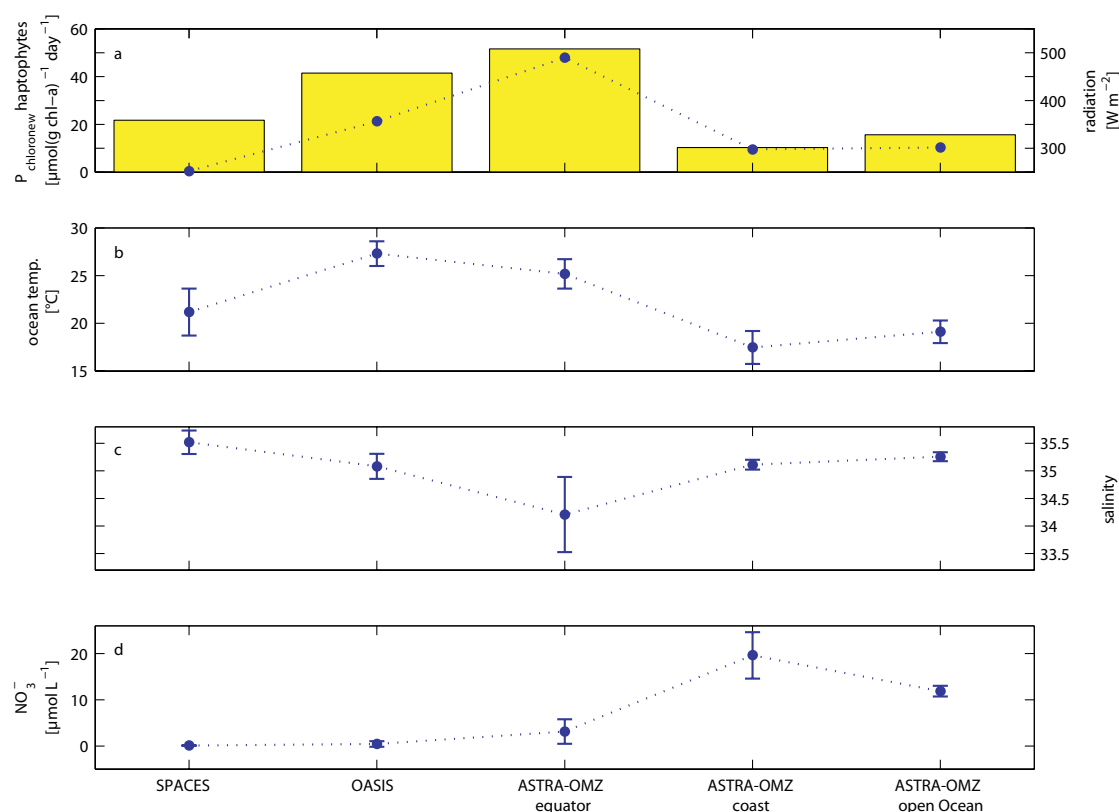
Figure 5.6: Mean values (± standard deviation) for (a) calculated $P_{chloronew}$ haptophytes (blue line) and global radiation (yellow bars), (b) ocean temperature, (c) salinity and (d) nitrate during SPACES/OASIS and ASTRA-OMZ (split into 3 different parts: equator, coast and open ocean).

In order to identify parameters that influence not only the chl-a normalized isoprene production rate of haptophytes, but the rate of all PFTs together, we calculated a normalized isoprene production rate (P_{norm}) independent from the absolute amount of each PFT. Hence, we divided each P_{calc} value at every station by the amount of the three most abundant PFTs:

$$P_{norm} = \frac{\sum_{i=1}^{3} P_{chloronew_i} \times [PFT]_i}{\sum_{i=1}^{3} [PFT]_i} = \frac{P_{calc}}{\sum_{i=1}^{3} [PFT]_i} \tag{5.11}$$

i = three most abundant PFTs during each cruise.

The P_{norm} value helps us to obtain more insight about the influencing factors at each station, rather than only one mean data point for each cruise. We plotted the P_{norm} values of each station versus the ocean temperature and color-coded them by nitrate concentration as a marker for the nutrient availability (Figure 5.7).
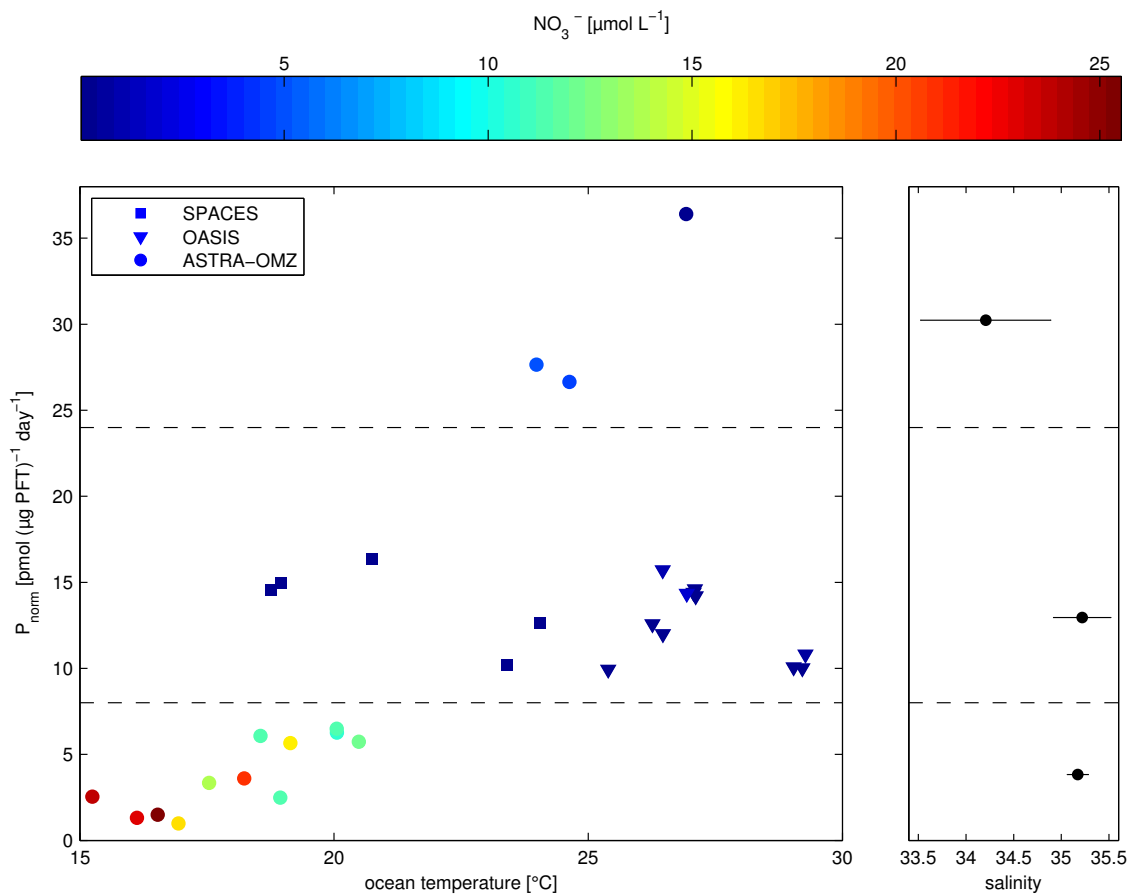
Figure 5.7: Relationship between P_{norm} in pmol $(\mu g\ PFT)^{-1}\ day^{-1}$ and ocean temperature in °C during SPACES (squares), OASIS (triangles), and ASTRA-OMZ (circles) color-coded by NO_3^- in $\mu mol\ L^{-1}$ (Left panel). Mean salinity (± standard deviation) of samples from left side plot in each box divided by dashed lines (Right panel).

During SPACES (squares) and OASIS (triangles), the normalized production rate is on average 12.8 ± 2.2 pmol $(\mu g\ PFT)^{-1}\ day^{-1}$ and independent from the ocean temperature, while the nitrate concentration is very low ($0.33 \pm 0.53\ \mu mol\ L^{-1}$). During ASTRA-OMZ

(circles) in the coastal and open ocean region, the nitrate concentrations were significantly higher (16.4 ± 5.5 μmol L^{-1}), but the P_{norm} values were lower (< 8 pmol (μg PFT)$^{-1}$ day^{-1}) correlating with lower ocean temperatures. In the equatorial region of ASTRA-OMZ, the production rates are significantly higher than during SPACES and OASIS, with up to 36.4 pmol (μg PFT)$^{-1}$ day^{-1}. On the right panel of Figure 5.7, the mean salinity for each P_{norm} dependent box (separated by the dashed lines) is shown. ASTRA-OMZ (equator) and SPACES and OASIS do not differ in ocean temperature or in nitrate concentration. However, the normalized production is significantly higher at the ASTRA-OMZ equatorial region, which may be caused by the low salinity there. In summary: 1) During ASTRA-OMZ (coast, open ocean) P_{norm} is comparably lower (< 8 pmol (μg PFT)$^{-1}$ day^{-1}) under "biogeochemically active" conditions (high nitrate concentration) but increases with increasing ocean temperature, 2) Under limited nutrient conditions P_{norm} is significantly increased likely due to nutrient stress 3) If the phytoplankton are additionally stressed due to lower salinity, P_{norm} is furthermore increased. These results show that there is no main parameter driving the isoprene production rate, resulting in a more complex interaction of physical and biological parameters influencing the phytoplankton to produce isoprene.

5.3.5 Loss processes

The comparison between P_{calc} and P_{need} in Figure 5.5b shows a mean overestimation of 10-20%. This is likely due to a missing loss term in the calculation, which would balance out the needed and calculated isoprene production. Chemical loss (red dashed line) and loss due to air sea gas exchange (black solid line) using the gas transfer parameterization of WANNINKHOF (1992) were already included in the calculation (Equation 10) and their loss rate constants are shown in Figure 5.8. For comparison, we added the k_{AS} values using the parameterizations of WANNINKHOF and MCGILLIS (1999) (black dotted line) and NIGHTINGALE et al. (2000) (black dashed line). They have different wind speed dependencies of gas transfer, which could influence the computed isoprene loss at high wind speeds. The parameterization of WANNINKHOF and MCGILLIS (1999) is cubic and will increase the loss rate constant of isoprene due to air sea gas exchange at high winds compared to the other parameterizations (Figure 5.8, OASIS). NIGHTINGALE et al. (2000) is a combined linear and quadratic parameterization, which would decrease the isoprene loss due to air sea gas exchange. However, during SPACES and ASTRA-OMZ the wind speed was between 8 and 10 m s^{-1} where the parameterization of WANNINKHOF (1992) is higher than both WANNINKHOF and MCGILLIS (1999) and NIGHTINGALE et al. (2000). Therefore the use of these alternative parameterizations would even lower the loss rate constant due to air sea gas exchange, leading to the need of an additional loss rate in order to balance the isoprene production.

To calculate the additionally required consumption rate ($k_{consumption}$), we only used stations where a loss term was actually needed to balance the calculated and needed production ($P_{calc} > P_{need}$). Those values were averaged within each cruise and are shown in Figure 5.8. For comparison, we added the loss rate constants due to bacterial consumption from PALMER and SHAW (2005) (blue dashed line; 0.06 day^{-1}) and an updated value
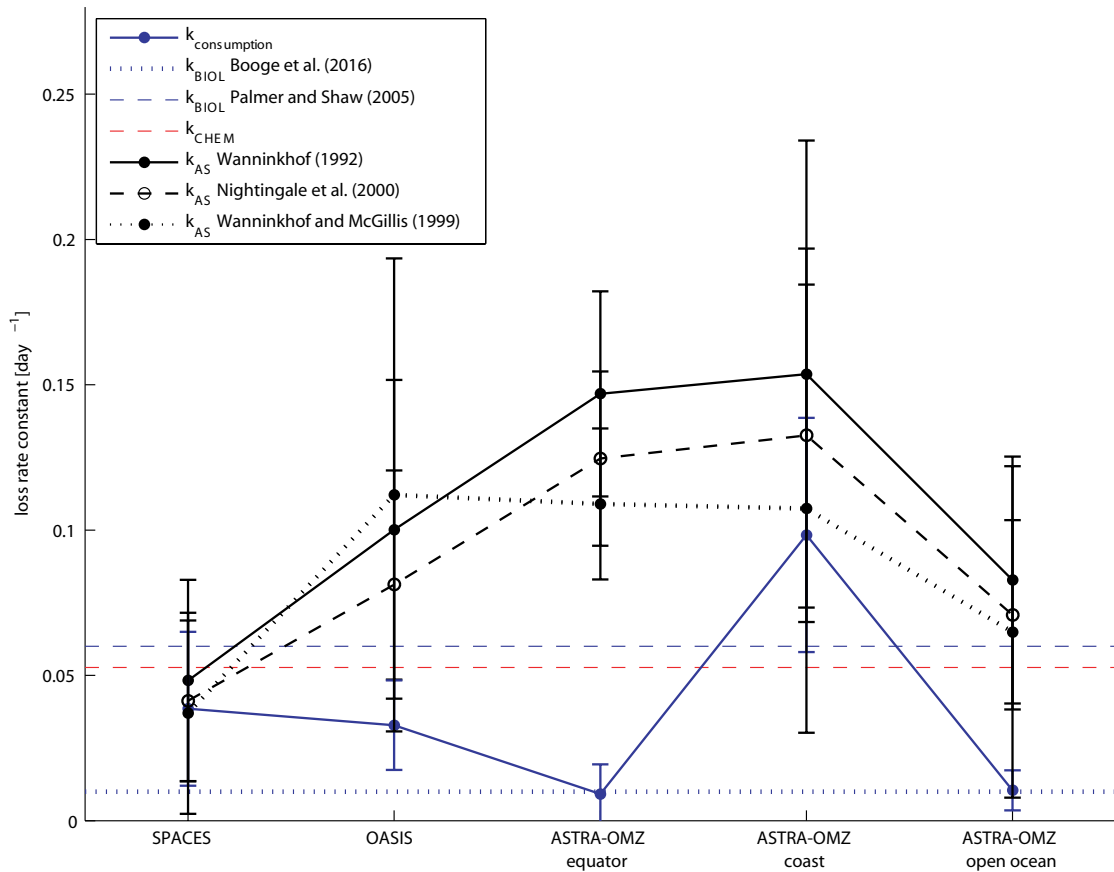
Figure 5.8: Different mean loss rate constants (± standard deviation) during SPACES, OASIS und AS-TRA-OMZ. Blue points: calculated loss rate ($k_{consumption}$), blue dotted line: k_{BIOL} from BOOGE et al. (2016), blue dashed line: k_{BIOL} from PALMER and SHAW (2005), red dashed line: k_{CHEM}, black points: calculated loss rate constants due to air-sea-gas exchange.

from BOOGE et al. (2016) (blue dotted line; 0.01 day^{-1}). Comparable to the chemical loss rate, the k_{BIOL} values were assumed to be constant (following the assumption of PALMER and SHAW (2005)), because no data about bacterial isoprene consumption in surface waters is available. Figure 5.8 clearly shows that the needed loss rate constant is not a constant factor. During SPACES and OASIS the loss rate constant is roughly in the middle of the assumed k_{BIOL} values of PALMER and SHAW (2005) and BOOGE et al. (2016), whereas during ASTRA-OMZ (equator and open ocean) the calculated loss rate constant fits quite well with the assumed value of BOOGE et al. (2016). In all four regions, the additional calculated sink is lower than the chemical loss and the loss due to air sea gas exchange, which is not true for the coastal region of ASTRA-OMZ. Here, the loss rate constant (0.1 day^{-1}) is about 10 times higher than in the open ocean region, resulting in a lifetime of isoprene of only 10 days, which is comparable to the lifetime due to air sea gas exchange during ASTRA-OMZ (open ocean) and OASIS. Physical loss, like advective mixing through the thermocline, cannot account for this sink, as this lifetime is assumed to be several years (PALMER and SHAW, 2005) and, therefore, negligible. Even a change in the chemical loss rate would only change the absolute value of the calculated loss rate constant, but not its variability. We tested a temperature dependent rate for the reaction with OH, but the mean difference of the temperature dependent k_{CHEM} to the non-

temperature dependent k_{CHEM} was less than 2% for all temperature regimes during the cruises and, therefore, negligible. It must be noted that the loss rate due to the reaction with OH is a gas phase reaction rate (ATKINSON et al., 2004) and the used rate for reaction with singlet oxygen derives from measurements in chloroform (MONROE, 1981), meaning that these rates might not be suitable for isoprene reactions in the water phase. These rates, involving possible temperature and pressure dependencies, have to be evaluated in seawater in order to determine the chemical loss in the water column.
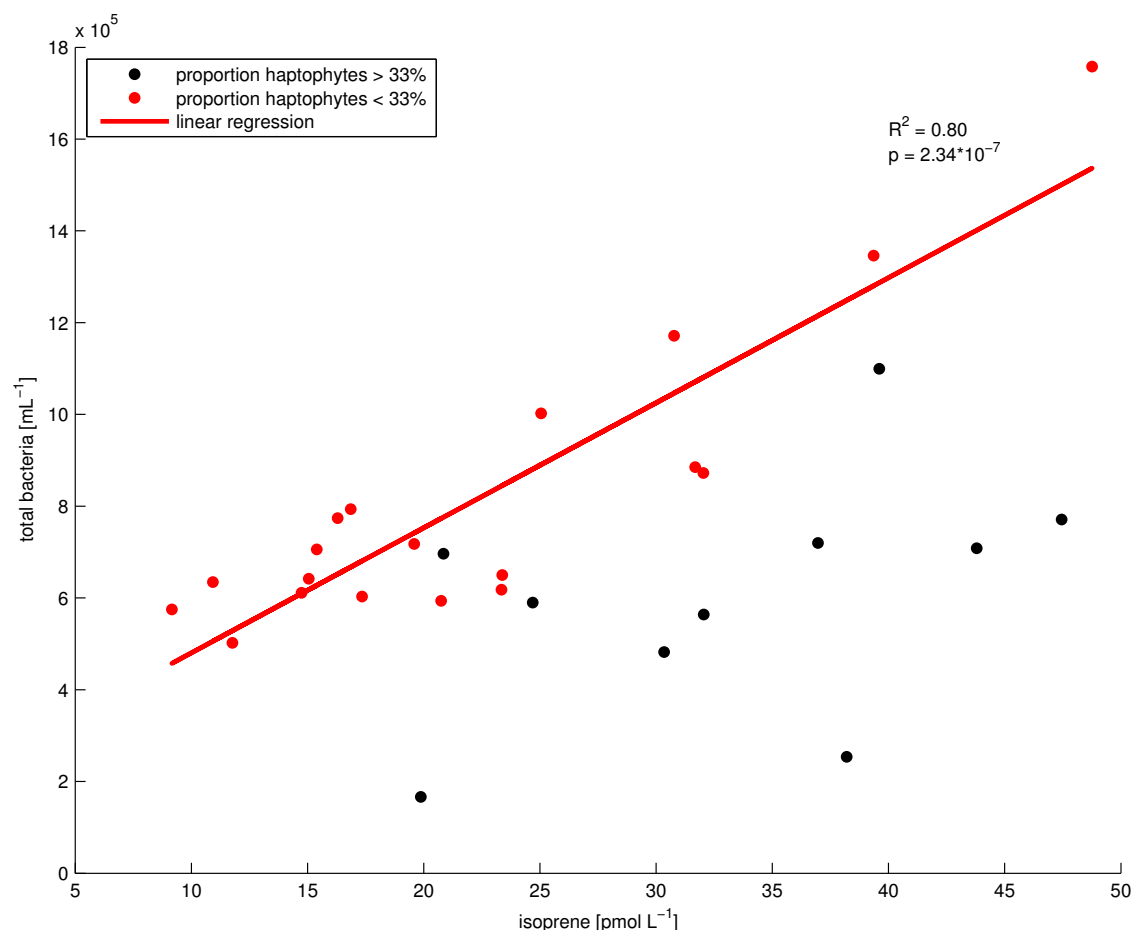
Figure 5.9: Relationship between isoprene concentration [pmol L^{-1}] and total bacteria counts [mL^{-1}] during SPACES/OASIS and ASTRA-OMZ. Black and red points represent samples where the contribution of haptophytes to the total phytoplankton chl-a concentration is higher and lower than 33%, respectively. Linear regression (R²=0.80, p=2.34*10^{-7}) for red points only.

Marine produced halocarbons, like dibromomethane and methyl bromide, are known to undergo bacterial degradation (GOODWIN et al., 1998). Compared to halocarbons, isoprene is not toxic and has two energy-rich double bonds and, therefore, may be even favored to be oxidized by heterotrophic marine bacteria (ACUÑA ALVAREZ et al., 2009). Figure 5.9 shows a comparison of total bacteria counts and isoprene concentration from each station in the MLD. The correlation between bacteria and the concentration of isoprene is only significant when haptophytes are less than 33% of the total phytoplankton chl-a concentration (R^2=0.80, p=2.34*10^{-7}). Haptophytes were one of the three dominant

PFTs during all cruises and had a mean calculated isoprene production rate of 17.9 μmol (g chl-a)$^{-1}$ day^{-1} (Table 5.3). This is a high isoprene production rate and we could assume higher isoprene concentrations with higher concentrations of haptophytes. This relationship, however, is not evident (data not shown), which may indicate that other processes mask this relationship. Multiplying the chl-a normalized isoprene production rate of 17.9 μmol (g chl-a)$^{-1}$ day^{-1} with the chl-a concentration of haptophytes results in a mean isoprene production rate of ~ 3 pmol L^{-1} day^{-1} which is about 4 times higher than the mean calculated loss rate due to bacterial degradation over all cruises (~ 0.8 pmol L^{-1} day^{-1}). This could hide the correlation of isoprene concentrations with bacteria when haptophytes are dominant (>33%). In addition, haptophytes themselves are suggested to be the main marine bacterial grazers, compared to other PFTs (UNREIN et al., 2014). This leads to the hypothesis that, if there is a lot of isoprene abundant which can be used (e.g. as energy source) by bacteria, also the bacteria abundance will increase, independent of any PFT. However, if the phytoplankton community is dominated (>33%) by haptophytes, the isoprene concentration is no longer correlated to the bacteria abundance, due to the grazing of bacteria by haptophytes (Figure 5.9, total bacteria cell counts of black points are lower than of the red points at similar isoprene concentrations).
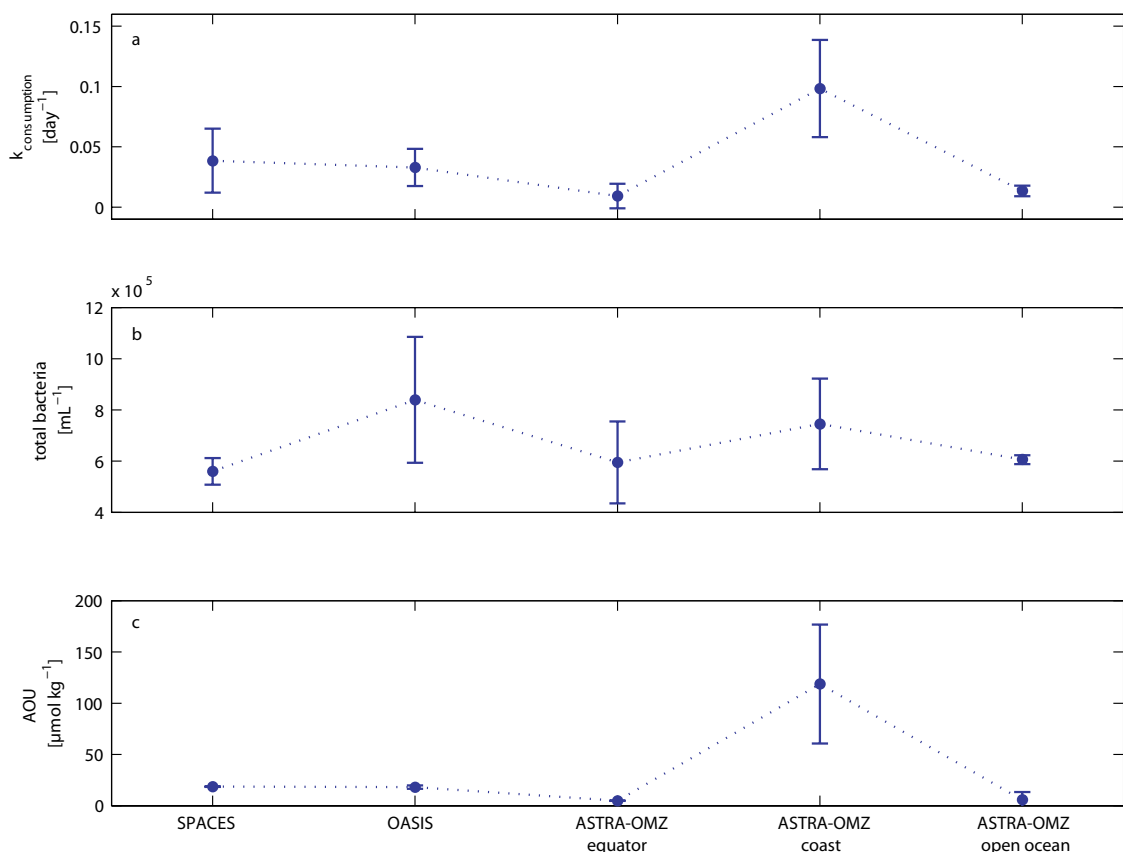
Figure 5.10: Mean values (± standard deviation) for (a) $k_{consumption}$ [day^{-1}], (b) total bacteria counts [mL^{-1}] and (c) AOU [μmol L^{-1}] during SPACES/OASIS and ASTRA-OMZ (split into three different parts: equator, coast and open ocean).

Due to the different loss rate constants of bacterial degradation (~0.01 day^{-1} during ASTRA-OMZ (equator) compared to ~0.1 day^{-1} in the coastal region of ASTRA-OMZ, Figure 5.8) in the different regions it is important to identify their dependence on environmental parameters. Unfortunately, the absolute amount of bacteria does not have a significant influence on $k_{consumption}$ (Figure 5.10a,b), which may be caused by different heterotrophic bacteria, each with a different ability to use isoprene as an energy source. However, we find a similar qualitative trend for $k_{consumption}$ and the apparent oxygen utilization (AOU) (difference of equilibrium oxygen saturation concentration and the actual measured dissolved oxygen concentration) during the three cruises (Figure 5.10c). The higher loss rate constant of isoprene due to possible bacterial consumption coincides with considerably higher AOU values in the coastal regime of ASTRA-OMZ, which may be caused by heterotrophic respiration. Even if this correlation is not significant, this trend points to the influence of environmental conditions on biological activity, which in turn influences the isoprene consumption.

5.4   Conclusions

For the first time, marine isoprene measurements were performed in the eastern Pacific Ocean. In addition, our isoprene measurements in the highly undersampled Indian Ocean further increase the small dataset of oceanic isoprene measurements in this region. The results from both oceans show that isoprene is well mixed in the MLD. Despite the known biogenic origin of isoprene, the marine isoprene concentrations cannot be described globally with a simple parameterization including chl-a concentration or SST or a combination of both. On regional scales this relationship might be sometimes significant (HACKENBERG et al., 2017; OOKI et al., 2015), but laboratory monoculture experiments show that isoprene production rates range widely over all different PFTs, as well as within one PFT (collection of literature values in BOOGE et al. (2016)). The production rates from laboratory experiments have to be evaluated in the field, as different PFTs are not distributed equally over the world ocean and are also influenced by temperature and salinity, as well as changing light levels. Therefore we used isoprene measurements as well as different phytoplankton marker pigment measurements to derive in-field production rates for haptophytes, cyanobacteria, *Prochlorococcus*, chlorophytes, and diatoms in different regions. The results confirm findings from previous laboratory studies that the isoprene production is influenced by light and ocean temperature, due to stress, and nutrients, due to their effect on changing phytoplankton communities and their abundances (e.g. DANI and LORETO, 2017; SHAW et al., 2010). Moreover, our data leads to the conclusion that isoprene production rates in the field, irrespective of phytoplankton communities and their abundance, are influenced by nutrient levels, which has never been shown before. Additionally, we show that isoprene production rates are influenced by salinity levels, which has also been shown in previous studies (RINNAN et al., 2014 and references therein). Our calculations also show that, besides chemical loss and the loss due to air sea gas exchange, another non-static isoprene consumption process has to be taken into account to understand isoprene concentrations in the surface ocean.

This loss may be attributed to bacterial degradation, or more generally, to heterotrophic respiration, as we could show a similar qualitative trend between the additional loss rate constant and the AOU. These results clearly indicate that further experiments are needed to evaluate isoprene production rates for every PFT in general, but additionally under different biogeochemical conditions (light, salinity, temperature, nutrients). With the help of incubation experiments under different conditions, the additional loss process can be investigated. The exact knowledge of the different production and loss processes, as well as their interaction, is crucial in understanding global marine isoprene cycling. Furthermore, the most appropriate wind speed based k parameterization to compute air sea gas exchange, the main loss process for isoprene in the ocean, must be used in future studies. Different parameterizations under different wind levels highly influence the loss term, which is additionally influenced by surface films at low or bubble generation at high wind speeds. Isoprene loss processes, in conjunction with the complexity of isoprene production, should be further examined in order to predict marine isoprene concentrations and evaluate the impact of isoprene on SOA formation over the remote open ocean.

5.5   Data availability

All isoprene data and bacterial cell counts are available from the corresponding author. Pigment and nutrient data from SPACES/OASIS and ASTRA-OMZ will be available from PANGAEA, but for now can be obtained through the corresponding author.

5.6   Acknowledgements

5.7   Supplementary material

Figure S5.1: Example for above and in-water radiation. (a) Data points represent hourly radiation measurements (converted from W m^{-2} into photosynthetic active radiation (PAR, µmol m^{-2} s^{-1}) as described in section 5.2.6) from the ship (mean values ± standard deviation from all cruises), blue line is the fitted data using a sine function. (b) Underwater mean calculated PAR over the course of a day depending on depth by applying the attenuation coefficient K_dPAR and Beer-Lambert's law. Dashed line represents mean mixed layer depth (MLD) for each cruise.
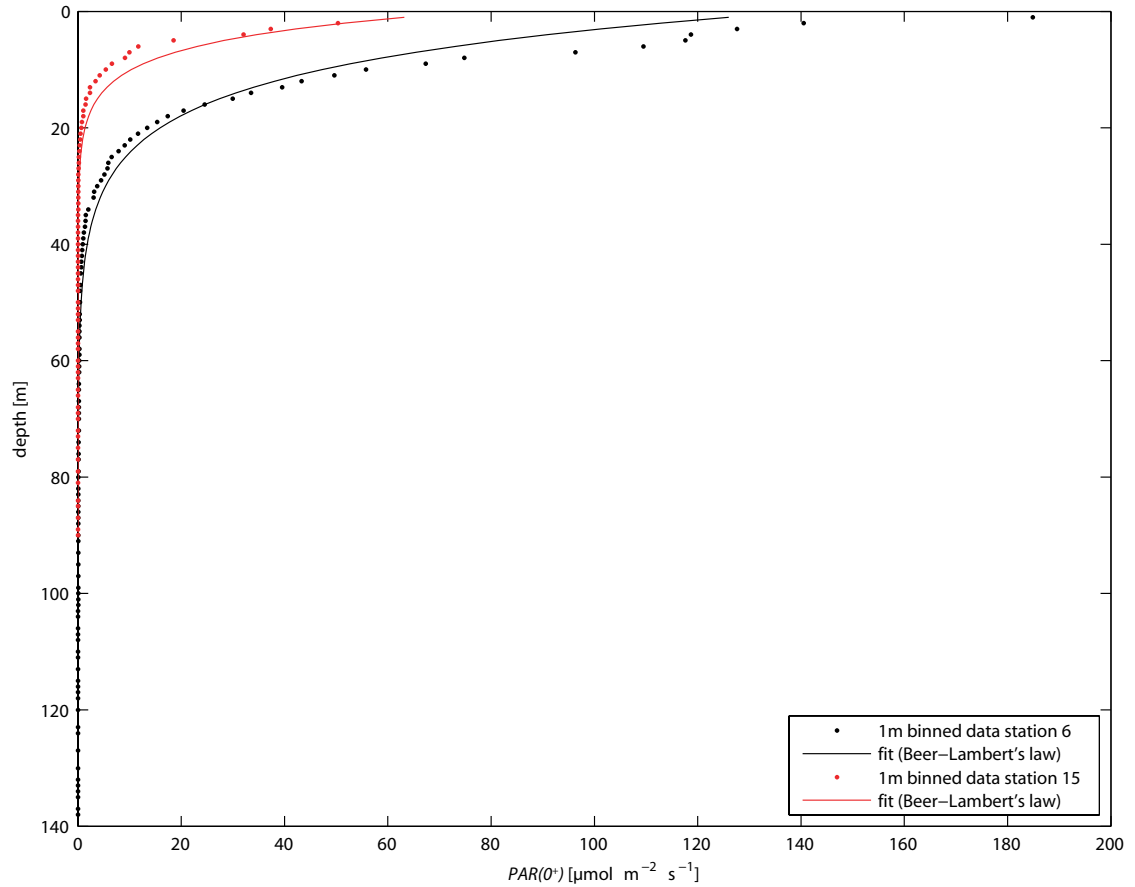
Figure S5.2: Example of two $PAR(0^+)$ depth profile measurements during ASTRA-OMZ. Data points are 1m binned data of station 6 (black) and station 15 (red). The line is calculated from $PAR(0^+)$ by applying Beer-Lambert's law using a mean attenuation coefficient K_dPAR obtained from all $E_dPAR(0^+)$ depth profile measurements during OASIS and ASTRA-OMZ.
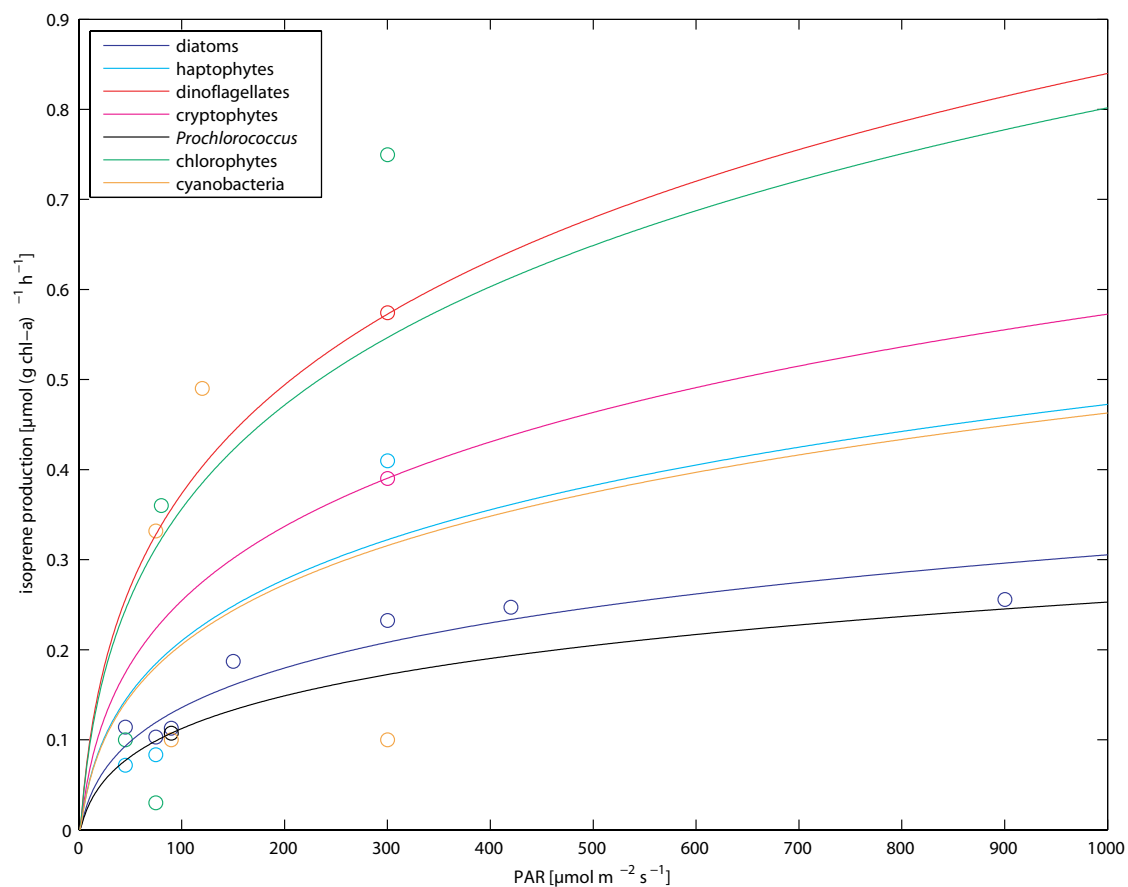
Figure S5.3: Single literature laboratory chl-a normalized isoprene production rates P_{chloro} (µmol isoprene (g chl-a)$^{-1}$ h^{-1}) (Table 5.2) as a log squared function of light intensity I(µmol m^{-2} s^{-1}).
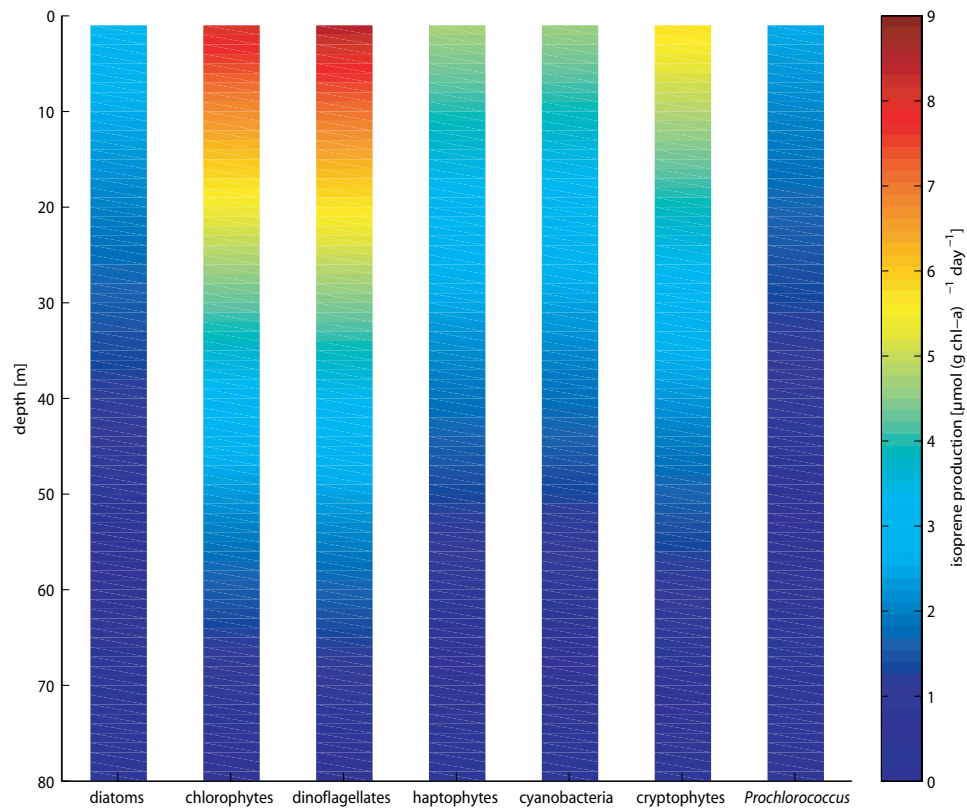
Figure S5.4: Example of calculated P_{chloro} values (µmol isoprene (g chl-a)$^{-1}$ day^{-1}) for each PFT at station 9 during SPACES depending on the depth in the water column.
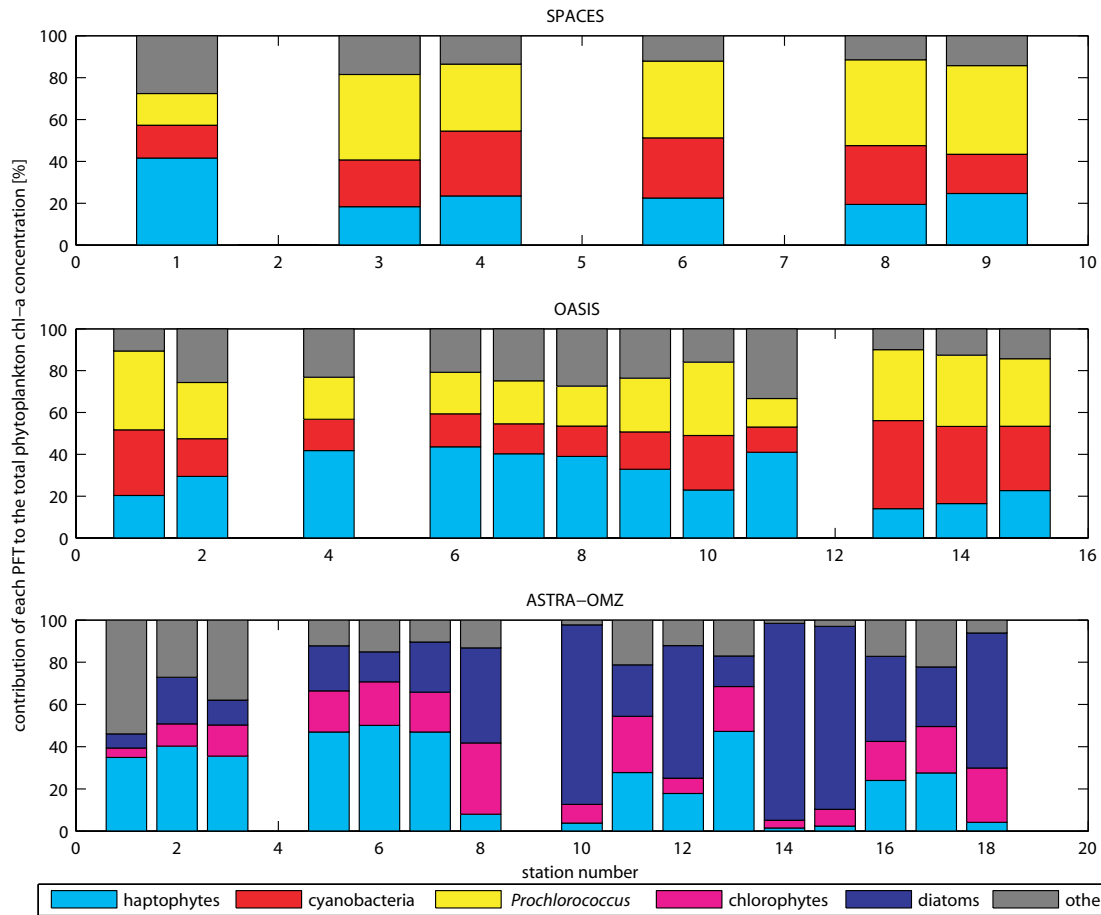
Figure S5.5: Contribution of each of the three most abundant PFTs to the total phytoplankton chl-a concentration at each station during SPACES (upper panel), OASIS (middle panel), and ASTRA-OMZ (bottom panel).

References

ACUÑA ALVAREZ, L., EXTON, D. A., TIMMIS, K. N., SUGGETT, D. J., and MCGENITY, T. J.: Characterization of marine isoprene-degrading communities, *Environmental Microbiology*, 11, 3280-3291, 10.1111/j.1462-2920.2009.02069.x, 2009.

AIKEN, J., PRADHAN, Y., BARLOW, R., LAVENDER, S., POULTON, A., HOLLIGAN, P., and HARDMAN-MOUNTFORD, N.: Phytoplankton pigments and functional types in the atlantic ocean: A decadal assessment, 1995-2005, *Deep-Sea Research Part Ii-Topical Studies in Oceanography*, 56, 899-917, 10.1016/j.dsr2.2008.09.017, 2009.

ANTTILA, T., LANGMANN, B., VARGHESE, S., and O'DOWD, C.: Contribution of isoprene oxidation products to marine aerosol over the north-east atlantic, *Advances in Meteorology*, 10.1155/2010/482603, 2010.

ARNETH, A., MONSON, R. K., SCHURGERS, G., NIINEMETS, Ü., and PALMER, P. I.: Why are estimates of global terrestrial isoprene emissions so similar (and why is this not so for monoterpenes)?, *Atmos. Chem. Phys.*, 8, 4605-4620, 10.5194/acp-8-4605-2008, 2008.

ARNOLD, S. R., SPRACKLEN, D. V., WILLIAMS, J., YASSAA, N., SCIARE, J., BONSANG, B., GROS, V., PEEKEN, I., LEWIS, A. C., ALVAIN, S., and MOULIN, C.: Evaluation of the global oceanic isoprene source and its impacts on marine organic carbon aerosol, *Atmos. Chem. Phys.*, 9, 1253-1262, 10.5194/acp-9-1253-2009, 2009.

ATKINSON, R., and AREY, J.: Atmospheric degradation of volatile organic compounds, *Chemical reviews*, 103, 4605-4638, 2003.

ATKINSON, R., BAULCH, D. L., COX, R. A., CROWLEY, J. N., HAMPSON, R. F., HYNES, R. G., JENKIN, M. E., ROSSI, M. J., and TROE, J.: Evaluated kinetic and photochemical data for atmospheric chemistry: Volume i - gas phase reactions of o_x, ho_x, no_x and so_x species, *Atmos. Chem. Phys.*, 4, 1461-1738, 10.5194/acp-4-1461-2004, 2004.

BAKER, A. R., TURNER, S. M., BROADGATE, W. J., THOMPSON, A., MCFIGGANS, G. B., VESPERINI, O., NIGHTINGALE, P. D., LISS, P. S., and JICKELLS, T. D.: Distribution and sea-air fluxes of biogenic trace gases in the eastern atlantic ocean, *Global Biogeochemical Cycles*, 14, 871-886, Doi 10.1029/1999gb001219, 2000.

BARLOW, R. G., CUMMINGS, D. G., and GIBB, S. W.: Improved resolution of mono- and divinyl chlorophylls a and b and zeaxanthin and lutein in phytoplankton extracts using reverse phase c-8 hplc, *Marine Ecology Progress Series*, 161, 303-307, 10.3354/meps161303, 1997.

BONSANG, B., POLLE, C., and LAMBERT, G.: Evidence for marine production of isoprene, *Geophysical Research Letters*, 19, 1129-1132, Doi 10.1029/92gl00083, 1992.

BONSANG, B., GROS, V., PEEKEN, I., YASSAA, N., BLUHM, K., ZOELLNER, E., SARDA-ESTEVE, R., and WILLIAMS, J.: Isoprene emission from phytoplankton monocultures: The relationship with chlorophyll-a, cell volume and carbon content, *Environmental Chemistry*, 7, 554-563, 10.1071/En09156, 2010.

BOOGE, D., MARANDINO, C. A., SCHLUNDT, C., PALMER, P. I., SCHLUNDT, M., ATLAS, E. L., BRACHER, A., SALTZMAN, E. S., and WALLACE, D. W. R.: Can simple models predict large-scale surface ocean isoprene concentrations?, *Atmos. Chem. Phys.*, 16, 11807-11821, 10.5194/acp-16-11807-2016, 2016.

BROADGATE, W. J., LISS, P. S., and PENKETT, S. A.: Seasonal emissions of isoprene and other reactive hydrocarbon gases from the ocean, *Geophysical Research Letters*, 24, 2675-2678, 10.1029/97gl02736, 1997.

BROADGATE, W. J., MALIN, G., KUPPER, F. C., THOMPSON, A., and LISS, P. S.: Isoprene and other non-methane hydrocarbons from seaweeds: A source of reactive hydrocarbons to the atmosphere, *Marine Chemistry*, 88, 61-73, 10.1016/j.marchem.2004.03.002, 2004.

CARLTON, A. G., WIEDINMYER, C., and KROLL, J. H.: A review of secondary organic aerosol (soa) formation from isoprene, *Atmospheric Chemistry and Physics*, 9, 4987-5005, 2009.

CHAVEZ, F. P., and MESSIÉ, M.: A comparison of eastern boundary upwelling ecosystems, *Progress in Oceanography*, 83, 80-96, http://dx.doi.org/10.1016/j.pocean.2009.07.032, 2009.

CHEN, B.: Patterns of thermal limits of phytoplankton, *Journal of Plankton Research*, 37, 285-292, 10.1093/plankt/fbv009, 2015.

DANI, K. G. S., and LORETO, F.: Trade-off between dimethyl sulfide and isoprene emissions from marine phytoplankton, *Trends in Plant Science*, 22, 361-372, 10.1016/j.tplants.2017.01.006, 2017.

DE BOYER MONTÉGUT, C., MADEC, G., FISCHER, A. S., LAZAR, A., and IUDICONE, D.: Mixed layer depth over the global ocean: An examination of profile data and a profile-based climatology, *Journal of Geophysical Research: Oceans*, 109, n/a-n/a, 10.1029/2004JC002378, 2004.

EXTON, D. A., SUGGETT, D. J., MCGENITY, T. J., and STEINKE, M.: Chlorophyll-normalized isoprene production in laboratory cultures of marine microalgae and implications for global models, *Limnology and Oceanography*, 58, 1301-1311, 2013.

GANTT, B., MESKHIDZE, N., and KAMYKOWSKI, D.: A new physically-based quantification of marine isoprene and primary organic aerosol emissions, *Atmospheric Chemistry and Physics*, 9, 4915-4927, 10.5194/acp-9-4915-2009, 2009.

GASOL, J. M., and DEL GIORGIO, P. A.: Using flow cytometry for counting natural planktonic bacteria and understanding the structure of planktonic bacterial communities, *Scientia Marina*, 64, 197-224, 2000.

GOODWIN, K. D., SCHAEFER, J. K., and OREMLAND, R. S.: Bacterial oxidation of dibromomethane and methyl bromide in natural waters and enrichment cultures, *Applied and Environmental Microbiology*, 64, 4629-4636, 1998.

GUENTHER, A., KARL, T., HARLEY, P., WIEDINMYER, C., PALMER, P. I., and GERON, C.: Estimates of global terrestrial isoprene emissions using megan (model of emissions of gases and aerosols from nature), *Atmos. Chem. Phys.*, 6, 3181-3210, 10.5194/acp-6-3181-2006, 2006.

GUENTHER, A. B., MONSON, R. K., and FALL, R.: Isoprene and monoterpene emission rate variability - observations with eucalyptus and emission rate algorithm development, *Journal of Geophysical Research-Atmospheres*, 96, 10799-10808, 10.1029/91jd00960, 1991.

GUENTHER, A. B., JIANG, X., HEALD, C. L., SAKULYANONTVITTAYA, T., DUHL, T., EMMONS, L. K., and WANG, X.: The model of emissions of gases and aerosols from nature version 2.1 (megan2.1): An extended and updated framework for modeling biogenic emissions, *Geoscientific Model Development*, 5, 1471-1492, 10.5194/gmd-5-1471-2012, 2012.

HACKENBERG, S. C., ANDREWS, S. J., AIRS, R., ARNOLD, S. R., BOUMAN, H. A., BREWIN, R. J. W., CHANCE, R. J., CUMMINGS, D., DALL'OLMO, G., LEWIS, A. C., MINAEIAN, J. K., REIFEL, K. M., SMALL, A., TARRAN, G. A., TILSTONE, G. H., and CARPENTER, L. J.: Potential controls of isoprene in the surface ocean, *Global Biogeochemical Cycles*, n/a-n/a, 10.1002/2016GB005531, 2017.

HEALD, C. L., HENZE, D. K., HOROWITZ, L. W., FEDDEMA, J., LAMARQUE, J. F., GUENTHER, A., HESS, P. G., VITT, F., SEINFELD, J. H., GOLDSTEIN, A. H., and FUNG, I.: Predicted change in global secondary organic aerosol concentrations in response to future climate, emissions, and land use change, *Journal of Geophysical Research-Atmospheres*, 113, 16, 10.1029/2007jd009092, 2008.

HENZE, D. K., and SEINFELD, J. H.: Global secondary organic aerosol from isoprene oxidation, *Geophysical Research Letters*, 33, 4, Artn L09812

10.1029/2006gl025976, 2006.

HOYLE, C. R., BERNTSEN, T., MYHRE, G., and ISAKSEN, I. S. A.: Secondary organic aerosol in the global aerosol - chemical transport model oslo ctm2, *Atmospheric Chemistry and Physics*, 7, 5675-5694, 2007.

HU, Q.-H., XIE, Z.-Q., WANG, X.-M., KANG, H., HE, Q.-F., and ZHANG, P.: Secondary organic aerosols over oceans via oxidation of isoprene and monoterpenes from arctic to antarctic, *Scientific Reports*, 3, 2280, 10.1038/srep02280

http://www.nature.com/articles/srep02280#supplementary-information, 2013.

HUERTAS, I. E., ROUCO, M., LÓPEZ-RODAS, V., and COSTAS, E.: Warming will affect phytoplankton differently: Evidence through a mechanistic approach, *Proceedings of the Royal Society B: Biological Sciences*, 278, 3534-3543, 10.1098/rspb.2011.0160, 2011.

JACOVIDES, C. P., TIMVIOS, F. S., PAPAIOANNOU, G., ASIMAKOPOULOS, D. N., and THEOFILOU, C. M.: Ratio of par to broadband solar radiation measured in cyprus, *Agricultural and Forest Meteorology*, 121, 135-140, http://dx.doi.org/10.1016/j.agrformet.2003.10.001, 2004.

JOHNSON, Z. I., ZINSER, E. R., COE, A., MCNULTY, N. P., WOODWARD, E. M. S., and CHISHOLM, S. W.: Niche partitioning among prochlorococcus ecotypes along ocean-scale environmental gradients, *Science*, 311, 1737-1740, 10.1126/science.1118052, 2006.

KAMEYAMA, S., YOSHIDA, S., TANIMOTO, H., INOMATA, S., SUZUKI, K., and YOSHIKAWA-INOUE, H.: High-resolution observations of dissolved isoprene in surface seawater in the southern ocean during austral summer 2010-2011, *Journal of Oceanography*, 70, 225-239, 10.1007/s10872-014-0226-8, 2014.

KURIHARA, M., ISEDA, M., IORIYA, T., HORIMOTO, N., KANDA, J., ISHIMARU, T., YAMAGUCHI, Y., and HASHIMOTO, S.: Brominated methane compounds and isoprene in surface seawater of sagami bay: Concentrations, fluxes, and relationships with phytoplankton assemblages, *Marine Chemistry*, 134–135, 71-79, http://dx.doi.org/10.1016/j.marchem.2012.04.001, 2012.

KURIHARA, M. K., KIMURA, M., IWAMOTO, Y., NARITA, Y., OOKI, A., EUM, Y. J., TSUDA, A., SUZUKI, K., TANI, Y., YOKOUCHI, Y., UEMATSU, M., and HASHIMOTO, S.: Distributions of short-lived iodocarbons and biogenic trace gases in the open ocean and atmosphere in the western north pacific, *Marine Chemistry*, 118, 156-170, http://dx.doi.org/10.1016/j.marchem.2009.12.001, 2010.

LELIEVELD, J., BUTLER, T. M., CROWLEY, J. N., DILLON, T. J., FISCHER, H., GANZEVELD, L., HARDER, H., LAWRENCE, M. G., MARTINEZ, M., TARABORRELLI, D., and WILLIAMS, J.: Atmospheric oxidation capacity sustained by a tropical forest, *Nature*, 452, 737-740, 10.1038/nature06870, 2008.

MATSUNAGA, S., MOCHIDA, M., SAITO, T., and KAWAMURA, K.: In situ measurement of isoprene in the marine air and surface seawater from the western north pacific, *Atmospheric Environment*, 36, 6051-6057, 10.1016/s1352-2310(02)00657-x, 2002.

MESKHIDZE, N., SABOLIS, A., REED, R., and KAMYKOWSKI, D.: Quantifying environmental stress-induced emissions of algal isoprene and monoterpenes using laboratory measurements, *Biogeosciences*, 12, 637-651, 10.5194/bg-12-637-2015, 2015.

MILNE, P. J., RIEMER, D. D., ZIKA, R. G., and BRAND, L. E.: Measurement of vertical-distribution of isoprene in surface seawater, its chemical fate, and its emission from

several phytoplankton monocultures, *Marine Chemistry*, 48, 237-244, Doi 10.1016/0304-4203(94)00059-M, 1995.

MONROE, B. M.: Rate constants for the reaction of singlet oxygen with conjugated dienes, *Journal of the American Chemical Society*, 103, 7253-7256, 10.1021/ja00414a035, 1981.

MOREL, A., and BERTHON, J. F.: Surface pigments, algal biomass profiles, and potential production of the euphotic layer - relationships reinvestigated in view of remote-sensing applications, *Limnology and Oceanography*, 34, 1545-1562, 1989.

MOREL, A., and MARITORENA, S.: Bio-optical properties of oceanic waters: A reappraisal, *Journal of Geophysical Research-Oceans*, 106, 7163-7180, 10.1029/2000jc000319, 2001.

MYRIOKEFALITAKIS, S., VIGNATI, E., TSIGARIDIS, K., PAPADIMAS, C., SCIARE, J., MIHALOPOULOS, N., FACCHINI, M. C., RINALDI, M., DENTENER, F. J., CEBURNIS, D., HATZIANASTASIOU, N., O'DOWD, C. D., VAN WEELE, M., and KANAKIDOU, M.: Global modeling of the oceanic source of organic aerosols, *Advances in Meteorology*, 16, 10.1155/2010/939171, 2010.

NIGHTINGALE, P. D., LISS, P. S., and SCHLOSSER, P.: Measurements of air-sea gas transfer during an open ocean algal bloom, *Geophysical Research Letters*, 27, 2117-2120, 10.1029/2000gl011541, 2000.

OOKI, A., NOMURA, D., NISHINO, S., KIKUCHI, T., and YOKOUCHI, Y.: A global-scale map of isoprene and volatile organic iodine in surface seawater of the arctic, northwest pacific, indian, and southern oceans, *Journal of Geophysical Research: Oceans*, 120, 4108-4128, 10.1002/2014JC010519, 2015.

PALMER, P. I., and SHAW, S. L.: Quantifying global marine isoprene fluxes using modis chlorophyll observations, *Geophysical Research Letters*, 32, 10.1029/2005gl022592, 2005.

RINNAN, R., STEINKE, M., MCGENITY, T., and LORETO, F.: Plant volatiles in extreme terrestrial and marine environments, *Plant, Cell & Environment*, 37, 1776-1789, 10.1111/pce.12320, 2014.

SCHOTT, F. A., XIE, S.-P., and MCCREARY, J. P.: Indian ocean circulation and climate variability, *Reviews of Geophysics*, 47, RG1002, 10.1029/2007RG000245, 2009.

SHAW, S. L., CHISHOLM, S. W., and PRINN, R. G.: Isoprene production by prochlorococcus, a marine cyanobacterium, and other phytoplankton, *Marine Chemistry*, 80, 227-245, http://dx.doi.org/10.1016/S0304-4203(02)00101-9, 2003.

SHAW, S. L., GANTT, B., and MESKHIDZE, N.: Production and emissions of marine isoprene and monoterpenes: A review, *Advances in Meteorology*, 10.1155/2010/408696, 2010.

SHENOY, D. M., KUMAR, M. D., and SARMA, V.: Controls of dimethyl sulphide in the bay of bengal during bobmex-pilot cruise 1998, *Proceedings of the Indian Academy of Sciences-Earth and Planetary Sciences*, 109, 279-283, 2000.

SPRACKLEN, D. V., ARNOLD, S. R., SCIARE, J., CARSLAW, K. S., and PIO, C.: Globally significant oceanic source of organic carbon aerosol, *Geophysical Research Letters*, 35, 5, 10.1029/2008gl033359, 2008.

SRIKANTA DANI, K. G., SILVA BENAVIDES, A. M., MICHELOZZI, M., PELUSO, G., TORZILLO, G., and LORETO, F.: Relationship between isoprene emission and photosynthesis in diatoms, and its implications for global marine isoprene estimates, *Marine Chemistry*, 189, 17-24, http://dx.doi.org/10.1016/j.marchem.2016.12.005, 2017.

STRAMMA, L., FISCHER, T., GRUNDLE, D. S., KRAHMANN, G., BANGE, H. W., and MARANDINO, C. A.: Observed el niño conditions in the eastern tropical pacific in october 2015, *Ocean Sci.*, 12, 861-873, 10.5194/os-12-861-2016, 2016.

SURRATT, J. D., CHAN, A. W. H., EDDINGSAAS, N. C., CHAN, M. N., LOZA, C. L., KWAN, A. J., HERSEY, S. P., FLAGAN, R. C., WENNBERG, P. O., and SEINFELD, J. H.: Reactive intermediates revealed in secondary organic aerosol formation from isoprene, *Proceedings of the National Academy of Sciences of the United States of America*, 107, 6640-6645, 10.1073/pnas.0911114107, 2010.

TAYLOR, B. B., TORRECILLA, E., BERNHARDT, A., TAYLOR, M. H., PEEKEN, I., RÖTTGERS, R., PIERA, J., and BRACHER, A.: Bio-optical provinces in the eastern atlantic ocean and their biogeographical relevance, *Biogeosciences*, 8, 3609-3629, 10.5194/bg-8-3609-2011, 2011.

TRAN, S., BONSANG, B., GROS, V., PEEKEN, I., SARDA-ESTEVE, R., BERNHARDT, A., and BELVISO, S.: A survey of carbon monoxide and non-methane hydrocarbons in the arctic ocean during summer 2010, *Biogeosciences*, 10, 1909-1935, 10.5194/bg-10-1909-2013, 2013.

UITZ, J., CLAUSTRE, H., MOREL, A., and HOOKER, S. B.: Vertical distribution of phytoplankton communities in open ocean: An assessment based on surface chlorophyll, *Journal of Geophysical Research: Oceans*, 111, n/a-n/a, 10.1029/2005JC003207, 2006.

UNREIN, F., GASOL, J. M., NOT, F., FORN, I., and MASSANA, R.: Mixotrophic haptophytes are key bacterial grazers in oligotrophic coastal waters, *Isme Journal*, 8, 164-176, 10.1038/ismej.2013.132, 2014.

VIDUSSI, F., CLAUSTRE, H., MANCA, B. B., LUCHETTA, A., and MARTY, J.-C.: Phytoplankton pigment distribution in relation to upper thermocline circulation in the eastern mediterranean sea during winter, *Journal of Geophysical Research: Oceans*, 106, 19939-19956, 10.1029/1999JC000308, 2001.

WANNINKHOF, R.: Relationship between wind speed and gas exchange over the ocean, *Journal of Geophysical Research: Oceans*, 97, 7373-7382, 10.1029/92JC00188, 1992.

WANNINKHOF, R., and MCGILLIS, W. R.: A cubic relationship between air-sea co2 exchange and wind speed, *Geophysical Research Letters*, 26, 1889-1892, 10.1029/1999gl900363, 1999.

ZINDLER, C., MARANDINO, C. A., BANGE, H. W., SCHÜTTE, F., and SALTZMAN, E. S.: Nutrient availability determines dimethyl sulfide and isoprene distribution in the eastern atlantic ocean, *Geophysical Research Letters*, 41, 3181-3188, 10.1002/2014GL059547, 2014.

6 INFLUENCE OF MARINE ISOPRENE EMISSIONS ON SOA FORMATION

6.1 Introduction

6.1.1 Global isoprene derived SOA

Due to the importance of aerosols in influencing the radiative balance of the Earth's system, it is crucial to understand their formation and impact in the atmosphere. Many model studies use laboratory and field measurements in order to determine actual organic aerosol concentrations and predict their concentrations in a changing climate (HODZIC et al., 2016). However, model results have large uncertainties due to the incomplete knowledge about secondary organic aerosol (SOA) composition or their physicochemical properties (LIN et al., 2012). Moreover, the SOA chemistry in the atmosphere is still not fully understood. This leads to highly uncertain estimates of SOA concentrations using different model set-ups (e.g. HEALD et al., 2005; KANAKIDOU et al., 2005). Furthermore, biogenic VOC emission inventories, as the most important SOA precursor, have large uncertainties (ARNETH et al., 2008). Biogenic precursors are estimated to contribute an order of magnitude more to SOA formation than anthropogenic sources, strengthening the need for precise emission estimates of biogenic VOCs (Table 6.1). SOA from biogenic sources ranges from 16.8 Tg yr^{-1} (TSIGARIDIS and KANAKIDOU, 2007) up to 107 Tg yr^{-1} (LIN et al., 2012) depending on model set-ups. Some more explicit model studies also determined SOA concentrations formed by just isoprene oxidation with different results, ranging from 4.6 Tg yr^{-1} (TSIGARIDIS and KANAKIDOU, 2007) to 19.2 Tg yr^{-1} (HEALD et al., 2008). The majority of these studies show that isoprene is by far the main contributor to the biogenic source of SOA. A recent model study from STADTLER et al. (2017) estimated the isoprene derived SOA formation to be 148 Tg yr^{-1}, which is one order of magnitude higher than results of other studies (Table 6.1). However, the uncertainty of these model estimations is still high, which mainly depends on the uncertainty in emission inventories used in each study.

Table 6.1: Global SOA modeling studies. E_{iso}: isoprene emissions, E_{bio}: biogenic VOC emissions, SOA_{iso}: SOA production from isoprene, SOA_{bio}: SOA production from biogenic sources, SOA_{tot}: total SOA production. Unless otherwise noted, all units in Tg yr^{-1}.

References	E_{iso}	E_{bio}	SOA_{iso}	SOA_{bio}	SOA_{tot}
Tsigaridis and Kanakidou (2007)	530	747	4.6	16.8	18.6
Heald et al. (2008)	562	539[a]	19.2[a]	22.9[a]	24.3[a]
Henze et al. (2008)	461	635	14.4	26.8	30.3
Hoyle et al. (2009)	220	386[b]	14	---	53.4
O'Donnell et al. (2011)	460	537	17	21.0	26.6
Lin et al. (2012)	---	590[a]	---	77-107	91-121
Hodzic et al. (2016)	---	---[c]	---	22-99	36-132
Stadtler et al. (2017)	445	---	148	---	---
Myriokefalitakis et al. (2010)[d]	1.0	---	0.1	5.1	---

[a] in Tg C yr^{-1}, [b] excluding isoprene emissions, [c] actual biogenic VOC emissions are not provided in the publication, [d] This model study uses only oceanic emissions to calculate marine-derived SOA.

6.1.2 Marine isoprene emissions

Meskhidze and Nenes (2006) demonstrated that marine biological productivity and SOA formation over the ocean are directly linked to each other influencing aerosol and cloud formation over the remote oceans. Since marine isoprene is biologically produced from phytoplankton and therefore could influence aerosol levels over the remote ocean significantly, a few model studies were carried out in order to determine the global strength of marine isoprene emissions (Table 6.2). Model simulations using isoprene concentrations in the water ("bottom-up"-method) calculated emissions ranging from 0.12 Tg yr^{-1} (Palmer and Shaw, 2005) to 1 Tg yr^{-1} (Gantt et al., 2009). Arnold et al. (2009) and Luo and Yu (2010) used atmospheric isoprene concentrations in the marine environment ("top-down"-approach) and calculated the ocean to be a source for isoprene of 1.9 Tg yr^{-1} and 13 Tg yr^{-1}, respectively. Since the discrepancies between bottom-up and top-down approaches are one order of magnitude, conclusions about the impact of marine emissions on global SOA formation are highly speculative (Anttila et al., 2010; Arnold et al., 2009; Gantt et al., 2009; Hu et al., 2013).

Table 6.2: Comparison of global oceanic isoprene emissions from different model simulations.

Reference	Model approach	Emission [Tg yr^{-1}]
PALMER and SHAW (2005)	bottom-up	0.12
ARNOLD et al. (2009)	bottom-up	0.31
ARNOLD et al. (2009)	top-down	1.9
GANTT et al. (2009)	bottom-up	1.0
LUO and YU (2010)	bottom-up	0.36
LUO and YU (2010)	top-down	13
BOOGE et al. (2016)	bottom-up	0.21

To date, only one model study concentrated on the global influence of marine isoprene on SOA formation (Table 6.1) assuming isoprene emissions of 1 Tg yr^{-1} (average value of different study emission estimates in Table 6.2) (MYRIOKEFALITAKIS et al., 2010). The global source of marine-derived SOA is estimated to be 5.1 Tg yr^{-1} in total, whereas only 0.1 Tg yr^{-1} is produced by oxidation of isoprene and monoterpenes. The main proportion of SOA (4 Tg yr^{-1}) is produced via methanesulfonic acid by the oxidation of DMS. However, the SOA production might be underestimated by using a two-product model based on ODUM et al. (1996), which neglects explicit chemical transformation when calculating the formation of SOA (STADTLER et al., 2017). Compared to the SOA$_{iso}$ values in Table 6.1, a yield of 0.1 Tg yr^{-1} from marine sources accounts only for <1% of biogenic derived SOA from total global isoprene sources. However, if the isoprene emissions are at least one order of magnitude higher as suggested by the top-down approach of LUO and YU (2010), the contribution of marine isoprene derived SOA could be significant (MYRIOKEFALITAKIS et al., 2010). This emphasizes the need to assess the SOA formation from marine isoprene emissions and to estimate their influence on total global SOA formation.

This study uses different monthly mean global marine isoprene emission inventories implemented into the global chemistry climate model ECHAM-HAMMOZ to calculate atmospheric isoprene concentrations and marine-derived iSOA formation, including their global iSOA distributions. Additionally, the importance of marine-derived iSOA on a regional and seasonal scale is discussed. The model results are used to investigate the direct radiative effect of marine-derived iSOA and its influence on a global marine aerosol scale.

6.2   Methods

6.2.1   Model description

Isoprene derived SOA concentrations for 2012 were calculated using the atmospheric chemistry climate model ECHAM-HAMMOZ. It couples the aerosol chemistry with the gas-phase reactions in the troposphere and stratosphere and is described in its actual version ECHAM6.3-HAM2.3-MOZ1.0 by SCHULTZ et al. (2017). The combination of the Hamburg Aerosol Model HAM2.3 and the Sectional Aerosol module for Large Scale Applications SALSA (KOKKOLA et al., 2008) is coupled to the Model for OZone And Related chemical Tracers MOZART (MOZ1.0) to simulate the interaction between trace gases and aerosols. In MOZ1.0, a semi-explicit isoprene oxidation mechanism JAM003 was implemented (STADTLER et al., 2017) describing the gas-phase chemistry of low volatile compounds. The horizontal resolution is 1.875° x 1.875° with 47 vertical layers from the surface to 0.01 hPa. Further information of each module and the coupling between HAM-SALSA and MOZ can be found in (STADTLER et al., 2017).

In this study isoprene emissions from terrestrial biogenic sources, from terrestrial biomass burning and from marine sources were used in order to calculate iSOA concentrations. Emission inventories of terrestrial biogenic isoprene (and other biogenic VOCs) are implemented using the Model of Emissions of Gases and Aerosols from Nature MEGAN (GUENTHER et al., 2012) and emissions from biomass burning were taken from the Atmospheric Chemistry and Climate Model Intercomparison Project ACCMIP (LAMARQUE et al., 2010). A complete list of emission inventories in the current version of the model is shown in SCHULTZ et al. (2017). For the first time, marine isoprene emission estimates were implemented and are described in the following section.

6.2.2   Marine isoprene emissions

Model runs were performed using four different marine isoprene emission set-ups for 2012:

ISO_land. During this model run, marine isoprene emissions were excluded. The resulting concentrations of isoprene and iSOA act as background concentrations assuming no marine emissions of isoprene. By subtracting the concentrations of this model output from the concentrations of other model runs, it is possible to determine the influence of marine isoprene emissions on iSOA formation.

ISO_orig. The revised PALMER and SHAW (2005) model from BOOGE et al. (2016) was used with monthly mean satellite data to calculate global monthly mean isoprene surface concentrations and emissions. The biological production in this steady-state model assumption is balanced by all loss processes (chemical loss, biological loss, physical loss due to mixing and loss due to air-sea gas exchange) following equation (4.1).

The biological production is calculated by monthly mean chl-a satellite data obtained from the Moderate Resolution Imaging Spectroradiometer (MODIS) instrument on board the Terra satellite which is converted into concentrations of six different PFTs using the parameterization from HIRATA et al. (2011). Each of the PFT concentrations was multiplied with the corresponding isoprene production rate obtained from Table 4.2. The quality of this parameterization was verified with actual PFT field concentrations and is shown in the supplement of BOOGE et al. (2016).

The chemical loss rate is parameterized by the rate of reaction of isoprene with OH radicals (ATKINSON et al., 2004) and singlet oxygen (MONROE, 1981) scaled with their corresponding concentrations in seawater (COOPER et al., 1988), yielding a total chemical loss rate constant of $0.0527 \, \text{day}^{-1}$. As no literature data is available regarding the strength of bacterial degradation, we estimated a biological loss rate of $0.01 \, \text{day}^{-1}$, dependent on temperature controlled natural seawater incubations (manuscript in preparation). The loss due to air-sea gas exchange is calculated by the gas exchange coefficient scaled with the mixed layer depth (DE BOYER MONTÉGUT et al., 2004). The gas exchange coefficient is calculated using the wind speed (obtained from the Quick Scatterometer (QuickSCAT) satellite) dependent parameterization from WANNINKHOF (1992), and the temperature dependent Schmidt number of isoprene (temperature obtained from the MODIS instrument on board the Aqua satellite), following equation (4.4). The lifetime of isoprene due to physical mixing to the deeper ocean is estimated to be >100s days, which is insignificant compared to other loss processes (PALMER and SHAW, 2005).

The air-sea gas exchange was calculated by multiplying the derived surface ocean concentration with the gas transfer coefficient, following equation (4.3) and assuming the atmospheric concentration of isoprene to be negligible. Figure 6.1 shows the global annual distribution of isoprene fluxes using the ISO_orig emission estimate. Highest emissions can be seen in the Southern Ocean and North Atlantic Ocean. High biological productivity and strong winds in these regions are the driving forces which lead to emission fluxes of more than $80 \, \text{nmol m}^{-2} \, \text{day}^{-1}$.
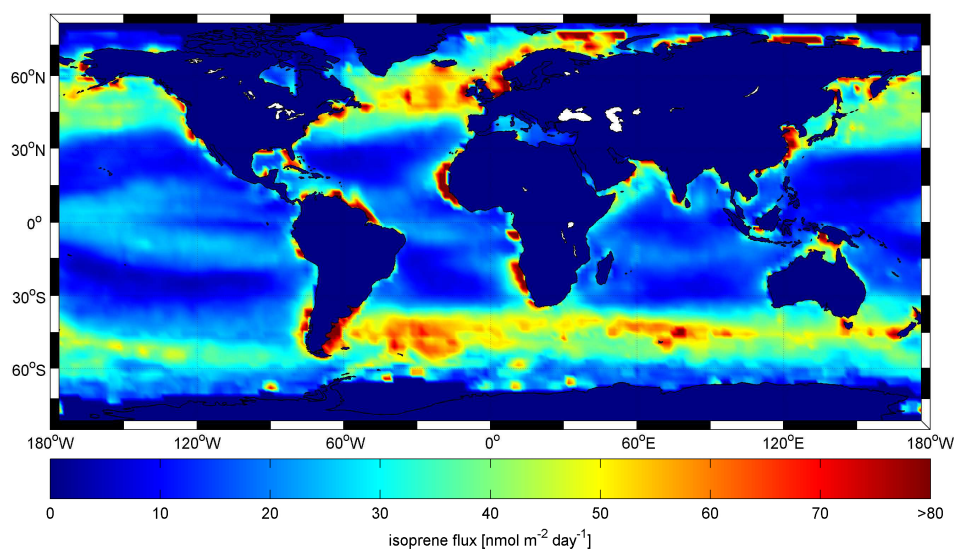

Figure 6.1: Annual mean global marine isoprene emissions for 2012.

ISO_x10 and ISO_x20. These emission estimates use 10 and 20 times higher emissions than ISO_orig. BOOGE et al. (2016) used measured surface ocean isoprene concentrations in a box model in order to compute the atmospheric isoprene concentrations assuming a lifetime of 1 and 4 h. The measured corresponding atmospheric isoprene concentrations were on average 45 times higher compared to the modeled values. Further calculations demonstrated that the sea-to-air flux must be 10 or 20 times higher using a lifetime of 4 and 1 h, respectively, in order to reach the measured atmospheric isoprene concentrations. One explanation for the discrepancy between measured and modeled atmospheric isoprene concentrations could be the photochemical production of isoprene in the surface microlayer (CIURARU et al., 2015) which is not captured by the model and is discussed in BOOGE et al. (2016). Annual global mean marine and terrestrial isoprene emissions of the different model simulations are shown in Table 6.3.

6.3   Results and discussion

6.3.1   Atmospheric isoprene distribution

Figure 6.2 shows the seasonal mean atmospheric isoprene mixing ratio over the ocean of the four different model simulations during December, January, and February (DJF) and during June, July, and August (JJA). During the ISO_land simulation, where the marine isoprene emissions were set to zero, only the coastal atmosphere contains significant amounts of isoprene (>5 ppt). These mixing ratios are due to transport from terrestrial sources, where the atmospheric isoprene mixing ratio can be up to 10 ppb, depending on the vegetation. The range of this transport depends on the wind speed but also on the isoprene mixing ratio at the source, which is highlighted e.g. off the coast of Australia and South America. During austral summer (DJF), where terrestrial isoprene emissions in both regions are higher than during austral winter (JJA), the range of isoprene transportation over the coastal ocean is higher. In general, due to the short atmospheric lifetime of maximum 4 hours, the atmosphere over the remote open ocean contains no isoprene. For the atmospheric mixing ratios from ISO_orig, ISO_x10, and ISO_x20 simulations in Figure 6.2, the ISO_land mixing ratios were subtracted in order to illustrate the influence of the marine isoprene emissions. The global variability of atmospheric isoprene over the open ocean is similar for all three model simulations and follows the marine isoprene emissions (Figure 6.1). During austral summer the mixing ratio is highest in the Southern Ocean, due to high biological production and high wind speeds driving isoprene gas exchange. During boreal summer mixing ratios are highest in the North Atlantic and in the Arctic, but also comparably high atmospheric marine-derived isoprene mixing ratios can be seen in the South Atlantic and South Indian Ocean (40°-50°S). Mixing ratios are lowest in the subtropical oceans. Also, local hot spots of marine isoprene production can be seen: Such as the upwelling off the coast of Mauretania which primarily is strongest from December to April is also visible with higher atmospheric

isoprene mixing ratios during DJF than during JJA. The same is true e.g. for the upwelling region off the coast of Namibia and Angola for JJA.
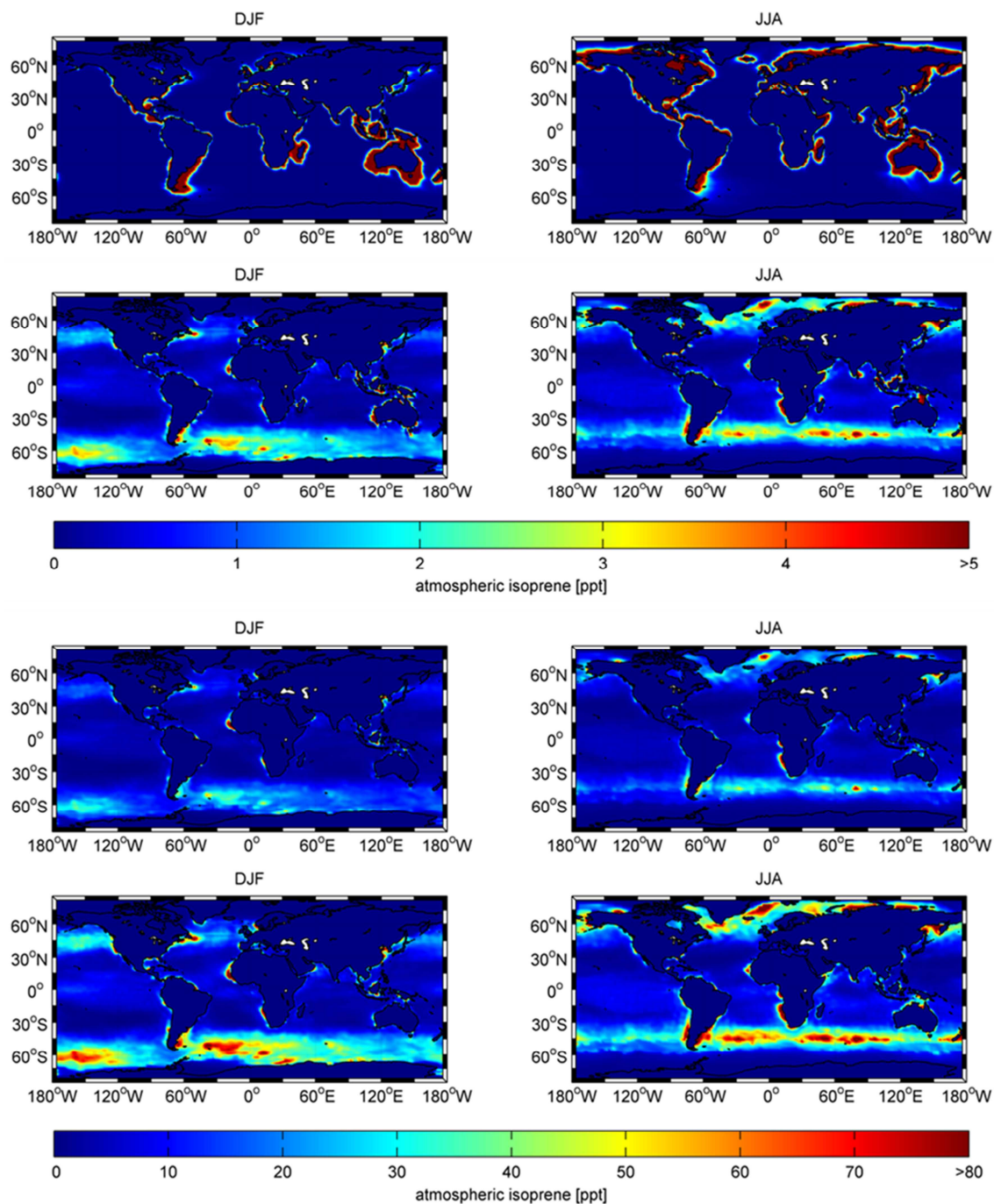
Figure 6.2: Seasonal mean atmospheric isoprene concentrations above the ocean for 2012. Left column: seasonal mean isoprene concentrations for winter months (DJF); right column: seasonal mean isoprene concentrations for summer months (JJA). First row: ISO_land; second, third and fourth row are mean atmospheric isoprene concentrations of ISO_orig, ISO_x10, and ISO_x20, respectively, with the ISO_land values subtracted.

The annual mean marine atmospheric isoprene mixing ratio using the ISO_orig model simulation is about 1 ppt with highest values up to 5 ppt in the biologically productive regions. These values are very low compared to atmospheric isoprene measurements in

the remote marine boundary layer (SHAW et al., 2010 and references therein.). Even in the oligotrophic subtropical Indian Ocean, mean measured values of 2.5 ppt (BOOGE et al., 2016) are more than twice as high compared to the modeled annual mean isoprene mixing ratio, leading to the conclusion that the ISO_orig model simulation is underestimating the atmospheric isoprene mixing ratio. Annual mean atmospheric isoprene mixing ratios are 8 ppt and 16 ppt for the ISO_x10 and ISO_x20 model simulations, respectively. In the area of the Indian Ocean (0°-30°S, 30°-60E), which is similar to the study area of BOOGE et al. (2016), the mean mixing ratio using ISO_x10 is 2.3 ppt, which is comparable to the findings of BOOGE et al. (2016). ISO_x20 overestimates the mixing ratio in this region (4.6 ppt), however, YASSAA et al. (2008) and COLOMB et al. (2009) measured mixing ratios of 26-187 ppt and 20-340 ppt in the Southern Ocean and Southern Indian Ocean, respectively. In these biological productive regions, ISO_x20 might even underestimate the atmospheric mixing ratio. Comparing to field data, ISO_x10 and ISO_x20 might simulate marine atmospheric isoprene mixing ratios best.

6.3.2   Global iSOA distribution

Figure 6.3 (upper panel) shows the seasonal mean surface iSOA concentration over the ocean of the ISO_land simulation during December, January, and February (DJF) and during June, July, and August (JJA). The global mean iSOA concentration over the ocean is 154 ± 92 ng m^{-3} and 236 ± 165 ng m^{-3} for DJF and JJA, respectively, using ISO_land. Lowest values are less than 0.01 ng m^{-3} over the Southern Ocean. Transport of terrestrially-derived isoprene is the only source for iSOA in this region, as the ISO_land model does not include oceanic isoprene emissions. Highest concentrations of iSOA can be found over the Tropical Ocean and in the coastal areas near terrestrial sources, with values higher than 1 µg m^{-3}. A decreasing gradient from the coast to the open ocean can be seen, due to transportation from terrestrial sources, especially in the outflow regions of South America and Africa. It is more likely that iSOA is transported over the remote oceans, as it has a lifetime of 4.2 days (STADTLER et al., 2017), whereas isoprene has a lifetime of only a few hours.

The influence of marine isoprene emissions on iSOA concentration is calculated by subtracting the iSOA concentration of the ISO_land simulation from the different simulations that include oceanic isoprene emissions (ISO_orig, ISO_x10, and ISO_x20). The results are shown in Figure 6.3 (lower three panels) for DJF and JJA. The global distribution of marine-derived iSOA mainly follows the distribution of marine isoprene concentrations (Figure 6.2) with high concentrations in the Southern Ocean during austral summer and elevated concentrations in the North Atlantic during boreal summer. Global mean surface marine iSOA concentrations are 0.004 ± 9.79 ng m^{-3}, 2.77 ± 7.11 ng m^{-3}, and 3.94 ± 7.46 ng m^{-3} for ISO_orig, ISO_x10, and ISO_x20, respectively. The high standard deviation is due to the high iSOA concentrations in the tropics. This region is the only region where global marine iSOA and atmospheric isoprene distributions are different. Atmospheric isoprene mixing ratios are low in the tropical regions due to low oceanic emissions. However, iSOA concentrations in the tropics are very high (~ 600 ng m^{-3}) due to transportation from terrestrial sources. Subtracting ISO_orig, ISO_x10, and ISO_x20
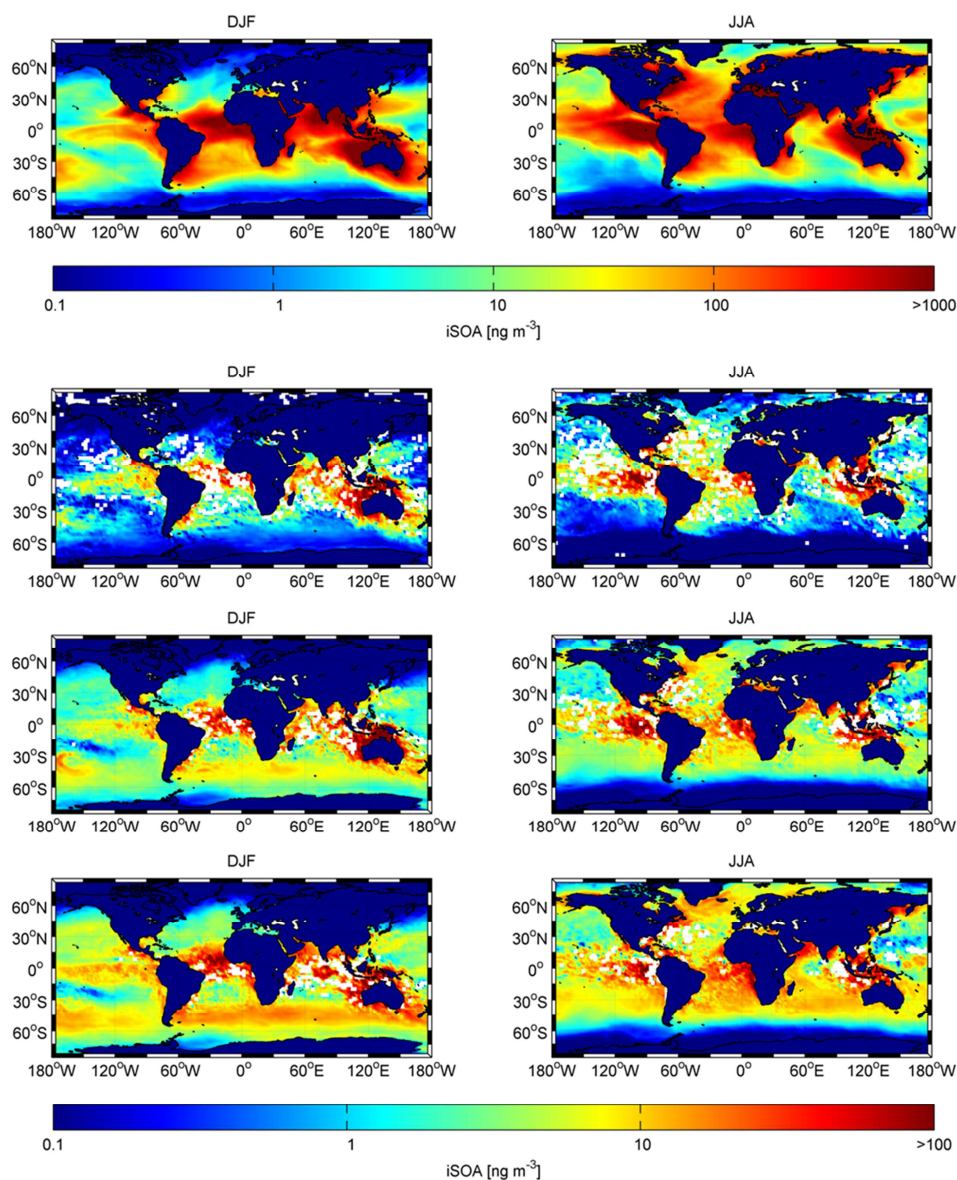
Figure 6.3: Seasonal mean iSOA concentrations for 2012. Left column: seasonal mean iSOA concentrations for northern hemisphere winter (DJF); right column: seasonal mean iSOA concentrations for northern hemisphere summer (JJA). First row: ISO_land; second, third and fourth row are mean iSOA concentrations of ISO_orig, ISO_x10, and ISO_x20, respectively, subtracted by ISO_land. White grid points indicate negative iSOA concentrations after subtraction.

from ISO_land also results in negative iSOA concentrations which are indicated as white grid points in Figure 6.3. This difference is mainly attributed to the noise of each model run and indicates that the oceanic isoprene emissions in those regions do not significantly influence the iSOA concentration. Variations in terrestrial isoprene emissions in different model simulations are a second reason for negative iSOA concentrations after subtraction. Table 6.3 shows the isoprene emissions and the resulting iSOA formation from the different model simulations. When implementing marine isoprene emissions, the terrestrial isoprene emissions derived from MEGAN are slightly lower than without marine isoprene emissions. The addition of marine isoprene emissions leads to a slight increase in aerosol concentration and therefore to a slight reduction in radiation reaching the Earth's surface, which is called global dimming. Hence, less light means less isoprene

production. Although the differences in different isoprene emission estimates are small, they influence the strength of the marine iSOA formation significantly due to the low marine isoprene emissions compared to terrestrial emissions. Subtracting the results of the ISO_orig simulation from the ISO_land simulation leads to negative marine iSOA formation, as the sum of marine and terrestrial emission in ISO_orig (443.85 Tg yr^{-1}) is less than the total isoprene emissions in ISO_land (443.87 Tg yr^{-1}).

Table 6.3: Annual global isoprene emissions and iSOA formation in Tg yr^{-1}.

Reference	Marine isoprene emissions	Terrestrial isoprene emissions	Marine iSOA formation	Terrestrial iSOA formation
This work				
ISO_land	---	443.87	---	147.79
ISO_orig	0.23	443.62	-0.21[a]	147.58
ISO_10x	2.27	443.82	0.39	148.17
ISO_20x	4.55	443.71	0.46	148.25
MYRIOKEFALITAKIS et al. (2010)				
marine isoprene	1.0	---	0.1	---

[a] negative value, because sum of marine and terrestrial isoprene emissions in ISO_orig is lower than terrestrial isoprene emissions in ISO_land alone.

On an annual global view the marine-derived iSOA concentrations account for 0.002%, 1.35%, and 1.91% of the total global iSOA concentration using ISO_orig, ISO_x10, and ISO_x20, respectively. Assuming a mean contribution of ~50% from isoprene derived SOA on total SOA following the model results listed in Table 6.1, the proportion of marine-derived iSOA on the total SOA concentration using ISO_x10 and ISO_x20 is less than 1%. However, marine-derived iSOA formation might contribute significantly to total marine aerosol concentrations because atmospheric marine aerosol numbers are lower by one order of magnitude compared to terrestrial aerosol numbers (SALTZMAN, 2013). Marine-derived organic aerosol concentrations at Mace Head were 360 ng m^{-3} on average when clean marine air was sampled (OVADNEVAITE et al., 2011). Additionally, GANTT et al. (2015) modeled total marine organic aerosol concentrations. Their results are in the same range as concentrations from field measurements, with annual mean global concentrations of ~130 ng m^{-3}. Marine-derived aerosol concentrations are highest (>2000 ng m^{-3}) in seasons and locations of high biological productivity but concentrations also drop below 100 ng m^{-3} in oligotrophic oceanic regions or in the dark winter months at high latitudes. Comparing these values to our calculated marine-derived iSOA concentration distribution (Figure 6.3) leads to the conclusion that marine-derived iSOA influences the aerosol distribution over the remote ocean basins like the Southern Ocean, where terrestrial sources of organic aerosols are negligible. Due to the short lifetime of isoprene, marine isoprene emissions appear to influence the iSOA con-

centrations, or even total organic aerosol concentrations, more significantly on regional scales. Moreover, BOOGE et al. (2016) could show that oceanic isoprene emissions are highly dependent on season and therefore might significantly influence the iSOA concentration even on a global scale during months with high oceanic isoprene emissions. The regional and seasonal impacts of oceanic isoprene emissions will be discussed in the following section.

6.3.3   Regional and seasonal impacts

Four different oceanic regions, dependent on isoprene emissions and iSOA concentrations as well as their seasonal variability, were chosen in order to investigate the regional and seasonal impacts of isoprene emissions on iSOA concentrations (Figure 6.4):

1. North Atlantic (38-58°N, 15-45°W): In this region the influence of terrestrial iSOA is moderate. The focus in this region lies on the seasonal impacts, as the North Atlantic has a strong variability in seasonal isoprene emissions and marine-derived iSOA concentrations.
2. South Indian Ocean (30-50°S, 40-100°E): This region is the counterpart in the southern hemisphere to the North Atlantic region having a strong seasonal variability in oceanic isoprene emission and only a moderate influence of terrestrial iSOA. Additionally the atmosphere above this region is even more likely to be marine air due to a constant westerly wind regime in this region.
3. Tropical Ocean (14°S-6°N, 85-110°W): The Tropical East Pacific is chosen as a region with a very high influence of terrestrial iSOA and very low oceanic isoprene emissions, showing almost no seasonality.
4. Southern Ocean (60-90°S): The marine atmosphere over this region contains almost no terrestrially derived iSOA, but has a strong seasonality with high isoprene mixing ratios during austral summer and almost no oceanic emissions during the dark austral winter.

Figure 6.4 (left panel) shows the annual mean isoprene emissions in the four different regions using ISO_orig, ISO_x10, and ISO_x20. Highest amounts of marine isoprene are emitted in the North Atlantic (cyan) followed by the South Indian Ocean region (blue). The strength of marine emissions in the tropics (red) is only half of the emission strength in the North Atlantic. On annual average, isoprene emissions to the atmosphere in the Southern Ocean region are lowest because marine isoprene is only produced during daylight, which is only available in austral summer. The absolute amount of emissions is dependent on the marine emission inventory used and ranges from 0.15 kgC yr^{-1} km^{-2} in the Southern Ocean using ISO_orig up to 18.8 kgC yr^{-1} km^{-2} in the North Atlantic using ISO_x20. However, the oceanic emissions do have different proportional contributions to the total iSOA formation in the corresponding regions (Figure 6.4). Using ISO_orig there is almost no increase in iSOA formation compared to ISO_land, suggesting that the oceanic emissions are not high enough to influence the iSOA concentration. The highest impact on iSOA formation can be seen in the Southern Ocean resulting in an increase
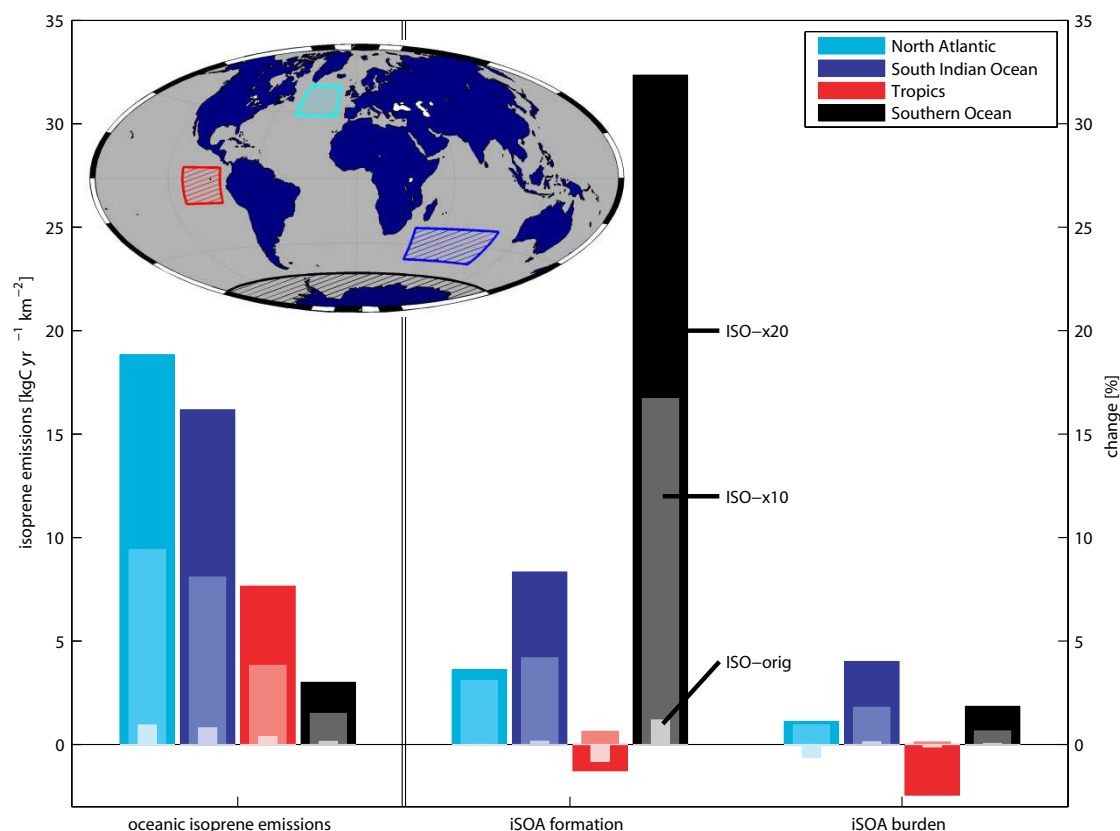
Figure 6.4: Impact of oceanic isoprene emissions on iSOA formation and iSOA burden. Left panel: Oceanic isoprene emissions in kgC yr^{-1} km^{-2} in four different regions using ISO_orig, ISO_x10, and ISO_x20. Right panel: The change in % of iSOA formation and iSOA burden using ISO_orig, ISO_x10, and ISO_x20 compared to ISO_land. The locations of the four different regions are shown on the world map in the upper left corner.

of 17% and 32% using ISO_x10 and ISO_x20, respectively. This high proportional increase is mainly due to the low absolute amount of 1.2 kgC yr^{-1} km^{-2} using ISO_land. However, this result indicates that even these low emissions have a significant impact on the total amount of marine iSOA over this remote ocean region. Oceanic emissions in the tropical region do not have a significant effect on the total iSOA formation, due to the already very high iSOA formation of 102 kgC yr^{-1} km^{-2} from terrestrial sources, which confirms the findings of the iSOA distribution discussed in section 6.3.2. The iSOA formation in the North Atlantic and the South Indian Ocean region is comparable when marine isoprene emissions are excluded, with an annual formation of 19 kgC km^{-2} and 21 kgC km^{-2}, respectively. However, using ISO_x20 the increase of 8% in the South Indian Ocean region is twice as high as in the North Atlantic region. This increase of 8% also leads to an increase of 4% in the yearly iSOA burden on the South Indian Ocean region using ISO_x20. The change in iSOA burden for the North Atlantic region and the Southern Ocean region is even smaller resulting in an increase of 1% and 2%, respectively, using ISO_x20. The absolute change in the annual mean marine iSOA concentration is shown in Figure 6.5a. A relative increase of 4%, 2%, and 1% corresponds to an annual mean marine-derived iSOA concentration of 11.0 ng m^{-3}, 1.2 ng m^{-3}, and 5.4 ng m^{-3} for the South Indian Ocean, Southern Ocean, and North Atlantic region, respectively.
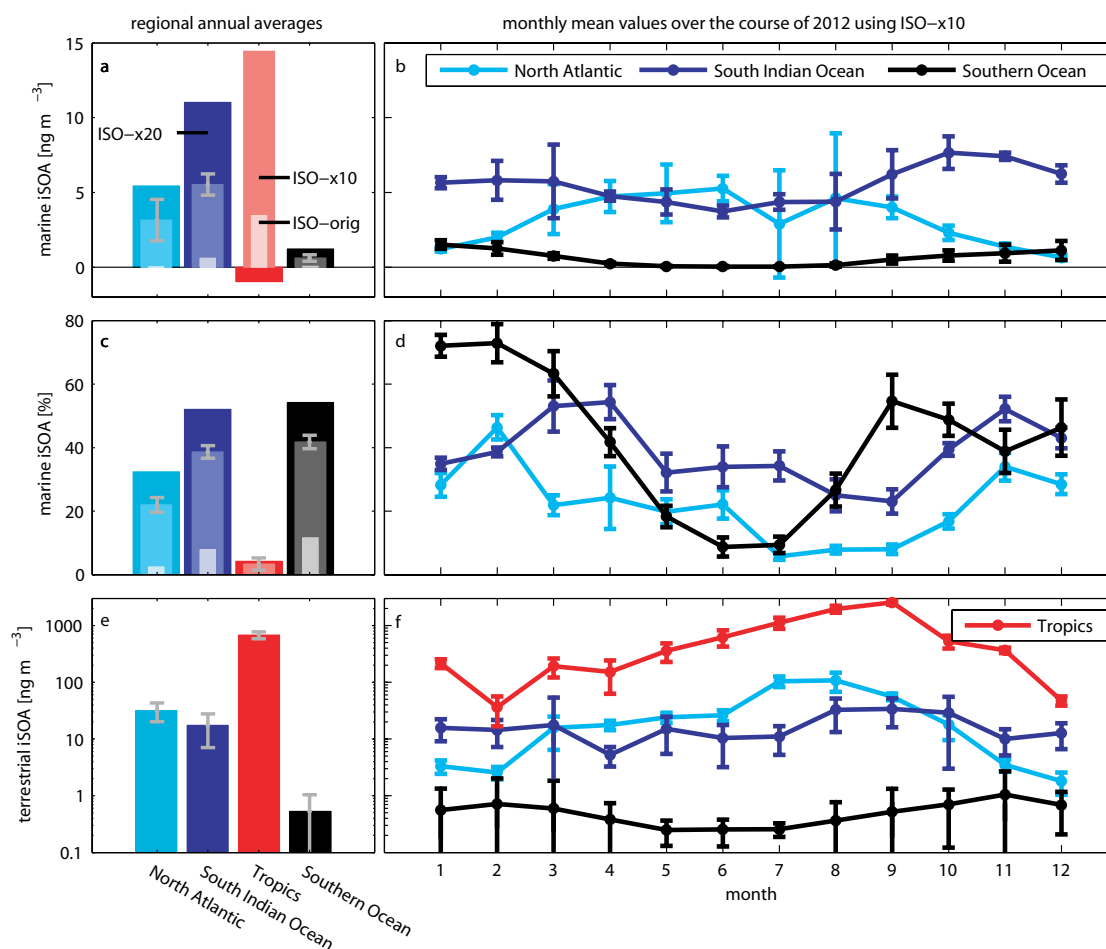
Figure 6.5: Annual mean and seasonal trend of marine-derived and terrestrially derived iSOA in four different regions. Annual mean (a) marine iSOA concentration in ng m^{-3}, (c) marine iSOA proportion from total iSOA in %, (e) terrestrial iSOA concentration in ng m^{-3}. Monthly mean (b) marine iSOA concentration in ng m^{-3} using ISO_x10, (d) iSOA proportion in % using ISO_x10, (f) terrestrial iSOA concentration in ng m^{-3}. Marine iSOA concentrations in Tropic region are not shown due to the large error bars. Seasonal trends for marine SOA in (b) and (c) is shown using ISO_x10 as a conservative estimate. Note the logarithmic scale for terrestrial iSOA in (e,f).

Annual mean marine-derived iSOA concentrations in the Southern Ocean region and the South Indian Ocean region account for more than 50% of total iSOA concentrations using ISO_x20 (Figure 6.5c) and could be as high as 75% during austral summer in the Southern Ocean region using ISO_x10 (Figure 6.5d). The marine-derived iSOA concentrations in the North Atlantic region also show seasonal variability, with higher values during boreal summer and lower values during boreal winter (Figure 6.5b, data shown using ISO_x10 as a conservative estimate). However, the contribution to total iSOA is highest during boreal winter and lowest during boreal summer, although the absolute concentrations of marine dervied iSOA are higher in summer. This contrasting trend leads to the conclusion that the North Atlantic open ocean region is influenced by terrestrially derived iSOA, especially in the boreal late summer months (July, August and September) (Figure 6.5f). In the South Indian Ocean and, even more, in the Southern Ocean region the seasonal trends of the marine iSOA concentration and the marine

proportion to total iSOA concentrations are similar. Marine-derived iSOA significantly influences the total iSOA concentration and variability in these regions in contrast to the tropical region, which is not influenced by marine-derived iSOA due to high terrestrial influence (Figure 6.5c,e,f).

6.3.4   Direct radiative effect

The results from analyzing the four different oceanic regions clearly indicate the importance of marine-derived iSOA in the South Indian Ocean and the Southern Ocean region with a proportion of 40% and 50% of the total iSOA concentration using the model simulation ISO_x10 and ISO_x20, respectively. The seasonal proportion of marine-derived iSOA can be as high as 72% and 83% in the austral summer months especially in the Southern Ocean using ISO_x10 and ISO_x20, respectively. The influence of the marine-derived iSOA on the global radiative balance of the Earth's system, the direct radiative effect, was estimated by comparing the incoming radiative flux at the surface of the different model simulations. In general, the absorption of solar radiation of the dark ocean, due to its low albedo (0.07) is higher than absorption of solar radiation by terrestrial surfaces (0.12-0.36) or ice/snow (0.62-0.66) (BRIEGLEB et al., 1986). Therefore, the effect of each particle over the ocean on the radiative balance in scattering or absorbing solar radiation might be stronger than over land. Using ISO_x20, the model with strongest marine isoprene emissions, the global annual mean radiation at the surface decreased by 0.0032%, which is within the uncertainty of the model and therefore negligible. The result confirms the findings made in section 6.3.2 that marine-derived iSOA has a negligible influence on total iSOA on a global scale. The influence of marine-derived iSOA on the radiative effect on regional and seasonal scale is calculated and shown in Figure 6.6. The annual mean direct radiative effect in the South Indian Ocean region as well as in the Southern Ocean region is negligible. Following the clear seasonal cycle in iSOA concentration in those two regions (Figure 6.5b) a seasonal influence on the radiative balance is visible too. However, the seasonal direct radiative effect is less pronounced. Surface radiation decreases in the tropical region by 0.2 W m^{-2} (annual mean surface radiation: ~220 W m^{-2}) when marine isoprene emissions are included in the calculation. Due to the very low emissions in this region it is highly speculative if the decrease in surface radiation is influenced by the marine emissions or if it is just the uncertainty in the model due to the strong terrestrial influence coming along with high iSOA concentrations. In the North Atlantic region the influence of marine-derived iSOA on the radiative balance shows a clear seasonal trend with a decrease in surface radiation in boreal summer (max: -1.25 W m^{-2}) and a slight increase in boreal winter times. Compared to the marine-derived iSOA concentration in Figure 6.5b, the direct radiative effect is strongest when the iSOA concentration is highest. Although the proportion of marine-derived iSOA in boreal summer is less than 25% (Figure 6.5d), the absolute iSOA concentration is high enough to significantly influence the incoming surface radiation. On a yearly average the mean surface radiation in the Atlantic Ocean region is 0.18 W m^{-2} lower when marine isoprene emissions are included in the model run.
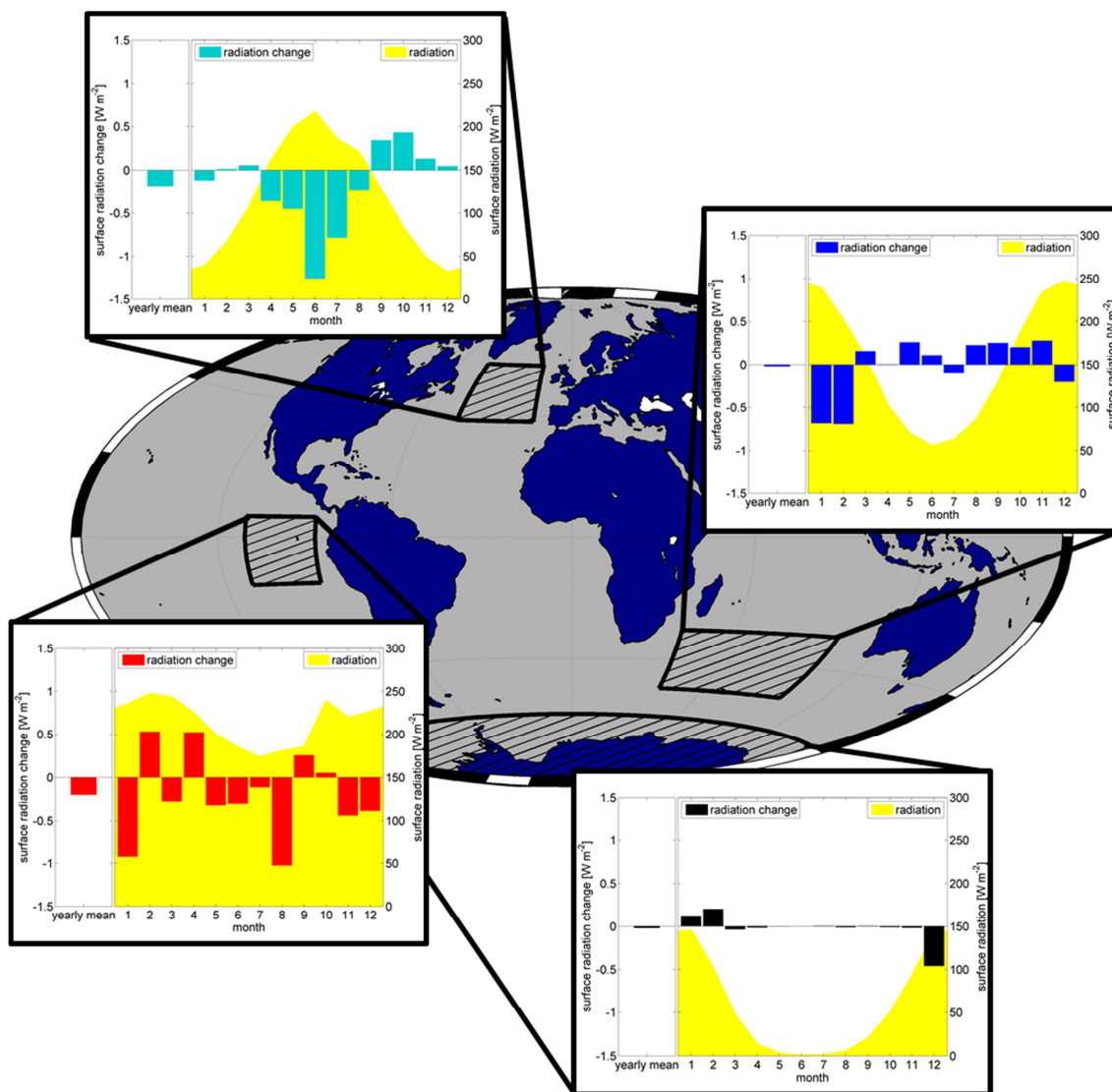
Figure 6.6: Direct radiative effect of marine-derived iSOA in four different ocean regions. Right part of each subplot: monthly mean change in radiative flux in W m^{-2} at the surface using ISO_x10 and ISO_x20 compared to ISO_land and the absolute radiative flux at the surface in W m^{-2} (yellow). Left part of each subplot: annual mean change in radiative flux of ISO_x10 and ISO_x20 compared to ISO_land at the surface in W m^{-2}.

Model and remote sensing studies suggest that the direct radiative effect of aerosols over the ocean is in the range of -5 to -6 W m^{-2} (BOUCHER and TANRÉ, 2000; MYHRE et al., 2007; REMER and KAUFMAN, 2006). This value is attributed to aerosols over the ocean and does not describe the effect of marine derived aerosols alone. It is highly influenced by terrestrial aerosols e.g. in outflow regions as West Africa and the Arabian Sea (compare Figure 6.3). REMER and KAUFMAN (2006) calculated an annual mean direct radiative effect of -2.9 W m^{-2} for the south tropical Pacific, a region which is hardly influenced by terrestrially derived aerosols. Therefore, this value might reflect the direct radiative effect of marine derived aerosols. The annual mean direct radiative effect from marine-derived iSOA in the North Atlantic region (-0.18 W m^{-2}) contributes ~6% to the total aerosol direct radiative effect (-2.9 W m^{-2}). This proportion is increased up to 43% in

June during boral summer. The contribution of marine-derived iSOA to the total aerosol radiative effect in the South Indian Ocean during late austral summer is ~25%. Although the annual mean marine iSOA concentration in the South Indian Ocean region is higher than in the North Atlantic region (Figure 6.5a), the direct radiative effect is weaker than in the North Atlantic region (Figure 6.6). Consequently, the absolute amount of particles is not the only driving force influencing the radiative balance.

Aerosol particles influence the scattering of light dependent on their size. They scatter the light in both directions, forward and backward. However, for larger particles it is more likely that the light is scattered in the forward direction (Mie scattering; WRIEDT, 2012). Hence, more light reaches the Earth's surface, when scattered by larger aerosol particles. Figure 6.7 shows the model-derived annual mean proportional size distribution of terrestrially derived (Figure 6.7a) and marine-derived iSOA (Figure 6.7b) for the four different regions, as well as the global (marine atmosphere) mean (Figure 6.7c). Particles from 3 nm to 10 µm in diameter are binned into ten different logarithmically spaced size bins. 50% of the global terrestrially derived iSOA (ISO_land) has a diameter within the range of 187 to 362 nm. Almost 90% of the aerosol particles have a diameter between 96.7 nm and 700 nm. Marine-derived iSOA (Figure 6.7b) was calculated by subtracting ISO_land from ISO_x10. The particle size distribution in marine-derived iSOA is clearly shifted to the direction of larger particles. 29% of marine-derived iSOA has a diameter of 0.7 − 4.12 µm, which is true only for 8% of the terrestrially derived iSOA. The total mean diameter is about two times higher in regions where the iSOA concentration is influenced mainly by marine isoprene emissions (Figure 6.7c). Hence, marine-derived iSOA is more likely to contribute to particle growth than to the initial formation of particles. The mean iSOA diameter in the tropical region is only slightly higher (689 nm) in marine-derived iSOA compared to terrestrially derived iSOA (538 nm). This confirms, as already stated in section 6.3.2, that the tropical region is mainly influenced by terrestrially derived iSOA. Additionally, the mean diameter of marine-derived iSOA is higher in the South Indian Ocean compared to the mean diameter of marine-derived iSOA in the North Atlantic Ocean region and, therefore, explains the lower direct radiative effect.

In summary, these results show that transport of terrestrially derived iSOA influences the concentration distribution over the ocean. Above the remote ocean, however, marine-derived iSOA influences the concentration of total iSOA, although the concentration of marine-derived iSOA might be negligible in comparison to terrestrially derived iSOA concentrations. Additionally, the size of already existing particles is increased by iSOA formation from marine isoprene emissions compared to terrestrial iSOA particle sizes, which lowers the influence of marine-derived iSOA on the direct radiative effect. However, the formation of marine-derived iSOA significantly influences the radiative balance over the open ocean. Therefore, one can differentiate between iSOA that is transported from terrestrial sources and iSOA that is formed from marine emissions due to their particle size distribution.
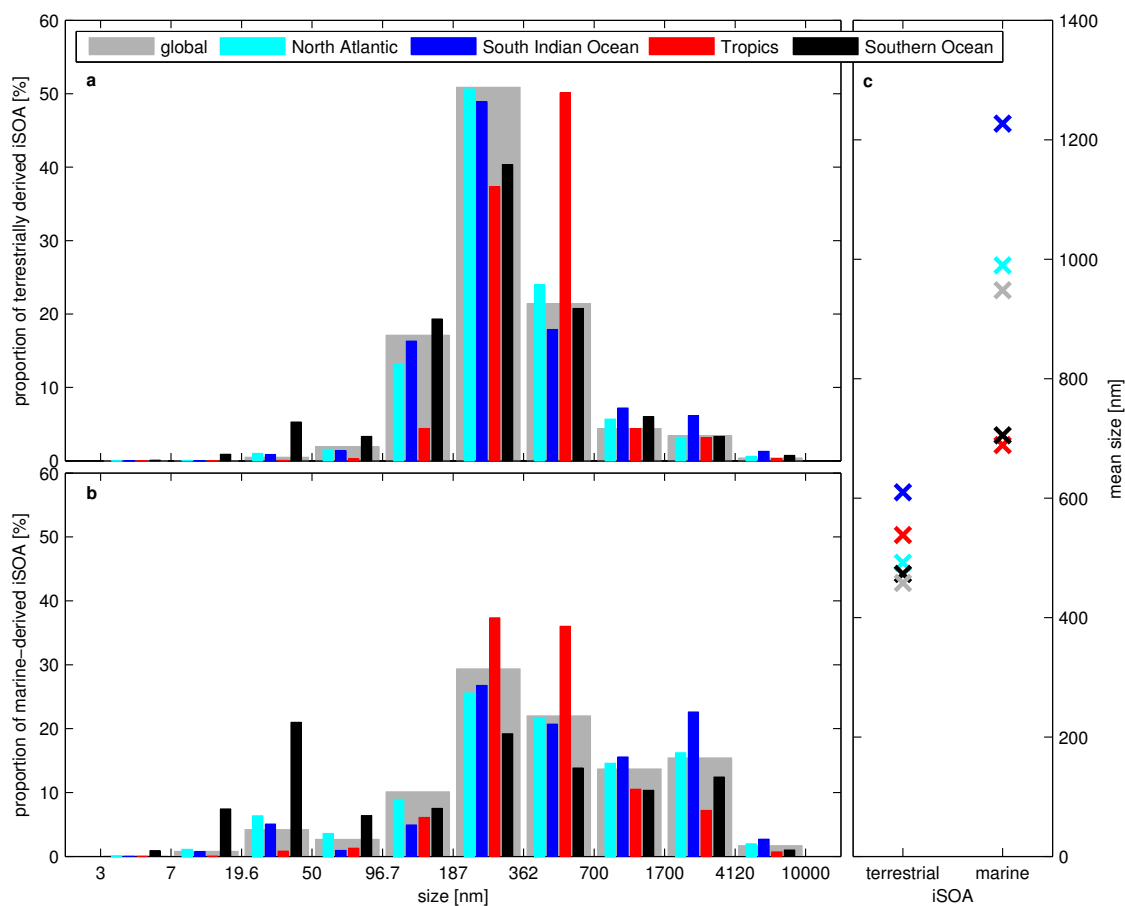
Figure 6.7: Size distributions of iSOA in different regions. Size distributions of (a) terrestrially derived iSOA (using ISO_land) and (b) marine-derived iSOA (using the difference of ISO_x10 (as a conservative estimate) and ISO_land) in different regions. (c) Comparison of mean size of iSOA in different regions. Size distribution of iSOA is split into 10 different size bins.

References

ANTTILA, T., LANGMANN, B., VARGHESE, S., and O'DOWD, C.: Contribution of isoprene oxidation products to marine aerosol over the north-east atlantic, *Advances in Meteorology*, 10.1155/2010/482603, 2010.

ARNETH, A., MONSON, R. K., SCHURGERS, G., NIINEMETS, Ü., and PALMER, P. I.: Why are estimates of global terrestrial isoprene emissions so similar (and why is this not so for monoterpenes)?, *Atmos. Chem. Phys.*, 8, 4605-4620, 10.5194/acp-8-4605-2008, 2008.

ARNOLD, S. R., SPRACKLEN, D. V., WILLIAMS, J., YASSAA, N., SCIARE, J., BONSANG, B., GROS, V., PEEKEN, I., LEWIS, A. C., ALVAIN, S., and MOULIN, C.: Evaluation of the global oceanic isoprene source and its impacts on marine organic carbon aerosol, *Atmos. Chem. Phys.*, 9, 1253-1262, 10.5194/acp-9-1253-2009, 2009.

ATKINSON, R., BAULCH, D. L., COX, R. A., CROWLEY, J. N., HAMPSON, R. F., HYNES, R. G., JENKIN, M. E., ROSSI, M. J., and TROE, J.: Evaluated kinetic and photochemical data for atmospheric chemistry: Volume i - gas phase reactions of o_x, ho_x, no_x and so_x species, *Atmos. Chem. Phys.*, 4, 1461-1738, 10.5194/acp-4-1461-2004, 2004.

BOOGE, D., MARANDINO, C. A., SCHLUNDT, C., PALMER, P. I., SCHLUNDT, M., ATLAS, E. L., BRACHER, A., SALTZMAN, E. S., and WALLACE, D. W. R.: Can simple models predict large-scale surface ocean isoprene concentrations?, *Atmos. Chem. Phys.*, 16, 11807-11821, 10.5194/acp-16-11807-2016, 2016.

BOUCHER, O., and TANRÉ, D.: Estimation of the aerosol perturbation to the earth's radiative budget over oceans using polder satellite aerosol retrievals, *Geophysical Research Letters*, 27, 1103-1106, 10.1029/1999GL010963, 2000.

BRIEGLEB, B. P., MINNIS, P., RAMANATHAN, V., and HARRISON, E.: Comparison of regional clear-sky albedos inferred from satellite observations and model computations, *Journal of Climate and Applied Meteorology*, 25, 214-226, 10.1175/1520-0450(1986)025<0214:corcsa>2.0.co;2, 1986.

CIURARU, R., FINE, L., PINXTEREN, M. v., D'ANNA, B., HERRMANN, H., and GEORGE, C.: Unravelling new processes at interfaces: Photochemical isoprene production at the sea surface, *Environmental Science & Technology*, 49, 13199-13205, 10.1021/acs.est.5b02388, 2015.

COLOMB, A., GROS, V., ALVAIN, S., SARDA-ESTEVE, R., BONSANG, B., MOULIN, C., KLÜPFEL, T., and WILLIAMS, J.: Variation of atmospheric volatile organic compounds over the southern indian ocean (3049s), *Environmental Chemistry*, 6, 70-82, http://dx.doi.org/10.1071/EN08072, 2009.

COOPER, W. J., ZIKA, R. G., PETASNE, R. G., and FISCHER, A. M.: Sunlight-induced photochemistry of humic substances in natural waters: Major reactive species, in:

Aquatic humic substances, Advances in chemistry, 219, American Chemical Society, 333-362, doi:10.1021/ba-1988-0219.ch022

10.1021/ba-1988-0219.ch022.

DE BOYER MONTÉGUT, C., MADEC, G., FISCHER, A. S., LAZAR, A., and IUDICONE, D.: Mixed layer depth over the global ocean: An examination of profile data and a profile-based climatology, *Journal of Geophysical Research: Oceans*, 109, n/a-n/a, 10.1029/2004JC002378, 2004.

GANTT, B., MESKHIDZE, N., and KAMYKOWSKI, D.: A new physically-based quantification of marine isoprene and primary organic aerosol emissions, *Atmospheric Chemistry and Physics*, 9, 4915-4927, 10.5194/acp-9-4915-2009, 2009.

GANTT, B., JOHNSON, M. S., CRIPPA, M., PRÉVÔT, A. S. H., and MESKHIDZE, N.: Implementing marine organic aerosols into the geos-chem model, *Geosci. Model Dev.*, 8, 619-629, 10.5194/gmd-8-619-2015, 2015.

GUENTHER, A. B., JIANG, X., HEALD, C. L., SAKULYANONTVITTAYA, T., DUHL, T., EMMONS, L. K., and WANG, X.: The model of emissions of gases and aerosols from nature version 2.1 (megan2.1): An extended and updated framework for modeling biogenic emissions, *Geosci. Model Dev.*, 5, 1471-1492, 10.5194/gmd-5-1471-2012, 2012.

HEALD, C. L., JACOB, D. J., PARK, R. J., RUSSELL, L. M., HUEBERT, B. J., SEINFELD, J. H., LIAO, H., and WEBER, R. J.: A large organic aerosol source in the free troposphere missing from current models, *Geophysical Research Letters*, 32, n/a-n/a, 10.1029/2005GL023831, 2005.

HEALD, C. L., HENZE, D. K., HOROWITZ, L. W., FEDDEMA, J., LAMARQUE, J. F., GUENTHER, A., HESS, P. G., VITT, F., SEINFELD, J. H., GOLDSTEIN, A. H., and FUNG, I.: Predicted change in global secondary organic aerosol concentrations in response to future climate, emissions, and land use change, *Journal of Geophysical Research-Atmospheres*, 113, 16, 10.1029/2007jd009092, 2008.

HENZE, D. K., SEINFELD, J. H., NG, N. L., KROLL, J. H., FU, T. M., JACOB, D. J., and HEALD, C. L.: Global modeling of secondary organic aerosol formation from aromatic hydrocarbons: High- vs. Low-yield pathways, *Atmos. Chem. Phys.*, 8, 2405-2420, 10.5194/acp-8-2405-2008, 2008.

HIRATA, T., HARDMAN-MOUNTFORD, N. J., BREWIN, R. J. W., AIKEN, J., BARLOW, R., SUZUKI, K., ISADA, T., HOWELL, E., HASHIOKA, T., NOGUCHI-AITA, M., and YAMANAKA, Y.: Synoptic relationships between surface chlorophyll-a and diagnostic pigments specific to phytoplankton functional types, *Biogeosciences*, 8, 311-327, 10.5194/bg-8-311-2011, 2011.

HODZIC, A., KASIBHATLA, P. S., JO, D. S., CAPPA, C. D., JIMENEZ, J. L., MADRONICH, S., and PARK, R. J.: Rethinking the global secondary organic aerosol (soa) budget: Stronger

production, faster removal, shorter lifetime, *Atmos. Chem. Phys.*, 16, 7917-7941, 10.5194/acp-16-7917-2016, 2016.

HOYLE, C. R., MYHRE, G., BERNTSEN, T. K., and ISAKSEN, I. S. A.: Anthropogenic influence on soa and the resulting radiative forcing, *Atmos. Chem. Phys.*, 9, 2715-2728, 10.5194/acp-9-2715-2009, 2009.

HU, Q.-H., XIE, Z.-Q., WANG, X.-M., KANG, H., HE, Q.-F., and ZHANG, P.: Secondary organic aerosols over oceans via oxidation of isoprene and monoterpenes from arctic to antarctic, *Scientific Reports*, 3, 2280, 10.1038/srep02280

http://www.nature.com/articles/srep02280#supplementary-information, 2013.

KANAKIDOU, M., SEINFELD, J. H., PANDIS, S. N., BARNES, I., DENTENER, F. J., FACCHINI, M. C., VAN DINGENEN, R., ERVENS, B., NENES, A., NIELSEN, C. J., SWIETLICKI, E., PUTAUD, J. P., BALKANSKI, Y., FUZZI, S., HORTH, J., MOORTGAT, G. K., WINTERHALTER, R., MYHRE, C. E. L., TSIGARIDIS, K., VIGNATI, E., STEPHANOU, E. G., and WILSON, J.: Organic aerosol and global climate modelling: A review, *Atmos. Chem. Phys.*, 5, 1053-1123, 10.5194/acp-5-1053-2005, 2005.

KOKKOLA, H., KORHONEN, H., LEHTINEN, K. E. J., MAKKONEN, R., ASMI, A., JÄRVENOJA, S., ANTTILA, T., PARTANEN, A. I., KULMALA, M., JÄRVINEN, H., LAAKSONEN, A., and KERMINEN, V. M.: Salsa – a sectional aerosol module for large scale applications, *Atmos. Chem. Phys.*, 8, 2469-2483, 10.5194/acp-8-2469-2008, 2008.

LAMARQUE, J. F., BOND, T. C., EYRING, V., GRANIER, C., HEIL, A., KLIMONT, Z., LEE, D., LIOUSSE, C., MIEVILLE, A., OWEN, B., SCHULTZ, M. G., SHINDELL, D., SMITH, S. J., STEHFEST, E., VAN AARDENNE, J., COOPER, O. R., KAINUMA, M., MAHOWALD, N., MCCONNELL, J. R., NAIK, V., RIAHI, K., and VAN VUUREN, D. P.: Historical (1850–2000) gridded anthropogenic and biomass burning emissions of reactive gases and aerosols: Methodology and application, *Atmos. Chem. Phys.*, 10, 7017-7039, 10.5194/acp-10-7017-2010, 2010.

LIN, G., PENNER, J. E., SILLMAN, S., TARABORRELLI, D., and LELIEVELD, J.: Global modeling of soa formation from dicarbonyls, epoxides, organic nitrates and peroxides, *Atmos. Chem. Phys.*, 12, 4743-4774, 10.5194/acp-12-4743-2012, 2012.

LUO, G., and YU, F.: A numerical evaluation of global oceanic emissions of α-pinene and isoprene, *Atmos. Chem. Phys.*, 10, 2007-2015, 10.5194/acp-10-2007-2010, 2010.

MESKHIDZE, N., and NENES, A.: Phytoplankton and cloudiness in the southern ocean, *Science*, 314, 1419-1423, 10.1126/science.1131779, 2006.

MONROE, B. M.: Rate constants for the reaction of singlet oxygen with conjugated dienes, *Journal of the American Chemical Society*, 103, 7253-7256, 10.1021/ja00414a035, 1981.

MYHRE, G., BELLOUIN, N., BERGLEN, T. F., BERNTSEN, T. K., BOUCHER, O., GRINI, A., IVAR, S. A. M., JOHNSRUD, I., MICHAEL, I. M., STORDAL, F., and TANRéE, D.: Comparison of the radiative properties and direct radiative effect of aerosols from a global aerosol model and remote sensing data over ocean, *Tellus B: Chemical and Physical Meteorology*, 59, 115-129, 10.1111/j.1600-0889.2006.00238.x, 2007.

MYRIOKEFALITAKIS, S., VIGNATI, E., TSIGARIDIS, K., PAPADIMAS, C., SCIARE, J., MIHALOPOULOS, N., FACCHINI, M. C., RINALDI, M., DENTENER, F. J., CEBURNIS, D., HATZIANASTASIOU, N., O'DOWD, C. D., VAN WEELE, M., and KANAKIDOU, M.: Global modeling of the oceanic source of organic aerosols, *Advances in Meteorology*, 16, 10.1155/2010/939171, 2010.

O'DONNELL, D., TSIGARIDIS, K., and FEICHTER, J.: Estimating the direct and indirect effects of secondary organic aerosols using echam5-ham, *Atmos. Chem. Phys.*, 11, 8635-8659, 10.5194/acp-11-8635-2011, 2011.

ODUM, J. R., HOFFMANN, T., BOWMAN, F., COLLINS, D., FLAGAN, R. C., and SEINFELD, J. H.: Gas/particle partitioning and secondary organic aerosol yields, *Environmental Science & Technology*, 30, 2580-2585, 10.1021/es950943+, 1996.

OVADNEVAITE, J., O'DOWD, C., DALL'OSTO, M., CEBURNIS, D., WORSNOP, D. R., and BERRESHEIM, H.: Detecting high contributions of primary organic matter to marine aerosol: A case study, *Geophysical Research Letters*, 38, 10.1029/2010gl046083, 2011.

PALMER, P. I., and SHAW, S. L.: Quantifying global marine isoprene fluxes using modis chlorophyll observations, *Geophysical Research Letters*, 32, 10.1029/2005gl022592, 2005.

REMER, L. A., and KAUFMAN, Y. J.: Aerosol direct radiative effect at the top of the atmosphere over cloud free ocean derived from four years of modis data, *Atmos. Chem. Phys.*, 6, 237-253, 10.5194/acp-6-237-2006, 2006.

SALTZMAN, E. S.: Marine aerosols, in: Surface ocean–lower atmosphere processes, American Geophysical Union, 17-35, 10.1029/2008GM000769.

SCHULTZ, M. G., STADTLER, S., SCHRÖDER, S., TARABORRELLI, D., FRANCO, B., KREFTING, J., HENROT, A., FERRACHAT, S., LOHMANN, U., NEUBAUER, D., SIEGENTHALER-LE DRIAN, C., WAHL, S., KOKKOLA, H., KÜHN, T., RAST, S., SCHMIDT, H., STIER, P., KINNISON, D., TYNDALL, G. S., ORLANDO, J. J., and WESPES, C.: The chemistry climate model echam6.3-ham2.3-moz1.0, *Geosci. Model Dev. Discuss.*, 2017, 1-43, 10.5194/gmd-2017-191, 2017.

SHAW, S. L., GANTT, B., and MESKHIDZE, N.: Production and emissions of marine isoprene and monoterpenes: A review, *Advances in Meteorology*, 10.1155/2010/408696, 2010.

STADTLER, S., KÜHN, T., SCHRÖDER, S., TARABORRELLI, D., SCHULTZ, M. G., and KOKKOLA, H.: Isoprene derived secondary organic aerosol in a global aerosol chemistry climate model, *Geosci. Model Dev. Discuss.*, 2017, 1-35, 10.5194/gmd-2017-244, 2017.

TSIGARIDIS, K., and KANAKIDOU, M.: Secondary organic aerosol importance in the future atmosphere, *Atmospheric Environment*, 41, 4682-4692, https://doi.org/10.1016/j.atmosenv.2007.03.045, 2007.

WANNINKHOF, R.: Relationship between wind speed and gas exchange over the ocean, *Journal of Geophysical Research: Oceans*, 97, 7373-7382, 10.1029/92JC00188, 1992.

WRIEDT, T.: Mie theory: A review, in: The mie theory: Basics and applications, edited by: Hergert, W., and Wriedt, T., Springer Berlin Heidelberg, Berlin, Heidelberg, 53-71, 10.1007/978-3-642-28738-1_2.

YASSAA, N., PEEKEN, I., ZÖLLNER, E., BLUHM, K., ARNOLD, S., SPRACKLEN, D., and WILLIAMS, J.: Evidence for marine production of monoterpenes, *Environmental Chemistry*, 5, 391-401, 10.1071/En08047, 2008.

7   CONCLUSION AND OUTLOOK

The main goal of this work was to provide a better understanding of the biogeochemical cycling of isoprene in the surface ocean in order to predict the global surface isoprene distribution and to assess the influence of marine-derived isoprene emissions on secondary organic aerosol (SOA) formation. SOA scatter and absorb solar radiation and, therefore, influence the radiative balance of the Earth. Current global atmospheric chemical models only use terrestrial isoprene emission inventories to estimate the influence of isoprene-derived SOA (iSOA), because marine isoprene emissions are thought to be negligible relative to terrestrial emissions. Furthermore, marine isoprene measurements are sparse and, therefore, are associated with large uncertainties. Due to the short atmospheric lifetime of isoprene and its oxidation products including iSOA, isoprene is known to influence atmospheric chemistry nearby its source. Therefore, model predictions of SOA concentrations in the atmosphere over the open ocean are highly speculative when no marine emissions are used in the calculation.

To assess the influence of marine isoprene concentrations on SOA, this thesis was split into three chapters. 1) Global marine isoprene distributions and resulting fluxes to the atmosphere on the basis of isoprene measurements in three different ocean basins were estimated, which 2) illustrated that an improved source and sink process understanding of isoprene in the surface ocean is needed. The resulting marine isoprene emissions were 3) implemented into a global atmospheric chemistry climate model to quantify marine-derived iSOA formation. Each chapter addresses one research question that was presented in the outline of this thesis (section 2). The questions will be answered in the following:

1) Can simple models predict large scale surface ocean isoprene concentrations?

To calculate global isoprene distributions an existing model was used, which assumes a steady-state concentration balanced by production and consumption processes of isoprene in the oceanic mixed layer. This model used monthly mean remotely sensed satellite data of chlorophyll *a* (chl-a) to parameterize the production of isoprene and sea surface temperature, wind speed, and mixed layer depth to parameterize the loss due to air-sea gas exchange. Additionally, the model accounted for chemical loss, biological consumption and physical loss (advective mixing) of isoprene in the surface ocean. The model output was verified against oceanic iso-

prene measurements from three different ocean basins (eastern Atlantic Ocean, Indian Ocean, eastern Pacific Ocean). This simple model underpredicted the measured oceanic isoprene concentration by a mean factor of 19±12 leading to the conclusion that such a simple model is not able to predict surface ocean isoprene concentrations.

The model was improved by using previously published phytoplankton functional type (PFT) dependent chl-a normalized isoprene production rates instead of one bulk chl-a normalized isoprene production rate for all different PFTs. To keep the model simple, PFT concentrations were parameterized from monthly mean remotely sensed satellite data of chl-a. Additionally, the loss rate for bacterial degradation of isoprene in the water column was decreased, dependent on results of isoprene incubation experiments under natural light conditions (data not shown). A comparison of the original and improved annual mean global model output for 2014 is shown in Figure 7.1. The predicted annual mean surface isoprene concentration of the improved model increased by a factor of four compared to the output of the original model.
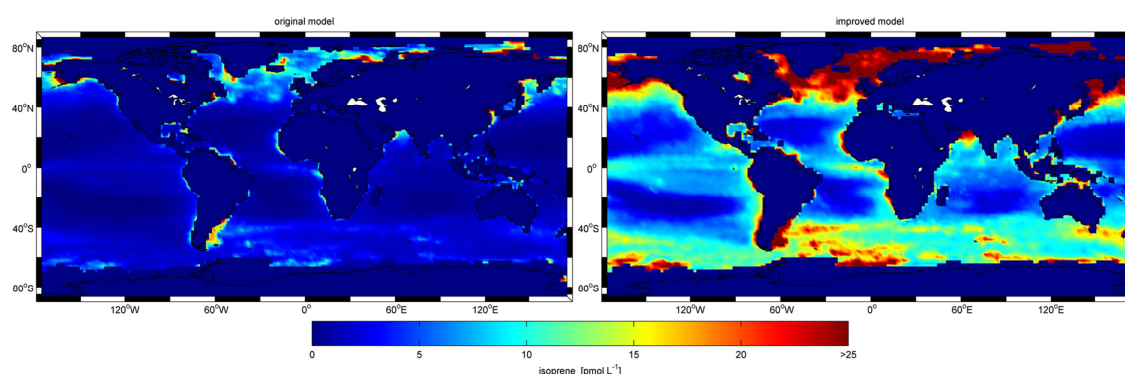
Figure 7.1: Modeled surface ocean isoprene concentrations. Left: original model. Right: improved model.

However, compared to the field measurements of the three different cruises, the resulting isoprene concentrations of the model were still a factor of two lower and did not always reflect the actual spatial distribution. Additionally, the sea-to-air fluxes and the resulting atmospheric mixing ratio of isoprene were calculated. The results showed that the isoprene flux had to be at least one order of magnitude higher to account for measured atmospheric concentrations. The discrepancies between modeled and measured oceanic isoprene concentrations, as well as between calculated and measured atmospheric mixing ratios, lead to the conclusion that the model still did not account for all production and consumption processes.

In summary, the improved model is able to predict large scale surface isoprene concentrations with some limitations on regional (limitation of resolution: e.g. resolution of mixed layer depth climatology is 2°x2°) and time scales (e.g. monthly mean satellite chl-a data cannot resolve short term changes in phytoplankton blooms). However, a better process understanding of the biogeochemical cycling of isoprene

and its preferably simple incorporation into the model would help to better predict surface ocean isoprene concentrations and subsequent emissions.

2) What are the in-field production and consumption rates of isoprene in the surface ocean?

The results of the first study showed that isoprene production and consumption processes in the surface ocean had to be better quantified to accurately predict surface ocean isoprene concentrations. Isoprene production rates for different PFTs are reported in the literature and are generally determined from incubation experiments of monocultures in the laboratory. However, monoculture laboratory experiments have limitations as there are different PFTs coexisting in the ocean and experiments are not able to account for various chemical, biological and physical processes which might influence the biogeochemical cycling of isoprene. Isoprene and pigment measurements in the Indian Ocean and the eastern Pacific Ocean were used to derive, for the first time, in-field isoprene production rates for haptophytes, cyanobacteria, *Prochlorococcus*, chlorophytes, and diatoms. The resulting in-field production rates were different for different PFTs, but also varied by oceanic region. These results generally confirmed the results of laboratory experiments that isoprene production is influenced by light and ocean temperature. Furthermore, this study showed that, irrespective of different PFTs, the production of isoprene is influenced by nutrient concentrations and salinity levels. PFT normalized calculated isoprene production rates could be split into three different categories: 1) low PFT normalized production rates between 1.0 and 6.5 pmol (µg PFT)$^{-1}$ day^{-1} were observed under high nutrient levels ([NO$_3^-$]>10 µmol L^{-1}), low ocean temperatures (<20.5°C), and low solar radiation (mean: <328 W m^{-2}). 2) medium PFT normalized production rates between 9.9 and 15.7 pmol (µg PFT)$^{-1}$ day^{-1} were observed under low nutrient levels ([NO$_3^-$]<2 µmol L^{-1}), independent of an ocean temperature regime, and medium light levels (mean: 408 W m^{-2}). 3) high PFT normalized production rates between 26.6 and 36.4 pmol (µg PFT)$^{-1}$ day^{-1} were observed under medium nutrient levels ([NO$_3^-$]<5 µmol L^{-1}), high light levels (mean: 469 W m^{-2}), and low salinity levels (mean: 34.2). The investigation of the biogeochemical cycling of isoprene also showed that a variable consumption process influenced the surface isoprene concentration. This loss process was attributed to bacterial degradation. However, the data showed that this consumption process might also be the result of a complex combination of bacteria and haptophyte concentration. Haptophytes are known to produce isoprene that might attract bacteria. However, haptophytes are also thought to be the main marine bacterial grazers. Therefore, this combination might be the reason for the variable loss rate constant between 0.01 and 0.1 day^{-1} dependent on ocean region.

3) How much do marine isoprene emissions impact the formation of total iSOA?

This question was answered in the third study, by incorporating three different possible isoprene emission estimates derived from the first study into a model experiment. The emission inventories were implemented into a global chemistry climate model that used a semi-explicit isoprene oxidation module with explicit aerosol tracer treatment to calculate iSOA formation. Using isoprene emission estimates that fit best to the measured atmospheric mixing ratios in the first study, the model calculations showed that marine-derived iSOA only contributed less than 2% to total iSOA formation on a global scale, which was attributed to the strong terrestrial source of isoprene. However, marine isoprene emissions did significantly impact the SOA formation over the open ocean, as the strong terrestrial isoprene emissions did not reach the open ocean due to the short atmospheric lifetime of isoprene (Figure 7.2). On a global scale in the atmosphere over the ocean, the annual mean contribution of marine-derived iSOA to total iSOA formation was 24% using the average of two emission scenarios that fit best to our measurements. This proportion was highly dependent on region and season. During boreal summer (Figure 7.2: left), marine-derived iSOA accounted for 6% and 25% of total iSOA formation in the northern and southern marine atmosphere, respectively. During austral summer (Figure 7.2: right), marine-derived iSOA accounted for 20% and 36% of total iSOA formation in the northern and southern marine atmosphere, respectively.
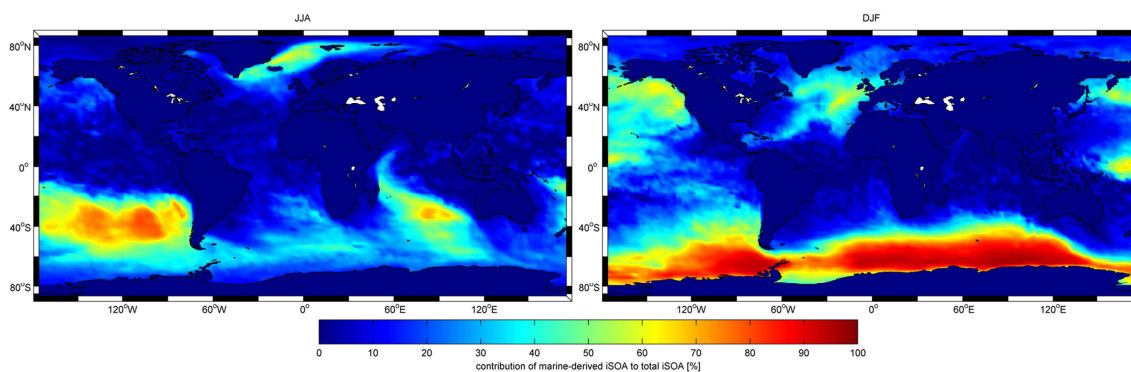
Figure 7.2: Contribution of marine-derived iSOA to total iSOA in %. Left: boreal summer (JJA). Right: austral summer (DJF).

The hemispheric differences in the marine-derived contribution to iSOA have a twofold explanation: 1) In the southern hemisphere the strength of marine-derived iSOA contribution to total iSOA is driven by the absolute concentration in marine-derived iSOA, as hardly any terrestrially derived iSOA reaches the open ocean regions, especially in the Southern Ocean. 2) In contrast, in the northern hemisphere the strength of marine-derived iSOA contribution to total iSOA is driven by the absolute concentration in terrestrially derived iSOA. This can be seen e.g. in the North Atlantic. During boreal summer, absolute concentrations of marine-derived iSOA

are higher than during austral summer. However, the contribution of marine-derived iSOA to total iSOA is stronger during austral summer. During austral summer, terrestrial emissions of isoprene in the northern hemisphere are low compared to boreal summer emissions, where terrestrially derived iSOA is transported over the ocean.

In summary, marine-derived isoprene emission significantly influence the total iSOA concentration over the ocean with higher contribution in the southern hemisphere up to almost 100% in the remote Southern Ocean during austral summer and also in the northern hemisphere up to 60% when terrestrial isoprene emissions are reduced.

Using the combined results of the three chapters of this thesis the overarching question will be addressed in the following:

How important are marine isoprene emissions in influencing the Earth's climate?

Marine isoprene emissions estimates from the first study were used in the third study to assess the influence of marine-derived isoprene on iSOA formation. Marine aerosols in general have a higher impact on the radiative balance as they scatter solar radiation that would have been more likely absorbed by the Earth's surface than aerosols over land. This is due to the much lower albedo of the ocean (0.07) compared to the albedo of the terrestrial surface (0.12-0.36) and ice/snow (0.62-0.66)(BRIEGLEB et al., 1986). Marine isoprene emissions significantly impact the climate over the open ocean in general, although their influence is reduced in the tropical regions, due to strong terrestrially derived iSOA concentrations which are transported to the atmosphere over the ocean. Marine-derived iSOA reduces the incoming solar radiation up to 1.25 W m^{-2} in seasons and regions where the contribution of marine-derived iSOA to total iSOA is strongest (e.g. North Atlantic, boreal summer). A decrease in incoming solar radiation of 1.25 W m^{-2} caused by marine-derived iSOA compared to the total aerosol direct effect in the clean atmosphere over the ocean of -2.9 W m^{-2} (REMER and KAUFMAN, 2006) demonstrates the significant contribution (up to 43%) of marine-derived iSOA to the total aerosol radiative effect. ANTTILA et al. (2010) reported modeled iSOA concentrations over the northeast Atlantic to be ~5 ng m^{-3} and stated that the iSOA contribution to organic aerosol (OA) is negligible. Their calculated marine-derived iSOA concentrations agree with the findings of this thesis in the northeast Atlantic. However, as this region is highly influenced by terrestrially derived aerosol, the results of this thesis demonstrate that a negligible contribution of marine iSOA to OA in the northeast Atlantic cannot be extrapolated to the global scale.

In addition to absolute number of aerosol particle, also the size distribution of iSOA influences the effect on scattering or absorbing solar radiation. The analysis of the global mean size distribution of marine-derived iSOA clearly showed that the mean radius was two times higher compared to terrestrially-derived iSOA. Larger particles are known to

scatter light mostly in the forward direction (Mie scattering; WRIEDT, 2012). Therefore, the results indicate a weakening of the direct radiative effect of marine-derived iSOA. However, a weakening of the direct radiative effect could increase the indirect radiative effect. MESKHIDZE and NENES (2006) hypothesized that marine isoprene emissions directly influence cloud properties over the bloom and calculated an indirect radiative effect of -15 W m^{-2} over the bloom area, which is comparable to highly polluted areas. However, the strength might be overestimated, as they overestimated the isoprene emissions. Additionally, they reported higher cloud droplet numbers and decreased particle size diameters. This in contrast to the results of this thesis that marine-derived iSOA contributes to the growth of already existing particles. To date, there is no clear positive link between marine isoprene emissions and cloud droplet numbers. Furthermore, laboratory experiments in a plant chamber show that isoprene emissions even might inhibit new particle formation in forests (KIENDLER-SCHARR et al., 2009).

The results of this thesis clearly show the importance of the influence of marine isoprene on SOA formation. However, it still needs further process understanding of both isoprene cycling in the ocean and isoprene oxidation pathways in the atmosphere to further assess the influence of marine isoprene on SOA formation. A schematic overview of the main isoprene pathways is given in Figure 7.3. Even though it is now known that production rates of isoprene are dependent on temperature and light, as well as on nutrient and salinity levels, the understanding of this complex interaction of different factors needs further investigation. This thesis shows that using PFT dependent isoprene production rates significantly improves the quantification of isoprene concentrations in the surface ocean. However, resolving the total composition of the phytoplankton community still needs actual field measurements. Different bio-optical algorithms have been developed to identify single PFTs from space using ocean-color satellite data. To date, these approaches either provide only the dominant PFT out of four different PFTs (ALVAIN et al., 2005) or are still limited to three particular PFTs (diatoms, coccolithophores, cyanobacteria) (WOLANIN et al., 2016). Improving the retrievals of PFTs from remotely sensed data will help to quantify the isoprene production in the surface ocean. To understand the biogeochemical cycling of isoprene in the ocean also includes the quantification of isoprene consumption in the surface ocean. The results of this thesis support recent findings of JOHNSTON et al. (2017) that marine isoprene is degraded by bacteria. Additionally, the mismatch between calculated and measured atmospheric isoprene concentrations in the first study leads to the hypothesis that the sea surface microlayer (SML) might be an additional source of isoprene. Laboratory experiments (CIURARU et al., 2015) indicate that the flux of isoprene produced in the SML could account for the mismatch between calculated and measured atmospheric isoprene concentrations. However, analytical trace gas sampling techniques have to be improved to reliably determine isoprene concentrations in the SML. This will help to quantify isoprene emissions and the resulting marine-derived atmospheric isoprene concentrations. The influence of marine-derived isoprene on SOA formation needs further research in understanding the atmospheric pathways of isoprene oxidation. The model used in the third study is the first one providing a semi-explicit isoprene oxidation module. However, WANG and RUIZ (2017) recently reported

SOA formation from chlorine-initiated isoprene oxidation under low-NO_x conditions, suggesting that tropospheric chlorine could contribute significantly to atmospheric OA loading.
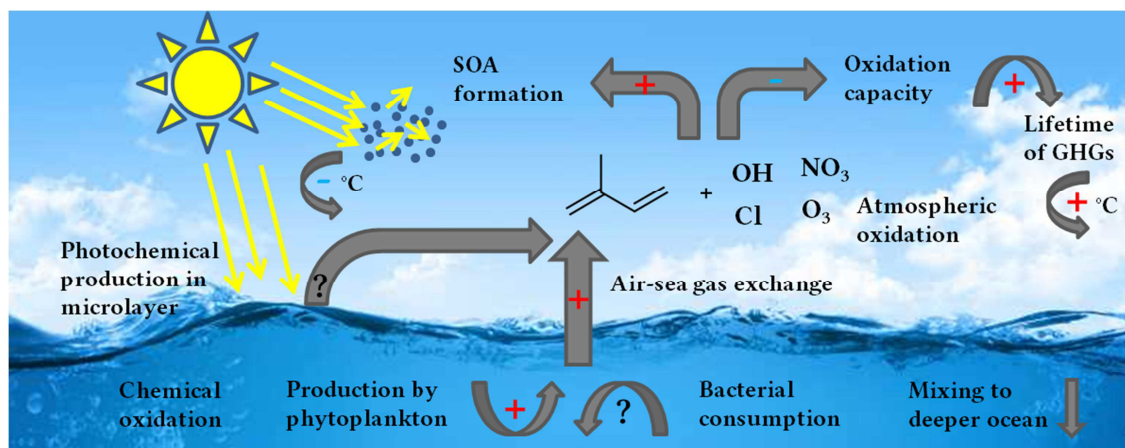

Figure 7.3: Schematic diagram of main isoprene pathways and processes in the marine and atmospheric environment including corresponding potential feedbacks in a warming climate. The potential feedback of a temperature increase in a future climate accompanied by increasing isoprene production in the surface ocean is shown using a red "+" and blue "-" for a positive and a negative feedback, respectively. SOA: secondary organic aerosols, GHG: greenhouse gas.

Current knowledge of the climate feedbacks of isoprene emissions is used today to assess the importance of isoprene emissions in a changing climate. Different studies tried to predict future scenario terrestrial isoprene emissions estimates with different results. SANDERSON et al. (2003) calculated an increase of terrestrial isoprene emissions up to 736 Tg yr^{-1} in 2090 as a result of climate change, however, with today's vegetation distribution. When they changed the vegetation accordingly to climate change in 2090 the emission estimate decreases to 697 Tg yr^{-1}, which is only a slight increase compared to today's terrestrial emission estimates (ARNETH et al., 2008). Other studies do not expect an increase of terrestrial isoprene emissions, as higher CO_2 concentrations could counteract the positive forcing of increasing temperatures (PACIFICO et al., 2012), although the temperature change was the primary control on isoprene emissions over the last 400 thousand years (HEALD et al., 2009). Future land-use is an additional uncertainty in future climate models and has to be taken into account as factor influencing isoprene emissions. Tropical deforestation would decrease future isoprene emissions (LATHIERE et al., 2006), whereas future spreading of oil palm plantations would increase isoprene emissions, as they are known to strong isoprene emitters (MISZTAL et al., 2011). Anthropogenic pollution might increase which would lead to higher NO_x levels. Thus, reaction with isoprene would increase tropospheric O_3 and increase the iSOA formation. Higher concentrations of SOA would cool the atmosphere counteracting the temperature increase by increased O_3 levels (PACIFICO et al., 2009). HEALD et al. (2008) assumed that the SOA burden from biogenic sources would increase by 35% in 2100.

The uncertainties in future terrestrial isoprene emissions and SOA formation complicate the assessment of the influence of marine-derived isoprene on a global scale. To
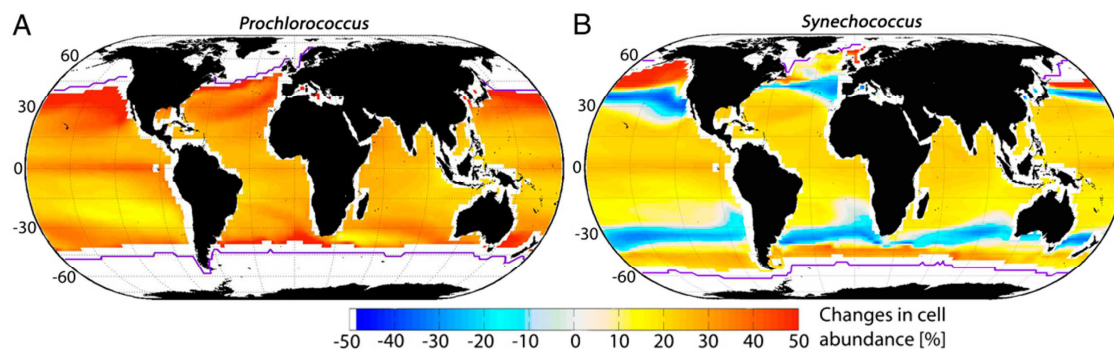
Figure 7.4: Projected change in global abundance of *Prochlorococcus* (A) and *Synechococcus* (B) for 2100 from FLOMBAUM et al. (2013).

date, no such future climate model studies for marine isoprene emissions were carried out. However, the dependence of isoprene production rates on environmental parameters, as shown in the second study, might help to predict future marine isoprene changes. Nutrient availability in the surface ocean will decrease due to increasing stratification. In contrast, eutrophication in coastal regions might increase, due to increasing anthropogenic influence (e.g. DIAZ and ROSENBERG, 2008). However, there are no published studies quantifying long-term trends of nutrient concentrations (IPCC, 2013). Mean global future salinity levels might not change, although the magnitude between high-saline and low-saline waters will increase (IPCC, 2013). This would have both, a positive and negative effect on isoprene production depending on the oceanic region. In a warming climate with increasing ocean temperatures one could expect that isoprene emissions would increase, 1) as the solubility of isoprene decreases with increasing temperature and 2) as temperature is known to positively influence isoprene production of different PFTs. However, temperature induced isoprene production of PFTs might only be a short term response, due to stress. Phytoplankton is known to migrate in the surface ocean due to nutrient limitation or due to light responses (JOHNSON et al., 2006). Likewise, temperature dependence would cause a shift of phytoplankton abundance in the global ocean under a changing climate. FLOMBAUM et al. (2013) observed complex changes in the abundance and distribution of two marine cyanobacteria (*Prochlorococcus* and *Synechococcus*) as a result of climate change in 2100 (RCP4.5 scenario) (Figure 7.4). On a global mean, they calculated an increase of cell abundances in general, with strongest increase towards higher latitudes for *Prochlorococcus* but also a decline of cell abundances around 35°N and 35°S for *Synechococcus*. The in-field production rates in the second study of this thesis for cyanobacteria (excluding *Prochlorococcus*) were calculated to be at the higher end of known isoprene production rates (up to 44.7 µmol (g chl-a)$^{-1}$ day^{-1}). Therefore, an increase in cell abundances and a shift in distribution of phytoplankton would have a regional as well as global effect on marine isoprene emissions.

Thus, further understanding of the biogeochemical cycling of isoprene in the surface ocean and the subsequent air-sea gas exchange is necessary to estimate the influence of marine isoprene on the oxidative capacity of the atmosphere. In combination with a better process understanding of atmospheric isoprene oxidation leading to iSOA formation this will help to predict the feedback of marine isoprene on our climate.

References

ALVAIN, S., MOULIN, C., DANDONNEAU, Y., and BREON, F. M.: Remote sensing of phytoplankton groups in case 1 waters from global seawifs imagery, *Deep-Sea Research Part I-Oceanographic Research Papers*, 52, 1989-2004, 10.1016/j.dsr.2005.06.015, 2005.

ANTTILA, T., LANGMANN, B., VARGHESE, S., and O'DOWD, C.: Contribution of isoprene oxidation products to marine aerosol over the north-east atlantic, *Advances in Meteorology*, 10.1155/2010/482603, 2010.

ARNETH, A., MONSON, R. K., SCHURGERS, G., NIINEMETS, Ü., and PALMER, P. I.: Why are estimates of global terrestrial isoprene emissions so similar (and why is this not so for monoterpenes)?, *Atmos. Chem. Phys.*, 8, 4605-4620, 10.5194/acp-8-4605-2008, 2008.

BRIEGLEB, B. P., MINNIS, P., RAMANATHAN, V., and HARRISON, E.: Comparison of regional clear-sky albedos inferred from satellite observations and model computations, *Journal of Climate and Applied Meteorology*, 25, 214-226, 10.1175/1520-0450(1986)025<0214:corcsa>2.0.co;2, 1986.

CIURARU, R., FINE, L., PINXTEREN, M. v., D'ANNA, B., HERRMANN, H., and GEORGE, C.: Unravelling new processes at interfaces: Photochemical isoprene production at the sea surface, *Environmental Science & Technology*, 49, 13199-13205, 10.1021/acs.est.5b02388, 2015.

DIAZ, R. J., and ROSENBERG, R.: Spreading dead zones and consequences for marine ecosystems, *Science*, 321, 926-929, 10.1126/science.1156401, 2008.

FLOMBAUM, P., GALLEGOS, J. L., GORDILLO, R. A., RINCÓN, J., ZABALA, L. L., JIAO, N., KARL, D. M., LI, W. K. W., LOMAS, M. W., VENEZIANO, D., VERA, C. S., VRUGT, J. A., and MARTINY, A. C.: Present and future global distributions of the marine cyanobacteria prochlorococcus and synechococcus, *Proceedings of the National Academy of Sciences*, 110, 9824-9829, 10.1073/pnas.1307701110, 2013.

HEALD, C. L., HENZE, D. K., HOROWITZ, L. W., FEDDEMA, J., LAMARQUE, J. F., GUENTHER, A., HESS, P. G., VITT, F., SEINFELD, J. H., GOLDSTEIN, A. H., and FUNG, I.: Predicted change in global secondary organic aerosol concentrations in response to future climate, emissions, and land use change, *Journal of Geophysical Research-Atmospheres*, 113, 16, 10.1029/2007jd009092, 2008.

HEALD, C. L., WILKINSON, M. J., MONSON, R. K., ALO, C. A., WANG, G., and GUENTHER, A.: Response of isoprene emission to ambient co2 changes and implications for global budgets, *Global Change Biology*, 15, 1127-1140, 10.1111/j.1365-2486.2008.01802.x, 2009.

IPCC: Climate change 2013: The physical science basis. Contribution of working group i to the fifth assessment report of the intergovernmental panel on climate

change, Cambridge University Press, Cambridge, United Kingdom and New York, NY, USA, 1535 pp., 2013.

JOHNSON, Z. I., ZINSER, E. R., COE, A., MCNULTY, N. P., WOODWARD, E. M. S., and CHISHOLM, S. W.: Niche partitioning among prochlorococcus ecotypes along ocean-scale environmental gradients, *Science*, 311, 1737-1740, 10.1126/science.1118052, 2006.

JOHNSTON, A., CROMBIE, A. T., EL KHAWAND, M., SIMS, L., WHITED, G. M., MCGENITY, T. J., and COLIN MURRELL, J.: Identification and characterisation of isoprene-degrading bacteria in an estuarine environment, *Environmental Microbiology*, 19, 3526-3537, 10.1111/1462-2920.13842, 2017.

KIENDLER-SCHARR, A., WILDT, J., MASO, M. D., HOHAUS, T., KLEIST, E., MENTEL, T. F., TILLMANN, R., UERLINGS, R., SCHURR, U., and WAHNER, A.: New particle formation in forests inhibited by isoprene emissions, *Nature*, 461, 381, 10.1038/nature08292

https://www.nature.com/articles/nature08292#supplementary-information, 2009.

LATHIERE, J., HAUGLUSTAINE, D., FRIEND, A., NOBLET-DUCOUDRÉ, N. D., VIOVY, N., and FOLBERTH, G.: Impact of climate variability and land use changes on global biogenic volatile organic compound emissions, *Atmospheric Chemistry and Physics*, 6, 2129-2146, 2006.

MESKHIDZE, N., and NENES, A.: Phytoplankton and cloudiness in the southern ocean, *Science*, 314, 1419-1423, 10.1126/science.1131779, 2006.

MISZTAL, P. K., NEMITZ, E., LANGFORD, B., DI MARCO, C. F., PHILLIPS, G. J., HEWITT, C. N., MACKENZIE, A. R., OWEN, S. M., FOWLER, D., HEAL, M. R., and CAPE, J. N.: Direct ecosystem fluxes of volatile organic compounds from oil palms in south-east asia, *Atmospheric Chemistry and Physics*, 11, 8995-9017, 10.5194/acp-11-8995-2011, 2011.

PACIFICO, F., HARRISON, S. P., JONES, C. D., and SITCH, S.: Isoprene emissions and climate, *Atmospheric Environment*, 43, 6121-6135, http://dx.doi.org/10.1016/j.atmosenv.2009.09.002, 2009.

PACIFICO, F., FOLBERTH, G. A., JONES, C. D., HARRISON, S. P., and COLLINS, W. J.: Sensitivity of biogenic isoprene emissions to past, present, and future environmental conditions and implications for atmospheric chemistry, *Journal of Geophysical Research: Atmospheres*, 117, n/a-n/a, 10.1029/2012JD018276, 2012.

REMER, L. A., and KAUFMAN, Y. J.: Aerosol direct radiative effect at the top of the atmosphere over cloud free ocean derived from four years of modis data, *Atmos. Chem. Phys.*, 6, 237-253, 10.5194/acp-6-237-2006, 2006.

SANDERSON, M. G., JONES, C. D., COLLINS, W. J., JOHNSON, C. E., and DERWENT, R. G.: Effect of climate change on isoprene emissions and surface ozone levels, *Geophysical Research Letters*, 30, n/a-n/a, 10.1029/2003GL017642, 2003.

WANG, D. S., and RUIZ, L. H.: Secondary organic aerosol from chlorine-initiated oxidation of isoprene, *Atmos. Chem. Phys.*, 17, 13491-13508, 10.5194/acp-17-13491-2017, 2017.

WOLANIN, A., SOPPA, M., and BRACHER, A.: Investigation of spectral band requirements for improving retrievals of phytoplankton functional types, *Remote Sensing*, 8, 871, 2016.

WRIEDT, T.: Mie theory: A review, in: The mie theory: Basics and applications, edited by: Hergert, W., and Wriedt, T., Springer Berlin Heidelberg, Berlin, Heidelberg, 53-71, 10.1007/978-3-642-28738-1_2.

CURRICULUM VITAE

Personal

Name:	Dennis Booge
Date of Birth:	21.05.1986
Place of Birth:	Elmshorn
Nationality:	German

Education

08/2013 – 12/2017	Ph.D. student at GEOMAR Helmholtz Centre for Ocean Research Kiel, Kiel, Germany
10/2010 – 11/2012	Studies of Chemistry, M.Sc. at Christian-Albrechts-Universität, Kiel, Germany
10/2007 – 9/2010	Studies of Chemistry, B.Sc. at Christian-Albrechts-Universität, Kiel, Germany
10/2006 – 9/2007	Studies of Math at Christian-Albrechts-Universität, Kiel, Germany
8/1996 – 5/2005	Elsa-Brändström-Gymnasium with German university entrance qualification (Abitur), Elmshorn, Germany

Work Experience

12/2012 – 07/2013	Research assistant at GEOMAR Helmholtz Centre for Ocean Research Kiel, Kiel, Germany
1/2012 – 3/2012	Industrial Internship at tesa® SE, Hamburg, Germany
4/2011 – 12/2011	Student Assistant at GEOMAR, Helmholtz Centre for Ocean Research, Kiel, Kiel, Germany
3/2011	Student Assistant at Institute for Inorganic Chemistry, Christian-Albrechts-Universität, Kiel, Germany

Research Expeditions

11/2015	SO243 ASTRA-OMZ, R/V Sonne Guayaquil (Ecuador) – Antofagasta (Chile)
07/2014 – 08/2014	SO234/2 and SO235 SPACES/OASIS, R/V Sonne Durban (South Africa) – Pt. Louis (Mauritius) – Malé (Maledives)
since 06/2010	several one-day cruises to time series station Boknis Eck, Eckernförder Bay (Baltic Sea)

Publications

Dennis Booge, Scarlet Stadtler, Christa A. Marandino: The influence of marine isoprene emissions on secondary organic aerosol concentration over the remote ocean, manuscript in preparation.

Alex Zavarsky, **Dennis Booge**, Alina Fiehn, Kirstin Krüger, Elliot Atlas and Christa Marandino: The influence of air-sea fluxes on atmospheric aerosols during the summer monsoon over the tropical Indian Ocean, *Geophys. Res. Lett.*, under review, 2017.

Dennis Booge, Cathleen Schlundt, Astrid Bracher, Sonja Endres, Birthe Zäncker, Christa A. Marandino: Marine isoprene production and consumption in the mixed layer of the surface ocean – A field study over 2 oceanic regions, *Biogeosciences Discuss.*, 2017, doi:10.5194/bg-2017-257.

Lennartz, S. T., Marandino, C. A., von Hobe, M., Cortes, P., Quack, B., Simo, R., **Booge, D.**, Pozzer, A., Steinhoff, T., Arevalo-Martinez, D. L., Kloss, C., Bracher, A., Röttgers, R., Atlas, E., and Krüger, K.: Direct oceanic emissions unlikely to account for the missing source of atmospheric carbonyl sulfide, *Atmos. Chem. Phys.*, 17, 385-402, 2017, doi:10.5194/acp-17-385-2017, 2017.

Dennis Booge, Christa A. Marandino, Cathleen Schlundt, Paul I. Palmer, Michael Schlundt, Elliot L. Atlas, Astrid Bracher, Eric S. Saltzman, Douglas W. R. Wallace: Can simple models predict large scale surface ocean isoprene concentrations?, *Atmos. Chem. Phys.*, 16, 11807–11821, 2016, doi:10.5194/acp-16-11807-2016, 2016.